UNIVERSITA' DEGLI STUDI DI PARMA

DOTTORATO DI RICERCA IN FISICA

CICLO XXXIII

IN COTUTELA CON LA UNIVERSIDAD DE GRANADA

PROGRAMA DE DOCTORADO EN FÍSICA Y MATEMÁTICAS

SYNCHRONOUS AND ASYNCHRONOUS DYNAMICS IN NEUROSCIENCE: A STATISTICAL PHYSICS APPROACH

Coordinatore: Chiar.mo Prof. Stefano Carretta

Tutore: Chiar.ma Prof. Raffaella Burioni

Tutore esterno: Chiar.mo Prof. Miguel Ángel Muñoz Martínez

Dottorando:

Victor Buendía Ruiz-Azuaga

Anni accademici 2017/2018 – 2019/2020

The doctoral candidate, Victor Buendía Ruiz-Azuaga, and the thesis supervisors, Raffaella Burioni and Miguel A. Muñoz guarantee, by signing this doctoral thesis, that the work has been done by the doctoral candidate under the direction of the thesis supervisor/s and, as far as our knowledge reaches, in the performance of the work, the rights of other authors to be cited (when their results or publications have been used) have been respected.

Il dottorando, Victor Buendía Ruiz-Azuaga, e i tutori della tesi, Raffaella Burioni and Miguel A. Muñoz, garantiamo, f rmando questa tesi di dottorato, che il lavoro è stato realizzato dat dottorando sotto la supervisione dei tutori della tesi, e per quanto di nostra conoscenza, nell'esecuzione del lavoro, si sono rispettati i diritti di altri autori a essere citati, quando sono stati utilizzati i loro risultati o pubblicazioni.

El doctorando, Victor Buendía Ruiz-Azuaga, y los supervisores de la tesis, Raffaella Burioni and Miguel A. Muñoz, garantizamos, al f rmar esta tesis doctoral, que el trabajo ha sido realizado por el doctorando bajo la dirección de los directores de la tesis, y hasta donde nuestro conocimiento alcanza, en la realización del trabajo, se han respetado los derechos de otros autores a ser citados, cuando se han utilizado sus resultados o publicaciones.

Parma, Granada, 22/ 12/ 2020

Victor Buendía Raffaella Burioni Miguel A. Muñoz

Contents

Acknowledgements

Una vez terminadas (espero) todas las correciones al texto de la tesis, queda solamente la tarea fundamental de agradecer a todas las personas que han colaborado conmigo, de algún modo, en su elaboración.

Me gustaría empezar por dar las gracias a mi director de tesis granadino, Miguel Ángel, por varios motivos. El primero, por confiar en mí para realizar una tesis doctoral, a pesar de aparecer por su despacho sin conocerle de nada, antes siquiera de entrar al máster, y decirle que me gustaría trabajar con él en una tesis. Después de empezar el doctorado, he escuchado cientos de veces que "la decisión más importante del doctorado es escoger bien a tu director" y puedo afirmar sin ninguna duda que acerté de pleno. Miguel Ángel siempre ha estado ahí para escuchar todas mis dudas y tratar de ayudarme a resolver los problemas que han surgido durante la investigación, y aún más importante –los problemas que nada tenían que ver con ella. Gracias por todos los consejos útiles y las ideas brillantes, y sobre todo, por tu visión personal de la vida en los momentos de flaqueza.

I also would like to thank Raffaella, who gave me the opportunity to do part of my PhD in Parma, a experience that has deeply changed my life, in many aspects. I want to thank you for your motivating and positive attitude during the thesis, your guidance, and your support –both academical, and personal. You demonstrated me from the very beginning that I can trust you for everything, and I really felt comfortable knowing that if something went bad, you were there. Thank you very much.

Por otro lado, quiero agradecer a los doctorandos (algunos ya doctores) del grupo de Física Estadística de la Universidad de Granada. A Ana Paula, Serena y a Nico, por muchos desayunos a media mañana, muchas conversaciones bastante frikis, y un montón de risas durante mi estancia en Granada. También a Rubén, por el intercambio productivo de conversaciones sobre divulgación y tecnologías libres, y a Guille, por el descubrimiento de las salidas a la Tertulia. A Álex, por amenizar la escritura de la tesis con algún streaming, y los post-it anónimos en mi mesa. A Matteo Sireci me gustaría agradecerle también unas cuantas largas conversaciones con tintes filosóficos, y el apoyo mostrado durante la realización de la tesis. Merece una mención especial Pablo Villegas, por las horas interminables discutiendo sobre inhibición, sincronización y otros aspectos de la vida durante los primeros meses de investigación. Estoy muy contento de haber podido

coincidir contigo, aunque fuera un período corto de tiempo, y espero que sigamos en contacto mucho tiempo más. El paper que explique "How the brain works" no se va a escribir solo, y no creo que pueda hacerlo sin ayuda...

Y además de los doctorandos, no me gustaría olvidarme de los profesores y personal del departamento: a Jose, por la ayuda técnica y su buen humor. A Daniel Manzano, Pablo Hurtado, Paco de los Santos y Joaquín J. Torres por las charlas distendidas sobre la academia y la vida científica. Y finalmente, a Pedro Garrido, por su particular sentido del humor y su interesante visión de la física, que ha conseguido contagiarme un poquito de su pasión durante nuestras (cortas) interacciones.

Me gustaría, por supuesto, darle las gracias a mis padres, por apoyarme siempre en mis decisiones, por locas que parezcan a veces. Sin ellos nada de esto hubiera sido posible, y agradeceré siempre que me hayáis permitido acertar (y equivocarme) libremente. Gracias a mi padre, por escucharme asesinar el piano durante buena parte de mi carrera académica y transmitirme la mayor de las aficiones por la música. Y sobre todo gracias a mi madre, por cuidarme tantísimo, apoyarme siempre, y conseguir finalmente enseñarme a vivir yo solo, a pesar del riesgo de que algún día se me olvide la cabeza. Gracias infinitas a los dos, porque sin vosotros esto no sería posible. Al igual que ocurre con el director de tesis, tener unos buenos padres te cambia la vida; pero en este caso no hay posibilidad de elegir, así que soy muy feliz de haberos tenido a vosotros. Esa es y será siempre mi lotería. Me gustaría también agradecer fugazmente a mi tío Fernando, por poner en mis manos un libro de matemáticas demasiado divertido a temprana edad, convirtiéndolo en culpable indirecto de la presente tesis.

Quiero mandar un caluroso abrazo a mis amigos de toda la vida, a Juan, a Aiden, Rafa, Chema, Héctor y a Fran, por años de quedadas para pasear, jugar a videojuegos o simplemente charlar del tema de la semana. Los encuentros prácticamente semanales, cuando estábamos todos juntos, han sido una de las rutinas más agradables que he tenido nunca. A pesar de los altibajos derivados del tiempo y la distancia, os considero a todos de las mejores personas que he conocido, y quiero que sepáis que sois una de las contribuciones más importantes a haber hecho de Granada mi hogar. Sé que todos vosotros estáis siempre ahí cuando lo necesito, y para mí es algo muy importante.

La realización de esta tesis hubiera sido muy distinta sin la pres-

encia de Elvira Asensio, a quien envío un abrazo muy grande desde aquí. Con su buen humor perpetuo, y su visión simple y reivindicativa de la vida, ella siempre ha sabido entender perfectamente cuál era el problema y cuál la solución, a pesar de que a mí me costara verlo. Y pasara lo que pasara, siempre ha sabido estar ahí. Podría extenderme durante páginas, pero en esta ocasión lo dejaré en que cuando esté lejos, echaré de menos los sábados soleados de invierno en la vega, con Sierra Nevada al fondo. Elvira, no tienes ni idea de cuánto me alegro de que cruzaras por mi vida. Realmente la has cambiado, en muchos sentidos... y lo mejor, es que sé que lo seguirás haciendo, siempre podré contar contigo, y eso me hace enormemente feliz.

Voglio ringraziare a miei amici in Italia, Gianluca, a Carlo, Bianca, e Chiara. Conoscere gente a Parma non ha stato facile, e sono veramente felice di avere trovato a loro. A Gianluca D'Amico, li ringrazio moltissimo tutte le passegiatte, le converse su musica, suonare insime, e la copia delle Danzas Chilenas, il mio presente di Natale favorito, che mi compromesso a publicitare a tutti posti. Parma non sarà mai lo stesso senza te, e spero che ci vediamo presto. Sono anche in debito con Bianca Massari, che ha fatto un disegno di frontespizio per la tesi veramente bello.

Grazie anche a Marco Mancastroppa, che ha fatto molto divertente la mia stanza al dipartimento di Parma, e anche l'ora di "comerrr". Mi dispiace non avere fatto una visita a Cremona, ma puoi essere sicuro che la mia stanza a Parma fosse stato diversa senza te. Anche devo ringraziare in questo senso a Michele Tizzani, per le jam insieme il primo anno, e Ifheanyi, Anjali e Cormac.

Agradecer también a mis amigos de la comunidad de Smash Granada, inicialmente juntos por la afición a los videojuegos, pero que con el tiempo se ha convertido en una amistad mucho más fuerte. Quiero mandar recuerdos a Luis, Casti, Álvaro, Mikel, Martha, Miki, Aarón, Ce, Jesús, Nacho, Silvia, Iker, Edu y Jose. Si tuviera que escribiros una dedicatoria con mi opinión de cada uno, la tesis tendría que duplicar su tamaño. Por tanto, quiero que sepáis que me alegro muchísimo de haberos conocido a todos, y que espero que nos sigamos viendo mucho, mucho tiempo (y no solo en el online de Smash).

I would like to say thanks to some of the international friends and collaborators I met during the thesis. First, to Johannes Zierenberg, for very engaging discussions, and his motivation, which always has

pushed me forward. I enjoyed a lot discussing with you during your visit to Granada –unfortunately short due to the pandemic. I have met a lot of wonderful people and brilliant scientists during these years, so many that unfortunately I could not list all... but allow me to also thank Jordi Soriano, Paul Spitzner and Susanna Manrubia, with whom I was lucky to collaborate with at some point during the thesis. I really hope that our paths will continue to cross in the future. Finally, I would like to say thanks to Maria Flores, for long discussions and complains about the PhD life, and her refreshing way of thinking; to Pehzman Ebraimzadeh, for the surprise visit to Granada; and to Veronika Rovnik, for beautiful photos and long conversations about academia and life.

Y para acabar, aunque no menos importante, muchísimas gracias a mi hermana, Ana. Por años y años juntos haciendo el idiota de todas las formas imaginables, las risas sobre cualquier tema, y todos los momentos ridículos en nuestras memorias de los que por desgracia (o casi más bien, por suerte) no queda testimonio gráfico. Por aguantarme hablar de física durante tanto tiempo. Por las videollamadas de las que es imposible colgar. Por todo lo que hay, y todo lo que queda.

Porque he llegado aquí gracias a todos vosotros.

Porque podría seguir escribiendo esta sección durante horas, y no llegaría a expresarlo todo.

De verdad, gracias, gracias a todos.

Victor

A small portion of the of the people I would like to thank. (A) My parents, at my father's birthday. (B) My friends from high-school, the day of my 25th birthday. (C) With Elvira, happy during her visit to Mallorca, in 2016. (D) Rare footage of a serious photo with my sister. (E) With my friends and PhD supervisors at Parma's national statphys conference 2018. Left to right, Pablo Villegas, myself, Serena di Santo, Miguel A. Muñoz, and Raffaella Burioni. The legendary authors of (di Santo et al. 2018a) in a single photo! (F) Enjoying Granada typical *tapas* with some friends from the Smash community. All photos are shared with permission of the people involved. Thank you *so* much again, to all of you!

Abstract

English

Understanding emergence, evolution and organization of natural systems is one of the main objective of science. Statisical physics has played a prominent role shedding light on the processes underlying order and complexity present in biological systems from a bottom-up approach, i.e. recovering the observed collective properties from our knowledge of the elementary components and their interactions. These ideas revolutionized our conception of science during the 20th century, and in the last decades they have become important in areas such as biology or neuroscience, leading to some exciting discoveries and hypotheses that are still in debate.

One of the most powerful conceptual ideas is the theory of *self-organized criticality* proposed by Bak and collaborators in 1987, which proposes that natural systems might be self tuned to the vicinity of a critical point, which would allow them to take advantage of characteristic critical properties such us long-range correlations, large susceptibility, or increased capacity for computation and information processing. Today there is experimental evidence that this the case for some systems in biology.

In 2003 Beggs and Plenz observed, in an experimental breakthrough, power-law distributed avalanches, which are usually manifested by critical systems, suggesting that the brain could also work at the edge of a critical phase transition in the universality class of the unbiased branching process, where activity does not grow nor shrink, on average. Almost twenty years later, there is still no conclusive evidence to close the debate on whether the brain, or at least some parts or it, are critical or not. The rich dynamical repertoire of the brain (including bistability, oscillations in several spectral ranges, large irregular outbursts...) has eluded a complete theoretical description in terms of simple models, and even recent experimental data is not completely conclusive on this respect.

It has been recently proposed that a way to bring together scale-free avalanches with brain rhythms is to consider synchronization phase transitions and their associated critical points. In this thesis, the *criti-*

cality hypothesis in the brain is studied from the perspective of synchronization phenomena, discussing under which circumstances synchronization transitions can generate power-law distributed avalanches, as well as their relation with other experimentally-observed aspects of the cortical dynamics such as the balance between excitation and inhibition or bistability. The thesis is organized in the following way:

Chapter 1 presents some basics concepts dynamical systems, and critical phenomena, as well as a summary of the issue of criticality in the brain and related philosophical aspects.

Chapter 2 is a review of theoretical models for neural and synaptic dynamics, as well as mesoscopic models describing whole regions in an effective way. Relevant concepts from synchronization theory are also sketched here.

Chapter 3 introduces the concept of "Jensen's force" by studying a discrete model that sheds light on the role on inhibition and sparsity in neural networks, and the effect of excitation-inhibition balance.

Chapter 4 presents the concept of hybrid synchronization, a novel regime where both partial synchronization and scale-free avalanches can be found together.

Chapter 5 presents a review of self-organization theory, including the new concept of self-organized bistability. These concepts are later applied to assess the relationship between self-organization and collective oscillations in cortical dynamics.

Chapter 6 sketches future work to develop from here on, including preliminary analyses of more realistic systems.

Chapter 7 includes a discussion on the thesis' results, as well as the conclusions.

Italiano

Capire come emergono, evolvono, e si organizzano i sistemi naturali è uno dei principali obiettivi della scienza. La fisica statistica ha svolto un ruolo chiave in questo processo, chiarendo i processi che stanno alla base della complessità e all'ordine presenti nei sistemi biologici con un approccio "bottom-up", che ricostruisce le proprietà collettive

osservate a partire della nostra conoscenza dei componenti elementari del sistema e delle sue interazioni. Tali idee hanno rivoluzionato la nostra concezione della scienza nel secolo XX, e negli ultimi deceni hanno diventato importanti in settori come biologia e neuroscienza, portando a nuove scoperte e ipotesi che ancora sono in discussione.

Une delle idee concettualmente più interessanti è la teoria della criticità auto-organizzata, proposta da Per Bak e collaboratori nel 1987, che suggerisce che i sistemi naturali si possono organizzare in modo autonomo nelle vicinanze di un punto critico, fatto che permetterebbe di sfruttare le proprietà caratteristiche della criticità come le correlazioni a lunga distanza, l'alta suscettibilità e una capacità maggiore di computazione di processare informazione. Attualmente c'è evidenza sperimentale che questo accada davvero per alcuni sistemi biologici.

Nel 2003 Beggs e Plenz hanno osservato, in un esperimento sorprendente, valanghe di attività cerebrali distribuite secondo leggi di potenza, una caratteristica propria dei sistemi critici, suggerendo quindi che il cervello potrebbe funzionare alla frontiera tra due fasi. L'esperimento suggeriva che il cervello potrebbe appartenere alla classe di universalità della directed percolation, dove l' attività non cresce né decresce, in media. Quasi venti anni dopo, il problema è ancora aperto e non c'è ancora una evidenza conclusiva sulla criticità del cervello. Il regime dinamico del cervello (che include bistabilità, oscillazioni in diversi intervalli di frequenza, valanghe di attività Irregolare) non è ancora completamente descritto in modo teorico a partire da modelli semplici, e anche i dati sperimentali recenti non sono conclusivi su questo aspetto.

Recentemente è stato proposto che un modo di spiegare contemporaneamente valanghe in un regime scale free e ritmi neuronali è considerare per l'atttività cerebrale delle transizioni di fase di sincronizzazione e corrispondenti punti critici associati. In questa tesi studieremo l' ipotesi di criticità dal punto di vista dei fenomeni di sincronizzazione, discutendo in quali circostanze le transizioni di sincronizzazione possono generare valanghe distribuite come leggi a potenza, e anche quale sia la relazione tra questa transizione e altri fenomeni osservati sperimentalmente come il bilancio tra eccitazione e inibizione e la bistabilità. La tesi è organizzata nel modo seguente:

Il capitolo 1 presenta concetti di base su sistemi dinamici e fenomeni critici, assieme ad una sintesi della ricerca attuale sulla criticità nel

cervello e sui problemi filosofici associati.

Il capitolo 2 rivede alcuni modelli teorici per sistemi neuronali e sinapsi, tra i quali i modelli mesoscopici per descrivere regioni estese in modo effettivo. Alla fine sono inclusi anche concetti rilevanti sulla teoria di sincronizzazione.

Il capitolo 3 introduce il concetto di "forza di Jensen", studiando un modello discreto che spiega il ruolo della inibizione in presenza di reti sparse. Inoltre si studia l'effetto del bilancio tra eccitazione e inibizione.

Il capitolo 4 presenta il concetto di sincronizzazione ibrida, una nuova regione dove è possibile osservare conteporaneamente valanghe scale free con sincronizzazione parziale.

Il capitolo 5 rivede la teoria dell'auto-organizzazione, compreso il nuovo concetto di bistabilità auto-organizzata. In seguito questi concetti sono applicati per capire la relazione tra auto-organizzazione e oscillazioni collettive nella dinamica corticale.

Il capitolo 6 discute le prospettive future di questa tesi, compreso una analisi preliminare di sistemi più realistici.

Il capitolo 7 include una discussione dei principali risultati della tesi, e le conclusioni.

Español

Comprender cómo emergen, evolucionan, y se organizan los sistemas naturales es uno de los principales objetivos de la ciencia. La física estadística ha jugado un papel clave en este aspecto, iluminando algunos de los los procesos que subyacen a la complejidad y el orden presentes en sistemas biológicos desde un planteamiento "ascendente", es decir, que recupera las propiedades colectivas observadas a partir de nuestro conocimiento de los componentes elementales del sistema y sus interacciones. Estas ideas revolucionaron nuestra concepción de la ciencia en el siglo XX, y en las últimas décadas han cobrado importancia en áreas como la biología o la neurociencia, llevando a nuevos descubrimientos e hipótesis que siguen en debate.

Una de las ideas conceptualmente más interesantes es la teoría de

la criticidad auto-organizada, propuesta por Bak y sus colaboradores en 1987, que sugiere que los sistemas naturales podrían organizarse de forma autónoma a las inmediaciones de un punto crítico, lo que les permitiría aprovechar las propiedades características de la criticidad como correlaciones a largo alcance, alta susceptibilidad, o una mayor capacidad de computación y procesado de la información. Actualmente hay evidencia experimental de que este es realmente el caso para algunos sistemas en biología.

En 2003 Beggs y Plenz observaron, en un experimento sorprendente, avalanchas distribuidas según leyes de potencias, una característica propia de sistemas críticos, sugiriendo que el cerebro podría funcionar en la frontera entre dos fases. Este pertenecería a la clase de universalidad de percolación dirigida, donde la actividad no crece ni decrece, en promedio. Casi veinte años después, aún no hay evidencia lo suficientemente conclusiva como para cerrar el debate sobre si el cerebro (o alguna de sus partes) es crítico o no. El régimen dinámico del cerebro (que incluye biestabilidad, oscilaciones en diversos rangos de frecuencia, avalanchas de actividad irregulares...) no ha podido ser descrito completamente de manera teórica a partir de modelos sencillos, e incluso los datos experimentales recientes no son definitivos en este aspecto.

Se ha propuesto recientemente que una forma de explicar de forma conjunta las avalanchas libres de escala con los ritmos neuronales es considerar transiciones de fase de sincronización y sus puntos críticos asociados. A lo largo de esta tesis, se estudia la *hipótesis de criticidad* desde el punto de vista de fenómenos de sincronización, discutiendo bajo qué circunstancias las transiciones de sincronización son capaces de generar avalanchas distribuidas como leyes de potencias, así como su su relación con otros fenómenos observados experimentalmente tales como el balance entre excitación e inhibición y la biestabilidad. La tesis se organiza de la forma siguiente:

El capítulo 1 presenta conceptos básicos sobre sistemas dinámicos y fenómenos críticos, así como un resumen de la investigación actual sobre criticidad en el cerebro, y problemas filosóficos asociados.

El capítulo 2 revisa algunos modelos teóricos para sistemas neuronales y sinapsis, así como modelos mesoscópicos para describir regiones completas de forma efectiva. Al final, se incluyen también conceptos relevantes sobre teoría de la sincronización.

El capítulo 3 introduce el concepto de "fuerza de Jensen", estudiando un modelo discreto que explica el rol de la inhibición junto con la baja densidad de conexiones, además de estudiar el efecto del balance entre excitación e inhibición.

El capítulo 4 presenta el concepto de sincronización híbrida, una nueva región donde es posible encontrar avalanchas libres de escala en conjunción con sincronización parcial.

El capítulo 5 revisa la teoría de auto-organización, incluyendo el nuevo concepto de biestabilidad auto-organizada. Después, estos conceptos se aplican para entender la relación entre la auto-organización y las oscilaciones colectivas en la dinámica cortical.

El capítulo 6 esboza el trabajo futuro por hacer a partir de ahora, incluyendo análisis preliminares de sistemas más realistas.

El capítulo 7 incluye una discusión sobre los resultados de la tesis, así como las conclusiones.

Chapter 1

Statistical Physics and Neuroscience: a brief overview

"Psychohistory dealt with no man, but with man-masses. […]. The reaction of one man could be forecast by no known mathematics; the reaction of a billion is something else again. […]. The laws of history are as absolute as the laws of physics, and if the probabilities of error are greater, it is only because history does not deal with as many humans as physics does atoms, so individual variations count for more."

- Isaac Asimov, in *Foundation and Empire*, 1952.

The intense effort devoted to understand the brain since ancient times is nothing but a reflect of the will to find out ourselves and our position in the world. This endeavor lasts until our days when, despite the astonishing advances in neuroscience during the last 50 years, a unified framework that explains how the brain works as a whole is still missing. Only disconnected pieces are available: the neuron doctrine initiated by Golgi and Ramon y Cajal in 1889 initiated an intense research that culminated with the identification of the most important parts of the building blocks that compose the brain, as well as the interactions among them. Unfortunately, the inverse (bottom-up) path –explaining high-level cortical function from the components– remains largely unsuccessful. In last decades, modern neuroimaging techniques, such as electroencephalography or functional magnetic resonance have allowed another qualitative jump, paving the way to connect structure and function in the brain. Although these are key advances to understand it, they do not even completely solve the *soft problem* in neuroscience: how the information provided by external stimuli is received by the sensory system, processed, stored, and how it evokes a response (Chalmers 1995). The *hard problem*, which involves understanding high-level cognitive functions (such as feelings or consciousness (Chalmers 1995)) remain unexplained at the neurological level.

Given the amount of literature dedicated to physiology, develop-

ment, functioning and disease of the brain, one could think that at least we have an extensive and systemic knowledge about our brain. Let me introduce a counterintuitive, curious story which illustrates very well that our knowledge of the brain as a whole is surprisingly limited, despite our extensive mapping of its individual components and areas.

John Lorber (1915 – 1996) was a medical doctor and professor at Sheffield. In 1979, a student told him that he often suffered from headaches. Lorber observed that the student head diameter was larger than usual, so he decided to run a scanner. The result was shocking: almost all his head was filled with cerebrospinal fluid. It was an extreme case of *hydrocephalus*. A normal brain would weight around one kilo and a half, and this one was less than 150g. Despite being almost brainless, this student always had a normal life, graduated with honours in Mathematics, and even presented a high CI (126). This story was published later by Lewin in Science, wondering if "*Is your brain really necessary?*" (Lewin 1980). Although hydrocephalus usually limited the cognitive capacity of the individuals, there are people that have almost no brain and does not even notice it. Another extreme case was reported in 2007, when Lionel Feuillet said from one of his patients that the brain was "virtually absent" (Feuillet et al. 2007); again, the patient had a normal life without complications. Despite it is known that the brain is able to re-wire via synaptic plasticity in case of tissue damage, this capacity to *self-organize* in order to function in these extreme cases is absolutely amazing, and make us wonder: how could all our knowledge about individual neurons, brain areas and brain topology explain this? What do we *really* know about how brain function at the large scale? The knowledge on brain basic building blocks or even on mesoscopic regions is not able to explain how these extreme cases work as a whole. The *collective behaviour* and the self-organization mechanisms of the whole-brain is still far from being understood.

During the last century, the application of statistical physics techniques and insights into the brain has helped to shed light on this problem. The novel *criticality hypothesis* –the idea that the brain obtains functional benefits by working near a phase-transition– and related concepts such complexity and self-organization have attracted a lot of attention, gaining traction both from the experimental neuroscience and physics communities. It has been already demonstrated that several biological systems can evolve or self-organize to such critical states

(Muñoz 2018), and it would serve to explain brain complexity and richness in an elegant, conceptual way. In this first chapter, we review some of the fundamental aspects of philosophy, as well as the theory of critical phenomena and the state of the art of the criticality hypothesis in the brain.

1.1 Philosophy, complex systems, and the brain

Physics has changed during the last century. To make ourselves an idea of how deep this evolution has been in the last years, we could take the clock back to one hundred years prior to this the writing of this thesis. In 1920, Rutherford just predicted the existence of the neutron; Rosalind Franklin, whose experiments where decisive for the discovery of DNA, was born this year; insulin was discovered by Banting and Best, being announced on 1921, the same year when Keynes published his *Treatise on Probability*, one of the fundamental pillars of Bayesian statistics. Even if all these milestones feel very old now, the time between these and our times is literally just a pair of generations.

Most of remarkable success of science during the XX century has been attributed to the advances in the natural sciences, as well as the technology that lead to the construction and popularization of computers. However, here I would like to insist on the -almost completely overlooked- role that philosophy of science has played during this period, helping researchers to make the great advances of the XX and XXI centuries, and being a tool as powerful as computers in order to make science. The philosophical approach can severely impact research methodology, and, therefore, the research results. For this reason, I will clearly state my philosophical posture during the realization of the thesis. Although this choice shapes all methodology implicitly, its consequences will be more evident at the discussion, in Chapter 6.

1.1 Philosophy, complex systems, and the brain

1.1.1 Philosophical alignment

In a nutshell, there has historically been two great opposed schools of thought: the realist view, and the instrumentalist one. The realist assumes that the systems we study possess objective properties (so for example, a body *has* mass, energy, or charge), which can be measured in a direct or indirect way. So, under the realist point of view, the energy is a real property that exist, and not a mathematical abstraction (Miller 2019). For the realist, the goal is to understand the properties that characterise the systems and their relations, in order to understand reality. On the other hand, the instrumentalist view often assumes that objects do not actually possess properties, or that we cannot know them. Under the instrumentalist glasses, all that we can hope for is to create theories or models that are able to predict the behaviour of systems in an accurate way -but an instrumentalist would not care about what actually the symbols represent in the equations, since they do not resemble any "real" property –they could be just abstractions.

A recurrent example is the development of quantum mechanics, which adopted the instrumentalist view at the Copenhaguen interpretation: properties of the quantum systems do not really exist until they are measured, just to cease its existence again. The difficulties interpreting what the wave function is and how it collapses led to the well-known mantra "Shut up and calculate!"[1], meaning that the only important results are the quantitative predictions obtained by solving the equations -but the interpretation of what the symbols in the equation *are*, in the ontological sense, should be ignored. The philosophy behind the development of quantum mechanics has greatly influenced other fields of research, like the Bayesian view of statistics and machine learning. The latest is the perfect example of modern instrumentalism: many applications of machine learning use "black boxes", where the researcher is not interested on how the underlying neural network learns, stores information or makes decisions.

This could sound an unappealing philosophy for a scientist that wants to understand the mechanisms underlying physical, chemical, or biological processes. However, completely understanding the be-

[1] Very often attributed to Richard Feynmann, but actually coined by David Mermin in 1989 (Mermin 2004).

haviour of a system turns out to be complicated, and making models and theories able to explain all the causal relations can be a daunting task. Often, physicists resort to oversimplified "toy models" where the system can be easily understood, shedding light over the key features of an observed phenomenon. But a simple model of the brain would not satisfy a neurophysiologist, since such constructions are not able to return exact quantitative results due to their underlying simplifications. Even worse, a medical doctor would find such a model useless for any kind of clinical application. Here instrumentalism would be of great help, and the instrumentalist's predictions can be used a posteriori in order to discern new phenomenology, even unveiling new, unexplored phenomena for basic science.

In addition to the already discussed realist-instrumentalist dichotomy, in the last half of century we found an additional problem: the difference between reductionism and holism. For many centuries, the idea of science has been to isolate systems, and study them separately, which makes easier to understand their components and write general theories. This turned out to be a powerful method, leading to many advances in fields such as biology or physics. Other fields, such as sociology, have tended to be integrative and holistic, arguing that is not possible to understand a system if we divide it into parts -everything is connected and single individuals cannot be explained without the whole (Bunge 2003). Both views, without an adequate perspective, could lead to philosophical (and hence scientific) problems. The case of holism is simpler to understand from the traditional scientific perspective, since it is the argument commonly employed by pseudoscience (as the "memory of water" in homeopathy or the astrological view that position of celestial bodies influence our lives), so I believe that it is now more important to argue against the reductionist view. An example of a blatant reductionist misconception is that unifying all the fundamental forces into a single theory would lead to a "theory of everything", since this theory would not explain turbulence in the Navier-Stokes equations, nor how does a neuron spike, or how random positive conditioning works in psychology. Even if the Navier-Stokes equations could be explicitly derived from the Standard Model, turbulence would have to be explained in terms of typical fluid properties (density, speed, Reynolds number), since connecting different levels of the description under a bottom-to-top

approach necessarily takes statistical averages that lead to a loss of information about individuals (Bunge 2003). Therefore, understanding how particles interact does not render knowledge on higher description levels. Reductionism seems to be good to find how components of each system work, but the idea that having a complete knowledge of the components will explain the full system is a naive -and many cases, incorrect- assumption. Some degree of holism is necessary in order to understand the system as a whole, re-connecting the pieces again. The idea that having a complete knowledge of the individual portions of the system does not render any knowledge of the system they form was explicitly claimed by Anderson in his paper *"More is different"* in 1972 (Anderson 1972). From this time on, many researchers in areas such as condensed matter physics, cosmology, biology or psychology have remarked the importance of the *interaction* between individuals, as well as the *emergency* of properties that are present in the collective motion, but not in the individual behaviour. Bunge remarks that such emergent, collective properties are *ontological*[2] and actually belong to the system (Bunge 2003), leading to the *systemic material realism*, the philosophical principles I will adopt during this text.

1.1.2 Statistical mechanics and brain modelling

The brain is the perfect example of what is understood by a "complex system". It is composed by many relatively simple elements that interact among themselves, organised in a hierarchical-modular structure. In the brain, there is not a single "micro-macro" limit, but instead we can find different description levels. Some of them are sketched in Fig. 1.1. For example, the cortex is similar to a two-dimensional sheet formed by cortical columns, which in turn are formed by several layers (Kandel et al. 2000; Breakspear 2017). Going up, we find different brain regions, each one composed by different kind of neurons and topology. Therefore, choosing an adequate description level for mod-

[2]This means that the usual definition of "emergent" as *collective properties that could not be predicted by just looking at the individual* has no sense –this just consider emergent properties those that are difficult to understand, but why should be emergency conditioned to our (subjective) difficulties to understand it? This is epistemological, while the definition we provided is objective and ontological.

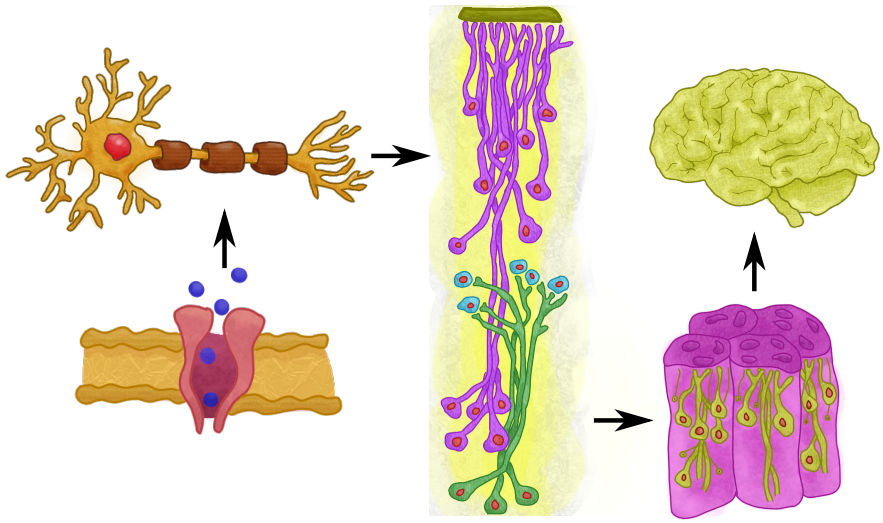

Figure 1.1: **Different scales at the brain.** The study of the brain ranges from the dynamics of the single neuron, synapses, ion channels or genetic networks, to that of the whole brain. The drawing depicts some of these explanation levels. Following the arrows: an ion channel, a neuron, a cortical column, a set of columns in the cortex, and the whole brain. Proper elaboration.

elling, as well as selecting the correct underlying assumptions for the neuronal tissue under study is very important if we are to impose a minimum level of realism into our models.

The first step is to understand its components and how they are organized. During the last century a vast amount of research has been devoted to characterise, classify, and understand each of the components of the brain. The pioneer work of Ramon y Cajal on the structure of the individual neuron and the subsequent advances in neurophysiology have provided a very deep understanding on how individual neurons work, and how they are connected, a field that still could reserve some surprises –as it was the discovery of the new rosehip neuron in 2018 (Boldog et al. 2018). Moreover, modern neuroimaging techniques have opened the door to study both structural and functional connectivities, unveiling the topology of both structural and functional neuronal circuits. At the current day, these technologies allow us for an identification of activity both in-vitro and in-vivo with unprecedented

spatial and temporal resolutions. All these achievements are key in our current image of how the brain works and very helpful for clinical practice. However, there are still many open questions, specially regarding how the brain works *as a whole*. For example, the processing and storage of information in the brain, the study high level cognitive function (consciousness, emotions, or creativity), the effect of the social environment of the subject in brain development and plasticity, or degenerative brain diseases. During the last 50 years, the study of the brain structure, function and dynamics has progressively integrated more fields of knowledge as psychology, statistical physics, or artificial intelligence, making it a science on its own. This is the modern concept of *neuroscience*, and it has to be necessarily understood as an interdisciplinary scientific field, if we want to have a complete, systemic, description of the brain (Bunge 2003).

In this thesis, we approach the problem from the statistical physicist point of view. Statistical mechanics provides a powerful set of tools in order to connect different description levels, starting from the individuals components, to the whole-system collective properties. Our aim is to shed light on the synchronization mechanisms that play an important role in brain processes, and how they are linked with the so called *criticality hypothesis*, which is described in detail below. To do that, we studied very simplified mathematical models of systems of coupled neurons and oscillators, that mimic, at the most possible abstract level, real neuronal tissue function. The main advantage of these models over the brute-force simulation of realistic models of neurons is that the results are easier to interpret, leading to a deeper understanding of the phenomena involved. The price we pay for the simplicity and elegance of the conceptual explanation is that toy models have little or no quantitative power, and could even miss qualitative features, making it is difficult to directly link the results with real-world experiments. Therefore, one must take this approach with (philosophical) care: models are not reality, and experimental evidence (as opposed to *computational evidence*) is always the one to judge whether the theoretical framework is suitable to explain reality (Bunge 2003). Studying computational models, making variations and adding ingredients to them *ad infinitum* without checking if its conclusions were in agreement with observations in the first place could lead to the automatic disprove of many years of collective theoretical effort. Due to

this problem, I will insist, during all the text, that results presented here should be always taken as *predictions for experiments that must be tested*, and that probably the way to dissipate incognita about criticality in the brain should now be more data-driven than discussions just over models. Of course, this theoretical-experimental dichotomy has been for enough time in my head to think about possible experimental links with the research we did, what the experimental loopholes could be, and which would be the best way to at least rule out some of the current theoretical proposals. I regret I had no time to evaluate every detail with the depth I would like to, but at least I am convinced that the theoretical advances we made during these years will certainly help to close very soon one of the long-standing debates in computational neuroscience: is the brain critical? Where does scale-free, power-law like distributions of neural activity come from?

1.2 Dynamical systems and bifurcation theory

In many classical models of statistical physics, the macroscopic behaviour can be explained by just analysing the deterministic part of the equations that govern the dynamics of the order parameters. In "simple models", the order parameter is just a scalar, meaning that a simple linear stability analysis is usually enough to understand all the system dynamics in mean-field. However, along this text we will face more complicated situations, making necessary a more in-depth view of *bifurcation theory*. Our discussion will be informal and not exhaustive, with the aim of being a practical guide on basic bifurcation theory of multidimensional, non-linear systems of differential equations. We will follow the concepts introduced by Strogatz (Strogatz 1994) and Kuznetsov (Kuznetsov 2004). The following section will not only serve to fix the notation but it will also render useful in the next chapters.

1.2.1 Stability of hyperbolic equilibria

A dynamical system can be written, in a general way, as

$$\frac{d\vec{x}}{dt} = \vec{F}(\vec{x}, \vec{c}) \tag{1.1}$$

where $\vec{x}(t)$ represents our desired observable (for example, a multidimensional order parameter) and $\vec{c}$ a set of control parameters. Note that the dimension of both vectors is usually different, i.e., $\vec{x} \in \mathbb{R}^n$ and $\vec{c} \in \mathbb{R}^m$. The function $\vec{F}\colon \mathbb{R}^n \times \mathbb{R}^m \to \mathbb{R}^n$ is called the *time evolution operator* (Kuznetsov 2004). The integer n is referred as the dimension of the system, while m is usually called the co-dimension. We are interested in stationary states of the system eq. (1.1), and hence we start by setting to derivative to zero, as $\vec{F}(\vec{x}^*, \vec{c}) = 0$. A system posed at $\vec{x} = \vec{x}^*$ will not evolve in time, since its temporal derivative vanishes. Hence, the points $\vec{x}^*$ are called *equilibria* of the system, and, in general, they depend on the value of the parameters $\vec{c}$. Let us start by fixing $\vec{c}$, so we can forget about the constants for a while. It is possible to know what is the behaviour of the system near the equilibria. If we evaluate the system at $\vec{x}_0 = \vec{x}^* + \vec{x}^p$, and expand around $\vec{x}_0 = \vec{x}^*$, we can linearize the system,

$$F_i(\vec{x}_0, \vec{c}) \simeq \sum_{j=1}^{n} \left.\frac{\partial F_i}{\partial x_j}\right|_{x_j = x_j^*} x_i^p + \mathcal{O}\left(\varepsilon^2\right). \tag{1.2}$$

Therefore, the system (1.1) can be approximated as a simple matrix-vector product, as the following linearization,

$$\frac{d\vec{x}^p}{dt} = \hat{J}(\vec{x}^*, \vec{c})\,\vec{x}^p. \tag{1.3}$$

where

$$J_{ij}(\vec{y}, \vec{c}) = \left.\frac{\partial F_i(\vec{x}, \vec{c})}{\partial x_j}\right|_{\vec{x}=\vec{y}} \tag{1.4}$$

is the Jacobian matrix of the system. Knowing the dynamics near the equilibrium points should be enough to construct a rough sketch of the phase space. In many situations, this is just enough in order to understand the dynamics of the system. Therefore, we only need to understand how to solve a linear system of differential equations in

order to estimate the dynamics of the non-linear one near the equilibrium points. Actually, if the Jacobian can be diagonalized, we can make a change of basis to that where the Jacobian is diagonal, which would allow us to solve the system in a straightforward way

$$\frac{dy_i^p}{dt} = \lambda_i y_i^p \rightarrow y_i^p(t) = e^{\lambda_i t}. \tag{1.5}$$

where λ_i are the eigenvalues of the Jacobian, and y_i^p its eigenvectors. If all eigenvalues are negative, the vector of perturbations $\vec{y}^p$ decays to zero at infinite time. Since the original vector $\vec{x}^p$ is related to $\vec{y}^p$ just by a change of basis, the limit $\vec{y}^p \rightarrow 0$ also means that $\vec{x}^p \rightarrow 0$. For a given equilibrium, if all its associated eigenvalues are negative, it is called *stable*, since it will always return to the equilibrium in exponential time. An equilibrium that has all its eigenvalues positive is called *unstable*, while an equilibrium with mixed number of positive and negative eigenvalues is called a saddle-node. Equilibria in which $\lambda_i \neq 0 \forall i$ are called hyperbolic. When an equilibrium is non-hyperbolic, the linear analysis does not give information about the system dynamics, and we are forced to analyse higher-corrections. Let us remark that complex eigenvalues pose no threat to our analysis, since the dynamics would obey $y_j^p = y_j^p(0)\, e^{t\,\mathrm{Re}\,\lambda_j} e^{i\,\mathrm{Im}\,\lambda_j}$. The imaginary part just contributes by adding oscillatory behaviour to the dynamics.

If we change our attention to eigenvectors, we can improve our knowledge of the dynamics near the equilibrium. For example, let assume that $\vec{x}^*$ is an equilibrium point with n_+ positive eigenvalues and n_- negative ones. If we construct a linear combination of the n_- eigenvectors corresponding to the negative eigenvalues, the iterative multiplication of the Jacobian matrix to this vector will lead to the equilibrium. This means that the vector subspace spanned by the eigenvectors corresponding to the negative eigenvalues correspond to a *local stable manifold*, while the subspace generated by the eigenvectors corresponding to positive eigenvalues form the *local unstable manifold*. The word local here is very important, because we are working with just an approximation near equilibrium values (Kuznetsov 2004).

1.2.2 Limit cycles

Although equilibrium points give key information about dynamical systems, they are usually not enough in order to understand their complete behaviour. An important phenomena that usually happens in physical and biological systems, which is core to the study of synchronization, is the appearance of limit cycles –oscillations in the system that are isolated. The difficulty analysing limit cycles arises from the fact that the derivative in cycle points is no longer zero, rendering useless our analysis above. We review now the basic standard formalism –which is equivalent to that of the equilibrium for the limit cycles– but considering that is of limit application in practice.

Let us assume that system eq. (1.1) has an isolated, periodical orbit, L. Assume that we take a point $\vec{x}^L \in L$, and at this point we define a cross-section Σ of the limit cycle, denoting its coordinates by $\vec{\xi}$. Assume that we take a perturbation near the limit cycle located inside the cross section $\vec{x}_0 \equiv \vec{\xi}_0 = \vec{x}^L + \vec{x}^p$. Then, after one approximately period, we will cross again the section Σ, this time at a different location, say $\vec{\xi}_1$. If we repeat this procedure many times, we will find $\vec{\xi}_k$. If $\vec{\xi}_k \to \vec{x}^L$, the limit cycle is stable (Kuznetsov 2004).

Formally, this construction is called a Poincaré map (Kuznetsov 2004; Strogatz 1994), $\vec{\xi}_{k+1} = P\left(\vec{\xi}_k\right)$. As with continuous systems, maps have equilibrium points (defined by $\vec{\xi}^*$ such that $\vec{\xi}_{k+1} = \vec{\xi}_k$) and their stability is governed by the behaviour of the Jacobian of the application P: an equilibrium point is stable if all the corresponding eigenvalues are inside the unit circle, i.e., $|\lambda_i| < 1 \forall i$. If the Poincaré map can be explicitly constructed, its analysis will lead to information about the local stable manifolds of the cycle, giving all the topological information that we need to create the phase space diagram. Therefore, the classification of a limit cycle as stable or unstable is obtained from the classification of the corresponding equilibria of the Poincaré map. However, in high dimensions, constructing such maps is very complicated, because it needs a priori information of the system trajectories, which usually need the system to be integrated exactly. For example, in the simplest two-dimensional case, the cross section is one-dimensional,

and it can be shown that the map has only one eigenvalue,

$$\lambda = \exp\left[\int_0^T \left(\vec{\nabla}\cdot\vec{F}\right)\left(\vec{x}^{L}(t)\right)dt\right] \tag{1.6}$$

where T is the minimum orbit period (Kuznetsov 2004). The parametric equation of the cycle $\vec{x}^{L}(t)$ is not usually known, rendering this method not very useful for most of analytical applications –but could still be used with success to determine the eigenvalues if the cycle can be determined numerically.

1.2.3 Bifurcations

Now that we have explored the basics of stability analysis and limit cycles for fixed parameters $\vec{c}$, we now wonder what happens when these parameters are changed. It is important to introduce the concept of topological equivalence: two different dynamical systems are called topologically equivalent if there exist a homeomorphism h that maps the trajectories of the first system into the second when the direction of time is preserved (Strogatz 1994; Kuznetsov 2004). Basically, h is a function able to deform the trajectories of the dynamical system in any way we wish, without making any two trajectories cross, or separating them, thus preserving the topology. Such definition can be made local, so two dynamical systems are locally topologically equivalent if there is a homeomorphism able to map the trajectories for a small neighbourhood around an equilibrium.

Then, it is possible to demonstrate the following theorem: two dynamical systems are locally topologically equivalent near their respective equilibrium points $\vec{x}^{*}_{A}$ and $\vec{x}^{*}_{B}$ if, and only if, the equilibria have the same number of positive and negative eigenvalues (Kuznetsov 2004). This theorem is very important because it tell us that, in practice, all the systems are topologically equivalent when we are close enough to an equilibrium, so it suffices to study them under the linearization (1.3). If we have a complete classification of equilibrium points of the linear system, we can apply such classification to any other dynamical system.

A bifurcation is the appearance of a non-equivalent phase space when the parameters $\vec{c}$ are changed. Bifurcations can appear in many

ways. A simple one is the appearance of new equilibria: when solving the equilibrium condition $\vec{F}(\vec{x}^*, \vec{c}) = 0$, equilibria is a function of the parameters, $\vec{x}^* = \vec{x}^*(\vec{c})$. It could be the case that a solution only exists for some set of values of $\vec{c}$, but not for others. An example is the saddle-node bifurcation, studied below in detail.

Another way at which a bifurcation can happen is by changing the stability of the fixed points. Since also the associated eigenvalues of equilibria depend on the parameters $\lambda_i = \lambda_i(\vec{c})$, a parameter change can affect the stability of the equilibria leading to a non topological equivalent diagram. Examples of these are pitchfork and transcritical bifurcations, also explained below.

Another important difference is the concept of local versus global bifurcations. A local bifurcation changes the phase space only at the neighbourhood of an equilibrium, so it suffices to study the local properties of the stability around it. Global bifurcations change the shape of whole regions in the phase space, making them difficult to analyse.

To conclude our small review on dynamical systems, we focus on the problem: what are the methods to detect and classify such bifurcations in real systems? How is it possible to know where bifurcations are, and how to classify them? Topological equivalency plays a very important role on the classification of bifurcations. Let us assume that we have a dynamical system that undergoes a local bifurcation. Just before and after the bifurcation, it is possible to construct a homeomorphism that maps these phase portraits to the corresponding linearized systems. Therefore, any model having a particular local bifurcation could be mapped to a simpler system that preserves all the key topological features at the bifurcation. This is called a *normal form* of the bifurcation (Strogatz 1994; Kuznetsov 2004). All local bifurcations have an associated normal form, as well as some global bifurcations. The study of the normal form provides simple criteria in order to classify different bifurcations, in terms of the values of $\vec{F}$ and its derivatives near equilibria.

Finding the equilibria is sometimes the main practical problem. The system $\vec{F} = 0$ could be highly non-linear, or involve transcendental equations, meaning that equilibria cannot be explicitly obtained. Without an analytical expression for equilibria, it seems that there is nothing to do, since all the analysis presented above relies on the expression of $\vec{x}^*$. Despite of this, a very simple trick in dynamical systems

consist in solving the equation $\vec{F} = 0$ together with the conditions for certain bifurcations; for example, for a saddle-node, this is $\det \hat{J} = 0$ (Strogatz 1994). If the variables we solve for are wisely chosen, it could be possible to obtain the bifurcation curves eliminating $\vec{x}^*$. In some cases, it is even convenient to write the bifurcations that depend on the equilibria as parametric equations, i.e., $\vec{c} = \vec{c}(\vec{x}^*)$. This method provides the coordinates of the bifurcations in parameter space, without the need to solve for the equilibria explicitly, and constitutes a powerful practical tool for analytics. When even this is not possible, numerical methods based on continuation analysis are still available (Kuznetsov 2004).

1.2.4 Potential dynamics

An useful way to characterise dynamical systems is defining a potential function. In one dimension, it is always possible (at least, formally), to define a potential function such that the general system (1.1) can be written as

$$\dot{x} = F(x, \vec{c}) = -\frac{dV(x, \vec{c})}{dx}, \tag{1.7}$$

where $V(x, \vec{c})$ is the potential function. Stationary states $\dot{x} = 0$ coincide with extrema of the potential. Stable fixed points fulfill the condition $\partial_x F = -\partial_x^2 V < 0$ and hence correspond to minima of the potential. Therefore, the use of the potential function could be beautifully linked with the idea of minimization of energy in physical systems. In the next this section, we will demonstrate that this link is deeper than just a formal idea. For higher dimensions, it is not always possible to write a potential for the dynamical system.

When looking at the potential function, bifurcations can be understood as changes in the energy landscape. Hence, if moving a parameter, a minimum becomes flat, the system is forced to move until finding a new minimum. We insist that not all systems have an associated physical potential function –but when they do, it makes easier to identify the dynamics of the system in intuitive, physical terms. Also, potential dynamics arise naturally in equilibrium statistical physics, as we will see in a moment.

1.2.5 Classification of bifurcations

For completeness, we include here a small classification of one and two-dimensional bifurcations. The description is not aimed to be exhaustive, but at least to provide information about the basic types of bifurcations, as well as the ones that will appear during this thesis.

In order to describe general conditions for the bifurcations, we can assume we can assume that $\vec{x}^* = 0$, since the system can be always translated to new variables $\vec{y} = \vec{x} - \vec{x}^*$, and that the bifurcation takes place at $\mu_c = 0$. In practical applications, the conditions for bifurcations have to be evaluated at $\vec{x}^*$, μ, or rescale parameters and equations accordingly.

Saddle-Node Bifurcation

Also known as a *fold bifurcation*. Its normal form in one dimension is given by

$$\dot{x} = \mu + \sigma x^2, \tag{1.8}$$

with $\sigma = \operatorname{sign} \partial_x^2 F(0,0)$. Any system with $\sigma \neq 0$ and $\partial_\mu F(0,0) \neq 0$ can be reduced to this normal form (Kuznetsov 2004). For $\mu < \mu_c$, a pair of stable-unstable equilibria exist, which coalesce into a saddle-node at the critical point $\mu_c = 0$. This bifurcation is characterised, at any dimensions, for having a zero eigenvalue at the Jacobian. In this case, the *center manifold* (the subspace corresponding to the projection of the critical $\lambda = 0$ eigenvalue) displays the normal form (1.8). Figure 1.2 depicts a saddle-node bifurcation.

Transcritical Bifurcation

The normal form for a transcritical bifurcation is given by

$$\dot{x} = \mu x + \sigma x^2 \tag{1.9}$$

with $\sigma = \partial_x^2 F(0,0)/2$. A necessary condition for reducing the system to this normal form is that $\partial_{x\mu} F(0,0) \neq 0$[3]. In a transcritical bifurcation, a pair of stable-unstable fixed points move linearly, collide at the

[3]This is because actually the linear term is actually given by $a\mu x$, and a is obtained through the derivative. If $a = 0$, no bifurcation is possible. However, we impose the condition and rescale the control parameter $\mu \to a\mu$ without loss of generality.

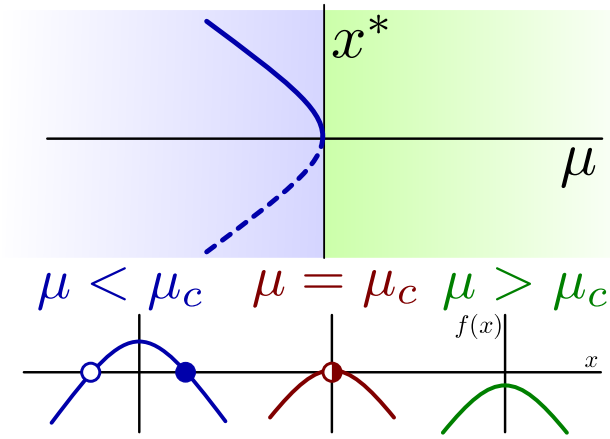

Figure 1.2: **The saddle-node or fold bifurcation.** Top, a schematic view of the bifurcation diagram; continuous lines indicate stable equilibria, dashed lines unstable equilibria. Bottom, sketch of the one-dimensional phase space for this bifurcation. Filled circles indicate stable equilibria, empty circles unstable solutions, and semi-filled circles saddle-nodes.

critical point at $\mu_c = 0$, and interchange their stabilities. This bifurcation is typical of systems that present an equilibrium that exists for any value of the parameters and does not depend on them, in contrast with saddle-node bifurcation. It cannot appear in systems with odd symmetries (i.e., $f(-x) = -f(x)$), since $\sigma = 0$ in this case. Figure 1.3 depicts a transcritical bifurcation.

Pitchfork bifurcation

In a pitchfork bifurcation, the normal form is given by

$$\dot{x} = \mu x + \sigma x^3$$

where in this case $\sigma = \partial_x^3 F(0,0)/6$. The name of the pitchfork bifurcation comes from the shape of its bifurcation diagram, that presents one equilibrium $\mu < \mu_c = 0$ and bifurcates intro three equilibria for $\mu > \mu_c$. If $\sigma < 0$, the transition is called supercritical, while $\sigma > 0$ is called subcritical. In supercritical bifurcations, the equilibrium $x^* = 0$ for $\mu < \mu_c$ is stable, while for $\mu > \mu_c$ only the states with $x^* \neq 0$ are stable. Subcritical bifurcations are the opposite, so $x(t)$ has the possibility to diverge

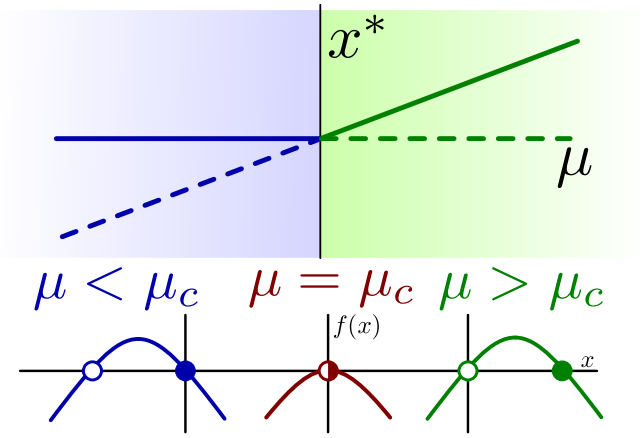

Figure 1.3: **The transcritical bifurcation.** Symbols are as in Figure 1.2.

for any value of the control parameter μ, leading to unphysical results. Therefore, subcritical bifurcations usually do not appear alone in physical systems. In this case stabilization is obtained by adding higher order terms, such as $-x^5$ (Strogatz 1994), but this does not correspond with a normal form. As in the transcritical, it happens when a fixed point exist for any value of the parameters, but for even symmetries. Figure 1.4 depicts a supercritical pitchfork.

Hopf bifurcation

For a system to display a Hopf bifurcation, it needs to have a minimum dimension of $n \geq 2$. In polar coordinates, the normal form of a Hopf bifurcation is given by

$$\dot{\rho} = \rho\left(\mu + \sigma\rho^2\right), \tag{1.10a}$$

$$\dot{\varphi} = \omega, \tag{1.10b}$$

which can be written in a compact way using complex numbers,

$$\dot{z} = (\mu + i\omega)\, z + \sigma z |z|^2 . \tag{1.11}$$

In this case, σ is defined as the sign of the first Lyapunov coefficient, which can be computed via expanding up to third order $F(\vec{x}, \mu)$

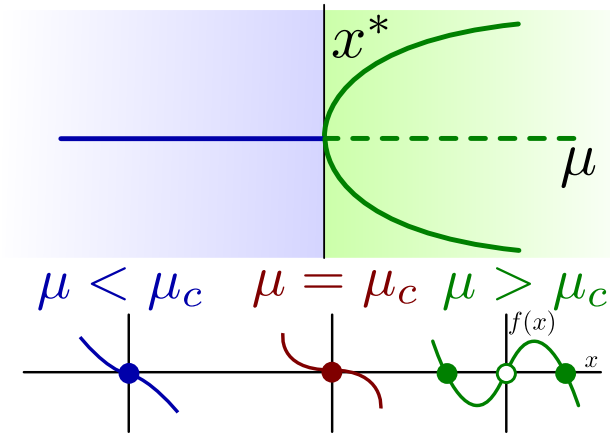

Figure 1.4: **The supercritical pitchfork bifurcation.** Symbols are as in figure 1.2.

and projecting over the center manifold (see the computational details e.g. in Kuznetsov (Kuznetsov 2004)). If $\sigma = -1$, we find the supercritical normal form, while $\sigma = +1$ leads to the subcritical one. As with the pitchfork, the subcritical form is usually not found alone in physical systems, due to the lack of stable states. A supercritical bifurcation displays a stable spiral, that loses stability giving birth to a limit cycle with constant angular speed ω and growing amplitude. The hallmark of the Hopf bifurcation at the critical point $\mu_c = 0$, is two eigenvalues becoming purely imaginary complex conjugates. The $n = 2$ system then fulfills $\mathrm{Tr}\,\hat{J} = 0$. At higher dimensions, the projection of the center manifold has also the normal form displayed by (1.11). Figure 1.5 depicts the phase space of the supercritical Hopf.

Homoclinic bifurcation

Homoclinic bifurcations are more involved, since they are global bifurcations, and hence normal forms cannot be explicitly constructed in general. There exist, however, some theorems that help finding numerically such bifurcations via continuation methods. The *split function* $\beta(\mu)$ acts as a control parameter, having a homoclinic orbit (that starts and end in a saddle equilibrium) when $\beta(\mu_c) = 0$. A homoclinic orbit is characterised by appearing with constant amplitude and growing period, that scales as $T \propto \log(\mu - \mu_c)$ (Strogatz 1994). Figure 1.6 shows a

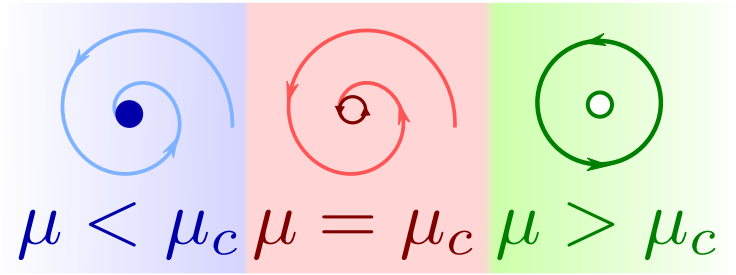

Figure 1.5: **The supercritical Hopf bifurcation in two dimensions.** Light colours represent system trajectories, while the bold line at $\mu > \mu_c$ indicates a stable limit circle. At $\mu = \mu_c$, the stable fixed point loses stability, creating a small limit circle.

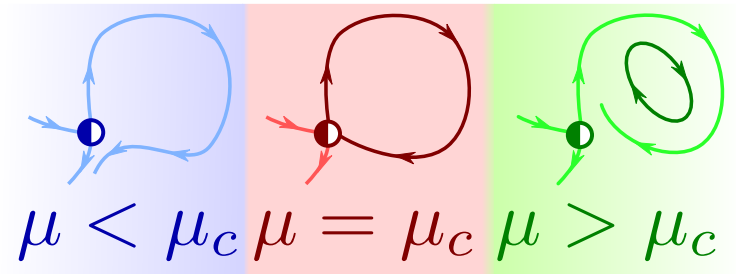

Figure 1.6: **The homoclinic bifurcation in two dimensions.** Bold curves indicate the existence of limit cycles, while light colours give system trajectories.

homoclinic bifurcation.

Saddle node on invariant circle (SNIC)

Although the name SNIC (or SNIPER, for saddle-node infinite period) is the most common name for this bifurcation, this is formally a *saddle-node homoclinic* (Kuznetsov 2004). Here, a saddle-node bifurcation happens, giving birth to a homoclinic cycle when the pair of fixed points coalesce. As it happens in a typical homoclinic bifurcation, the amplitude is constant and the angular speed grows with the control parameter. However, now the process dynamics is governed by the speed at which both equilibria merge, making the period to scale as $T \propto \left|\mu - \mu_c\right|^{-1/2}$ instead of the logarithmic scaling (Strogatz 1994;

Kuznetsov 2004). Figure 1.7 shows a SNIC bifurcation.

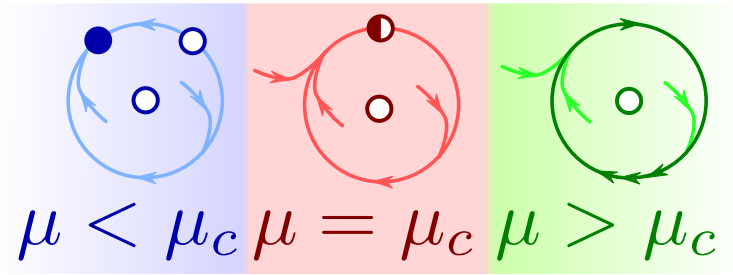

Figure 1.7: **The SNIC bifurcation in two dimensions.** Bold curves indicate the existence of limit cycles, while light colours give system trajectories.

Cusp bifurcation

We leave codimension-1 bifurcations to focus on codimension-2 from now on. Let us assume that we are near a saddle-node bifurcation, and hence the center manifold of our system is described by the normal form (1.8) with $\mu = 0$. While tracking the saddle-node bifurcation curve, it might happen that $\sigma = 0$. This is known as a cusp bifurcation. Since all the contributing orders of (1.8) become 0 at this point, it is necessary to go to higher orders to obtain the normal form of the cusp bifurcation,

$$\dot{x} = \mu_1 + \mu_2 x + \sigma x^3. \tag{1.12}$$

where now $\sigma = \operatorname{sign} \partial_x^3 f(0,0)$. Intuitively, the cusp is presented as the point where two branches saddle-node intersect in a *cusp*. In one dimension, the branches have the shape of the semicubic parabola

$$4\mu_2^3 - 27\mu_1^2 = 0, \tag{1.13}$$

which gives a curve in the parameter space (μ_1, μ_2), with the cusp at $(0,0)$. In high dimensions, computing σ needs of more refined methods that we will not cover here (Kuznetsov 2004). A diagram of the cusp bifurcation is shown in Fig. 1.8

Bogdanov-Takens (BT)

As we mentioned before, following the saddle-node entails several options. Another one, while keeping $\sigma \neq 0$ this time, is to find another

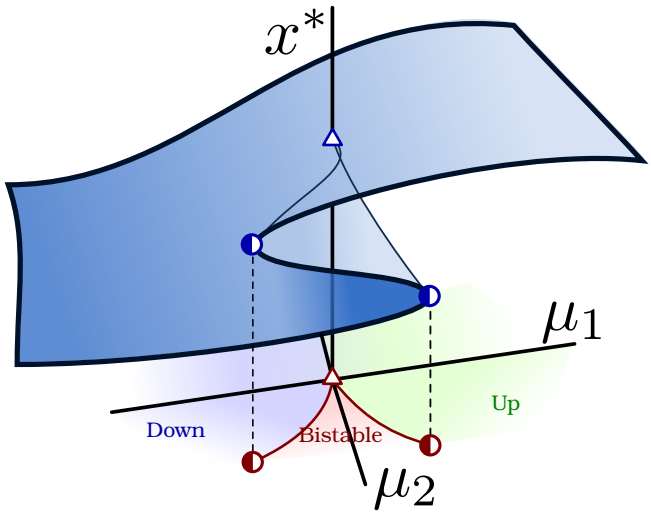

Figure 1.8: **A sketch of the cusp bifurcation.** Surface of equilibria is plotted, along with the projection of the saddle-node branches. The surface is stable, except the bent sheet between the saddles, giving rise to a bistable configuration with hysteresis.

eigenvalue $\lambda_2 = 0$. This is the *double-zero* or Bogdanov-Takens bifurcation. Since we need at least two eigenvalues, this bifurcation only appears in systems with dimensions $n \geq 2$. For a two-dimensional system, the normal form reads

$$\dot{x} = y \tag{1.14a}$$

$$\dot{y} = \mu_1 + \mu_2 x + x^2 + \sigma x_1 x_2 \tag{1.14b}$$

and $\sigma = \pm 1$ depending on the Taylor expansion of $f(\vec{x}, \vec{\mu})$. The bifurcation lies at the origin of the parameter space, $\vec{\mu}_c = 0$. It is possible to analyse the bifurcation diagram by obtaining the bifurcation curves. For example, $\phi_{SN} = \left\{(\mu_1, \mu_2) : 4\mu_1 - \mu_2^2 = 0\right\}$ is a curve of saddle-node bifurcations, that displays two branches. It is also easy to check that if $\mu_1 = 0$, the region $\mu_2 < 0$ corresponds to a line of Hopf bifurcations. Finally, it is even possible to demonstrate analytically the existence of a homoclinic bifurcation going out of the BT point, $\phi_{Hom} = \left\{(\mu_1, \mu_2 < 0) : \mu_1 + 6\mu_2/25 + \mathcal{O}\left(\mu_2^2\right) = 0\right\}$. Finding Bogdanov-Takens bifurcations is easier than cusps, in practice, due

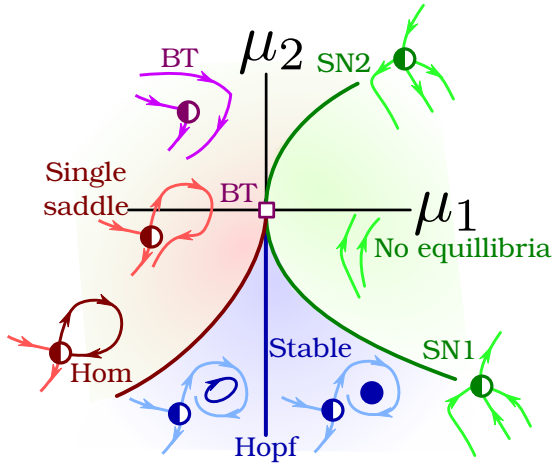

Figure 1.9: **Parameter space of the Bogdanov-Takens bifurcation.** This bifurcation presents four phase. A sketch of the phase space at each phase, as well as at the bifurcations, is included.

to the double-zero condition, and doing so means that Hopf, saddle nodes and homoclinic bifurcations are also involved (Kuznetsov 2004). In particular, if a Hopf and a saddle-node lines end, merging tangentially, we have a Bogndanov-Takens. A complete view of the phases and bifurcations surrounding this transition is shown in Fig. 1.9.

Saddle-node-loop (SNL)

The saddle-node-loop is another global bifurcation difficult to identify in practice. Limit cycles can appear via common saddle-node bifurcations, SNICs, and in homoclinic bifurcations, among others (Strogatz 1994; Kuznetsov 2004; Izhikevich 2006). The saddle-node-loop bifurcation acts as a separatrix between a saddle node bifurcation of cycles, and a SNIC bifurcation. It happens when a homoclinic bifurcation intersects a saddle-node curve. A complete view of the phases and bifurcations surrounding this transition is shown in Fig. 1.10.

Notice that, since Bogdanov-Takens bifurcations involve both homoclinic and saddle-nodes, it is usual to see that the homoclinic later intersects with the saddles, leading to a SNL bifurcation. We will see this is often the case in neuronal systems (Borisyuk and Kirillov 1992;

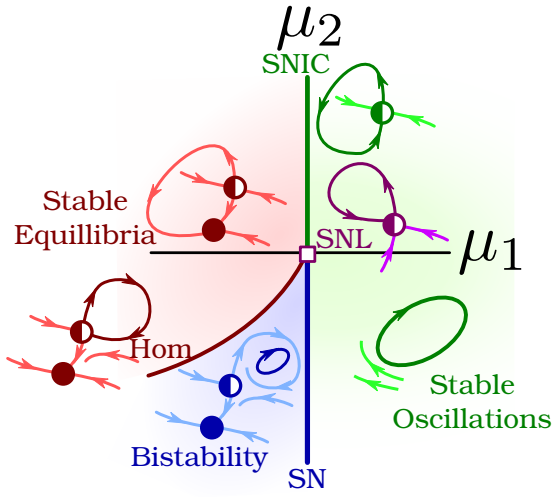

Figure 1.10: **Parameter space of the saddle-node-loop bifurcation.** This bifurcation presents three phases around it. A sketch of the phase space at each phase, as well as at the bifurcations, is included.

Tsumoto et al. 2006; Hesse et al. 2017; Schleimer et al. 2019).

1.3 Statistical physics

The mathematical formalism of dynamical systems has demonstrated to be a powerful tool to describe the behaviour of systems in fields such as physics, chemistry, economics, or biology. This formalism is adequate to model both the behaviour of either single elements or collective variables, but, unfortunately, is not completely exhaustive: it leaves outside stochastic systems, discrete models as cellular automata, or equilibrium systems in physics. The concepts of statistical physics complement and reinforce the ideas presented above for systemic modelling, remarking the importance of the interactions among the individuals and with the environment.

In particular, fluctuations play a very important role in physical and biological systems. The source of randomness in macroscopic systems

are the microscopic (possibly chaotic) dynamics[4]. Statistical physics gives a bottom-to-top approach, explaining macroscopic phenomena that describes the *phases of matter*, as well as the behaviour of the system at *phase transitions*, i.e., at the boundaries between such phases, from microscopic interactions. But, unlike the usual phases of matter, biological systems are out of equilibrium, since they receive a non-negligible amount of energy from the its interaction with the environment. Therefore, if we are to understand biology, we are forced to extend the tools of equilibrium statistical physics to non-equilibrium systems.

We now briefly review the classical theory of critical phenomena in equilibrium statistical mechanics, which will allow us to introduce useful concepts as critical exponents and universality classes, and then jump to the study of non-equilibrium phase transitions. Although long, our description will give an insight on the deep relationship between bifurcation theory and critical phenomena in physics.

1.3.1 Landau-Ginzburg theory of phase transitions

The basic ideas of equilibrium statistical mechanics were developed in order to understand the phases of matter and the transitions between them. The simplest systems one can study are gases. The main principles underlying the formalism of equilibrium statistical physics are those of *phase space* and *state counting*. Given the Hamiltonian of the system, it is possible to evaluate the volume that each possible state takes in the phase space. A macroscopic property can arise from many different microscopic configurations, so counting the number of configurations compatible with each macroscopic state will give us its probability distribution (Kardar 2007b; Pathria and Beale 2011).

The most important quantity in statistical physics is the *partition function* of the system, called Z. Intuitively, the partition function

[4]For this reason, some philosophers consider that, when the underlying processes are deterministic, the macroscopic system is not random at all and talking about probabilities in this setting is formally wrong (Bunge 2003). I consider that in this case, macroscopic randomness is an emergent property, hence it is ontological and we are actually entitled to speak about true random events.

is nothing but a (weighted[5]) sum over all the possible system states, which leads to the volume of the system in the phase space. Its relevance comes from the fact that all thermodynamics variables and observables can be derived if we know the partition function (Le Bellac 1991; Binney et al. 2001; Kardar 2007a; Pathria and Beale 2011). For example, the Helmholtz free energy is given by

$$A = -\frac{1}{\beta}\log Z, \tag{1.15}$$

with $\beta = kT$, being k the Boltzmann constant and T the temperature (Pathria and Beale 2011). The main difficulty is obtaining a closed expression for the partition function Z. Let us use the paradigmatic Ising model to illustrate the theory. This model is composed by spins, that can either be "up" or "down", and are able to interact among them. Two spins will minimise their energy if they point to the same direction. The system can also interact with an external magnetic field, h, which favors one of the two possible orientations. The well-known Ising model Hamiltonian is given by

$$\mathcal{H} = -\sum_{i,j=1}^{N} s_i J_{ij} s_j + h\sum_{j=1}^{N} s_j, \tag{1.16}$$

where $J_{ij} > 0$ is the coupling among the spins (Le Bellac 1991). Spins can flip randomly due to the effect of temperatures, and the coupling among them is the only thing that prevents the system to be completely disordered and uncorrelated. We can set the matrix J_{ij} in any network topology we like, but the usual thing is to assume that spins are situated in a d-dimensional lattice, with $d \geq 2$, and coupling $J_{ij} = J/(2d)$ for connected spins. This model is the paradigm for second-order critical phase transitions: for low couplings, $J \leq J_c$, the effect of noise dominates, and the system is completely demagnetized. However, if $J > J_c$, clusters of identically oriented spins emerge, leading to a net magnetization of the system (Le Bellac 1991; Binney et al. 2001; Pathria and Beale 2011). The magnetization is called the *order parameter*, since it

[5]Depending on the ensemble chosen. Here we will work with the canonical ensemble, so the weight factor for each macroscopical state is $\exp(-\beta\mathcal{H})$, that suppresses energies far away from the thermal energy $k_b T$.

gives a measure of how ordered are the spins, from completely uncorrelated to perfectly aligned (Binney et al. 2001). If we want to obtain the thermodynamic observables of the Ising magnet, the only thing that remains is the "easy" task of evaluating the partition function,

$$Z = \sum_{\{s\}} \exp\left(-\beta \mathcal{H}\right), \tag{1.17}$$

where the sum is over all possible spin configurations $\{s\}$. Of course, the problem here relies on computing all the possible system states when the number of spins $N \to \infty$.

Hundreds of pages have been already devoted to the study of the Ising system and similar models. I believe that no further discussion of the model is necessary in this context, redirecting the interested reader to textbooks such as (Le Bellac 1991; Binney et al. 2001; Kardar 2007a; Pathria and Beale 2011). Despite of this, I believe that introducing all these concepts will prove useful later.

In order to explain phenomenologically critical phase transition of the Ising model, Landau assumed that the free energy of the system could just be expanded in series of the order parameter around the critical point. The discussion Landau does about phase transitions is mostly in terms of the fundamental changes of symmetry (related with changes in *order* in the system) at the phase transition, so the series expansion is motivated by symmetries argument alone (Landau and Lifshitz 1964). Further developments lead to a more formal way of obtaining those series expansion, in the so-called Landau-Ginzburg theory (Binney et al. 2001; Kardar 2007a). Its basic idea is based on scattering experiments in gases: we would like to measure the magnetization of small parts of the Ising ferromagnet, but our measure instrument is not powerful enough in order to detect the orientation of individual spins; it will necessarily average over a small region, composed by a certain number of spins, large enough to make averages consistent, but small compared with the whole system size (Binney et al. 2001; Kardar 2007a). Therefore, we would be measuring the magnetization at each point in the lattice, $\phi(\vec{x})$. It is possible to formally demonstrate (Binney et al. 2001) that the Ising partition function can be written near the critical point in terms of this new variable as

$$Z = \int \mathcal{D}\phi \exp\left(-\beta \mathcal{H}_{LG}\right), \tag{1.18}$$

where

$$\mathcal{H}_{LG}[\phi] = \int d\vec{x}\left(\frac{\mu}{2}\phi^2(\vec{x}) + \frac{\lambda}{4!}\phi^4(\vec{x}) + \frac{D}{2}\left|\vec{\nabla}\phi(\vec{x})\right|^2 + h\phi(\vec{x})\right) \tag{1.19}$$

is the Landau-Ginzburg Hamiltonian, with $\lambda, D > 0$, and where μ plays the role of the distance to the critical temperature. Now we can work with a continuous model, which should be easier to tackle. Notice how the sum over configurations changed to an integral over all possible magnetization functions, or *fields*. From (1.18), it is clear that configurations with large energy values are exponentially suppressed. Then, we could take the field $\phi_0(\vec{x})$ that minimizes the Hamiltonian $\mathcal{H}_{LG}$, and it would be the largest contribution to the partition function. This approximation is often called the *saddle point approximation*, since it assumes that only the saddle-node of the energy surface survives the procedure of exponentiating (Kardar 2007a). The field that minimizes $\mathcal{H}_{LG}$ has to be homogeneous, since $D\left|\vec{\nabla}\phi\right|^2 > 0$ for any value of ϕ, so $\phi_0(\vec{x}) \equiv \phi_0$, and hence the partition function is given by $Z = \exp(-\beta\mathcal{H}_{LG}[\phi_0])$. The intensive[6] free energy then can be easily obtained as

$$A = h\phi_0 + \frac{\mu}{2}\phi_0^2 - \frac{\lambda}{4!}\phi_0^4, \tag{1.20}$$

which is nothing but a series expansion of the order parameter for the free energy, the same Landau proposed in 1936 (Landau and Lifshitz 1964). Notice that ϕ_0 can be considered the average magnetization of the system, that has been homogeneously distributed over all the system. Still, we have to minimize the free energy A in order to perform the saddle-point integration. The result of this procedure will determine the value of the magnetization ϕ_0 at equilibrium.

However, minimising an energy to find the stable states of a system is something we already did: if we identify the free energy with the potential function $V(x)$ defined in Section 1.2.4, it is exactly the same concept. Actually, the condition $\partial_\phi A(\phi = \phi_0) = 0$ leads to the finding of the equilibria of the normal form of the pitchfork bifurcation (see the previous discussion on normal forms). In equilibrium physical systems, following Landau theory, the free energy is written as the minimum Taylor expansion of the order parameters to be minimized.

[6] Since the field ϕ_0 is constant, the integral over $d\vec{x}$ yields the volume of the system.

As a consequence, the result is always potentials dynamics. However, we will not necessarily arrive at the normal forms of bifurcations. For example, the ϕ^6-model leads to a 5th degree polynomial, which contains a subcritical (destabilizing) pitchfork bifurcation, as well as two stabilizing saddle-nodes (Strogatz 1994; Binney et al. 2001).

We have finally a formal link between statistical physics and dynamical systems theory. This will help us to classify the different nature of each phase transitions. As we saw in the classification of bifurcations, these can happen either by creating new solutions discontinuously, or just changing the stability of the already existing equilibria. This is the formal background of the phenomenological Ehrenfest criterium of phase transitions: a phase transition is of order k if the free energy is discontinuous in its k derivative (Binney et al. 2001; Pathria and Beale 2011). Therefore, first order phase transitions are discontinuous, since a discontinuity in the potential function means the appearance of a new equilibrium point. Second order phase transitions are continuous, since in this case we only have a change of stability of already-existing equilibria. Higher-order transitions are linked to more exotic bifurcation conditions, but they have been also reported in physical systems (Ma and Wang 2011; Cunden et al. 2017).

Let us come back to the Landau-Ginzburg model after this small digression. We will continue exploring the links between the ideas of statistical physics and dynamical systems very soon. Minimization of the free energy at zero external field $h = 0$ leads to the existence of two distinct phases,

$$\partial_\phi A = 0 \rightarrow \begin{cases} \phi_0 = 0, \\ \phi_0 = \pm\sqrt{\frac{6\mu}{\lambda}}. \end{cases} \tag{1.21}$$

The demagnetized phase is stable only for $\mu > 0$, and unstable for $\mu < 0$. It is possible to check that the phase transition is of second order, with a critical point at $\mu = 0$ where the symmetries of both phases are present at some extent (Landau and Lifshitz 1964). From the point of view of statistical mechanics, we are now interested in the value of macroscopic observables near criticality. Since μ already plays the role of distance to criticality, equation 1.21 tell us that the magnetization $\phi \sim \mu^{1/2}$. The number $\beta = 1/2$ is called a *critical exponent*, and it will allow us to classify different phase transitions (Binney et al. 2001; Kardar 2007a). It is possible compute critical exponents associated with more

observables, as the specific heat capacity or the magnetic susceptibility (Le Bellac 1991; Binney et al. 2001; Kardar 2007a) .

When analysing critical phenomena, we are particularly interested in deriving the critical exponents of the system. The reason is that it was experimentally observed that many different transitions display the same set of critical exponents. Near criticality, all second order transitions with the same set of exponents as the Ising ferromagnet behave as the ferromagnetic-paramagnetic transition, which has deep implications for the *universality* of symmetry changes that take place during phase transitions (Landau and Lifshitz 1964; Binney et al. 2001; Kardar 2007a). Although this is an amazing feature of criticality from the point of view of physical phenomena, is no surprising from the prism of bifurcation theory: near a critical point of a phase transition, we are approaching a local bifurcation of an equilibrium. Since any local bifurcation is topologically equivalent to its normal form, the behaviour at the critical point is governed by that of the normal form (Kuznetsov 2004).

Formally speaking, alterations in microscopical symmetries at the transition are responsible for topological changes in the phase space of the macroscopic variables.

Another characteristic that will be important for the subsequent analyses is the appearance of large fluctuations at criticality, as well as diverging correlation lengths. Our mean-field analysis is able to account for the existence of large fluctuations, for example by computing the magnetic susceptibility to small external fields, that goes as $\chi(h \to 0) \sim \mu^{-1}$, hence diverging at critical point. However, the mean-field theory is unable to give answers for the large correlations found in critical systems, since we assumed from the very beginning that the magnetization field is homogeneous. Furthermore, the theory is valid only for infinitely sized systems, while both experiments and simulations are limited by a finite size.

The power law distributions at criticality have another important implication, which is that the system presents *scale invariance*. Take, for example, the correlation length at criticality, which scales as $P(\xi) \propto \xi^{-\alpha}$ (Kardar 2007a). If we scale the system length by a factor b, as $\xi' = b\xi$, then $P(\xi') \propto b^{-\alpha} P(\xi) \propto \xi^{-\alpha}$, leaving the distribution invariant again. This means that at the critical point, there is no characteristic correlation length (Binney et al. 2001; Muñoz 2018).

1.3.2 Road to non-equilibrium: Langevin equations

Thus far, we have used the formalism of classical statistical physics to study phase transitions. Despite its utility, it only describes systems at equilibrium. For this reason, time is absent in the formalism, and there is no way to obtain dynamical properties. As it was already pointed out, most biological systems are outside of equilibrium. In particular, in the brain, temporal dynamics play a very important role in processes as information transmission and computation. Brain waves and synchronization, which are fundamental aspects of neuroscience, are intrinsically temporal phenomena. As a consequence, if we are to understand how the brain works, we need to extend our tools in order to be able to describe also non-equilibrium phenomena.

We will move to non-equilibrium demonstrating, in first place, how to add dynamical properties to equilibrium problems, and then making the bridge with microscopical stochastic processes that present paradigmatic non-equilibrium phase transitions. When the Landau-Ginzburg theory was introduced, the field $\phi(\vec{x})$ was presented as the magnetization of a small region of space. In equilibrium, the properties of each "realization" or ensemble of the system are completely equivalent, so time can be safely disregarded. However, in a real system, the value of the magnetization would fluctuate with time: the variable $\phi(\vec{x},t)$ is stochastic (Hohenberg and Halperin 1977; Binney et al. 2001). Let us assume that we perturb a small, isolated region of the system, to a non-equilibrium state, and let it relax to equilibrium. The relaxation would occur by minimizing the energy. If we do not constrain the fields to be homogeneous as before, it is possible to interpret the full Hamiltonian $\mathcal{H}_{LG}[\phi]$ as a potential energy to minimize and write dynamical equations for the magnetization (Kardar 2007a). This fact is formalized assuming that the process is mainly dissipative (so inertial terms can be neglected, $\mathcal{O}\left(\partial_t^2\right) \sim 0$), that the fluctuations in each site are Gaussian and uncorrelated, and that the order parameter is not conserved, so

$$\partial_t \phi(\vec{x},t) = -\frac{\delta \mathcal{H}_{LG}}{\delta \phi(\vec{x},t)} + \sigma \eta(\vec{x},t) = -\mu\phi - \frac{\lambda}{6}\phi^3 + D\vec{\nabla}^2\phi + \sigma\eta(\vec{x},t). \quad (1.22)$$

where the white noise fulfills

$$\langle \phi(\vec{x},t)\rangle = 0, \tag{1.23a}$$
$$\langle \phi(\vec{x},t)\,\phi(\vec{y},t')\rangle = \delta(\vec{x}-\vec{y})\,\delta(t-t'). \tag{1.23b}$$

Notice that if the magnetization of the model is homogeneous, then the potential coincides with the minimum of the free energy in the saddle point integration. If we wanted the order parameter to be conserved, the time evolution should be derived from the divergence of a current, which is usually known as the Hohenberg-Halperin model B (Hohenberg and Halperin 1977; Kardar 2007a). For our interests, model A –no conservation– will suffice.

An interesting dynamical consequence of criticality is the so-called *critical slowing down*. Writing eq. (1.22) in momentum space it is possible to demonstrate that the dynamics at zeroth order (Gaussian model, $\lambda \to 0$) are governed by the momentum-dependent timescale $\tau_q = 1/\left(\mu + Dq^2\right)$, with $\phi \propto \exp\left(t/\tau_q\right)$. Since the correlation length diverges at the critical point $\mu = \mu_c$, then $\tau_q \sim \mu^{-1}$, and the time needed to reach equilibrium diverges. Systems at criticality need infinite time to relax! The relation between time and space scales in dynamical systems at criticality is very important, and it has its own critical exponent, called z. The dynamical version of the Gaussian model has $z = 2$, as can be easily checked (Kardar 2007a).

1.3.3 Stochastic processes on lattices

Let us finish with a fast glance at stochastic processes on lattices. Until now, what we did was to extend the formalism of equilibrium behaviour to dynamical variables. However, many microscopic processes are also intrinsically outside of equilibrium, and their study allow us to understand and classify better the behaviour of non-equilibrium systems.

Microscopic dynamical processes are usually posed in terms of stochastic reactions (Hinrichsen 2000; Gardiner 2009). In this case, systems are modelled as a number of states (discrete or continuous) and the possible transitions among them. In Markovian processes, the

transition rates depend only on the initial and final states, and not on system's previous history (Gardiner 2009). Therefore, all the system information can be stored in the stochastic matrix ω_{ij} that represents the transition rates from state i to j. Equilibrium phenomena can be also represented using this formalism. For example, the Ising model can be simulated by just setting appropriate transition rates for spin flips (like, for example, Glauber dynamics) (Binney et al. 2001). We will, however, focus on the *contact process* (CP), a paradigmatic non-equilibrium microscopic model with important implications on neural criticality (Hinrichsen 2000). In the CP, we work with a lattice or network, in which each site i can be either active ($n_i = 1$) or inactive ($n_i = 0$). Active sites decay to inactive at a rate β, but they can propagate their activity to neighbouring sites with rate λ. It is possible to fix the timescale $\beta = 1$ so λ is the control parameter. The order parameter is the number of active sites in the system, $n(t) = \sum_{i=0}^{N} n_i(t)$. At low transmission rates all active nodes will decay, leading the system to an *absorbing state*, in which all the nodes in the lattice are inactive. At this point, activity cannot propagate any longer and the dynamics stops.

In order to study the macroscopic dynamics of the system, one needs to obtain the transition rates of states from having n active sites to $n \pm 1$. In a lattice, in the thermodynamic limit ($N \to \infty$) this is an almost impossible task. The transition rate of the state with n particles to the state with $n \pm 1$ heavily depends on the spatial configuration of active and inactive sites, rendering an excessively high number of configurations.

To tackle the problem, let us assume the simplest case, that of mean-field theory, where all sites are mutually connected so knowing *which* particle is active becomes irrelevant. Transition rates can now be easily computed: the global inactivation rate is given by β multiplied by the probability of picking an active site, hence $\omega(n \to n-1) = \beta n/N \equiv \omega_-$, while the global activation rate is given by the probability of finding a pair of active-inactive sites, $\omega(n \to n+1) = \lambda n(N-n)/N^2 \equiv \omega_+$. Since the total number of active sites at a given time is a stochastic variable, we can ask ourselves for the probability distribution $p(n,t)$. The model is Markovian (all transition rates are independent of time), and hence this probability depends only on the system state at the last timestep. In order to have

n particles at time t, either

1. we had $n-1$ active sites at $t-dt$ and an activation occurred,
2. we had $n+1$ active sites and a site decayed, or
3. we had n and nothing happened.

This allow us to write a *master equation* for the probability,

$$\partial_t p(n,t) = \omega(n+1 \to n)\, p(n+1,t) - \omega(n-1 \to n)\, p(n-1,t) - \\ -[1-\omega_- - \omega_+]\, p(n,t). \quad (1.24)$$

Solving the master equation means obtaining a closed expression for $p(n,t)$, hence the ability to compute any statistical moment of the variable n at any time. In general, analytical solutions to master equations are not available, and we have to jump to more sophisticated methods. One possibility is to use the Van Kampen finite size expansion (Gardiner 2009), that profits from the fact that all the rates ω that appear in the master equation are functions of the system size, N. The expansion assumes that the variance of the variable n scales as $N^{1/2}$ according with the central limit theorem. At first order in size, one obtains a Fokker-Planck equation,

$$\partial_t p(n,t) = \partial_n \left[-f(n)\, p(n,t) + \frac{1}{2} g(n)\, \partial_n [g(n)\, p(n,t)] \right] + = -\partial_n J(n,t), \quad (1.25)$$

where

$$f(n) = \sum_k k\omega(n \to n-k), \quad (1.26a)$$

$$g(n) = \sum_k k^2 \omega(n \to n-k). \quad (1.26b)$$

and the $J(n,t)$ is called the *probability current.* The Fokker-Planck equation gives a simplified version of the master equation, which is easier to solve, since it is just a partial differential equation instead of a functional equation (Gardiner 2009). Another advantage is that from the Fokker-Planck it is possible to identify a Langevin equation, as

$$\partial_t n = f(n) + g(n)\, \xi(t), \quad (1.27)$$

in the Îto sense[7]. Therefore, it is now possible to compare to equilibrium processes. Before, we commented that equilibrium processes usually have additive noise. The reason behind this is that the stationary solution of the Fokker-Planck, i.e., $\partial_t p(n,t) = 0$, for a constant value of noise, $g(n) = \sigma$, is given by

$$p_{st}(n) = \exp\left[-\frac{2}{\sigma^2}\int dt f(n,t)\right] \equiv \exp\left(\frac{2V(n)}{\sigma^2}\right), \tag{1.28}$$

so the probability to find the system is higher at the minima of the associated deterministic potential $V(n)$. When the noise is multiplicative, sometimes we can speak about an effective potential $\tilde{V}(n)$ that control the stationary dynamics. Such potential may have different minima than the deterministic potential, and hence noise could be able to completely deform the phase space. Actually, many non-equilibrium systems do not only display an "effective potential", but also add a rotational shear that cannot be described by any means in potential terms (for an application in neuroscience read e.g. (di Santo et al. 2018b)). In particular, neuronal dynamics seem to benefit noticeably from such shear, as we will see in our study of the Wilson-Cowan model and hybrid type synchronization transitions (also c.f. **santo2018JSM**; (Buice and Cowan 2007; Benayoun et al. 2010)). Returning to the CP, the associated mean-field Langevin equation is given by

$$\partial_t \rho = (\lambda - 1)\rho - \lambda\rho^2 + \sqrt{\frac{(\lambda+1)\rho - \lambda\rho^2}{N}}\xi(t), \tag{1.29}$$

where we wrote the equation for densities of active sites $\rho = n/N$. The deterministic part of the equation corresponds to a simple transcritical bifurcation, with a critical point $\lambda_c = 1$ which separates two possible phases: the absorbing state $\rho_0 = 0$, and the active state $\rho^* = \sqrt{(\lambda-1)/\lambda}$. Hence, the critical exponent $\beta = 1/2$ in mean field. Since we are usually interested in the properties of the system near criticality, we take $\lambda \simeq \lambda_c$, so $\rho \ll 1$ and the noise term can be approximated to $\sqrt{(\lambda+1)\rho/N} \equiv \sigma\sqrt{\rho}$. If order to have a full description of the contact process, the

[7] Langevin stochastic equations need to a criterium for the integration of the noise in order to be fully determined. Since $\xi(t)$ is a random Dirac-delta train, the integral $\int_t^{t+\Delta t} \xi(s)\,ds$ is completely different depending if we take left, right, or centered Riemann sums -or if we weight them in any mean (Gardiner 2009).

easiest way now is to assume that the mean-field equation we derived was for a very small region of the space, and connection among regions is given in a diffusive way[8]. The result is the stochastic equation that corresponds to Reggeon field theory (Hinrichsen 2000)

$$\partial_t \rho(\vec{x},t) = (\lambda-1)\rho(\vec{x},t) - \lambda\rho^2(\vec{x},t) + D\vec{\nabla}^2\rho(\vec{x},t) + \sigma\sqrt{\rho(\vec{x},t)}\xi(\vec{x},t), \quad (1.30)$$

which is similar in spirit to the the Landau-Ginzburg theory: take the continuum limit of the lattice, and study the evolution of the coarse-grained density $\rho(\vec{x},t)$. It is easy to see that this equation still preserves the absorbing state $\rho(\vec{x},t)=0$, due to the multiplicative noise, characteristic of non-equilibrium dynamical process.

As we already commented, dynamical non-equilibrium processes have also static critical exponents, such as $\beta = 1/2$ presented above. Critical exponents for susceptibilities and correlations can be similarly computed (Hinrichsen 2000). However, we will be more interested in dynamical exponents, such as the ones that corresponds to *avalanche behaviour*. Activity in the CP only survives for $\lambda > \lambda_c$, while any other value $\lambda \leq \lambda_c$ will lead the system to the absorbing state. The time that the system needs to reach the absorbing state is exponential in the subcritical phase, but potential at criticality –another reflection of the critical slowing down. Let us assume that we start the system at the absorbing state, and slightly perturb it, activating one site (alternatively, making $\rho(\vec{x}_0,0)=h\ll 1$). At criticality, the system is dominated by fluctuations, and propagation of activity is marginal, so the system might increase a lot its activity before falling again to the absorbing state, in an event called an *avalanche*. The duration of such avalanches is defined by just the time at which the absorbing state is reached again, $\rho(\vec{x},T)=0$, while the avalanche sizes can be found by integrating the total activity during the event $S=\int_0^T dt\int_V d\vec{x}\rho(\vec{x},t)$. The distribution of sizes and times at criticality is distributed as a power law, meaning that $P(S)\propto S^{-\tau}$ and $P(T)\propto T^{-\alpha}$, where $\tau=3/2$ and $\alpha=2$ in the case of mean-field CP (Hinrichsen 2000). Notice that a power law distribution means that avalanches are scale-free in the sense that there is no "typ-

[8] We could go back to the beginning of the derivation, computing the transition rates taking in account spatial structure, and obtaining a master equation for $n(\vec{x},t)$. The result is the same.

ical size" or "typical duration" of avalanche, so the largest avalanche values obtained are only limited by system sizes.

The contact-process belongs to a more general universality class, that of *directed percolation* (DP), shared among many non-equilibrium phenomena. The DP universality class is so robust that it has been conjectured that every non-equilibrium absorbing-active transition, with a scalar order parameter, short range interactions, and no additional elements such extra symmetries belong to this class. (Hinrichsen 2000).

Finally, let me state some conclusions about critical phenomena, equilibrium vs non-equilibrium, and dynamical systems theory. Both equilibrium and non-equilibrium processes can be described by Langevin equations. In the case of systems at equilibrium, the Hamiltonian provides a deterministic potential that rules the whole dynamics. This potential is only disturbed by an additive noise, in the case of non-conserved order parameters. On the other hand, non-equilibrium phenomena are formally characterised by the lacking of a potential function, either because the deterministic part cannot be written in potential form, or because the multiplicative noise changes the "effective" potential –even creating rotational contributions. At criticality, both kinds of transitions have similarities: diverging correlation lengths and susceptibilities, critical slowing down, scale-free distributions... However, non-equilibrium phase transitions have their own universality classes, characterised also by dynamical exponents of scale-free events (avalanches) found at criticality (Muñoz et al. 1996; Marro and Dickman 2005; Ódor 2008).

1.4 The criticality hypothesis: state of the art

In physics, we are used to find systems at a certain phase, just perfectly ordered, like solids, or disordered, like liquids or gases. In striking contrast with common physical systems, biology seems to often display structures that are not completely ordered, neither random. And the most surprising fact is that these structures are formed spontaneously, without any lead: ants coordinate to find resources, creating long lines of hundreds of individuals and constructing complex nests

in the soil, but all the individuals are equal; bacteria are able to make collective decisions depending on their environment and population density; each decision is just taken by a network of proteins that self-regulate, without any apparent supervision, or design; and our brains are just formed by an incredibly large number of neurons, which need no leader to coordinate another incredibly complex amalgam of organs and cells, generating not only simple responses to external physical stimuli, but also high-level cognitive states such as "consciousness" or "feelings", so complex that until now have eluded all our attempts to be linked with brain states and function, being just defined in psychological constructs.

The idea that collective phenomena in biology could arise from criticality is recent, in scientific timescales. It has two basic roots: one is the famous observation by Mandelbrot of fractal, scale-free spatial distributions in physical, geological and biological systems (Mandelbrot 1983). The other important realization was the ubiquity of $1/f$ noise in many systems, i.e., noise whose power spectrum scales as a power law. Basically, this is the lack of characteristic spatiotemporal scales, as well as large spatial and temporal correlations, a phenomenon that is known to happen at criticality, as previously mentioned. This motivated Bak, Tang and Wiesenfeld in 1987 and 1988 to develop the theory of self-organized criticality, an allegedly universal mechanism that would "tune" many systems to a critical point of a second-order phase transition (Bak 1996; Bak et al. 1987).

Since the proposal of this revolutionary idea, evidence in favor of criticality has astonishingly increased. The arguments that support that criticality and self-organization in biology are that critical points allow the systems to enhance correlations, increase the response to stimulus, and allows better information processing, among other (Muñoz 2018). Although all these features could be clearly favoured by natural selection, determining in experiments whether a biological system is actually critical has proven to be a daunting task. One problem is the choice of order and control parameters, as well as studying the relationship between them. In this sense, biology is similar to astrophysics, and regulating control parameters in some systems can be challenging –so observation and simulation is the best we can hope for in many cases. Another important complication is that biological system sizes range from dozens to some hundreds of

individuals, while the phase transition formalism is defined in the thermodynamic limit of infinite individuals. Despite of the problems, there are several systems that have proven to live at the edge between order and disorder, while others are just suspected to, but no conclusive experimental and theoretical evidence has been gathered (Muñoz 2018).

One of these elusive systems is the brain. Many features of the brain could be easily understood under the umbrella of criticality: maximal information capacity and transfer (Shew et al. 2011), information processing and computing (Denève and Machens 2016; Yu et al. 2017; Michiels van Kessenich et al. 2019), large dynamical range (Kinouchi and Copelli 2006; Shew et al. 2009), maximal synchronization variability (Yang et al. 2012), among others (Shew and Plenz 2013). In 2003, experiments by Beggs and Plenz were able to resolve the temporal structure of activity bursts in EEG recordings (Beggs and Plenz 2003). The distribution of sizes and time of the burst, when measured correctly (see Appendix A for details) follows a power-law distribution. Surprisingly, the critical exponents coincided with the ones suggested by the DP-conjecture (Beggs and Plenz 2003; Beggs and Plenz 2004). If this was true, it would mean that the brain worked near a second-order phase transition, between an absorbing and an active state, and that the dynamics of the brain would be those of the critical branching process[9]. This discovery generated a lot of interest in both the statistical physics and neuroscience communities, that have been trying to answer the question "*Is the brain working near a critical transition?*" until today. We will try to shed light to this question during the thesis, at least partially.

Let me remark some of the advances I consider to be relevant from 2003 to understand the current situation, and put the content of the thesis in context. From the experimental side, many experiments have replicated the observations of scale-free avalanches in cultures and *in-vitro* slices (Shew et al. 2009; Pasquale et al. 2008; Yang et al. 2012; Yaghoubi et al. 2018), as well as *in vivo*, obtaining scale-free burst in many animal species both at rest (Petermann et al. 2009; Ribeiro et al. 2010; Hahn et al. 2010; Bellay et al. 2015; Yu et al. 2014; Karimipanah et al. 2017) and during stimuli or task performing (Palva et al.

[9]For small review on the branching process, see (di Santo et al. 2017).

2013; Karimipanah et al. 2017; Yu et al. 2017). Moreover, the results seem to be consistent among the observations using different techniques (Miller et al. 2009; Palva et al. 2013). The exact value of the critical exponents, however, is a delicate matter. Many experiments have found exponents compatible with the critical branching process (Petermann et al. 2009; Klaus et al. 2011; Bellay et al. 2015; Karimipanah et al. 2017) i.e., $\alpha = 1.5$ and $\tau = 2$, but most recent evidence tends to consistently deviate to values $\alpha \sim 1.65$ and $\tau \sim 1.9$, as found in (Pasquale et al. 2008; Hahn et al. 2010; Friedman et al. 2012; Yaghoubi et al. 2018; Fontenele et al. 2019),. We would like to highlight the work by Friedman (Friedman et al. 2012) and Fontenele *et al.* (Fontenele et al. 2019) that found that even when the measurements of the size and time critical exponents are different, the relationship between the size of an avalanche and its duration is also a power law $P(T|S) = T^{\gamma}$ whose exponent fulfills the hyperscaling relation

$$\gamma = \frac{\alpha - 1}{\tau - 1}, \tag{1.31}$$

and demonstrated its validity along a large sets of experiments and models. In particular, Fontenele *et al.* dismissed the hypothesis of the critical branching process (Fontenele et al. 2019). Another recent breakthrough is the finding of power-law distributed avalanche behaviour in the complete nervous system of the zebrafish (Ponce-Alvarez et al. 2018). It is the first time that the whole-brain is analysed in this sense, and it presented scale-free avalanches with exponents compatible with the 3D Ising random field model (Ponce-Alvarez et al. 2018). However, the hyperscaling relation (1.31) was still fulfilled.

From the modelling approach, there has been many attempts to recover scale-free avalanche behaviour, to check what dynamical regimes are compatible with experimental data, and possibly shed light on the criticality hypothesis. Although no model is able to reproduce exactly the behaviour of the whole brain, *universality* is expected to play an important role here, so a model with just the necessary ingredients should also display the same critical exponents, as it happened one century ago with phenomenological Landau theory.

On one hand, simple stochastic models have demonstrated to display neuronal avalanches (Benayoun et al. 2010; Larremore et al. 2014; Brochini et al. 2016), but they have been also found in realistic realizations of simulated neurons, as in (Levina et al. 2007; Millman et

al. 2010; Brochini et al. 2016; Choi et al. 2012; Scarpetta et al. 2018) or even in mesoscopic and whole-brain models (Deco and Jirsa 2012; Villegas et al. 2014; di Santo et al. 2018a). Models present different scenarios that could be compatible with criticality. One of the most commonly accepted is that of E/I balance, i.e., the idea that at each single neuron excitatory and inhibitory inputs are compensated in average (Vreeswijk and Sompolinsky 1996; Brunel 2000; Denève and Machens 2016). It has been claimed that such a balance contributes to the asynchronous irregular state observed in the cortex (Denève and Machens 2016; Buendía et al. 2019), and that it provides a plethora of functional advantages (Shew et al. 2011; Deco et al. 2014; Denève and Machens 2016; Sadeh and Clopath 2020). Many models present criticality at a balanced state (Brunel 2000; Vogels et al. 2011; Poil et al. 2012; Denève and Machens 2016; Politi et al. 2018; Ullner et al. 2018), which seems to be correlated with the finding of power-law distributed avalanches in experiments (Shew et al. 2011; Poil et al. 2012).

From the modelling point view, it has been recently proposed that the universality class behind the neuronal avalanches might not be the critical branching processes, but synchronization transitions. Synchronization among neurons, or even complete regions in the brain, manifest at a macroscopic level as *brain waves* or neuronal rhythms, which were in fact one of the first collective phenomena ever observed in neuroscience (Buzsáki 2006). The role and function of synchronization in the brain has been extensively discussed in the literature, both in experiments (Gray et al. 1989; Segev et al. 2001; Gireesh and Plenz 2008; Yang et al. 2012; Palmigiano et al. 2017; Daffertshofer et al. 2018b; Aguilar-Velázquez and Guzmán-Vargas 2019) as well as in models (Corral et al. 1995; Brunel 2000; Cabral et al. 2011; di Santo et al. 2018a; Porta and Copelli 2019). Although some of these models present synchronization jointly with critical balance, we would like to highlight the breakthrough by di Santo and her collaborators (di Santo et al. 2018a), that demonstrated explicitly for the first time (up to my knowledge) that scale-free avalanches with critical exponents compatible with experimental ones arise at the edge of a synchronization transition. The main advantage the hypothesis of the synchronization transition over the critical branching process is that we do not need to suppose that the brain is arbitrarily near to an absorbing state of "no activity", which is not consistent with the constant chat-

ting of neurons observed in experiments, and it reconciles the view of critical phenomena with brain waves propagation, which needs the recruiting of synchronous spiking of neurons or regions (Buzsáki 2006). The interplay between criticality and synchronization has been also explicitly studied in other experiments (Gireesh and Plenz 2008; Yang et al. 2012; Markram et al. 2015; Miller et al. 2019), as well as models (Poil et al. 2012; Breakspear et al. 2010; Pittorino et al. 2017; Yang et al. 2017; Daffertshofer et al. 2018a; Aguilar-Velázquez and Guzmán-Vargas 2019; Porta and Copelli 2019). Moreover, hints of a synchronization transition appear at the whole-cortex brute-force simulations performed in the Blue Brain project (Markram 2006; Markram et al. 2015). However, synchronization transitions in the brain are still not well understood. The universality class and the underlying statistical physics of the Landau-Ginzburg model of di Santo *et al.* (di Santo et al. 2018a) have not been completely explained, and other more complicated models remain so. An important part of this thesis is to classify, understand, and shed light on the remaining mysteries of synchronization phase transitions in neuronal models, obtaining general laws for these phenomena and stating a new, thrilling hypothesis: synchronization alone is not enough to explain critical-like behaviour, and *excitability* is a necessary ingredient in order to observe such scale-free phenomena in the brain, creating *hybrid type synchronization transitions*. This hypothesis will be further explored and explained in detail in Chapter 4.

It is important to remark that the criticality hypothesis in general has also received strong and valid criticism from both the theoretical and the experimental sides. For instance, Alain Destexhe and Jonathan Touboul have pointed out that scale-free avalanches can be obtained from uncorrelated Poisson processes (Touboul and Destexhe 2010; Touboul and Destexhe 2017). Moreover, they have measured bursting activity of *in vivo* brains among different animal species, and conducted very stringent statistical test power-law distributions in recordings. Their results show that some data was more consistent with exponential or lognormal distributions, when the data is processed carefully (Clauset et al. 2009; Touboul and Destexhe 2010; Dehghani et al. 2012). This remind us that fitting power laws is a delicate matter, specially when the available data does not span for many decades, as it usually happens with neuronal data. A similar proposal

was suggested recently by Viola Priesemann and Oren Shriki, arguing that external inputs may drive the system to distributions that are critical-like, but not exactly power laws (Priesemann and Shriki 2018). Priesemann has also insisted on the role of subsampling on critical systems and how it affects power law observations (Priesemann et al. 2009; Levina and Priesemann 2017), remarking that real data is more consistent with subcritical states[10] (Priesemann et al. 2014). However, if subsampling is taken in account, it could be corrected to discern between critical and non-critical states (Levina and Priesemann 2017). Even the father of the field, John Beggs, stated that the matter of criticality in the brain should be taken with care, in an imagined dialogue between two fictional scientists (Beggs and Timme 2012). Hence skepticism of the criticality hypothesis is absolutely valid and healthy, and reminds us that no definitive empirical and theoretical evidence of critical processes in the brain has been collected so far.

Under my point of view, criticality in the brain still lacks some support from both theory and experimental sides, and even when most of the evidence collected seems to be in favor of it, the reasons to remain skeptical are strong still today. Let me sum up some of the observations that would convince me that the brain is critical, or, conversely, what I believe it remains to be done in order to gather conclusive evidences:

1. The measurements employed (see Appendix A for detail) depend very strongly on the choice of the timebin width, which is arbitrarily taken to be the average of the inter-event interval. The fact that firing rates must be measured via time-binning makes comparisons difficult, and prevent measuring avalanches in time series as we in non-equilibrium processes such as the contact process. Being able of measuring avalanches on continuous models, or establishing a strong theoretical reason to use the current method seems to be necessary in order to have a formal definition of "avalanche". We will suggest a solution through this thesis, in Chapter 6.

2. Modelling evidence is sometimes contradictory, but there is no

[10] In my opinion, the obtained values of the branching parameters in these studies are so close to criticality that it does not make really a difference for brain functioning. For example, (Priesemann et al. 2014) reports an estimation of $m = 0.98$, with criticality being at $m = 1$.

clear explanation on why. For example, there are models that present scale-free avalanches as a consequence of excitation-inhibition balance, but many classical models usually link balance with asynchronous irregular regimes that present very low correlations –in contrast with large critical correlations, and in odds the idea of the with synchronization critical points. Is something missing? Or are those different faces of the phenomena and biases are preventing us from seeing what all those models have in common?

3. We should define what is *exactly* criticality in the brain. It is not the same to say that the brain as a whole is working near a critical point, than to say that the cortex is, or that a layer of pyramidal neurons inside the cortex shows critical-like phenomena. And moreover, if both the cortex and the whole brain are working at criticality, is this criticality the same? It is certainly different to have a Hopf bifurcation, than to couple many oscillators near a Hopf bifurcation. A Stuart-Landau oscillator just at the Hopf bifurcation is critical. A set of such oscillators display more bifurcations and transitions collectively, including chaotic dynamics, and the boundaries of those critical bifurcations do not coincide with those of the single oscillator (a more in-detail discussion can be found in Chapter 7). Therefore, a different kind of criticality might emerge from the coupling of already critical-systems, while sometimes we talk about "criticality in the brain" without specifying the scale at which we are looking at.

4. The final proof would be to have biological evidence that the brain is able to self-organize to such states, maybe from the point of view of evolutionary and developmental biology and not only from plasticity mechanisms. The regulatory mechanisms that lead the brain to criticality –or to any other dynamical state it works– should be known if we want to have a complete image of how the brain works. Additionally, knowing the pathways to the healthy brain could help to diagnose and prevent disease in a fast and accurate way, with its associated clinical benefits.

Chapter 2

Neuronal models and synchronization

"When you know about something, it stops being a nightmare.
When you know how to fight something, it stops being so threatening."

- Andrzej Sapkowski, in *Blood of Elves*, 1994.

After introducing the necessary tools of bifurcation theory and non-equilibrium statistical physics, our objective is to give an overview on neuronal models, both at microscopic and mesoscopic scales. We will also discuss synchronization theory, which will be useful later to asses collective behaviour in neuronal models.

2.1 Neuron Physiology

The neuron is one of the main building blocks of the brain. Its behaviour has been extensively studied, leading to a good understanding of the biophysical mechanisms that govern the dynamics of spiking and coupling to other neurons.

Neurons are composed by a cellular body (or *soma*), a set of fractal-shaped branches called dendrites coming out of the soma, and a long axon, that finishes in synapses connecting to other neuron dendrites. The soma contains organelles such as the nucleus, mitochondria, and the Golgi apparatus; axons, albeit growing as prolongations of the soma, have their own cytoskeleton and are usually recovered by myelin (Kandel et al. 2000). Not all neurons are identical: they different dendritic trees and axon lengths, depending on their particular role; some neurons even display special genetic programs dedicated to perform certain actions, as the circadian pacemakers of the suprachiasmatic nucleus (Golombek and Rosenstein 2010; Albrecht 2012). Cellular diversity is important for correct brain functioning, though often disregarded in computational neuroscience models.

2.1 Neuron Physiology

At rest, neurons present a non-zero potential, called the *resting potential*, which is around -60 mV, but can be found in an interval between -40 mV and -90 mV (Kandel et al. 2000). Neurons generate this potential by regulating the concentration of ions inside their cellular membrane (Kandel et al. 2000; Izhikevich 2006). Permeability to ions in the neuron is accomplished by *ion channels*, proteins in the membrane that react to changes in the potential, "opening" and "closing" and creating physical space for ions to cross the cellular membrane. For example, the resting potential is due to the permeability to K^+, but when the membrane *becomes* permeable to Na^+ due to channel opening, the potential can rise about to +50mV. Channel opening happens due to electrical currents arriving from neighbouring neurons and *depolarizing* the membrane. If the depolarization is strong enough, channels open and an *action potential*, also called a *spike*, is generated. *Hyperpolarizing* currents, on the other hand, do not usually trigger any response, except on some special kinds of neurons (Izhikevich 2006).

The action potential travels through the axon until reaching the synapse. This travel happens by the depolarization of the axon, but the process is aided by the myelin that covers it. At the axon, the action potential travels by opening and closing of ionic channels, not by electric conduction; this process would be too slow to transmit information efficiently. In contrast, the myelin sheath that covers the axon is able to conduct the electrical signal quickly, but its potential tends to immediately hyperpolarize again. As a result, myelin sheaths do not cover the entire axon, and the signal travels by jumping between the axon (where the membrane potential is actively depolarized) and sheath (where the depolarized signal travel faster but the current decreases). This process reduces considerably the time needed for the signal to reach the synapse. Depolarization of the synapse releases neurotransmitters to the intracellular medium, increasing the permeability of the neighbouring cell, and producing its depolarization. The synapse needs some time to recover its neurotransmitters to be "used" again (Kandel et al. 2000).

Permeability of the neuronal membrane, or equivalently, its conductance, can be physically modelled. Hodgin and Huxley created an accurate model of the dynamics of the membrane potential and its conductance. The model, which consist in four coupled non-linear differential equations, was an important breakthrough due to its remarkable

accuracy. More impressively, Hodgin and Huxley were not aware of the existence of the ion channels themselves –whose dynamics allow to derive the model in an easier way– but only of the membrane permeability changes. Actually, they postulated some of the channel properties (Kandel et al. 2000; Izhikevich 2006).

2.2 Deterministic neuron models

Although the Hodgin-Huxley model is able to reproduce very well dynamics of the action potentials, it is computationally expensive and analytical computations are cumbersome. In practice, this limits the number of neurons that can be simulated in a reasonable time. For this reason, there is a plethora of neuronal models obtained by simplifying or reducing the Hodgin-Huxley model, that are more amenable to analytical or numerical treatment. We review here some that I consider to be relevant in our context, and that will help us to understand better the contents of this thesis.

2.2.1 Integrate and fire

The integrate-and-fire neuron is one of the most popular set of models in neuroscience, due to its simplicity, that allows giving analytical treatments in some cases, as well as very fast numerical simulations that allow for large system sizes. These models come from the view of neurons as simplified electrical circuits. The most basic model is the leaky integrate and fire, firstly introduced by Lapicque in 1907[1] (Brunel and van Rossum 2007), that gives a single equation for the potential membrane,

$$\tau_m \dot{V} = -(V - V_r) + R_m I(t), \tag{2.1}$$

where V is the potential membrane, V_r the resting potential, R_m is the membrane electrical resistance, and τ_m a characteristic timescale of the

[1] Incredibly early considering that Ramon y Cajal started studying the neuron in 1887 and received the Nobel prize in 1906!

equivalent RC circuit. Equation (2.1) is not complete by itself, and has to be understood with a threshold and reset potential. If $R_m I > V$, then the membrane potential just diverges exponentially, so the solution has to be reset to the resting potential, $V = V_r$, when $V \geq \theta_T$.

A more realistic integrate-and-fire model is the exponential integrate and fire (Gerstner 2014), that includes a non-linear response of the membrane potential to perturbations, as

$$\tau_m \dot{V} = -(V - V_r) + \Delta_T \exp\left(\frac{V - V_T}{\Delta_T}\right) + R_m I(t), \tag{2.2}$$

where the new parameters V_T and Δ_T control the initiation of the action potential. When $V \geq V_T$, the exponential starts to grow very fast, diverging and initiating the action potential. As before, this has to be cut when $V \geq \theta_T \gg V_T$, resetting the membrane potential to V_r. Note that in the limit $\Delta_T \to 0$ the leaky integrate and fire model is recovered, effectively setting $\theta_T \simeq V_T$. The exponential integrate and fire model can be justified by several ways, such as directly reducing the Hodlin-Huxley model, or just fitting the shape of the starting spike. From the Hodgin-Huxley model, it suffices to reduce it to a one-dimensional system by eliminating the slow timescales –situating all them at its equilibrium values–, keeping just the equation for the membrane potential, and noticing that at its equilibrium value, the opening of the sodium channel $m(V) \propto \exp(V - V_T)$ (Gerstner 2014). Up to my knowledge, of all the one-dimensional integrate and fire models available, the exponential integrate and fire is the most realistic one, making it very suitable for numerical computation.

However, other options are possible. Let us assume a neuron close to its threshold, so V_T is not actually much larger than V_r. This could happen, for example, if the neuron is subject to some external constant input that depolarizes its membrane. Then, the exponential can be further simplified by its Taylor series up to second order (Gerstner 2014). In general, the result can be summarized as

$$\tau_m \dot{V} = (V - V_r)(V - V_T) + R_m I(t), \tag{2.3}$$

where V_r and V_T are not formally the same as in the exponential model before. As before, the model will be reset to V_r when $V \geq \theta_T$. This is called the quadratic integrate-and-fire neuron, due to the quadratic

term V^2 (Izhikevich 2006). A common choice to simplify this model is just to take $V_r = -V_T$, so the right-hand side simplifies to $V^2 - V_r^2 + R_m I(t)$. Taking in account that the height of sodium-induced action potential is around +50 mV, V_T should be just slightly positive, making V_r close to 0; this model the behaviour of a neuron excited via an external current, that has a very small or even no threshold so any external input would activate the neuron spiking. This last scenario is exactly the "canonical type-I" model of the theta neuron (Izhikevich 2006), that will be explained in detail below.

2.2.2 Two dimensional systems

Let us now present two popular reductions of the Hodgin-Huxley: the Fitzhugh-Nagumo and the Morris-Lecar models[2]. Both are two-dimensional systems, more amenable to analytical treatment, and often used as toy model to study neuronal dynamics. Their main advantage over the integrate-and-fire models is that they are more biologically plausible, and the threshold-reset rule is not necessary. This rule, though easy to implement numerically, poses a number of problems for purely theoretical study. FN and ML models present a membrane potential and a slow adaptation variable, with a reduced number of parameters with respect to the Hodgin-Huxley, so it is possible to do phase plane and bifurcations analyses (Izhikevich 2006; Gerstner 2014). The study of these models has uncovered many universal and essential features of neuronal dynamics, such as excitability.

The Fitzhugh-Nagumo model is defined by

$$\tau_m \dot{V} = V - \frac{1}{3}V^3 - W + RI(t), \tag{2.4a}$$

$$\tau_w \dot{W} = a + bV - W, \tag{2.4b}$$

[2] An important, non-written rule of neuronal modelling is that you need exactly two scientists to develop a successful model: Hodgin-Huxley, Fitzhugh-Nagumo, Morris-Lecar, Ermentrout-Kopell, Jansen-Rit, Hindmarsh-Rose, or Wilson-Cowan are excellent examples of well-known models created by pairs. A popular Spanish pun would be to include Ramon y Cajal in the list.

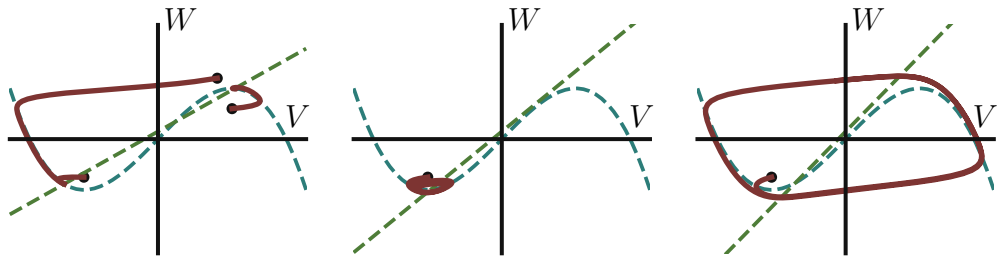

Figure 2.1: **Phase plane of the Fitzhugh-Nagumo model.** From left to right, the stable equilibrium becomes unstable through a Hopf bifurcation. As the oscillations grow, the trajectory goes outside of the stable manifold causing large amplitude oscillations (spikes). Initial conditions marked with grey filled circles. Parameters: $\tau_m = 1$, $\tau_w = 10$, $a = 0.1$. From left to right, $b = 0.545$, $b = 0.795$, and $b = 0.995$.

which should be familiar at this point: the membrane potential is a perturbation to the normal form of the pitchfork bifurcation. Actually, it is exactly the same dynamical equation as the Ising model with an external field W, which adapts following the membrane potential. Although the membrane potential is called V, note that our definition of the Fitzhugh-Nagumo model (which is the standard) comes from several changes of variables and rescaling, so it does not describe physiologically accurate values of the membrane potential or adaptation potential (Gerstner 2014). In this form, it is just a mathematical toy to understand neuronal dynamics in a qualitative way. Figure 2.1 shows the basic spiking dynamics of the Fitzhugh-Nagumo model.

Let us say a few words about this model, from which we can extract a few valuable analytical conclusions. When analysing a dynamical system, one of the first steps is to compute the *nullclines*, i.e., the curves $\dot{V} = 0$ and $\dot{W} = 0$ (Strogatz 1994; Izhikevich 2006). This helps to draw and understand the dynamics in the phase space. Let us assume the simple case of no external current, $I = 0$. The nullcline $\dot{V} = 0$ is $W(V) = V - V^3/3$, a S-shaped cubic polynomial, which is a typical feature of excitable systems, as we will see shortly. The particularity of the Fitzhugh-Nagumo model is that the shape of this polynomial does not depend on the parameter choice, and hence the topology of the phase space depend only on the $\dot{W} = 0$ nullcline, which turns out to be sim-

ply $W(V) = a + bV$. In order to determine the number of fixed points, it suffices to see how much intersections the line has with the S-shaped cubic polynomial, for example, by fixing a and using the slope b as a control parameter. Hence, just one or three solutions are possible. Figure 2.1 shows the evolution of the system for low a. At the beginning, there are three crossings in the S-shaped polynomial, where the one in the centre is unstable, while the other are stable spirals. Note, however, that the stable manifold for the point is divided by the cubic, so a point very near to the up equilibria might be attracted instead to the left bottom part of the diagram, as depicted in Fig. 2.1a. Both stable spirals will undergo a Hopf bifurcation at the extrema of the cubic, leading to small amplitude oscillations. The amplitude of such oscillations increases as b grows, leading the trajectory outside of the stable manifold, to large amplitude oscillations. This is possible because the "up state" equilibrium, after the Hopf, disappeared through a saddle-node bifurcation, when the line stop touching the upper branch.

The neuronal interpretation of this behaviour is the following one: for (adequate[3]) low values of b, the only possible state is the fixed point at the lower branch, that is identified as the membrane resting potential $V^* < 0$. The large excursions around the phase space corresponds with spikes, while the small cycles generated by the Hopf bifurcation are subthreshold oscillations. Of course, in the real neuron all these behaviours are triggered by changing the value of the external intensity, $I(t)$, as a control parameter.

This behaviour, which is common accross neuroscience models, is called *excitability*. A *excitable system* is defined as a system at a stable equilibrium, but where perturbations in the adequate direction can drive it into excursions that go around all the phase space (Izhikevich 2006; Lindner 2004; Prescott 2014). The mathematical reason behind this phenomena is that the stable manifold of the equilibrium has a small area in the direction of the perturbation. Many physical and biological systems exhibit excitability (Lindner 2004). When the external intensity changes, neuronal models might start spiking from the Hopf

[3]For $a < b$, there is a set of b values for which only the lower branch is stable. For our example (see parameters in Fig. 2.1), the Hopf bifurcation cycle appears at $b = 0.805$, while the saddle-node that destroys stability in the upper branch takes place before, at $b = 0.718$. So, for $b \in [0.718, 0.805]$, the only stable point is the resting potential.

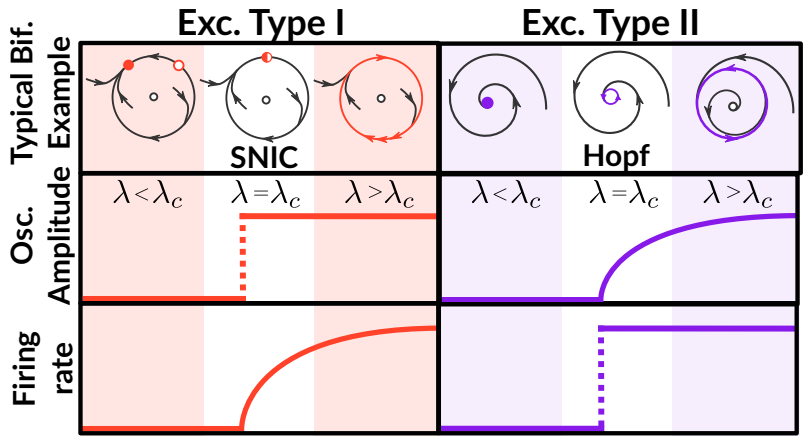

Figure 2.2: **Comparison of excitability classes I and II.** The comparison is done through representative bifurcations corresponding to each excitability class. Note that the firing rate is directly related with frequency of oscillations: vanishingly-small firing rates correspond to arbitrarily large firing frequencies. (Buendía et al. 2020b)

or saddle-node bifurcations (among others), which have a very different behaviour, as explained in Chapter 1. The Hopf presents a finite period and growing amplitude, while the saddle node has finite amplitude and growing period, as illustrated in Fig. 2.2.

The differences in response to a constant input were previously observed in real neurons, which lead to a classification into "excitability classes" by Hodgkin (Hodgkin 1948; Izhikevich 2006). The classification goes as follows,

1. Type I excitability corresponds to neurons that start spiking with constant amplitude and infinite period when they are fed with an external, constant current I. In this case, the minimum current able to elicit a response at infinite time is called the *rheobase current*.

2. Type II excitability corresponds to neurons that start spiking with fixed frequency, regardless of the input current.

3. Type III excitability when the input current generates a single spike. Regular spiking happens only for very high input currents.

In models, in order to have a certain excitability class, it suffices to cross a bifurcation generating large-amplitude limit cycles in an excitable system. Two representative examples of bifurcations corresponding to classes I and II are the creation of cycles through saddle nodes, and Hopf bifurcation, respectively, as sketched in Fig. 2.2. The homoclinic bifurcation is common in neuronal models (Schleimer et al. 2019), and belongs to class I neuronal excitability, as the SNIC bifurcation.

Let us move towards a more realistic, two-dimensional neuronal model, the Morris-Lecar neuron, defined as

$$C\dot{V} = -g_{Na}m_{\infty}(V)(V - V_{Na}) - g_K W(V - V_K) - g_L(V - V_L) + I(t), \tag{2.5a}$$

$$\dot{W} = \tau^{-1}(V)[W_{\infty}(V) - W], \tag{2.5b}$$

where V_{Na} and V_K are the equilibrium reversal potentials of sodium and potassium, and the functions $m_{\infty}(V)$ and $W_{\infty}(V)$ control ionic channel activations and are given by sigmoids. The adaptation variable W is actually representing the dynamics of potassium gating, while the dynamics of the sodium variable are faster and approach the value $m_{\infty}(V)$ immediately. When both ions are considered, we have the $I_{Na} - I_K$ model (see for example Izhikevich (Izhikevich 2006)). The timescale that controls the adaptation dynamics depends on the membrane potential, as

$$\tau(V) = \frac{\tau_w}{\cosh\left(\frac{V-a}{b}\right)}, \tag{2.6}$$

although a constant value for $\tau(V)$ is commonly used for simplicity. If its parameters are fit correctly, the Morris-Lecar model is able to describe realistic neuronal behaviour, making it popular for applications and theoretical studies (Cabrera et al. 2013; Ditlevsen and Greenwood 2013; Montejo et al. 2005; Wang et al. 2013). However, as can be seen in Fig. 2.3, the nullcline shapes are very similar to the ones presented by the Fitzhugh-Nagumo model, meaning that the dynamics of the model can be understood in a similar way. This Figure displays the behaviour of the Morris-Lecar model for sodium and potassium channels for different values of the external current, showing how spiking activity start at low frequencies, being an example of a type I excitability class.

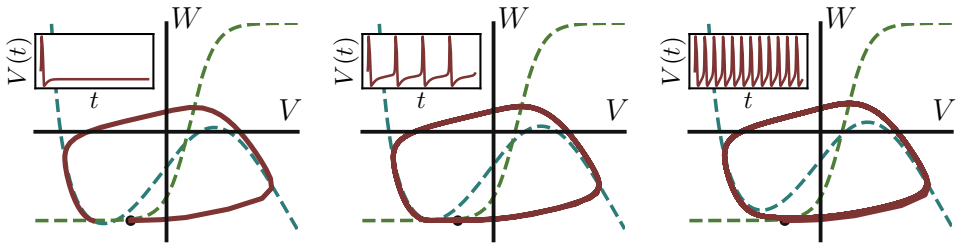

Figure 2.3: **Type I excitability at the Morris-Lecar model under external constant current.** The Morris-Lecar for a set of realistic parameters, subject to a constant external current. The spikes start at low frequency, which increases with I. All insets are drawn for a fixed time of 60 ms. Parameters were obtained from Izhikevich (Izhikevich 2006): $V_L = -80$ mV, $V_K = -60$ mV, $V_{Na} = 60$ mV, $g_L = 8$, $g_K = 10$, and $g_{Na} = 20$. Both timescale constants $C = 1$ and $\tau(V) = 1$ ms. Sigmoids are given by $S(V) = 1/\{1 + \exp[(V_{1/2} - V)/k]\}$, with $V_{1/2} = -20$ mV, $k = 15$ for m_∞ and $V_{1/2} = -25$ mV and $k = 5$ for W_∞.

Although here the Morris-Lecar model is shown to have a type I excitability, it is also able to display type II behaviours, as well as more complex firing patterns (Liu et al. 2014). Moreover, type I spikes can start either from saddle-node or homoclinic bifurcations, whose firing rate have a different dependence on the input current (Tsumoto et al. 2006; Liu et al. 2014).

Finally, let us remark that for the sake of modelling, thousands of variations can be done in already-existing models, easily converting integrate and fire neurons to computationally convenient higher-dimensional models. For example, Izhikevich complemented a quadratic integrate-and-fire neuron with a linear leakage, and used an adaptive variable to account for ionic channels opening (Izhikevich 2003). The result, known as the Izhikevich neuron, is a mixture between an integrate-and-fire model, and the two-dimensional models discussed in this section. The Izhikevich neuron has plethora of possible spiking behaviours that are found in real neuronal systems (see Fig. 2.4), and its main advantage is its computational simplicity.

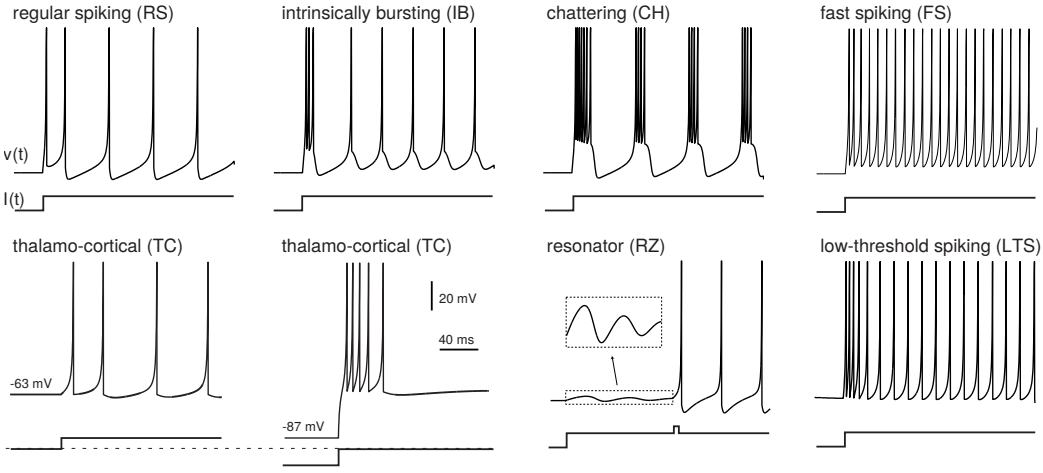

Figure 2.4: **Real neuronal behaviours reproduced by Izhikevich model**. Reproduced with permission of the author. Electronic version of the figure and reproduction permissions are freely available at www.izhikevich.com.

The model is defined by

$$\dot{V} = 0.04V^2 + 5V + 140 - W + RI(t), \tag{2.7a}$$

$$\dot{W} = a(bV - W), \tag{2.7b}$$

in conjunction with a reset rule $V = V_r$, $W = W + W_r$ when $V \geq \theta_T$. The coefficients of the membrane potential are already fitted in order to capture the dynamics of real neurons, so the only free parameters are a and b.

2.2.3 Synaptic dynamics

The models described above are just for single neurons, which receive an external current denoted just by $I(t)$. In order to understand neuronal networks, it is very important to discuss the dynamics of the interaction among neighbours. As discussed above, when a neuron spikes, the action potential reaches the synapses, releasing neurotransmitters to the medium. These neurotransmitters bind to the post-

synaptic neuron's neuronal membrane, facilitating the flux of ions that lead to changes in membrane potentials.

It is possible to build detailed models of this process, by studying the dynamics of neurotransmitter release and binding, as well as treating the neuron as a spatially distributed system (Gerstner 2014). However, here we consider the simplest and popular case of the point-like neuron that receives an input current from the spike of neighbouring cells. Under this assumption, electrical intensity effectively felt by a neuron is given by the sum of all the presynaptic action potentials,

$$I(t) = \sum_{i=1}^{k} \sum_{\{t_m^i\}} \int_{-\infty}^{t} dt' G\left(t_m^i - t', V\right) \delta\left(t_m^i - t'\right), \tag{2.8}$$

where k is the number of neurons whose axon points to the individual considered, $\left\{t_m^i\right\}$ are the set of times at which the i-th neuron spiked, and $G(t, V)$ is a kernel that returns the strength of the interaction after a spike. Note that integrate-and-fire models usually have a very well-defined "spike-time", which is estimated just by computing the time needed for the membrane potential to diverge after reaching the threshold θ_T (Montbrió et al. 2015; Börgers and Kopell 2005). Models such as the Fitzhugh-Nagumo, which do not present any divergence at all, define the spike at its maximum membrane potential. This is an important difference because in such models we retain information about the membrane voltage of the action potential, which cannot be described by integrate-and-fire models. For this reason, integrate-and-fire models usually employ eq. (2.8) directly, which is a *current input* to the neuron, while models with no divergences often add a term $V - V_s^i$ into the sum in eq. (2.8), converting it into a *synaptic input* (Börgers et al. 2010; Izhikevich 2006). The voltage V_s^i is the reversal membrane potential of the i-th neuron synapsis, which is large and positive for excitatory interactions, and below the resting potential for inhibitory synapses. The difference between current input and synaptic inputs is usually not relevant qualitatively (Börgers et al. 2010), so in the computational neuroscience literature they are used commonly interchangeably. We will stick for simplicity to input currents.

The dynamics of the synapse are then dominated by the behaviour of the kernel $G(t, V)$. This is usually written as separate variables, as

$G(t,V) = g_s \alpha(t)\beta(V)$, with g_s the maximum conductance of the membrane potential at spike time, which is assumed to be at $t = 0$. The kernel can be interpreted in the biological sense as the permeability dynamics on the postsynaptic neuron after the arrival of the spike. A common choice is to let $\alpha(t \geq 0) = \exp(-t/\tau)/\tau$, being τ the typical decay time (Rothman 2013). However, this leads the spike strength to be directly one at $t = 0$. A more realistic option, with finite rise time, is given by a double exponential function (Rothman 2013; Gerstner 2014). Usually, the dependence on the membrane potential is not used, so $\beta(V) = 1$.

Finally, the number of neurotransmitters in the vesicles is generally reduced after each spike, hence reducing the effectiveness of the synapse for some time. This short-term plasticity of the synapsis is usually taken in account by adding dynamics to the maximum conductance g_s, with a charge-discharge mechanism following fast-slow time dynamics (Rothman 2013; Gerstner 2014). Adaptation will be discussed in more detail in Chapter 5.

Despite not modelling explicitly all the physiological processes, the synapse equation (2.8) is still complicated, and hence further assumptions are usually made. A typical one is to assume that synapses are *fast*, so the neuron is only affected by spikes in a small time window $[t-\tau, t]$. This is equivalent to set $G(0 \leq t \leq \tau) = 1/\tau$, for $\tau \ll 1$ (Brunel 2000; Montbrió et al. 2015). Given these assumptions, the neuron only feels the spikes that take place at recent times, leading to

$$I(t) = \frac{1}{\tau} \sum_{i=1}^{k} \int_{t-\tau}^{t} dt' \delta\left(t^i - t'\right), \tag{2.9}$$

which is nothing but the average number of action potentials that took place in a small, recent time window. This is a very common way of coupling integrate and fire models, due to its extreme computational simplicity (see for example (Brunel 2000; Montbrió et al. 2015; Borges et al. 2020)).

As another practical variation, we can take the model by Brunel (Brunel 2000), a network of simple leaky integrate-and-fire neurons, where a delay D is added to mimic the time needed by the action potential to affect the post-synaptic neuron, changing the Dirac delta to $\delta\left(t_m^i - t - D\right)$ and selecting a unit kernel in order to make spikes affect

instantaneously. Therefore, it can be seen that eq. (2.8) is a rather general and robust way to write chemical synapses. "Electrical synapses", which are formally called *gap junctions*, are just mutually connected by diffusive interaction of the membrane potential of the different neurons. Their qualitative effect on neuronal coupling is completely different; however, they are not very common in the brain[4], except for particular areas and functions (Izhikevich 2006; Kandel et al. 2000).

2.3 Neural mass models and stochastic effects

After describing models for single neurons, we go through a small review of mathematical models for mesoscopic regions. These can be postulated just phenomenologically, or derived by doing the large size limit of the dynamics of single neuron models. To understand the behaviour of neural networks, we study simpler, stochastic toy models, that will allow us to follow the bottom-up philosophy based on emergent and universal properties, and then study one of the best-known models of neural masses: the Wilson-Cowan model.

2.3.1 Stochastic models

Stochastic neuronal modelling benefits from simplifying physiological details to the minimum, which allow us to perform analytical computations on neuron networks, both at mean-field and network topologies. The simplest approach to understand neuronal dynamics are binary neuron models (Vreeswijk and Sompolinsky 1996; Rubin et al. 2017; Buendía et al. 2019) such as the one proposed by Larremore *et al.* (Larremore et al. 2014; Buendía et al. 2019). The model consists in a network composed by nodes that evolve with time. At any given

[4] Although they are not common for *synaptical* connections, they constitute an excellent way to model the junction between the myelin sheath and the axon, making them useful for compartmental models of the neuron (Gerstner 2014), in contrast with our point-like models.

(discrete[5]) time t, the i-th neuron can be either active, $s_i(t) = 1$ or inactive, $s_i(t) = 0$. Each neuron integrates the activity of its neighbours, becoming active with a probability p_i given by

$$p_i \equiv f\left(\Lambda_i = \frac{1}{k}\sum_j A_{ij}s_j(t)\right) = \begin{cases} 0 & \Lambda_i < 0 \\ \Lambda_i & 0 \leq \Lambda_i \leq 1 \\ 1 & \Lambda_i > 1 \end{cases}, \tag{2.10}$$

and inactivating with probability $1 - p_i$. The function $f(\Lambda_i)$ is a transfer function of the input, which takes in account the possible spiking of the k neighbours; The matrix A_{ij} is called the weighted adjacency matrix, which controls the coupling between neurons. A fraction α of the neurons is considered inhibitory, while the others are excitatory. For simplicity, and the sake of comparison between models, let us take $A_{ij} = \omega_e > 0$ for excitatory connections and $A_{ij} = \omega_i < 0$ for inhibitory ones. (Buendía et al. 2019).

Let us consider the mean-field case, where all the individuals are mutually connected. Let E and I be the total number of excitatory and inhibitory active neurons at a given time. These quantities evolve stochastically according to a master equation, in a similar way to the contact process discussed in Chapter 1. Therefore it is possible to write such a master equation by computing the global rates of activation and inactivation of the model. Let us compute the rate at which excitation is destroyed in the system. If we have E excitatory inactive neurons, and each neuron has a rate $1 - f(\Lambda_i)$ to become inactive, then the total rate is given by its sum, $\Omega(E \to E-1) = \sum_i^E (1 - f(\Lambda_i))$. It is possible to assume that in the macroscopic limit $N \to \infty$ all nodes are equivalent, so the rate can be approximated to $\Omega(E \to E+1) \simeq E(1 - f(\Lambda))$, where we assumed that $\Lambda_i \simeq \Lambda$. This reasoning can be applied to all stochastic

[5] Using a continuous time makes no qualitative difference, but the discrete version makes analytics easier.

reactions, to get

$$\Omega(E \to E-1) = E(1-f(\Lambda)), \tag{2.11a}$$
$$\Omega(E \to E+1) = [N(1-\alpha)-E]f(\Lambda), \tag{2.11b}$$
$$\Omega(I \to I-1) = I[1-f(\Lambda)], \tag{2.11c}$$
$$\Omega(I \to I+1) = [N\alpha-I]f(\Lambda), \tag{2.11d}$$

that allow us to write a master equation, followed by a van Kampen expansion. Now, we are interested in using just fractions of excitatory and inhibitory particles, which are more useful in the thermodynamic limit $N \to \infty$. There are two ways of defining this, either (1) the total fraction over the total number of sites, $x = E/N$ and $y = I/N$, or (2) the fraction of E/I active neurons, $x = E/[(1-\alpha)N]$, $y = I/(N\alpha)$. Though I find the former more natural, most of the literature tends to use the latter. For this reason, the second option[6] will be considered. Then, the associated coupled Langevin equations are

$$\dot{x} = f(\Lambda) - x + \sqrt{x + f(\Lambda)(1-2x)}\xi_x(t), \tag{2.12a}$$
$$\dot{y} = f(\Lambda) - y + \sqrt{y + f(\Lambda)(1-2y)}\xi_y(t), \tag{2.12b}$$

and they completely determine the system dynamics. Solving both equations is still difficult, but its symmetry suggests using the change of variables $s = (x+y)/2$, and $q = (x-y)/2$, which leads to the simpler system

$$\dot{s} = f(\Lambda) - s + \xi_s(t), \tag{2.13a}$$
$$\dot{q} = -q + \xi_q(t), \tag{2.13b}$$

where the noise terms have been defined by grouping the respective noise terms. The first variable is proportional to the system activity[7]. Finally, observe that if we take averages over these two equations, noise

[6] The analysis done in Chapter 3 uses the former.

[7] Using the "natural" option for x and y variables discussed earlier, s is formally the total activity of the system, and the input depends only on q, although the mathematics are slightly more involved.

vanishes and the evolution of $\langle \dot{s} \rangle$ does depends on q only through the input Λ. Hence, solving

$$\langle \dot{s} \rangle = \langle f(\Lambda) \rangle - \langle s \rangle, \tag{2.14a}$$
$$\langle \dot{q} \rangle = -\langle q \rangle, \tag{2.14b}$$

allow us to determine the most important order parameter, the average activity of the system. The detailed computations, along with their results and discussion are the main topic of Chapter 3. For the moment, let us say that the Langevin equations (2.12) are not convenient for mathematical analysis in real networks, since determining the exact value of the neuronal input Λ *from the stochastic variable*s is only possible in fully connected, mean-field systems, as $\Lambda = \omega_e x - \omega_i y = \omega_- s + \omega_+ q$, with $\omega_\pm = (\omega_e \pm \omega_i)/2$. At this moment, we are just interested to see that $\langle q \rangle = 0$ is a necessary condition in order to have a fixed point, meaning that *the same fraction of excitatory and inhibitory neurons has to be active*, i.e., that excitation and inhibition must be in dynamical balance, a hypothesis that we used in our paper (Buendía et al. 2019) just backed by numerical evidence. Let us compute the Jacobian of the deterministic system (2.14), evaluated at the fixed point $\langle s^* \rangle = s_0, \langle q \rangle = 0$.

$$\hat{J}(s_0, 0) = \begin{pmatrix} -1 + \omega_- \langle f'(\Lambda_0) \rangle & \omega_+ \langle f'(\Lambda_0) \rangle \\ 0 & -1 \end{pmatrix}. \tag{2.15}$$

where $\langle f'(\Lambda_0) \rangle \simeq f'(\langle \Lambda_0 \rangle)$ in mean-field systems, which can be easily evaluated (Buendía et al. 2019). However, we do not need to assume that fluctuations vanish in order to see that if $\omega_- = 0$ (the case we study in Chapter 3), then all fixed points of the system are always stable. However, the Jacobian matrix presented here is not diagonalizable, due to the off-diagonal zero.

Let us compare these results with another remarkable model proposed by Benayoun et al. (Benayoun et al. 2010). As the model by Larremore *et al.*, it presents binary state neurons, where inactive nodes integrate neighbouring inputs Λ and activate with rate $f(\Lambda)$. Active nodes remain in that state for a typical time, decaying at a rate β. The difference with the Larremore *et al.* model is that the inactivation process does not depend on the neighbour's state. This apparently innocent variation between the models leads to great discrepancies in the

macroscopic limit, remarking how small changes in individual couplings can lead to completely different emergent macroscopic properties. The procedure for the analysis is the same we carried out before, but now the rates are (slightly) modified to

$$\Omega(E \to E-1) = E\beta, \tag{2.16a}$$
$$\Omega(E \to E+1) = [N(1-\alpha) - E] f(\Lambda), \tag{2.16b}$$
$$\Omega(I \to I-1) = I\beta, \tag{2.16c}$$
$$\Omega(I \to I+1) = [N\alpha - I] f(\Lambda), \tag{2.16d}$$

which leads to the Langevin equations

$$\dot{x} = -\beta x + (1-x) f(\Lambda) + \sqrt{\beta x + (1-x) f(\Lambda)}\,\xi_x(t), \tag{2.17a}$$
$$\dot{y} = -\beta y + (1-y) f(\Lambda) + \sqrt{-\beta y + (1-y) f(\Lambda)}\,\xi_y(t), \tag{2.17b}$$

which are actually very similar to the one derived for the Larremore *et al.* model. There are just one key difference between the two, and it is just the $(1-x)$ term that multiplies the response function, annihilating the second term at high activities. Making, as before, a change to the variables s and q and taking averages we arrive to the deterministic equations

$$\langle \dot{s} \rangle = -\beta \langle s \rangle + \langle (1-s) f(\Lambda) \rangle, \tag{2.18a}$$
$$\langle \dot{q} \rangle = -\beta \langle q \rangle + \langle q f(\Lambda) \rangle, \tag{2.18b}$$

with a situation that is similar to the one at the Larremore model. Note that for fully-connected, mean-field systems, higher order moments as $\langle q f(\Lambda) \rangle \simeq \langle q \rangle f(\langle \Lambda \rangle)$. This condition constrain fixed points to lie in $\langle s^* \rangle = s_0$, $\langle q \rangle = 0$ as before. The Jacobian for this deterministic system is finally given by

$$\hat{J}(s_0, 0) = \begin{pmatrix} -[\beta + f(\langle \Lambda_0 \rangle) + (1-s_0)\omega_- f'(\langle \Lambda_0 \rangle)] & (1-s_0)\omega_+ \\ 0 & -(\beta + f(\langle \Lambda_0 \rangle)) \end{pmatrix}. \tag{2.19}$$

As before, this system cannot be properly diagonalized, being again a *non-normal matrix*. But in this case both eigenvalues can vanish, leading to a saddle-node bifurcation, or a Bogdanov-Takens. What Benayoun *et al.* (Benayoun et al. 2010) demonstrate is that collective behaviour such as neuronal avalanches and large fluctuations can appear even without fine-tuning the system to critical bifurcations, just by taking the balanced limit $\omega_+ \gg \omega_-$. Note that, near a fixed point, $\langle \Lambda_0 \rangle = s_0\omega_-/2$, so if $\omega_+ \gg \omega_-$, both diagonal entries of the Jacobian are very small compared to the off-diagonal term. This means that any fluctuation around the equilibrium will result into activity feedback, a mechanism termed *balanced amplification of fluctuations* (Benayoun et al. 2010). From the dynamical systems point of view, the balanced amplification just brings $\hat{J}$ to be similar to a Bognadov-Takens normal form (Benayoun et al. 2010; Cowan et al. 2016). For finite sizes, the amplification of fluctuations is able to drive the system out of the stable manifold, generating large excursions around the phase plane. In the limit $N \to \infty$, fluctuations vanish, so the system (formally at a stable fixed point) remains at equilibrium. In the thermodynamic limit the only way to effectively generate critical dynamics is posing the system at the Bogdanov-Takens bifurcation.

The balanced amplification of fluctuations is actually an explicit manifestation of the non-potential shear that we mentioned in Chapter 1. Here it can be seen how shear, which results from the interplay between balance and noise, can produce rich neuronal dynamics in the Benayoun *et al.* model, and it has been shown to play an important role in neuronal dynamics (Murphy and Miller 2009; Benayoun et al. 2010; Hidalgo et al. 2012).

2.3.2 Wilson-Cowan model

The deterministic part of the model by Benayoun *et al.*, under mean-field assumptions, is called the Wilson-Cowan model. It was originally derived by Wilson and Cowan in the early 70s (Wilson and Cowan 1972), and it has become one of the most relevant mesoscopic models for mathematical neuroscience (Cowan et al. 2016).

The original derivation of the model is not based on stochastic mod-

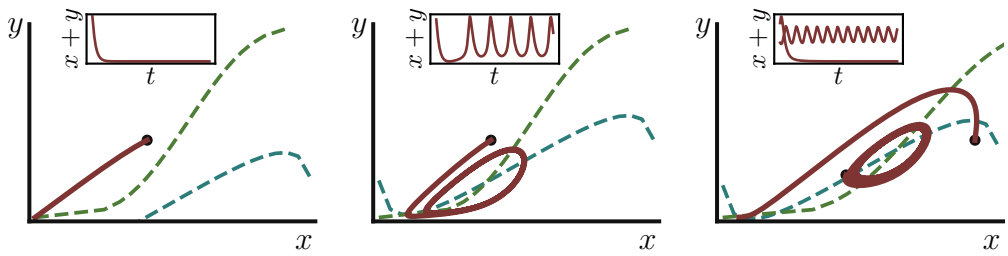

Figure 2.5: **Dynamics of the Wilson-Cowan model.** The Wilson-Cowan equations display many different dynamical regimes. Here, a single stable fixed point of no activity, stable oscillations, and bistability between oscillations and a fixed point are shown –but there are more possibilities. Parameters: $\omega_{ee} = 16$, $\omega_{ei} = 12$, $\omega_{ii} = 3$, both $r_e = r_i = 1$, and $Q = 0$. The sigmoidal function used is $S(x, x_0, k) = \tilde{S}(x, x_0, k) - \tilde{S}(0, x_0, k)$, with $S(x, x_0, k) = 1/(1 + \exp(-k(x - x_0)))$. Sigmoid parameters are $x_{0e} = 4$, $x_{0i} = 3.7$, $k_e = 1.3$, $k_i = 2$. From left to right, the tuple (ω_{ie}, P) is given by $(15, 0)$, $(15, 1.15)$, and $(11.5, 1)$ respectively.

els, but rather on arguments over some general dynamics of the neurons and action potentials. No underlying physical models for the neurons are necessary, which makes the equations a very general tool to analyse mesoscopic neural regions. We reproduce here a very short, conceptual derivation of the model, for completeness, redirecting the interested reader to the seminal work of Wilson and Cowan (Wilson and Cowan 1972).

Let us assume a population of neurons composed by both excitatory and inhibitory neurons. Suppose that all individuals have exactly the same name of neighbours (in-degree k) pointing to them, and its spiking threshold follows certain distribution. Then, under constant excitatory input, the population fraction whose threshold is below the input will spike. The *response function* of the system receiving an input is given by

$$f(\Lambda) = \int_0^\Lambda I_{rh}(\zeta)\, d\zeta, \tag{2.20}$$

where $I_{rh}(\zeta)$ is the distribution of rheobase intensities[8]. Note that we

[8]The rheobase current is the minimum current that, applied for an infinite time,

could have assumed, conversely, that all neurons have the same threshold but a distribution of in-degrees, as long as the number of synaptic inputs is large enough. Under adequate conditions for $I_{rh}(\zeta)$, the response function grows monotonically with the input, and it is usually sigmoidal. Let us by x and y the proportion of cells that are instantaneously firing at a time t, as we did before, and assume that neurons have a short refractory period, r. It is possible to obtain the number of neurons that have already spiked and hence are not available for spiking again until $t+r$, just by integrating $x(t)$ from $t-r$ to t. Therefore, the fraction of active neurons at a time $t+\Delta t$ is the product of the fraction sensible to incoming spikes and their response function. For the excitatory population,

$$x(t+\Delta t) = \left[1 - \int_{t-r}^{t} x(t')\,dt'\right] f_e(\Lambda_e), \tag{2.21}$$

and an analogous equation holds for the inhibitory population. A subindex e was added both to the sigmoid response function and its input in order to be able to make differences among the populations. When writing eq. (2.21), no correlation between the amount of sensible neurons and fraction that responds to the input is assumed. Although this includes in some sense equivalent the mean-field assumption taken in the Benayoun *et al.* model above, these correlations are more general and could be induced by also other mechanisms, as adaptation regulating neuronal thresholds. The input to the neuron is to be interpreted in the sense of (2.8), as

$$\Lambda_e(t) = \int_{-\infty}^{t} dt' G(t-t')\left[c_{ee}x(t') - c_{ei}y(t') + P(t')\right], \tag{2.22}$$

where c_{ee} and c_{ei} are the excitatory and inhibitory couplings to the excitatory population, respectively, and $P(t)$ is an external current. We could stop here and use the equations in their current state, solving them numerically; however, further analytical progress is possible by performing temporal coarse graining. The idea is to replace fast-oscillating variables by their mean value, so a periodic function $g(t)$ with a period $T \ll r$ would be replaced by its average,

$$\overline{g}(t) = \frac{1}{r}\int_{t-r}^{t} g(t')\,dt'. \tag{2.23}$$

is able to elicit a response in the neuron at $t \to +\infty$ (Izhikevich 2006).

Coarse graining is applied in both equations (2.21) and (2.22). In (2.21), this eliminates any oscillation faster than the timescale associated with the refractory period, changing $\int x(t')\,dt' \to r\overline{x}(t)$. At the input, we assume that the kernel $G(t-t')$ has a characteristic timescale, so we can apply the same procedure. Examples of this are a pulse function (which leaves the integration between $[t-\tau, t]$), or an exponential decay with parameter τ. If, again, fast synapses are considered ($\tau \ll 1$) it is possible to set $\int G(t-t')E(t')\,dt' \to k\overline{x}(t)$. The last step is to take the left-hand side of equation (2.21), and Taylor expand to first order around a small timestep,

$$x(t+\Delta t) = x(t) + \Delta t \frac{dx}{dt} + \mathcal{O}\left(\Delta t^2\right). \tag{2.24}$$

Putting all together we finally find the celebrated Wilson-Cowan equations. Renaming $\overline{x}, \overline{y} \to x, y$ again for clarity of notation,

$$\dot{x} = -x + (1-rx)\,f\left(\omega_{ee}x - \omega_{ei}y + p_e\right), \tag{2.25a}$$
$$\dot{y} = -y + (1-ry)\,f\left(\omega_{ie}x - \omega_{ii}y + p_i\right), \tag{2.25b}$$

where all the parameters were rescaled as $\omega_{ee} = kc_{ee}$, $\omega_{ei} = kc_{ei}$, $p = kP$, and so on. The most remarkable feature of this derivation is that no underlying model was assumed for the spiking neurons, and only simple hypotheses about the behaviour of spiking dynamics were necessary.

The phase plane analysis of the model is more involved than in the previous two-dimensional models, and a complete, formal bifurcation diagram has been elusive for exactly 20 years since the publication by Wilson and Cowan (Wilson and Cowan 1972), which was performed by Borisyuk and Kirillov (Borisyuk and Kirillov 1992). The phase plane for the Wilson-Cowan equations are two S-shaped nullclines, that can intersect in different points. As it happens with other neuronal models, the Wilson-Cowan equations are able to show excitability, hysteresis, and oscillations, as depicted in Figure 2.5, but the Wilson-Cowan is also able to exhibit more exotic behaviours. We reproduce, in Figure 2.6, the diagram by Borisyuk and Kirillov (Borisyuk and Kirillov 1992), which displays a zoo of bifurcations, including some codimension 2 points. Among all the possible phases in the bifurcation diagram, the authors found that a small particular region where stable fixed points

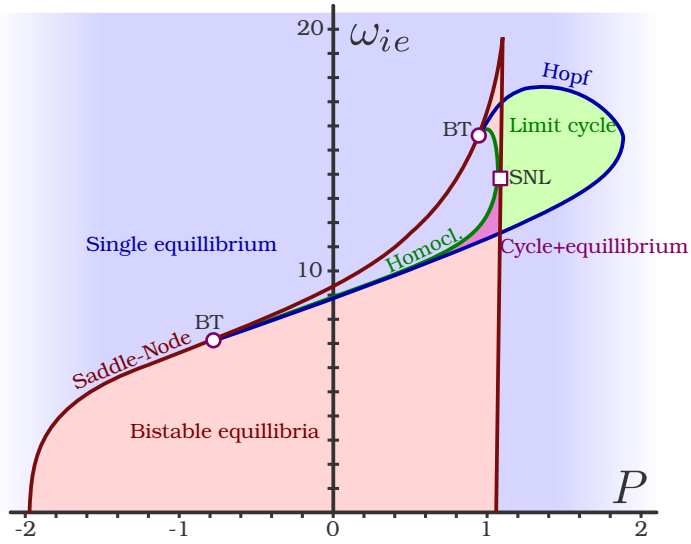

Figure 2.6: **Bifurcation diagram of the Wilson-Cowan model.** Bifurcations are drawn by thick, coloured lines: blue, Hopf; red, saddle-node; green, homoclinic. Different macroscopic regions are marked with different colours: green, single stable limit cycle; red, bistability between two stable equilibria; blue, a single stable equilibrium; and purple, bistability between a limit cycle and a fixed point. The blue regions are macroscopically very similar. Bogdanov-Takens bifurcations are symbolized by empty circles, and a saddle-node-loop by an empty square. Parameters are as in Figure 2.5. This figure was adapted from (Borisyuk and Kirillov 1992).

and stable limit cycles coexist, stating that such a region "may be of interest to neurophysiologists" (Borisyuk and Kirillov 1992). Almost 30 years later, one of the main results of this work is that this bifurcation topology could be not only ubiquitous in many neuronal systems, but indeed responsible for the critical avalanches and complex phenomena in the brain. Although we will revisit and discuss this matter in detail Chapter 4, let us remark that this is a theoretical hypothesis, which needs to be studied in more models, as well as the necessary experimental support.

2.3.3 The "Landau-Ginzburg" approach

Another model which is of special relevance to this thesis is the recent model proposed by di Santo, Villegas, Burioni and Muñoz (di Santo et al. 2018a) in order to explicitly understand the role of critical synchronization in the brain. The philosophy behind this approach is to write the simplest possible parsimonious model that accounts for activity and adaptation in the cortex. The idea is to write an equation for the mesoscopic activity of the region in the same way Landau did for equilibrium statistical physics, using just a low-order polynomial, and complement this with an adaptation mechanism, that accounts for the amount of neurotransmitters available to the region, which allow the system to spike. The S-shape nullcline found in all these models, including the Wilson-Cowan, suggest that a third-order expansion for the activity is enough. Finally, the adaptation follows Tsodyks-Markram short-term plasticity dynamics (Tsodyks and Markram 1997). The model for a single cortical region is

$$\dot{\rho} = (R - a)\rho + b\rho^2 - \rho^3 + \sigma\sqrt{\rho}\eta(t), \tag{2.26a}$$

$$\dot{R} = \frac{1}{\tau_R}(\xi - R) - \frac{1}{\tau_D}\rho R, \tag{2.26b}$$

where the only control parameter is ξ, the maximum allowed density of calcium ions, and the noise has been chosen to be square root multiplicative noise, typical of non-equilibrium demographic processes (Hinrichsen 2000). The system has an absorbing phase at $\rho = 0$, as well as a fixed point $\rho^* \neq 0$. The timescales τ_R and τ_D control the charge and depletion dynamics, respectively. Let us focus now on the noiseless, mean-field description of the model. In this case, the fixed points have a complicated analytical form.

For $\xi < a$, the linear term of the activity equation is always negative. This leads always to the absorbing phase $\rho = 0$ (as the linear term controls the stability of points, see the pitchfork bifurcation in Chapter 1). For $\xi > a$, the linear term can become positive for a while, allowing the system to spike, discharge, and fall into the absorbing phase. While in this phase, the resources will charge again, eventually moving the system to the up branch again, re-starting the cycle. This can be seen

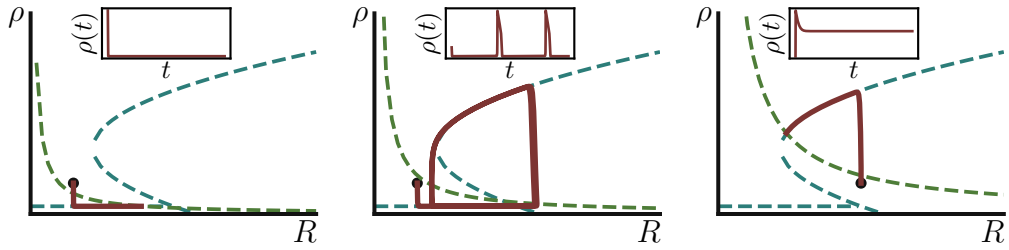

Figure 2.7: **Phase plane of the Landau–Ginzburg model.** The mesoscopic region presents both up and down states, as well as oscillations, depending on the control parameter value. The oscillations turn to bistability if the charge timescale is faster than depletion. Parameters: $a = 1$, $b = 1.5$, $\tau_R = 10^3$, $\tau_D = 10^2$. From left to right, $\xi = 0.8$, $\xi = 1.5$, and $\xi = 5.0$.

if we compute $R^* = \tau_R^{-1}\xi / \left[(\tau_R^{-1} + \tau_D^{-1})\rho\right]$. When the timescale separation is large enough, this becomes $R^* \simeq \Delta\xi/\rho$, with $\Delta = \tau_D/\tau_R$. If the charge time is slower than the depletion, then $R^* \simeq 0$, indicating that the system will tend to deplete its resources. But when we are in the absorbing state, $\rho = 0$, leading to $R^* = \xi/\tau_R$. Since $\xi > a$, the system will be allowed to jump again into the active state, generating a limit cycle. The cycle emerges at the bifurcation $\xi = a$, which is homoclinic[9]. The limit cycle disappears through a Hopf bifurcation to a stable fixed point in the up branch.

The main idea of the Landau-Ginzburg model was to couple many of these units together through a simple diffusion mechanism. When this is done, the collective dynamic of mesoscopic units change as a function of the control parameter ξ. Di Santo *et al.* (di Santo et al. 2018a) demonstrated that single units, that behave as non-linear oscillators, undergo a synchronization phase transition from synchronous regular to asynchronous irregular states. At the critical point ξ_c, all main features from criticality are recovered, as large susceptibilities in the order parameter and scaling. When avalanches are measured mimicking the experimental protocol used in neuroscience (see Appendix A), power-law distributed avalanches can be found, with critical expo-

[9] In (Buendía et al. 2020c) we said that this is a SNIC bifurcation, but a more careful analysis revealed it was actually a homoclinic.

nents compatible with the experimental observations (di Santo et al. 2018a).

2.4 Oscillations and phase reductions

The systems described above are written in terms of variables such as membrane potentials, or collective neuronal activity. Although these variables are very useful to understand the system dynamics, they do not render much information about brain waves, i.e., about synchronization of neurons.

Rhythmic oscillations found in neuronal images and EEG, as well as spiking bursts in cultures, imply the recruiting of large numbers of individuals spiking in consonance, meaning that the action potentials of many individuals happen in a synchronous way (Buzsáki 2006). Single neurons can spike periodically under a constant input current $I(t)$ (Izhikevich 2006; Kandel et al. 2000). If we couple many of these neurons together, do their activity synchronize? But even at larger scales, models are able to display this behaviour: limit-cycle oscillations in the Wilson-Cowan model are a reflect of pulsating microscopic spiking activity, regulated by inhibition; in the Landau-Ginzburg model, the whole mesoscopic region displays periods of activity, followed by quiescence when resources are depleted. If we couple several oscillating mesoscopic regions, under which conditions do they synchronize?

Our objective now is to review methods to reduce periodically spiking neurons or regions to phase models, and then use the theory of non-linear coupled oscillators to study synchronization phenomena in the brain.

2.4.1 The theta-neuron

A very simple example to start the study of phase models is the so-called "theta-neuron", or the "canonical type-I Ermentrout-Kopell" model (Ermentrout and Kopell 1986; Izhikevich 2006). We start, as already discussed above, from the quadratic integrate-and-fire neuron,

eq. (2.3), and assume that $V_r = -\theta_T \simeq 0$. Then, the model reads

$$\dot{V} = V^2 + I(t), \tag{2.27}$$

with the additional reset rule $V(t) = V_r$ when $V(t) \geq \theta_T$. If a constant input current $I(t) \equiv I$ is assumed, for $I < 0$ the membrane potential stabilizes at $V = \sqrt{I}$, while if $I \geq 0$, then $V(t)$ spikes periodically. Solving the differential equation, we see that $V \propto \tan t$, meaning that in absence of the reset rule, the spike happens at $V \to +\infty$ and the potential grows again from $V \to -\infty$. Therefore, the change of variables $V = \tan(\varphi/2)$ is able to absorb the divergence and lead to

$$\dot{\varphi} = (1 - \cos\varphi) + (1 + \cos\varphi) I(t) \equiv (I + 1) + (I - 1)\cos\varphi, \tag{2.28}$$

which the canonical form of the SNIC bifurcation, with control parameter I. What Ermentrout and Kopell demonstrated in 1986 (Ermentrout and Kopell 1986) was that all neuronal systems close to the spiking threshold could be approximated by this equation, in the spirit of normal forms. The theta neuron has a clear advantage over the quadratic integrate-and-fire neuron: the reset rule is not needed anymore. The spike is produced exactly at $\varphi = \pi$. This also allow one to perform analytical computations easily, such as the spiking period. The equation can be readily integrated, obtaining an expression for $\varphi(t)$. Imposing $\varphi(t) = \varphi(t + T)$ it is possible to obtain the period $T = \pi/\sqrt{I}$, following the expected scaling of the SNIC bifurcation.

If an additional leaky voltage $-aV$ is introduced in the simplified quadratic model, then (in a similar fashion to the membrane potential of the Izhikevich model), the explicit expression for $V(t) \propto \tan t$ can be still obtained, so performing the same variable change we arrive at

$$\dot{\varphi} = (I + 1) + (I - 1)\cos\varphi_j - a\sin\varphi_j, \tag{2.29}$$

which is again a normal form for a SNIC transition, that takes place at $I_c \simeq a - 1$. Therefore, for $a > 1$ we need larger currents to trigger a spike. We could also wonder what would happen if we start from the general equation of the non-linear oscillator $\dot{\varphi} = \omega + a\sin\varphi$ and did the reversal change of variables. The result is given by the equation $2\dot{V} = \omega + 2aV + \omega V^2$ where ω now makes the role of external input, but it is also coupled to the quadratic term.

2.4.2 More general phase reductions

The quadratic integrate-and-fire case is very simple, since it deals with periodic signals in just one dimension, so an adequate change of variable is able to render a phase reduction. However, for the two-dimensional systems such as the Fithugh-Nagumo, the situation gets more complicated. In general, one could be tempted to analyse this problem just by changing the origin of coordinates to a point inside the cycle[10], and moving to polar coordinates. However, by doing this we still have to retain both the amplitude and the angle, which in many cases will not decouple; in higher dimensions, we need all the equations to understand the behaviour of the system. But a limit cycle is always a one-dimensional manifold, so a single angular variable should be sufficient to describe the dynamics, once we constrain ourselves to such a line. Once the system is posed at limit cycle, angles can be chosen due to homeomorphism of the cycle with a unit circle, so the phase corresponding to $t = 0$ is $\varphi = 0$ and the phase corresponding to $t = T$ is $\varphi = 2\pi$, linearly interpolating between both values. It is possible to demonstrate that, if all the oscillators are identical, then we can move a corotating frame of reference, so the angular speed of each oscillator will be given by the fluctuation to the global angular speed, ω. The procedure is done in detail in Appendix B, and the result is given by

$$\frac{d\varphi_j}{dt} = \omega_j + \sum_i c_{ij} \sin\left(\varphi_i - \varphi_j + \psi_{ij}\right), \tag{2.30}$$

which is nothing but the celebrated Kuramoto-Shinomoto model of synchronization (Izhikevich 2006). Therefore, we see that this simple popular model arises from any general set of coupling limit cycles, when the systems are assumed to interact weakly.

Another important remark that we could do at this point is that phase-reduction procedure considered deals only with oscillators that present a constant angular speed. This is because we just interpolated linearly through the complete curve, completely ignoring that often real oscillators tend to pass more time some parts of the cycle than

[10] Index theory can be used to demonstrate that at least one unstable equilibria should be inside the cycle, which could be a good reference point.

others. For example, the theta neuron for $I \gtrsim 0$ goes very fast near $\varphi = \pi$, being very slow at $\varphi = -\pi$. The simplicity of this model allowed us to obtain a variable change that is able to retain this non-linear information. Although it could seem that the general method is losing information, angular reductions are always one dimensional, so a non-linear oscillator $\dot{\varphi}_j = \omega\left(\varphi_j\right)$ can be casted into a linear one with arbitrary angular speed Ω by the chain rule

$$\frac{d\tilde{\varphi}}{dt} = \Omega = \frac{d\tilde{\varphi}}{d\varphi}\dot{\varphi} = \frac{d\tilde{\varphi}}{d\varphi}\omega(\varphi) \rightarrow \tilde{\varphi} = \Omega \int \omega(\varphi)\, d\varphi, \tag{2.31}$$

paying the price of more complicated interaction terms H_{ij} when performing the changes of variables from φ to $\tilde{\varphi}$. Hence, there is no difference between using linear or non-linear phase models, and it reduces to mathematical conveniences.

2.5 Synchronization of coupled oscillators

We finally review the mathematical background that will be used to speak about synchronization dynamics in coupled neuronal systems. We start by considering the classical Kuramoto model as an example to develop the formalism, which will be applied later in Chapters 4 and 6 for more complicated, realistic cases.

2.5.1 The Kuramoto Model

We consider the classical Kuramoto model in mean-field in order to develop our tools for studying coupled oscillators. This model presents a synchronization transition, and its simplicity and generality has made it the reference model for synchronizing behaviour in physics, biology or chemistry (Pikovsky et al. 2003; Acebrón et al. 2005). The model consists in a series of phase oscillators that move with a certain angular frequency, subject to (quenched or annealed) noise and modulated by an attractive coupling. If the coupling is large enough, oscillators may get together and synchronize, as sketched in Figure 2.8.

We start by taking eq. (2.30) and setting $\psi_{ij} = 0$, $c_{ij} = J/N$, and obtaining the frequencies ω_j from a distribution $g(\omega)$. Then, the model we want to study is

$$\dot{\varphi}_j = \omega_j + \frac{J}{N}\sum_{i=1}^{N}\sin\left(\varphi_i - \varphi_j\right). \tag{2.32}$$

The oscillators become synchronized depending on the differences in ω_j due to the distribution $g(\omega)$ and the attractive coupling J. We start its study by introducing the Kuramoto complex order parameter,

$$Z(t) = R(t)\,e^{i\psi(t)} = \frac{1}{N}\sum_{j=1}^{N} e^{i\varphi_j(t)}, \tag{2.33}$$

which has $R = 1$ if all the oscillators are synchronized, and $R = 0$ if all of them are completely asynchronous. The angle ψ is the average global phase of the system –which is well-defined only for at least partially synchronized systems. One could argue that $Z = 0$ not only on desynchronized cases, but also when for example exactly half of the oscillators at a phase φ and the other half are at $\varphi + \pi$, but those cases are usually unstable and can be analysed with the mathematical machinery we review here. The coupling in equation (2.32) can be rewritten using the order parameter, as

$$\dot{\varphi}_j = \omega_j + JR\sin\left(\psi - \varphi_j\right) = \omega_j + \frac{J}{2i}\left(Ze^{-i\varphi} + \overline{Z}e^{i\varphi}\right), \tag{2.34}$$

where the bar stands for complex conjugate. The right-hand side of the equation, despite looking more complicated, has the advantage of retaining the order parameter in its complex form, a fact that we will exploit shortly. Although some information can be obtained from this change of variables, such as the existence of synchronous solutions, it is not particularly useful for analytics. We consider then the thermodynamic limit $N \to +\infty$, and then study the density of oscillators $P(\varphi, \omega, t)$, that is, the fraction of oscillators with angular speed ω with phases in the interval $[\varphi, \varphi + d\varphi]$ at time t. This distribution fulfills

$$\int_{-\infty}^{+\infty} d\omega \int_{0}^{2\pi} d\varphi P(\varphi, \omega, t) = \int_{-\infty}^{+\infty} d\omega\, g(\omega) = 1, \tag{2.35}$$

since at each time the total distribution of phases has to be $g(\omega)$, which is normalized by definition. In the continuum, the complex order parameter can be computed as

$$Z(t) = \int_{-\infty}^{+\infty} d\omega \int_0^{2\pi} d\varphi P(\varphi, \omega) e^{i\varphi}. \tag{2.36}$$

Note that in theory we should also modify eq. (2.32) in a similar way, adding up all the integrals, but since the definition of the order parameter has also changed equation (2.34) can be used just by omitting its indices (Pikovsky et al. 2003). Now it remains to obtain an equation for the density of oscillators. This is done through the continuity equation,

$$\frac{\partial P}{\partial t} + \frac{\partial (P\dot{\varphi})}{\partial \varphi} = 0, \tag{2.37}$$

where $\dot{\varphi}$ is given by eq. (2.34). After inserting $\dot{\varphi}$ and simplifying, the continuity equation for the Kuramoto model reads

$$\partial_t P = -\omega \partial_\varphi P - \frac{J}{2i}\left[Z e^{-i\varphi}\left(\partial_\varphi P - iP\right) + \overline{Z} e^{i\varphi}\left(\partial_\varphi P + iP\right)\right]. \tag{2.38}$$

Solving the partial differential equation gives complete information about the model. A particularly useful way to tackle this problem is to expand the density P in Fourier series, which can be done since $P(\varphi, \omega, t) = P(\varphi + 2\pi, \omega, t)$ by definition. Writing

$$P(\varphi, \omega, t) = \frac{g(\omega)}{2\pi} \sum_{k=-\infty}^{+\infty} p_k(\omega, t) e^{ik\varphi}, \tag{2.39}$$

and substituting into the continuity equation, it is possible to find an equation for the evolution of each mode $p_k(\omega, t)$. Note that Fourier harmonics are given by

$$p_k(\omega, t) = \int_0^{2\pi} d\varphi P(\varphi, \omega, t) e^{ik\varphi}, \tag{2.40}$$

which reminds the definition of the Kuramoto order parameter. Actually, this suggests a generalization of the order parameter definition to

$$Z_k(t) = \int_{-\infty}^{+\infty} d\omega \int_0^{2\pi} d\varphi P(\varphi, \omega, t) e^{ik\varphi} = \int_{-\infty}^{+\infty} d\omega \overline{p}_k(\omega, t) g(\omega), \tag{2.41}$$

where we used the Fourier expansion and $p_{-k} = \overline{p}_k$. These are known as the Kuramoto-Daido order parameters (Pikovsky et al. 2003; Ott and Antonsen 2008). Therefore, this relationship allow us to obtain Z_k from the harmonics p_k. Ott and Antonsen observed in 2008 that the ansatz

$$p_k(\omega, t) = [p_1(\omega, t)]^k, \tag{2.42}$$

provides an exact solution to the Kuramoto model (Ott and Antonsen 2008). Later formal advances have shown that this is a solution of an entire family of coupled oscillators, so for most cases the Ott-Antonsen ansatz provides an exact, closed form for the distribution $P(\varphi, \omega, t)$ (Ott and Antonsen 2008; Tyulkina et al. 2018; Goldobin et al. 2018; Montbrió et al. 2015).

If, additionally, we use the common assumption that $g(\omega)$ is a Lorentzian distribution, then contour integration and the residue theorem allow to explicitly integrate eq. (2.41) for $k = 1$,

$$Z(t) = \int_{-\infty}^{+\infty} d\omega \frac{\overline{p}_1(\omega, t)\sigma}{\pi\left[(\omega - \omega_0)^2 + \sigma^2\right]} = \overline{p}_1(\omega_0 - i\sigma, t), \tag{2.43}$$

as long as $p_1(\omega, t)$ is well-behaved. The only thing that remains is to bring everything together and perform the long, boring computations. In summary, the method is as follows: we obtained the continuity equation, and expanded it using Fourier series, obtaining a set of infinite differential equations $\dot{p}_k$, one per each mode; then, use the Ott-Antonsen ansatz (2.42) to reduce the infinite set of differential equations to just a complex differential equation for $p_1(\omega, t)$, as $\dot{p}_k = k p_1^{k-1} \dot{p}_1$. And finally, assuming that $g(\omega)$ is Lorentzian, take complex conjugates and set $\omega = \omega_0 - \sigma i$, to write equation for the usual Kuramoto order parameter instead of the first harmonic. The resulting (simple) equation for the Kuramoto order parameter is

$$\dot{Z} = i\omega_0 Z + \frac{1}{2}(J - 2\sigma) Z - J Z |Z|^2, \tag{2.44}$$

which is the normal form of the Hopf bifurcation. As we discussed in the first chapter, the equilibria corresponding to this normal form are $Z = 0$, the asynchronous state, and a stable limit cycle with constant amplitude, which is partial synchronization. The critical transition happens at $J_c = 2\sigma$. Note that the complex term $i\omega_0 Z$ couples only

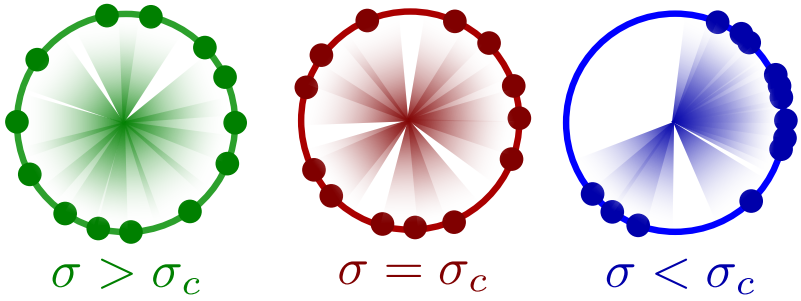

Figure 2.8: **The Kuramoto model.** Oscillators move with angular frequencies picked with a distribution with variance σ (or, conversely, with homogeneous frequencies subject to white noise with variance σ). If the noise is large (left), the system will be synchronous. If the noise is low (right), then the coupling starts to form synchronization clusters that move together. At criticality (center) the mean synchronization is zero, but fluctuations can still create clusters.

with the global phase, leading to $\dot{\psi} = \omega_0$, meaning that the synchronized system rotates with the mean angular speed ω_0.

2.5.2 Noisy oscillators

Although the analysis done above is very general, one could think that it is unrealistic for our interest applications. Synaptic input is known to be noisy by nature, and many neurons receive external inputs usually modelled as white noise. Therefore, reducing the study of synchronization to deterministic systems does not seem to be useful. Let us adapt the formalism also for stochastic systems. In order to do so, we study a common noisy variant of the Kuramoto model (Acebrón et al. 2005; Pikovsky et al. 2003),

$$\dot{\varphi}_j = \omega_0 + \frac{J}{N}\sum_{i=1}^{N}\sin\left(\varphi_i - \varphi_j\right) + \sqrt{2\sigma}\xi_j(t), \tag{2.45}$$

where all oscillators now share the same frequency ω_0, subject to white Gaussian noise $\left\langle \xi_j \right\rangle = 0$, $\left\langle \xi_i(t)\,\xi_j(t') \right\rangle = \delta_{ij}\delta(t-t')$ of strength σ. The continuity equation is now given by the associated Fokker-Planck

equation,

$$\frac{\partial P}{\partial t} + \frac{\partial (P\dot{\varphi})}{\partial \varphi} = \sigma \frac{\partial^2 P}{\partial \varphi^2}, \tag{2.46}$$

which is similar to the continuity equation above, but additive noise enters as a diffusive term. We then can follow the procedure explained above, expanding P in Fourier series and analysing the modes. This case seems to be even easier than the preceding one, since the distribution $g(\omega) = \delta(\omega - \omega_0)$, and hence (2.41) automatically renders $Z_k = \overline{p}_k$, without the need of integration. Performing again all the whole procedure as before leads again to (2.44).

At this point just could be tempted to think that the role of both quenched and temporal noises is exactly the same, and that nothing special happens in this case –just that the quenched noise was distributed by a long-tailed Lorentzian distribution, while here the noise statistics are Gaussian.

However, numerical simulation will immediately point problems to us. While in the deterministic system, the equation $J = 2\sigma$ predicts the location critical point with great accuracy, at the noisy system it fails for large values of noise. This is because in the Kuramoto model, as in any other deterministic system, the Ott-Antonsen is exact, but in noisy system, it only renders an approximation which is correct up to order $\mathcal{O}(\sigma)$, which turn to be far away from the actual results when the noise grows. Here we present some solutions for noisy systems (Tyulkina et al. 2018; Goldobin et al. 2018).

First, one could wonder what the Ott-Antonsen ansatz means exactly for the angle distribution. If we are to guess the functional form of the solution, maybe it is just easier to try to write directly an ansatz for $P(\varphi, t)$ than for the Fourier harmonics. The most naive idea one can think of is a Gaussian distribution, so the angle distribution could be described using the global phase $\psi(t)$ and its variance $\Delta(t)$. In order to fulfill periodicity in the angles, it becomes necessary to "wrap" the distribution, by letting

$$P(\varphi, t) = \frac{1}{\sqrt{2\pi\Delta}} \sum_{k=-\infty}^{+\infty} \exp\left[-\frac{(\psi - \varphi + 2\pi k)^2}{2\Delta}\right], \tag{2.47}$$

then we can use the definition of the Kuramoto-Daido parameters, 2.41, to obtain Z_k, and then try to relate Z_k recursively from lower

harmonics. When we do this, we get

$$Z_k = |Z|^{k^2-k} Z^k, \tag{2.48}$$

which is another possible ansatz for the oscillators, similar to the one studied by Ott and Antonsen. The Ott-Antonsen ansatz, as $Z_k = Z_1^k$ turns out to be nothing but the underlying assumption that the angles are distributed in a Lorentzian, at any time[11]. The ansatz 2.48 was (unwittingly) used by Zaks *et al.* (Zaks et al. 2003), to study a system of non-linear oscillators, five years before Ott and Antonsen published their method. Although the ansatz works better than the Ott-Antonsen when the oscillators are very well synchronized, in general its results are poorer.

So far, it seems that the best we can hope for is to get a clever ansatz that allow us to get an approximate solution. Recently, a systematic approach was derived by Tyulkina, Goldobin, Klimenko and Pikovsky (Goldobin et al. 2018; Tyulkina et al. 2018), where they demonstrate that the Ott-Antonsen ansatz is just the "first-order", so we should look for deviations from the manifold of Ott-Antonsen solutions. The way to do this is defining a moment generating function,

$$F(k,t) = \left\langle \exp\left(k e^{i\varphi}\right)\right\rangle = \sum_{m=0}^{\infty} Z_m(t)\frac{k^m}{m!}, \tag{2.49}$$

so the Kuramoto-Daido parameter $Z_k = \left\langle e^{ik\varphi}\right\rangle$ can be obtained by making derivatives, as

$$Z_m = \left.\frac{\partial^m F}{\partial k^m}\right|_{k=0}. \tag{2.50}$$

Then, the infinite set of equations for the Kuramoto-Daido parameters can be transformed into a partial differential equation for the moment-generating function, F, analogously to the moment-generating function formalism studied in stochastic processes (Gardiner 2009). Although this PDE is usually easier to tackle than the Fokker-Planck equation directly, in most cases it does not turns out a very convenient

[11] Using the ansatz means that angles are Lorentzian-distributed regardless of the $g(\omega)$.

approach. However, from the generating function it is possible to compute the *cumulants* of the distribution, as

$$k\frac{\partial \log F}{\partial k} \equiv \sum_{m=1}^{+\infty} \vartheta_m(t)\, k^m. \tag{2.51}$$

After a short computation, it is possible to see that the cumulants are given by

$$\vartheta_m = m\frac{\partial^m \log F}{\partial k^m}\bigg|_{k=0}, \tag{2.52}$$

which is the typical expression for the cumulants of a statistical distribution. Although it is difficult to find a closed expression for the cumulants in terms of the derivatives of the generating function[12], the computation using the derivatives is easy –just tedious. The first cumulants are given by

$$\vartheta_1 = Z_1, \tag{2.53a}$$
$$\vartheta_2 = Z_2 - Z_1^2, \tag{2.53b}$$
$$\vartheta_3 = Z_3 - 3Z_2Z_1 + 2Z_1^3, \tag{2.53c}$$
$$\vartheta_4 = Z_4 - 4Z_3Z_1 - 3Z_2^2 + 12Z_1^2Z_2 - 6Z_1^4. \tag{2.53d}$$

Observe that when we choose the Ott-Antonsen solution, $\vartheta_1 = Z_1$, and all the other cumulants become zero. Note that even when the ansatz gives a value for all orders in Z_m, all of them contribute just to first order in ϑ_m. Then, using the second approximation with $\vartheta_1, \vartheta_2 \neq 0$ does not mean to neglect from Z_3 –since the Ott-Antonsen already takes in account these orders– but to include corrections to the assumption of Lorentzian distributed angles. Actually, it is possible to explicitly identify $P(\varphi, t) = P_{OA}(\varphi, t) + P_C(\varphi, t)$, where P_{OA} is the Lorentzian distribution assumed for the Ott-Antonsen solution, and P_C encodes the corrections (Goldobin et al. 2018). In this thesis, we will test and compare for the first time (up to my knowledge) the predictions ansatz in different kind of bifurcations for a system noisy non-linear oscillators. This computations will be carried out in Appendix C.

[12] Which can be done using Faà di Bruno formula.

Neuronal inhibition: the Jensen's force

"A man will be imprisoned in a room with a door that's unlocked and opens inwards; as long as it does not occur to him to pull rather than push."

- Ludwig Wittgenstein.

Our objective in this chapter is to shed light on the effect of inhibitory mechanisms in the brain, as well as their possible relations with synchronization. In order to do it so, we study in detail a model originally proposed by Larremore *et al.* (Larremore et al. 2014), consisting in a network of excitatory and inhibitory units. By simplifying some of the model assumptions, we uncover the roots of the the asynchronous irregular state in balanced networks, a fluctuation-driven mechanism we termed *Jensen's force*. At the end, we argue why this is an important concept for both theoretical and experimental future research.

3.1 Inhibition, balance and synchrony

Many simple abstract models for activity propagation are built upon networks of excitatory units. Paradigmatic example of spreading activity include epidemic dynamics and information transmission on the internet (Serazzi and Zanero 2004; Pastor-Satorras et al. 2015). However, there are many biological systems that cannot be modeled using just excitatory units. Nodes that repress further activations are essential components of neuronal circuits in the cortex (Wilson and Cowan 1972; Isaacson and Scanziani 2011; Buendía et al. 2019), as well as of gene-regulatory, signaling, and metabolic networks (Ozbudak et al. 2004; Davidson and Levin 2005).

3.1 Inhibition, balance and synchrony

In general, systems where inhibition is present posses a richer dynamical behaviour, including the possibility of limit cycles and collective oscillations. An example is the Wilson-Cowan model reviewed in the last chapter (Cowan et al. 2016). These regimes have been also studied experimentally (Chen and Dzakpasu 2010; Poil et al. 2012; Denève and Machens 2016). More in general, inhibition sheds light on the problem of dynamical range in neuroscience: each neuron in the cortex is connected to many others, but individual synapses are relatively weak, so that each single neuron needs to integrate inputs from many others to become active; for excitatory-only networks, this leads to a first-order (discontinuous) phase transition between a quiescent and an active phase (Isaacson and Scanziani 2011), so the network is either quiescent or almost saturated (Buendía et al. 2019). The existence of such a transition would severely constrain the set of possible network dynamical regimes, and hence reducing the number of possible responses to different inputs. The role of inhibition in allowing richer dynamical ranges in the real cortex has been already empirically studied (e.g., in (Pouille et al. 2009; Liu et al. 2011)) where inhibition leads to a continuous transition, allowing for smaller populations to become active. This is consistent with the well-known empirical fact that neurons in the cerebral cortex remain slightly active even in the absence of stimuli (Softky and Koch 1993; Abeles 1991; Arieli et al. 1996). In such a state of low self-sustained activity neurons fire in a steady but highly-irregular fashion at a very low rate and with little correlations among them. This is the so-called *asynchronous state*, which has been argued to play an essential role for diverse computational tasks (Rubin et al. 2017; Denève and Machens 2016; Sippy and Yuste 2013).

The current scientific consensus is that such an asynchronous irregular state emerges from the interplay between excitation and inhibition, and, in particular, from a *balance* between both. Balanced excitatory-inhibitory (E-I) networks present in average a very small input to each individual node, and they have been first predicted by models (Brunel 2000; Brunel and van Rossum 2007; Vreeswijk and Sompolinsky 1996; Vreeswijk and Sompolinsky 1998) and later empirically observed (Shu et al. 2003; Treviño 2016; Haider et al. 2006; Dehghani et al. 2016; Barral and Reyes 2016).

In spite of solid theoretical and experimental advances, many aspects of the E-I asynchronous irregular networks are not still fully

understood (Buendía et al. 2019). For instance, there has been controversy regarding whether irregular, low activity can be sustained in the absence of external inputs to the system. Although it has been argued that external inputs from stimuli or other brain areas are required in order to sustain the asynchronous irregular phase (Destexhe 2009), recent approaches have reported situations where the system spiking alone is enough to maintain the activity (Borges et al. 2020). Furthermore, it is still not clear whether the asynchronous states can present low levels of activity (Destexhe 2009; Kriener et al. 2014; Borges et al. 2020).

From the point of view of statistical physics, these problems can be summarized in one question: is the asynchronous state a well-defined macroscopic phase, as the quiescent and active phases? Or does need external input in order to be stable? If it constitutes a novel phase, what are the phase transitions at its boundaries? Models such as the classical model by Brunel (Brunel 2000) predict phase boundaries between synchronous regular and asynchronous irregular phases –under the presence of external stimuli. Understanding these boundaries could and shed light on the criticality hypothesis, which is the main objective of this thesis. In particular, we are interested in the interface between synchronous and asynchronous transitions, so understanding how the asynchronous irregular state emerges could be of great value for us.

In order to tackle this problem, we study a simple neuronal stochastic model in an attempt to construct a parsimonious approach for E-I networks. We demonstrate, both analytically and computationally, that inhibitory interactions in combination with sparse networks lead to a stable, self-sustained phase of low activities, which lies between the conventional quiescent and active phases. Remarkably, this new phase emerges from fluctuations into node inputs owing to the combined effect of inhibition and network sparsity. The low-activity intermediate phase (LAI phase) shares all its fundamental properties with asynchronous states, so we argue that the model constitutes the simplest possible statistical-mechanics representation of asynchronous endogenous cortical activity (Buendía et al. 2019).

3.2 Jensen's force and asynchronous states

In an engaging paper by Larremore *et al.*, it was argued that inhibition induces "ceaseless" activity in networks with excitation and inhibition (Larremore et al. 2014). This is a counterintuitive result, since inhibition does not "generate" activity. Though it was already briefly discussed in Chapter 2, here we give all the detailed computations not only under the mean-field approximation, but for any network topology, shedding light on the dynamics of the asynchronous irregular state, remarking the role of sparsity in neuronal systems.

3.2.1 Mean-field vs sparse networks

The simplest approach to capture the basic elements of E-I networks are two-state neuron models (Vreeswijk and Sompolinsky 1996; Rubin et al. 2017). We work here with a model recently proposed by Larremore *et al.* (Larremore et al. 2014), but simplifying the ingredients relative to network topology. The network has N nodes or neurons, where a fraction α is inhibitory, and the rest are left as excitatory. In simulations we take fixed $\alpha = 0.2$, as observed in experiments (Soriano et al. 2008; Barral and Reyes 2016). We consider the connectivity graph to be an undirected hyperregular network, meaning that each node will have exactly k neighbours, but also that each of them receives exactly $k\alpha$ inhibitory connections and $k(1-\alpha)$ excitatory ones. A small network is shown in Figure 3.1. The steps followed to construct such networks are the following:

1. Two random regular networks, one purely excitatory and one purely inhibitory are generated, with connectivities $k(1-\alpha)$ and $k\alpha$, respectively.

2. Then, the inhibitory nodes need still $k(1-\alpha)$ links in order to have k in total. Therefore, for each inhibitory node, $k(1-\alpha)$ excitatory nodes are randomly chosen. The inhibitory node is mutually connected with the chosen excitatory ones. An excitatory

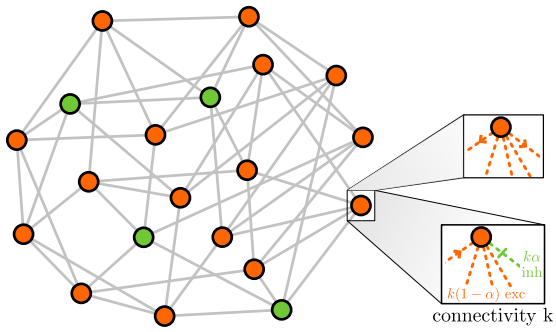

Figure 3.1: **An example of hyper-regular network.** Hyper-regular network with $N = 20$ nodes and connectivity $k = 5$. Orange nodes are excitatory, while green ones are inhibitory. The out- and in- connectivity for a particular node are also displayed. Note that when the node is mutually connected to five other neurons, the out-connection for the inhibitory node is excitatory, while the in-connection is inhibitory.

node is susceptible to be picked if it has less than k links (so it still needs inhibitory inputs), and the link is not repeated. This simple procedure can get stuck at the end, meaning that it is sometimes not possible to fulfill all the requirements. To avoid such a pitfall, the network is restarted after a large number of unsuccessful attempts to generate the links.

The state of each neuron is modelled by a Boolean variable, being either active when $s_i = 1$ and inactive when $s_i = 0$. For simplicity, time t is chosen to advance in discrete steps. At each step, each node i integrates the activity of its neighbours, becoming active at $t+1$ with a probability $\mathcal{P}_i$ given by

$$\mathcal{P}_i \equiv f\left(\Lambda_i = \frac{1}{k}\sum_{j=1}^{N} A_{ij} s_j(t)\right) = \begin{cases} 0 & \Lambda_i < 0 \\ \Lambda_i & 0 \le \Lambda_i \le 1 \\ 1 & \Lambda_i > 1 \end{cases}, \tag{3.1}$$

where $f(\Lambda_i)$ is a transfer function of the input Λ_i received by the i-th node, and A_{ij} is the weighted adjacency matrix of the graph. For simplicity, we set $A_{ij} = +\gamma$ for excitatory connections, and $A_{ij} = -\gamma$

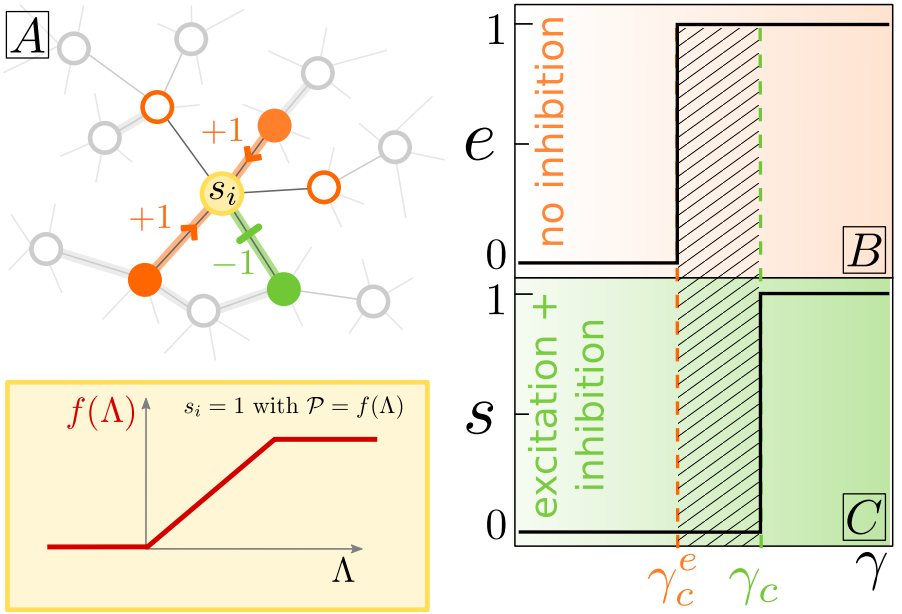

Figure 3.2: **A simple model for inhibition. A.** Sketch of the network dynamics. The yellow node receives (weighted) input from the active neighbours (filled circles), and activates following the transfer function shown below. **B.** Average activity in a mean-field network consisting of $N(1-\alpha)$ excitatory nodes, exhibiting a first-order first transition between the quiescent and the fully active states at $\gamma_c^e = 1/(1-\alpha)$. **C.** As before, but now we add $N\alpha$ inhibitory nodes. The phase transition is displaced to the point $\gamma = 1/(1-2\alpha)$.

for inhibitory ones. Two disconnected nodes have $A_{ij} = 0$, and self-connections are not allowed. The model is kept purposely simple in an attempt to reveal the basic mechanisms of its collective behavior, but more complex possibilities will be explored later in order to verify the robustness of the results (Buendía et al. 2019).

Let us start again by the simplest case, a mean-field approach. In Chapter 2, the Langevin equations for the system were derived in detail. Let us remark that in contrast with the notation chosen in Chapter 2, the fraction of active excitatory and inhibitory neurons $x = E/N$ and $y = I/N$ are used instead of the variables $x = E/[N(1-\alpha)]$ and $y = I/(N\alpha)$. In this way, the actual activity of the system is given just by $s = x + y$. From the microscopic rates it is possible to obtain the

Langevin equations for the fractions x, y, and then perform the change of variables $s = x + y$ and $q = x - y$, and average to eliminate the noise. The mean-field equation for the average activity $s \equiv \langle s \rangle$, $q \equiv \langle q \rangle$ is given by

$$\dot{s} = \langle f(\Lambda) \rangle - s, \tag{3.2a}$$
$$\dot{q} = (1 - 2\alpha) \langle f(\Lambda) \rangle - q. \tag{3.2b}$$

As we argued in our introduction of the model in Chapter 2, in the steady state excitation and inhibition become spontaneously balanced, which lead to $x\alpha = y(1-\alpha)$. As a consequence, in the fully-connected the input to a neuron can be written as $\langle \Lambda \rangle = \gamma q = \gamma(1-2\alpha)s$. In the thermodynamic limit, the mean-field assumption allows us to disregard the fluctuating input, $\left\langle \Lambda^2 \right\rangle = \langle \Lambda \rangle^2$. In this regime, equation (3.2) can be simplified and

$$\dot{s} = f(\gamma(1-2\alpha)s) - s \tag{3.3}$$

is exact. If γ is low, then $f(\langle \Lambda \rangle) = \langle \Lambda \rangle$ and the only fixed points are the quiescent and saturated states, $s^* = 0$ and $s^* = 1$ respectively. If γ is large enough, then $f(\langle \Lambda \rangle) = 1$ and the saturated state is the only stable equilibrium. The quiescent phase is stable below the critical value $\gamma_c = 1/(1-2\alpha)$, while at the transition point $\gamma = \gamma_c$ both states are marginally stable. Therefore, the system experiences a first-order, discontinuous phase transition at γ_c. Note that as we introduce inhibition in the system, the coupling γ_c needed to stabilise the active phase grows, as one could have expected intuitively. The nature of the transition is, however, independent of the fraction α of inhibitory neurons.

Let us move from fully-connected, mean-field populations, to simulations of the model in large, sparse networks. These reveal a richer phenomenology, in comparison with the mean-field case. Figure 3.3 shows the phase diagram obtained after averaging several runs, which is richer in comparison with the mean-field analysis. As the network connectivity k is reduced, the phase transition becomes progressively smoother, and a novel phase where the overall phase activity is neither 0 or 1 emerges. This intermediate phase does not appear when only excitatory nodes are considered, meaning that it has its roots in inhibition.

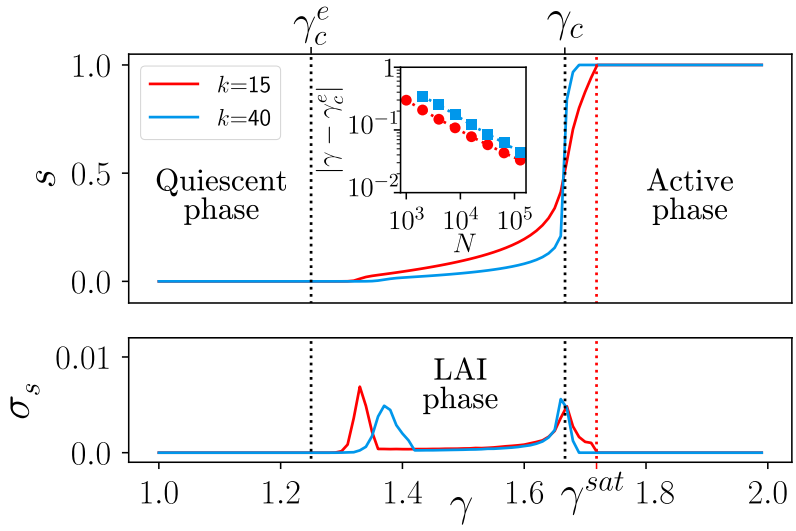

Figure 3.3: **Phase diagram of the Larremore et al. model**. The average value of activity (top) and its variance (bottom) across runs for the E-I hyperregular network is plotted against the control parameter, the coupling γ between nodes. The variance presents two peaks, indicative of phase transitions: one comes from the mean-field transition γ_c, while the other converges to the excitatory-only prediction γ_c^e as we approach the thermodynamic limit (see inset). Between both transitions, we find a low-activity phase, not previously predicted by the mean-field approach. Parameters: $N = 16000$, $\alpha = 0.2$. Results were averaged over 10^4 MonteCarlo steps, across 10^3 runs.

In order to assess the variability of the network, we measured the ensemble variance σ^2 across simulations. First, we compute the average activity over a long time window, obtaining an average value $\bar{s}$. We then compute averages and variance over the set of $\bar{s}$ obtained in different realizations (see Fig. (3.3)). The variance displays two marked peaks, which suggest the presence of two phase transitions (Binney et al. 2001; Henkel et al. 2008). The first corresponds to an absorbing-active transition from the quiescent to the LAI phase. The exact location of this transition, denoted by γ_c^e, depends on the system size. When the thermodynamic limit $N \to \infty$ is taken, it approaches to the location of the excitatory-only mean-field transition

with $N(1-\alpha)$ units, $\gamma_c^e = 1/(1-\alpha)$ (see Fig. 3.2) , which justifies the notation with superindex e. On the other hand, the second peak lies at $\gamma_c = 1/(1-2\alpha)$, which is the same location of the mean-field discontinuity for the fully connected networks. These two transitions delimit the LAI phase (Buendía et al. 2019). It is also possible to analytically locate the saturation point γ^{sat}, at which all network nodes become active. When we approach the mean-field limit (as $k \to \infty$) both points γ_c^e, γ^{sat} converge to γ_c making the transition discontinuous.

In order to understand the novel LAI phase, it is essential to realise that in the sparse connectivity case, the input received by a given node does not necessarily take its mean-value, being a stochastic variable, and thus making necessary to consider eq. (3.2), rather than its mean-field counterpart (Buendía et al. 2019). It turns out that to compute the average $\langle f(\Lambda) \rangle$, one only needs to determine the probability distribution of the inputs. Assuming that all nodes are statistically equivalent (since we are in a hyperregular network), then one only has to focus on the number of active neighbours of the node. If j is the number of active excitatory neighbours and l is the number of active inhibitory ones, then the input is just given by $\Lambda = \gamma(j-l)/k$. Therefore, in order to obtain the distribution $p\left(\Lambda_{jl}\right)$ it suffices to obtain the probability of picking active neighbours. In the original work of Larremore *et al.* (Larremore et al. 2014) the approach is to work with the network architecture, thus analysing the spectral properties of the adjacency matrix. Instead of using the "quenched" architecture, we propose to simplify even more the problem: consider that at each time step, the node *randomly selects* $k(1-\alpha)$ excitatory nodes and $k\alpha$ inhibitory ones, i.e., an "annealed" version of the original model. As it can be seen in Fig. 3.4, numerical computations confirm that annealed and quenched (hyperregular) versions of the model are exactly equivalent, and can be used interchangeably (Buendía et al. 2019).

The advantage of the annealed version is that it simplifies the analytical computations of the averages. Let us assume that of the k nodes randomly chosen, n turn out to be inhibitory. Hence, if we denote by $p(j|k-n)$ the probability of finding j active excitatory nodes out of $k-n$ excitatory ones, and do the same with the inhibitory population, then $p\left(\Lambda_{jl}|n\right) = p(j|k-n)\,p(l|n)$. If the average activity of the network at this time is $s(t)$, then a random node will be active with probability

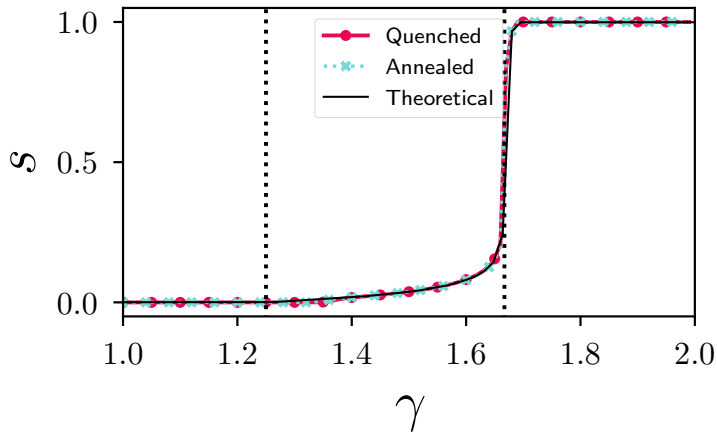

Figure 3.4: **Comparison between annealed and quenched networks.** The simulation results are marked with symbols, while the analytical solution is drawn in a black line. The agreement between both sets of data with analytical results is excellent. Parameters: $k = 40$, $N = 16000$. Analytical solution was evaluated solving eq. (3.2), evaluating exactly $\langle f(\Lambda)\rangle$ via the numerical computation of the sum eq. (3.5).

$s(t)$, regardless of its type due to the balance condition. Therefore, the probability $p(l|n)$ is given by the binomial distribution,

$$p(l|n) = \binom{n}{l} s^l (1-s)^{n-l}, \tag{3.4}$$

and the same goes for $p(j|k-n)$. Finally, the probability to find an arbitrary input can be readily written as

$$p\left(\Lambda_{jl}\right) = \sum_{n=0}^{k} \delta_{n,k\alpha}\, p\left(\Lambda_{jl}|n\right) = \binom{k\alpha}{l}\binom{k(1-\alpha)}{j} s^{j+l}(1-s)^{k-j-l}, \tag{3.5}$$

where the first Kronecker delta is introduced because the number of inhibitory nodes that we pick in every timestep is fixed. Now we see that the probability to obtain certain input at the microscopic level depends only on the average activity of the network, so $p\left(\Lambda_{jl}\right) \equiv p_{lj}(s)$. Using eq. (3.5) it is possible to evaluate any averages involving functions of

the input. In particular,

$$\langle \Lambda \rangle = \sum_{j=0}^{k-n} \sum_{l=0}^{n} p_{lj}(s) \Lambda_{jl} = \tilde{\gamma} k s (1-2\alpha) = \gamma s (1-2\alpha), \tag{3.6a}$$

$$\langle \Lambda^2 \rangle = \tilde{\gamma}^2 \Big[k s^2 \Big((1-2\alpha)^2 k - 1 \Big) + k s \Big], \tag{3.6b}$$

where $\tilde{\gamma} = \gamma/k$ in order to make the notation simpler. Then, input fluctuations can be analytically computed as

$$\sigma^2(\Lambda) = \tilde{\gamma}^2 k s (1-s). \tag{3.7}$$

Note that the variance scales as $\sigma^2(\Lambda) \sim 1/k$, meaning that fluctuations in the input go to zero in the mean-field limit where $k \to +\infty$. Actually, the standard deviation scales as $k^{-1/2}$, as expected from the central limit theorem, a result often found in the balanced network literature (Vreeswijk and Sompolinsky 1996; Barral and Reyes 2016). The activity $s = 1/2$ maximizes fluctuations, coinciding with the mean-field situation at $\gamma = \gamma_c$.

Given the probability eq. (3.5) it is possible to evaluate $\langle f(\Lambda) \rangle$. In this case, the non-linearity of the transfer function prevents us from obtaining a closed form, although the sum can be numerically computed with ease. The numerical solution to equation (3.2) is shown in Fig. 3.4, and it fits exactly the simulation results. Therefore, this approach, taking in account all fluctuations, is able to solve exactly the problem of the emergence of the novel LAI phase.

Moreover, the critical points can be obtained analytically, by Taylor expanding eq. (3.2) in order to obtain information about the behaviour of the system near $s^* = 0$ and $s^* = 1$. Let us start near the quiescent phase. Equation (3.5) contains the term $s^{j+l}(1-s)^{k-j-l}$, so for k large enough and $j + l \geq 2$ the term $(1+s)^{k-j-l} \sim \mathcal{O}\left(s^2\right)$. Then, the only pairs (j,l) that contribute to first order in activity are $(0,0)$, $(1,0)$, and $(0,1)$. Noting that $f(\Lambda_{00}) = f(\Lambda_{01}) = 0$, we get

$$\langle f(\Lambda) \rangle \simeq f(\tilde{\gamma}) \binom{n}{0} \binom{k-n}{1} s (1-s)^{k-1} \simeq k s f(\tilde{\gamma})(1-\alpha) + \mathcal{O}\left(s^2\right). \tag{3.8}$$

When this result is plugged into eq. (3.2), a simple bifurcation analysis shows that the quiescent state loses its stability at $\gamma = \gamma_c^e =$

$1/(1-\alpha)$. After the bifurcation, the activity tends to increase, rendering the first-order analysis useless, except near γ_c^e. For values of the coupling slightly larger than the critical point, the activity scales as $s \sim 1/k$, in accordance of what was observed by Larremore *et al.* (Larremore et al. 2014).

For the saturation of the activity it is possible to follow the same procedure near the point $s^* = 1$. The pairs that contribute to first order around this value are $(k-n, n)$, $(k-n-1, n)$, and $(k-n, n-1)$. Observe that $f\left(\Lambda_{jl}\right)$ is non-vanishing for the three terms, so now we have to deal with

$$\langle f(\Lambda)\rangle = f(\Lambda_0)[1+k(1-s)] + (1-s)(k-n)f(\Lambda_-) + nf(\Lambda_+) \tag{3.9}$$

where we have defined $f(\Lambda_0) \equiv f[\tilde{\gamma}(k-2n)]$ and $f(\Lambda_\pm) \equiv f[\tilde{\gamma}(k-2n\pm 1)]$. Thus, depending on the synaptic strength, some of the transfer function terms may saturate, becoming 1. If $\gamma > \gamma_c$, then always $f(\Lambda_0) = f(\Lambda_+) = 1$, and the bifurcation analysis gives us the value at which the fixed point $s^* = 1$ loses stability,

$$\gamma^{sat} = \frac{1-k(1-\alpha)}{(1-\alpha)-k(1-\alpha)(1-2\alpha)}, \tag{3.10}$$

which coincides accurately with numerical results. Finally, if none of the transfer functions saturate, we recover again the expression of γ_c. Thus, in contrast with mean-field expectations there exists a whole intermediate region, $\gamma_c^e < \gamma < \gamma^{sat}$, where activity does not vanish nor saturate. Such a region emerges as a consequence of input fluctuations and, hence, stems from network sparsity (Buendía et al. 2019). When inhibition is not present, i.e., when $\alpha = 0$, then $\gamma_c^e = \gamma^{sat}$ and the intermediate region vanishes.

3.2.2 Jensen's force

If we want to understand the origin of the LAI phase beyond the perturbative analysis, we must notice that the difference between the exact result and the mean approximation is just that $\langle f(\Lambda)\rangle \neq f(\langle\Lambda\rangle)$. Then, the non-trivial effects in the sparse network stem from the difference between both, as

$$F(\tilde{\gamma}, s) \equiv \langle f(\Lambda)\rangle - f(\langle\Lambda\rangle). \tag{3.11}$$

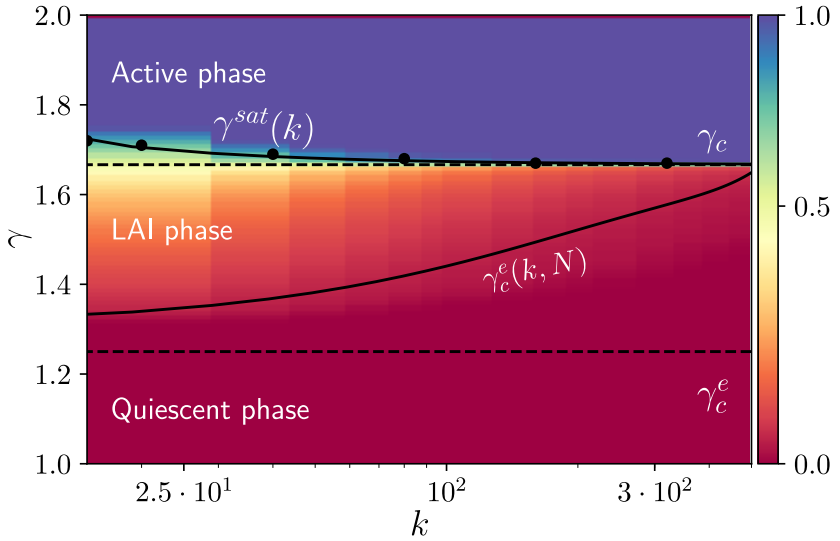

Figure 3.5: **Phase diagram as a function of the connectivity.** Horizontal dashed lines indicate the position of the discontinuous transition in mean-field, both for only excitatory populations and for E-I systems. Background colour codes average simulated activity. The curve $\gamma^{sat}(k)$ is obtained from eq. (3.10), while points are simulation-obtained values for comparison. The curve $\gamma_c^e(k,N)$ is obtained by interpolating simulation values, and it gives the transition from the quiescent to LAI phases. Note that formally $\gamma_c^e(k,N\to\infty)=\gamma_c^e$, but as we approach the mean-field limit larger sizes are needed to appreciate this effect. System size for all simulations was $N = 16000$.

Since the terms in the right hand are functions of the activity s, then $F(\tilde{\gamma},s)$ can be interpreted as a stochastic force. We showed above that the fluctuations of inputs to any given node scale as $\sigma \sim k^{-1/2}$, as expected by the central limit theorem. If the transfer function f was linear, then we would have $\langle f(\Lambda)\rangle = f(\langle\Lambda\rangle)$, but if f was a convex[1] function, then Jensen's inequality of statistics implies that $\langle f(\Lambda)\rangle > f(\langle\Lambda\rangle)$. Note that indeed the transfer function f is convex near the origin, due to its definition as a piecewise function where $f(\Lambda \le 0) = 0$, and concave near $\Lambda = 1$, since it saturates as $f(\Lambda \ge 1) = 1$. Then, for low inputs,

[1] Here "convex" means with the positive second derivative, as in $y = x^2$.

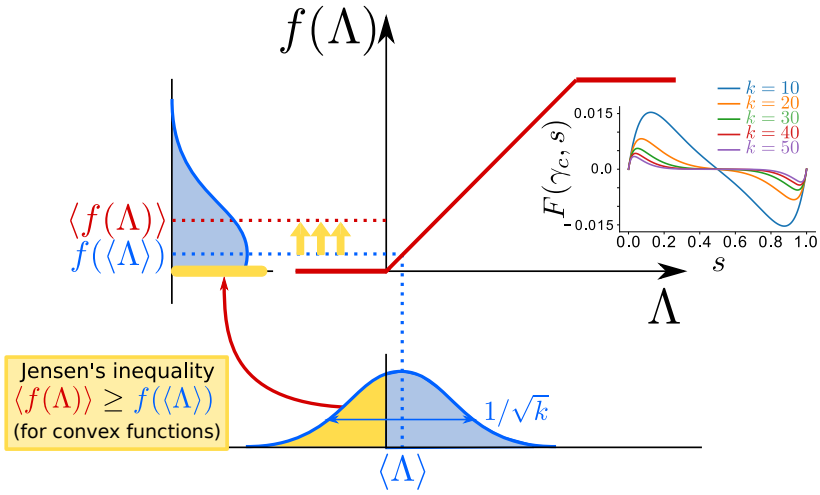

Figure 3.6: **Origin of the Jensen's force.** The input received by a node in the network is a random variable distributed with mean $\langle\Lambda\rangle$ and standard deviation $\sigma(\Lambda) \sim 1/\sqrt{k}$, sketched below the axes. The distribution is mapped through the transfer function $f(\Lambda)$; since the transfer function is convex at the origin, the mapping for low inputs fulfills Jensen's inequality –so $f(\langle\Lambda\rangle)$ (blue) is mapped below $\langle f(\Lambda)\rangle$ (red), due to negative inputs mapping all to zero. The inset shows the Jensen's force $F(\gamma = \gamma_c, s)$ for different connectivity values.

it is clear that $F(\tilde{\gamma}, s) > 0$, while for large inputs, $F(\tilde{\gamma}, s) < 0$.

For this reason, we propose to call $F(\tilde{\gamma}, s)$ *Jensen's force*. This force is positive for low values of the inputs, and hence responsible for destabilizing the quiescent state, pushing activity to grow, and generating the LAI phase. On the other hand, when the input is high and the transfer function is near saturation, then the concavity of f causes a negative Jensen's force that decreases the activity, justifying the reduction of the activity near γ_c with respect to the mean-field predictions (see Figure 3.6). However, note that both phases, $s = 0$ and $s = 1$, are absorbing when stable, so the system will stay in them without fluctuations if they are reached. In general, Jensen's force can be computed numerically, as in Fig. 3.6, where it can be seen how its magnitude decreases as the connectivity grows. In some cases, it is possible to obtain an analytical closed form for $F(\tilde{\gamma}, s)$. We will show an example later, generalising our results for different shapes of the transfer functions.

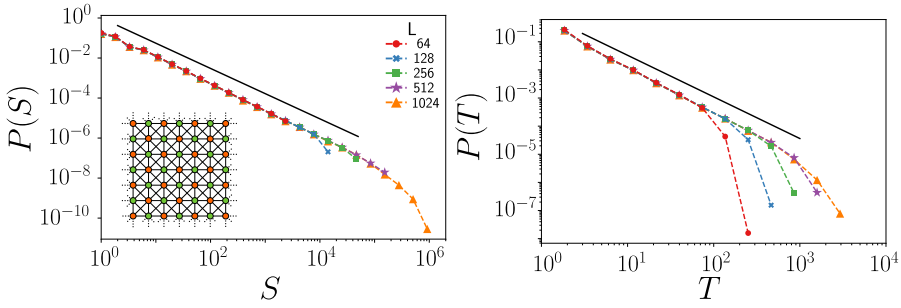

Figure 3.7: **Avalanche size and durations for 2D systems.** The exponents are those predicted by the directed percolation universality class. Avalanches present excellent finite size scaling. Lattice construction is as shown in the leftmost inset, with excitatory neurons being orange, and inhibitory neurons being green.

Summing up, the sparsity-induced Jensen's force is responsible for the emergence of a LAI phase in E/I networks below the mean-field critical point, γ_c as well as for a reduction in the overall level of activity with respect to the mean-field limit in a region above γ_c (Buendía et al. 2019).

3.2.3 The boundaries of the LAI phase

The LAI phase is surrounded by two phase transitions, as demonstrated by the variance peaks in Figure 3.3. At the leftmost one, γ_c^e, an absorbing-active transition takes place. We performed standard avalanche analysis for non-equillibrium systems, as explained in the first chapter and Appendix A: the absorbing state was perturbed with a small amount of activity –making active just one excitatory node– and analysed the statistics of duration and size to return to the quiescent phase.

Numerical experiments reveal that at the quiescent-active critical point γ_c^e, the system displays scale-free distributed avalanches, with exponents compatible with those of the unbiased branching process (Henkel et al. 2008; di Santo et al. 2017). Actually, the critical exponents obtained at this transition in lower dimensional networks (such as the two-dimensional lattice) are compatible with those of directed

percolation universality class (Hinrichsen 2000; Henkel et al. 2008). However, the model does not present correlation among different avalanches, which is typical of experimental settings (Bellay et al. 2015). On the other hand, no sign of scale-free critical avalanches could be found at the second point γ_c; this could be explained from the fact that this second transition becomes discontinuous in mean-field.

It is important to remark that the analysis performed here was the formal one employed in non-equillibrium physical systems, while in neuroscience the experimental procedure is different (see Appendix A). Therefore, comparing both procedures is essential in order to understand avalanche dynamics, and rule out any actual link with the experiments.

3.2.4 The asynchronous irregular state

It is possible to demonstrate that the novel LAI phase represents the so-called asynchronous irregular state in cortical networks. This state is characterised by several key features, which include the following: large variability, as measured by the coefficient of variation (see Appendix A) (Softky and Koch 1993); the average Pearson correlation among pairs of neurons decays with the system size, reflecting a lack of coherent behaviour (Destexhe 2009; Renart et al. 2010; Harris and Thiele 2011); and there is a short time lag between the temporal series of excitation and inhibition, usually known as *E-I lag*. This lag happens because excitation tends to increase activity, just to be rapidly compensated by inhibition. In this way, inhibition acts as a regulatory mechanism, actively decorrelating neuronal populations and stabilizing the activity, as it was first theoretically predicted (Ginzburg and Sompolinsky 1994; Brunel and Wang 2003; El Boustani and Destexhe 2009; Renart et al. 2010) and later confirmed by experiments (Okun and Lampl 2008; Sippy and Yuste 2013).

The LAI phase displays all these key features, as shown in Figure 3.8. In particular, the coefficient of variation is slightly over unity at the LAI phase, but vanishes both in the quiescent and active phases. More complex network topologies or transfers functions could help to obtain larger values of the CV, close to those observed in experiments

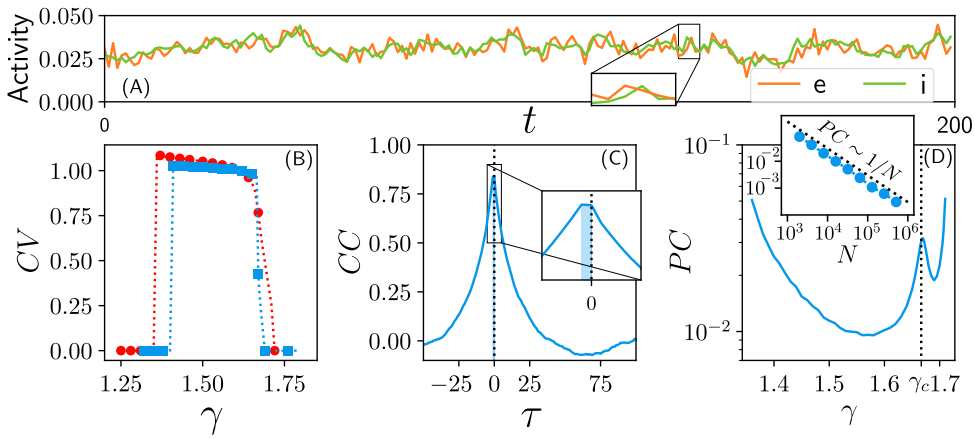

Figure 3.8: **Features of the asynchronous irregular state. (A)** Temporal series of the activity of both excitatory and inhibitory populations. The zoom shows how excitation slightly precedes inhibition. **(B)** Coefficient of variation as function of the coupling strength; high values ($CV \sim 1$) are obtained only in the LAI phase. **(C)** Cross-correlation $CC(\tau)$ of the excitatory and inhibitory time series. Maximum correlation, which is close to unity, is reached at $\tau = -1$, showing that the inhibitory population lags behind the excitatory one. **(D)** Average pairwise correlations are very small and tend to decrease with system size, as shown in the inset. Computations were performed for a network with $N = 16000$ nodes, during 10^4 time steps; pairwise correlations are computed sampling 500 random pairs, averaging over 1000 different networks.

(Bellay et al. 2015). As demonstrated by the cross-correlation, there is also an excitation-inhibition lag of just one timestep, so inhibitory neurons tend to follow excitatory activity delayed by just one step. Finally, average correlation between any pair of neurons in the system is measured is very small, and tends to decrease with the system size as $PC \sim 1/N$, implying that at the thermodynamic limit neuronal spiking is completely decorrelated.

Moreover, in agreement with the original claim for asynchronous states (Vreeswijk and Sompolinsky 1996; Vreeswijk and Sompolinsky 1998), we verified that the dynamics is chaotic exclusively at the LAI phase (Buendía et al. 2019). In order to do that, we analysed the dy-

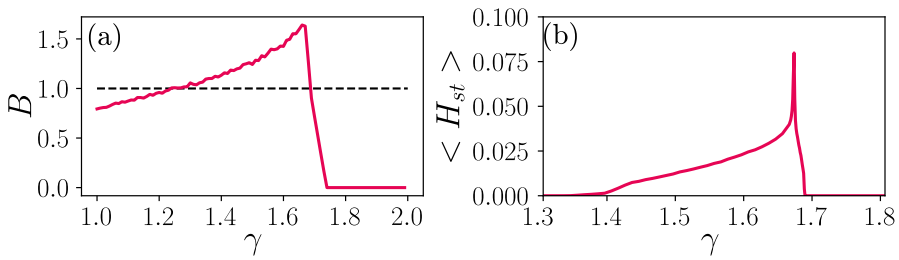

Figure 3.9: **Damage spreading experiment.** (a) The branching parameter $B > 1$ only in the LAI phase, meaning that the intermediate phase has chaotic dynamics. (b) The average Hamming distance used to obtain the branching parameter. Remarkably, maximum distance is reached at with the maximum situated at γ_c, while both quiescent and active phases have a distance close to zero.

namics of a damage spreading process. Two replicas of the model are created, and one of them is slightly perturbed. Both are simulated at the same time, computing the Hamming distance H between them[2]. The Hamming distance is averaged over many realizations of the model, allowing us to obtain the branching parameter B. If $B > 1$, perturbations tend to grow, meaning that the network is posed at a chaotic state, while if $B < 1$ the network tends to eliminate the perturbations with time. The value $B = 1$ is a critical point. The result of these measures is shown in Figure 3.9, where indeed a value $B > 1$ is obtained all across the LAI phase. Therefore, we find chaotic behaviour as suggested for the asynchronous irregular states. The Hamming distance at the LAI phase has values compatible with those of the network activity s, meaning that after some time the system decorrelates completely. Thus, in synthesis, all the chief features of cortical asynchronous states are also distinctive and exclusive characteristics of the LAI phase (Buendía et al. 2019).

[2]Given two strings, the Hamming distance is the number of positions at which both strings have different symbols.

3.3 Model Generality

3.3.1 Network balance

Is it possible to maximize the span of the LAI phase? If so, asynchronous irregular states would emerge without any need for fine tuning parameters, just by increasing the width of the interval $[\gamma_c^e, \gamma_c]$. We discovered that a possibility to achieve this is using tightly balanced networks, also known as detailed balanced networks (Vogels and Abbott 2009; Denève and Machens 2016). In these networks, the mean input received by each neuron is $\langle \Lambda \rangle \simeq 0$, so excitation and inhibition are almost perfectly compensated. To achieve it, we set different strength for excitatory and inhibitory synapses, ω_e and ω_i, as we did in Chapter 2. This shifts the critical points, being $\gamma_c^e = 1/(\omega_e(1-\alpha))$ and

$$\gamma_c = \frac{1}{(\omega_e(1-\alpha) - \omega_i \alpha)}. \tag{3.12}$$

Here γ_c^e only depends on ω_e, so it is fixed, while ω_i can be tuned in order to change $\gamma_c \to +\infty$. Let us remark that making the denominator vanish also leads to $\langle \Lambda \rangle = \gamma\,(\omega_e x - \omega_i y) = \gamma s\,(\omega_e(1-\alpha) - \omega_i \alpha) = 0$, i.e., to the tightly balanced state. Thus, tightly balanced networks maximize the span of the LAI phase.

It is important to observe that two different, alternative concepts of balance appear here simultaneously. The first one, dynamical balance, leads to $x\alpha = y(1-\alpha)$ so $x = (1-\alpha)s$ and $y = \alpha s$, and it is always reached after some simulation time, independently of ω_e and ω_i. This corresponds to the necessary condition to have a fixed point discussed earlier in Chapter 2, and it is related with the fact that activity does not distinguish between excitatory and inhibitory nodes; however, dynamical balance is compatible with an input $\langle \Lambda \rangle \neq 0$ –which has been the case during the whole text so far. Tight balance is a stronger constrain that forces the average input to vanish (Denève and Machens 2016).

3.3.2 Non-linear transfer functions

One could argue that the effect of the Jensen's force could be due to the piecewise linear shape of the transfer function, or the discontinuous nature of the transition induced by this choice. Here we demonstrate that the effects discussed above are largely independent of the transfer function choice, as long as Jensen's inequality holds.

In order to do so, let us return for a moment to the mean-field approximation, so $\langle f(\Lambda)\rangle = f(\langle\Lambda\rangle)$ with $\langle\Lambda\rangle = \gamma(1-2\alpha)s$. Then, the equation for the activity reads $\dot{s} = f(\langle\Lambda\rangle) - s$, whose bifurcation diagram strongly depends on the choice of the transfer function. Following again the basic ideas of statistical mechanics and dynamical systems, we could just expand the transfer function for low inputs, obtaining then a "Landau expansion". From the point of view of dynamical systems, this give us different normal forms of bifurcations near the quiescent state, allowing us to shape the mean-field phase diagram at our will. Then, we set

$$f(\Lambda) = a\Lambda + b\Lambda^2 + c\Lambda^3 + \ldots, \tag{3.13}$$

where a, b and c are free parameters. Note that, since we are letting $\Lambda = \langle\Lambda\rangle \propto s$, the linear term a can absorb the linear term of the mean-field equation (3.3). The choice of signs of the free parameters will determine the behaviour of the stable equillibria of our system. For example, the original (linear) piecewise function corresponds to $b = c = 0$, and has a discontinuous transition at $a_c = 0$. Figure 3.10 shows different mean-field phase diagrams corresponding to different parameter choices. In the Figure, the terms kept in the expansion are odd polynomial powers, to resemble the Taylor expansion of the usual sigmoid function $f(\Lambda \geq 0) = \tanh\Lambda$.

In all the cases shown in Figure 3.10, the LAI phase is still present when the model is studied in sparse E-I networks, as we demonstrate in Figures 3.11 and 3.12. Let us focus first on the continuous transition. In this case, one could wonder if the low-activity in the LAI phase is dynamically different from the arbitrary low activity that the system presents near a continuous transition. This question is equivalent to asking whether the active phase emerging after a second-order, continuous transition, is also an asynchronous irregular regime. The

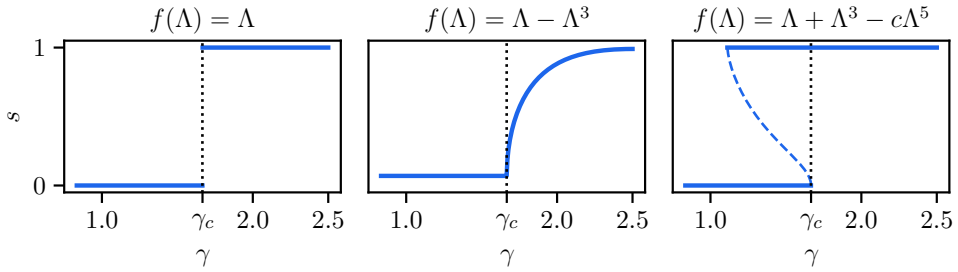

Figure 3.10: **Mean-field phase diagrams with different non-linear transfer functions. (Left)** The linear term is the choice used during the analysis **(Center)** Keeping the first term and adding a negative cubic for stabilization leads to a continuous transition (pitchfork bifurcation). **(Right)** If we make both terms positive and add $-\Lambda^5$ to stabilise, we find bistability around a hysteretic cycle. Discontinuous blue line shows unstable equillibria.

answer is given by the computation of the CV and CC, which are illustrated in Figure 3.11. During the LAI phase, both the coefficient of variation and the cross-correlation among populations are fairly high. When we enter into the active phase, both observables start to decrease immediately, indicating that the dynamical regime of the active phase is not an asynchronous state. Therefore, the dynamical properties of the LAI phase cannot be found in a regular active phase, even when this also displays relatively low activity (Buendía et al. 2019).

Moreover, following the Landau approach, it is possible to analytically estimate the value of the Jensen's force. When the transfer function is expanded in Taylor series, we can obtain Jensen's force by computing the infinite series

$$F(\Lambda) = \sum_{n=0}^{+\infty} \frac{f^{(n)}(0)}{n!} (\langle \Lambda^n \rangle - \langle \Lambda \rangle^n), \tag{3.14}$$

for positive inputs. As we saw before, it is possible to evaluate the moments of the distribution $\langle \Lambda^n \rangle$ using eq. (3.5), and then obtain an analytic approximation to any order. If we use, for example, $f(\Lambda \geq 0) = \tanh \Lambda$, we get, up to third order, that

$$F(\Lambda) \equiv F(s) \simeq \frac{\gamma^3}{3} \alpha(1-\alpha)(1-2\alpha) k s(1-s)(1-2s), \tag{3.15}$$

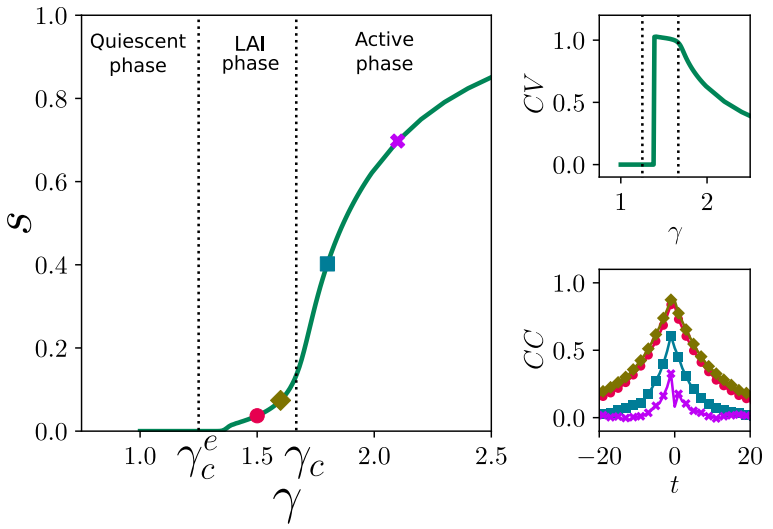

Figure 3.11: **The LAI phase is different from active phases.** Left, phase diagram obtained in a sparse hyperregular network, using $f(\Lambda \geq 0) = \tanh \Lambda$, which induces a continuous phase transition. Observe that the LAI phase still emerges between the quiescent and the active phases. At right, the coefficient of variation (top) and cross-correlations (bottom) at selected coupling values –marked in the left phase diagram. The CV is larger than one only in the LAI phase, decreasing fast; the correlations decrease as we go into the active phase. Parameters: $N = 16000$, $k = 40$.

which tell us that Jensen's force vanishes at $s = 0$, $s = 1$, and $s = 1/2$, as obtained in Fig. 3.6 for the linear piecewise function[3]. Note that the first term contributing to $F(s)$ is the third moment. In the tightly balanced case, the mean-field equation is given just by $\dot{s} = F(s)$, which turns out to be of the form $\dot{s} = as - bs^2$, that displays a continuous quiescent-active transition only.

Now we move to the case where the response function has bistability and hysteresis. Does the LAI phase coexist with the active or

[3]Note, however, that the piecewise definition prevents the hyperbolic tangent function to be derived at $\Lambda = 0$. Although it is possible to assume that the expansion formally holds for larger input values, it does not give all the contribution to Jensen's force: If we apply this procedure to the piecewise linear function, we get $F = 0$ exactly, so all Jensen's force is coming from the discontinuity in the derivative.

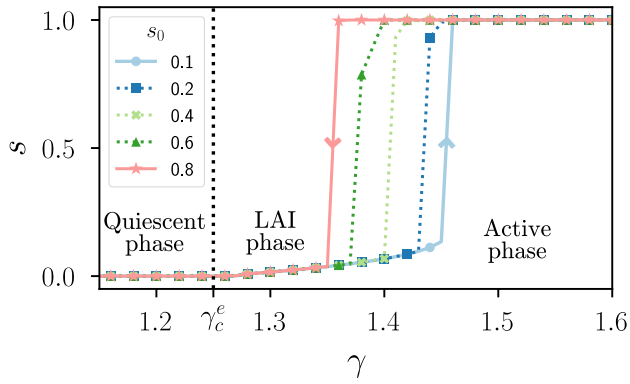

Figure 3.12: **Bistability between the LAI and the active phase.** Phase diagram using the transfer function $f(\Lambda \geq 0) = \Lambda + \Lambda^3 - \Lambda^5$. Simulations were run using different initial conditions on the activity $s(0)$, in order to detect the hysteresis cycle. There is bistability between the LAI phase and the active phase in a large interval couplings. Parameters: $N = 128000$ and $k = 15$.

quiescent phases? Considering $f(\Lambda) = \Lambda + \Lambda^3 - \Lambda^5/2$, we run simulations for different initial conditions, obtaining the results shown in Figure 3.12: the quiescent phase destabilises first to the LAI phase. As we keep increasing γ, a stable active branch appears, coexisting with the LAI phase. This continues for a while, until the LAI phase becomes unstable, leaving only the active phase. Therefore, there is a bistable region between the active and LAI phases.

3.3.3 Network structure

As it was discussed earlier, the simulations for annealed and quenched hyperregular networks give the same computational results, which coincide with analytics predictions. Therefore, the essence of Jensen's force mechanism is not related at all with network topology. However, we computationally verified our results in networks different from the hyperregular model. In particular, Erdös-Rényi random networks also reveal the emergence of the LAI phase, as well as using heterogeneity

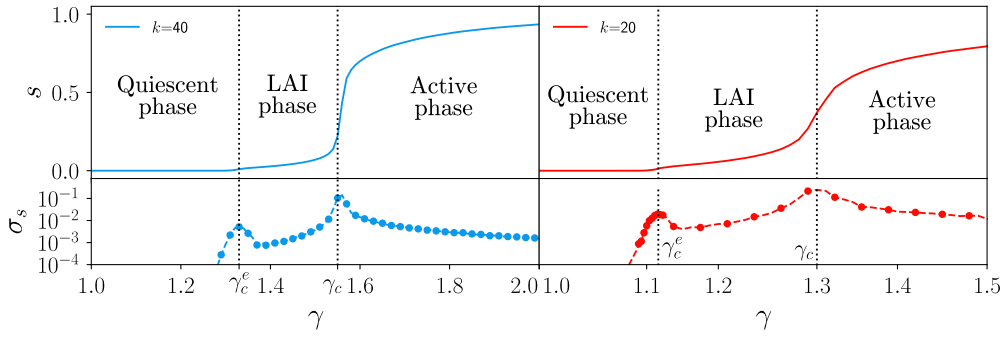

Figure 3.13: **Phase diagram for Erdös-Rényi networks.** The LAI phase emerges also on more heterogeneous networks topologies. (Left) Unweighted Erdös-Rényi network with $k = 40$. (Right) Gaussian weight distribution with $k = 20$. System size is $N = 16000$.

in the weight distribution. The results are displayed in Fig. 3.13.

From the analytical point of view, it is also possible to bring network structure into the equation. Note that in equation (3.5) we assumed that the number of inhibitory neighbours is fixed, as it happens in the hyperregular network. In a similar way, we can introduce the degree distribution $g(k)$ of the network by letting k itself to be a random variable. This generalization changes eq. (3.5) to

$$p(\Lambda_{jl}) = \sum_{k=1}^{+\infty} \sum_{n=0}^{k} \binom{n}{l} \binom{k-n}{j} g(k) h(n|k) s^{j+l} (1-s)^{k-j-l} \tag{3.16}$$

where $h(n|k)$ is the probability of having a total number of n inhibitory neighbours, given a degree k. This sum cannot be worked out analytically, but is still possible to obtain numerical results from it. For the simple case of Erdös-Rényi networks, then $g(k)$ should be a Poisson distribution, and $h(n|k)$ a binomial with probability α.

3.3.4 Experimental measurements

We have discussed ways of directly observing the effect of Jensen's forces in experimental setups. A tentative protocol for doing so would be the following:

1. Make measurements of the network firing rate $s(t)$ as a function of time. Since the firing rate has to be measured in finite time bins (see Appendix A), the activity would already be in "discrete" time steps. The next step is to compute $s(t+1)$ as a function of $s(t)$ for all times observed, and average in order to obtain good statistics. This will be an empirical estimation of the transfer function, $s(t+1) = \langle f(\Lambda) \rangle_{exp}$.

2. Extract individual neurons from the tissue under study, and obtain its associated transfer function f_{exp}. This is currently feasible (Wolfart et al. 2005; La Camera et al. 2006). Heterogeneity among neuronal populations should be averaged. $f_{exp}(\Lambda)$.

3. Using patch-clamp techniques, it should be possible to estimate the input received by a neuron in the network. Therefore, using the function f_{exp} previously determined, one could compute $f_{exp}(\langle \Lambda \rangle)$ by averaging over the input. Then, Jensen's force $F(\Lambda) = \langle f(\Lambda) \rangle_{exp} - f_{exp}(\langle \Lambda \rangle)$ can be computed.

Actually, an alternative and easier procedure to estimate the Jensen's force would be to just obtain f_{exp}, and include this realistic transfer function into simulations, which would allow us to make a numerical, rough estimation of $F(\Lambda)$. For experimental low activity states, we would expect Jensen's force to be positive, pushing the fluctuating activity to larger values.

Although we are conscious that this program is very likely to need changes and present a number of pitfalls, the experimental determination of Jensen's forces in neuronal tissues could bring new light to the study of balanced states and asynchronous irregular, low activity regimes.

3.4 Discussion

As it has been already discussed in the thesis, cortical regions present diverse levels of synchronization (Latham et al. 2000; Brunel 2000). Although the role of collective, synchronous spiking has been long studied (Buzsáki 2006) the function of the background asynchronous ac-

tivity has remained more elusive (Renart et al. 2010). Now, scientific consensus is that such a state emerges from an interplay of (balanced) excitation and inhibition, which is essential for stability and computational capabilities (Sippy and Yuste 2013; Rubin et al. 2017; Sadeh and Clopath 2020).

The main goal of this chapter was to elucidate the origin of low-activity regimes in simple E-I networks, through the statistical mechanics approach. The idea was to make the model as simple as possible, containing the minimum ingredients able to generate stable low-activity phases in the thermodynamic limit. In order to do so, we employed a model proposed by Larremore *et al.* (Larremore et al. 2014), that was later simplified. Their original approach used an Erdös-Rényi directed network, with uniform distributed weights. We eliminated all these heterogeneities, moving to the fixed-coupling, hyperregular network approach.

The study of this minimal model reveals a non-trivial low-activity phase that emerges between the standard quiescent and active phases. The necessary ingredients for the LAI phase to emerge are network sparsity, and dynamical balance between the excitatory and inhibitory populations. These are enough in order to produce fluctuations in the inputs received by the neurons, even in an extremely homogeneous setup. The fact that heterogeneity is not necessary to generate the LAI phase rules out underlying phenomena such as *Griffiths phases* to be an explanation its emergence. Griffiths phases are similar, appearing in the middle between quiescent and active phases, and it has been claimed that they could play a relevant role in cortical dynamics (Moretti and Muñoz 2013). However, Griffiths phases emerge only due to structural heterogeneity, so it they are not related with the new LAI phase. Still, it would be worth to study the effect of heterogeneities in the asynchronous irregular states, an issue that could unveil new phenomena (Litwin-Kumar and Doiron 2012).

Another important issue to remark is the effect of neuronal threshold. The nodes do not have any spiking threshold, since a single active excitatory neighbour is able elicit activation, even when the probability γ/k is low. Near γ_c^e, the activity is of order $s \sim 1/k$. Therefore, for large connectivities, very large system sizes are needed in order to see the LAI phase, specially near γ_c^e. Thresholds imply that there a minimum amount of activity is required to cause an activation. As

a consequence, large neuronal thresholds hinder the asynchronous irregular phase. For example, if we let $f(\Lambda < \Lambda_T) = 0$, being $\Lambda_T > 0$ but small, we need some active neighbours in order to become active, so the LAI phase does not start at γ_c^e, needing larger couplings. If the threshold Λ_T is large enough, the transition will become discontinuous again. There are several ways of overcoming this problem. One is using an external firing rate to each neuron, that counters the effect of the threshold. Other is also explored in classical works on E-I balance, as the seminal work of van Vreeswijk and Sompolinski (Vreeswijk and Sompolinsky 1996), where the synaptic couplings are not constant but grow as $\sqrt{k}$, therefore scaling the fluctuations of the input, making them to be of the order of the neuronal threshold.

In order to verify that more realistic ingredients such as this threshold do not rule out the possibility of finding the LAI phase, we reviewed the recent literature, finding at least two recent computational analyses of E/I networks of integrate-and fire neurons confirming the emerge of similar regimes with high variability (Kriener et al. 2014; Borges et al. 2020). Furthermore, a careful analysis of dynamics in the original Brunel model (Brunel 2000), as well as integrate-and-fire neurons with leaky synapses have revealed that synchronization dynamics is strongly influenced by input fluctuations in the individual neurons, revealing that "up" and "down" neuronal states are nothing but a reflect of (balanced) stochastic fluctuations. We discuss this more in detail in Chapter 6.

To close this chapter, let us go back to our main objective in this thesis: the problem of the "criticality hypothesis", from the perspective of synchronization. Shockingly, (balanced) asynchronous states and criticality, which have been both proposed to explain the background cortex activity, have almost opposite features. In particular, criticality is characterised by long range correlations, in blatant contrast with the decorrelation produced by inhibition in balanced systems. It is necessary to clarify which is the interplay between both interpretations, in order to have a complete view of neuronal activity (Stepp et al. 2015; Wilting and Priesemann 2019). A possibility to obtain synchronization is using synaptic plasticity (as in the work of di Santo *et al.* (di Santo et al. 2018b)) to create oscillations in the system, letting it to self-organize. In this direction, Recio and Torres studied a similar version of the model including also long-term plasticity mechanisms. In

this case, it is possible to induce memory states into the system (Recio and Torres 2016), which reflects the flexibility of the model to account for new phenomena if the adequate ingredients are considered.

Hybrid Type Synchronization: Avalanches and Synchronization

"It matters little who first arrives at an idea, rather what is significant is how far that idea can go."

- Sophie Germain.

The model previously studied shed light on the dynamics of inhibition on sparse networks, as well as on the origin of the asynchronous irregular state of the cortex. However, the phase transitions surrounding the LAI phase turned out to be not new: the quiescent-LAI transition belongs to the directed percolation universality class, while the LAI-active transition does not present scale free distributed avalanches. Moreover, synchronous states, one of the most robust experimental evidences in neural data (Buzsáki 2006), are missing from the simple Larremore *et al.* model. Therefore, we decided to move to a more complex approach, with the objective of unveiling the properties of the synchronization transition observed, for example, in di Santo et al. (di Santo et al. 2018a). This quest will lead us to formulate an exciting new hypothesis regarding criticality in the brain.

4.1 Avalanches and Synchronization

As we discussed in the previous chapter, neurons in the cerebral cortex fire in an irregular, sparse, self-sustained manner (Softky and Koch 1993; Arieli et al. 1996; Abeles 1991), in which is regarded as the resting state of the brain. At the end of the day, our goal is to understand how does such background activity engages in cortical information processing (Latham et al. 2000; Deco et al. 2008; Breakspear 2017).

Spontaneous neuronal activity presents (at least) two distinctive faces: *synchronization* and *scale-free avalanches*. Although we have already discussed both in detail in Chapter 1, performing also a small

literature review, let us do a short summary to situate ourselves. Synchronization is the microscopic process underlying brain waves, which are characterised by different frequency ranges, depending on functional state and region. Such waves are crucial in order to share information between distant brain regions (Buzsáki 2006; Buehlmann and Deco 2010; Muller et al. 2018), while asynchronous states play an important role in information coding (Renart et al. 2010; Denève and Machens 2016; Sadeh and Clopath 2020). We also discussed the possibility of the brain to work at the edge of a synchronization phase transition, half-way between a perfect synchronization and irregular states, allowing for more complex dynamical regimes (Cabral et al. 2011; Markram et al. 2015; Breakspear 2017), as well as more flexibility to explore the synchronous-asynchronous spectrum. From the clinical point of view, abnormal synchronization levels have been linked with pathological functioning (Kandel et al. 2000).

We also discussed in detail the phenomenon termed neuronal avalanches, outbursts detected over the background activity, following scale-free distributions for both their sizes and durations. Moreover, the exponents characterising such distributions are power laws $P(S) \sim S^{-\tau}$, $P(T) \sim T^{-\alpha}$ whose exponents are not independent but fulfill the hyperscaling relation (1.31), $\gamma = (\alpha - 1)/(\tau - 1)$, that links the average avalanche size with avalanche duration, $\langle S(T) \rangle \sim T^{\gamma}$, and it is typical of critical systems. (Muñoz et al. 1999; Friedman et al. 2012). Although the values of the critical exponents are very similar to the ones of the critical branching process (Beggs and Plenz 2003; Petermann et al. 2009; Bellay et al. 2015; di Santo et al. 2017), we have discussed that recent observations seem to agree that the universality class in indeed different (Friedman et al. 2012; Ponce-Alvarez et al. 2018; Yaghoubi et al. 2018; Fontenele et al. 2019; Porta and Copelli 2019).

The Landau-Ginzburg model of the brain brought together synchronization and critical avalanches, suggesting that the cortex operates near to a synchronization phase transition. At this point, both scale-free avalanches and marginal synchronization occur in concomitance (di Santo et al. 2018a), a proposal backed by both theoretical and experimental evidence (Gireesh and Plenz 2008; Poil et al. 2012; Markram et al. 2015; Porta and Copelli 2019). But the Landau-Ginzburg model does not solve many important questions

regarding criticality: which is the minimal model able to display a synchronization transition compatible with experimental observations? What is its universality class? We dedicate this chapter to find detailed answers to those questions.

4.1.1 Avalanche distribution in the Kuramoto model

In Chapter 2, we derived the canonical model for phase synchronization, i.e., the Kuramoto model, from very general phase reduction principles. The Kuramoto model has been widely employed, usually being the go-to option to understand synchronization behaviours in many areas, including neuroscience (Breakspear et al. 2010; Cabral et al. 2011; Villegas et al. 2014; Ferrari et al. 2015). Therefore, it seems the perfect candidate to explore in a simple way the critical synchronization dynamics proposed by di Santo *et al.* (di Santo et al. 2018a). In other words, we are interested to know if the Kuramoto model is able to display scale-free neuronal avalanches with the observed critical exponents at the synchronization phase transition. We consider here the "stochastic Kuramoto" counterpart (eq. (2.45)), assuming that all frequencies are the same, since heterogeneity is not essential for observing avalanches[1]:

$$\dot{\varphi}_j(t) = \omega + \frac{J}{N}\sum_{i=0}^{N}\sin\Big(\varphi_i(t) - \varphi_j(t)\Big) + \sigma\eta_j(t), \tag{4.1}$$

where the phase $\varphi_j(t)$ describes the dynamical state of the j-th oscillatory unit, with $j = 1, 2, \ldots, N$, ω is the common intrinsic frequency, $\eta_j(t)$ a zero-mean unit-variance Gaussian white noise with amplitude σ, and J is the coupling strength with all the neighbors (Strogatz 2000; Pikovsky et al. 2003; Acebrón et al. 2005). As we discussed in Chapter 2, equation (4.1) exhibits a synchronization phase transition at $J = \sigma^2$ according to the Ott-Antonsen ansatz, where the Kuramoto order parameter $Z = \left\langle e^{i\varphi} \right\rangle$ experiences a Hopf bifurcation from a fixed point to a limit cycle, revealing the emergence of collective oscillations (Acebrón et al. 2005).

[1] For example, the model by di Santo *et al.* that we want to understand is completely homogeneous.

4.1 Avalanches and Synchronization

Avalanche events are measured following the standard protocol in neuroscience (Beggs and Plenz 2003; Plenz and Niebur 2014) (see also Appendix A). This measure works with events at the raster plot, so first we have to define what constitutes such events in an oscillator model. We set a spike each time an oscillator crosses the phase value $\varphi = \pi$, following the convention for other phase models such as e.g. theta-neurons (see Chapter 2), and in analogy to the active rotators defined below. The resulting raster plots are shown in Figure 4.1.

It is possible now to fix parameters $J = 1$ and $\omega = 1$ without loss of generality, leaving σ as the control parameter. According to the Ott-Antonsen ansatz, the mean-field critical transition happens near $\sigma_c = 1$. However, the actual value of the critical point could be affected by higher order corrections[2], as well as finite size effects, so it has to be estimated through numerical methods. In order to determine numerically σ_c, we take the point at which the variance of the Kuramoto order parameter is maximum (Acebrón et al. 2005; Pikovsky et al. 2003; di Santo et al. 2018a). The result of this analysis is shown in Fig. 4.1a and b. At criticality, one should strictly have $R = 0$, but this requires many averages and very large sizes, so in our simulations a finite value of R is approached. Avalanche analyses reveal no scale-free distributed events at any of the studied points (subcritical, critical and supercritical). Surprisingly, all the three values present an exponential decay of avalanche sizes and durations, as seen in Fig. 4.1. A possible explanation for this could be that the Kuramoto order parameter experiences a Hopf bifurcation, where (regular) oscillations emerge with a fixed frequency (Strogatz 1994). This could induce a strong characteristic timescale in the system, which is not compatible with the scale invariance displayed by critical avalanches.

Note, however, that the lack of scale-free avalanches measured in this way does not go against criticality itself in the stochastic Kuramoto model's synchronization transition. If we take the order parameter R, and analyse its temporal behaviour (see Appendix A), we find that R experiences scale-free avalanches with exponents $\tau \sim 4/3$ and $\alpha \sim 3/2$, which are typical for random walks (di Santo et al. 2017), and in accordance with recent results (Ódor and Kelling 2019).

[2] Remember that in stochastic systems, the Ott-Antonsen gives the result correct up to $\mathcal{O}\left(\sigma^2\right)$.

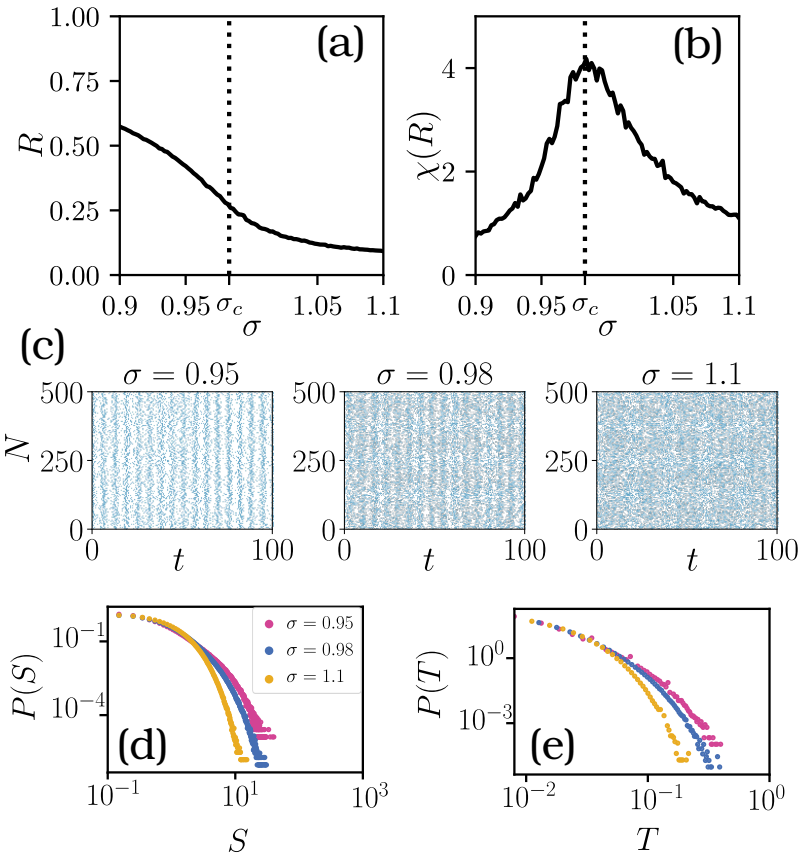

Figure 4.1: **Avalanche statistics in the stochastic Kuramoto model on fully connected networks.** **(a)** Kuramoto order parameter (R) as a function of the noise intensity σ for a finite size $N = 500$. **(b)** The Kuramoto critical point is defined as the point of maximum variance of the order parameter, χ, which occurs at $\sigma_c = 0.98$ (vertical dashed line). **(c)** Raster plots of the Kuramoto model at the synchronous phase ($\sigma = 0.95$, left plot), the critical point ($\sigma_c = 0.98$, central plot) and the asynchronous phase ($\sigma = 1.1$, right plot). **(d)** Distributions of size events in the three phases for the same representative values of σ as above. **(e)** Distribution of time events in all the three phases for the same parameter values. Let us underline the lack of power-law distributions at criticality, i.e., when the system undergoes a collective Hopf bifurcation. Parameter values: $\omega = 1$ and $J = 1$.

Finally, let us remark that avalanche measures are very sensible to time binning and related problems. When we integrate the differential equations, the integration step Δt needs sufficient time resolution. If we let Δt to be large enough, it will affect as a "time binning" itself, thus affecting avalanche measures. In particular, at the asynchronous phase, in the limit $N \to +\infty$ the interevent interval $\langle \mathrm{IEI} \rangle \to 0$, where avalanches are pathologically defined. Since the raster gets "denser" as we increase N, the timestep Δt should be decreased as $1/\sqrt{N}$ in order to avoid ill-defined results.

4.2 The active rotator model

4.2.1 Model analysis

From the above analysis, it is therefore clear that the Kuramoto model alone is not rich enough in order to explain the observed scale-free avalanches in the cortex, as well as to understand the universality class of the synchronization transition in the Landau-Ginzburg model. But if this transition is not explained by the usual Kuramoto universality class, then what could it possibly be?

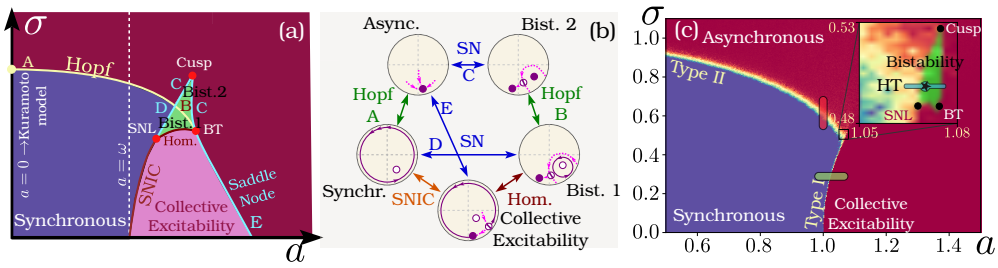

Figure 4.2: **Mean-field phase diagram and bifurcations of the active rotator model. (a)** Sketch of the phase diagram obtained solving eqs. (4.5) using the Ott-Antonsen ansatz; it reveals the existence of synchronous and asynchronous states, as well as a collectively-excitable regime. The central triangular-shaped region (green) describes a regime of bistability; its vertices correspond to codimension-2 bifurcations. **(b)** Sketch of the different regimes represented in terms of the complex Kuramoto order parameter. Each regime is represented by a point in the unit circle (since $|Z_1| \leq 1$) with filled circles describing stable fixed points, open circles standing for unstable fixed points, and mixed-color circles describing saddles. Bifurcations between different regimes are indicated as arrows, labeled with capital characters as in panel (a). **(c)** Phase diagram computed using direct simulations of a fully-connected system with $N = 5000$ oscillators. Collective oscillations are computationally detected with the Shinomoto-Kuramoto order parameter. The location of the bistability region (inset zoom) was established by numerically solving eqs. (4.5) for the first $k = 50$ harmonics (imposing $Z_{51} = 0$), which is very accurate in the thermodynamic limit. The three segments (red, green and blue) indicate three possible types of transition to synchronization (as considered in Fig. 4.3 and 4.4) (Buendía et al. 2020b)

Let us return for a moment to the Landau-Ginzburg model of di Santo *et al.* (di Santo et al. 2018a). As it was explained in detail in Chapter 2, the model consist on a lattice of mesoscopic units, which are diffusively coupled. As the control parameter is increased, the individual unit goes through a homoclinic bifurcation, where the unit's activity and the synaptic resources start oscillating at increasing frequency. Moreover, small external perturbations are able to make the system spike before falling again into the quiescent state. Therefore,

according to the Hodgin excitability classification, the model would correspond to type-I excitability. Finally, if we continue increasing the control parameter, the units get synchronized through a phase transition. At this point, scale-free avalanches emerge (di Santo et al. 2018a).

Note that the behaviour of the Landau-Ginzburg unit (oscillator) is essentially different from the Kuramoto oscillator. The missing ingredient is *excitability*, which can be added by considering a model of "active oscillators", in which the angular speed is no longer constant but depends itself on the phase, as

$$\dot{\varphi} = \omega + a \sin \varphi, \tag{4.2}$$

where ω is the oscillator natural frequency and a are parameters (Strogatz 1994). For $a > \omega$ the deterministic dynamics of each isolated unit exhibits two fixed points at $\varphi^*_{\pm} = \pm \arcsin(\omega/a)$. While φ^*_- is a stable equillibria, φ^*_+ is a saddle-node. When $\omega \simeq a$, both equillibria are close to each other, distancing as we increase the excitability. If stochastic noise is added, the angle fluctuates around φ^*_-, eventually reaching φ^*_+, and forcing the system to do a complete cycle to return again to the stable fixed point. This is exactly the same mechanism that drive spikes in 2D models such as the Fitzhugh-Nagumo, as explained in the Chapter 2.

When $a < \omega$, the system is able to oscillate, with the period increasing as $T \propto 1/\sqrt{\omega - \alpha}$, the hallmark of the SNIC bifurcation (Strogatz 1994). The model presented here is again nothing but the canonical Ermentrout-Kopell type-I model, that can be coupled through Kuramoto-like interactions. We argue that

$$\dot{\varphi}_j = \omega + a \sin \varphi_j + \frac{J}{M_j} \sum_{i \in n.n.j}^{M_j} \sin\Big(\varphi_i - \varphi_j\Big) + \sigma \eta_j(t) \tag{4.3}$$

captures the properties of neuronal systems in a more realistic way than Kuramto units, due to its excitable behaviour, as demonstrated by Ermentrout and Kopell (Ermentrout and Kopell 1986). Note that although the transition from fixed points to oscillations is SNIC, while in the Landau-Ginzburg is homoclinic, both belong to type-I excitability.

We consider versions of the model both in mean-field (fully-connected networks) which are useful for analytical approaches

and on two-dimensional lattices, mimicking the topology of cortical columns in the cortex (Breakspear 2017). Eq. (4.3) is also known as the Shinomoto-Kuramoto model or Winfree's ring model (Shinomoto and Kuramoto 1986b; Winfree 2001), and it has been previously studied in the literature (Shinomoto and Kuramoto 1986b; Sakaguchi et al. 1987; Zaks et al. 2003; Tyulkina et al. 2018).

At this stage, one could be tempted to use the Kuramoto order parameter in order to characterise synchronization in the system. However, it turns out that it is far from enough. Note that when $\omega \simeq a$, although the single unit can oscillate, the period can be very long, so most of the units will stay around $\varphi \simeq -\pi$ for a long time. Hence, computing the Kuramoto order parameter for many uncoupled ($J = 0$) oscillators still gives a non-trivial value for R. There are several solutions to this problem. One is to use the change of variable (2.31) to linearise the equation. A very similar (numerical) approach is the linear interpolation of spikes described in Chapter 2 and in Appendix B. A possible solution is to consider the complete family of Kuramoto-Daido parameters,

$$Z_k = \langle e^{ik\varphi} \rangle \equiv \frac{1}{N} \sum_{j=1}^{N} e^{ik\varphi_j} \equiv R_k e^{i\psi_k}, \tag{4.4}$$

that render complete information of the system. Since the system includes stochastic noise, higher order moments have to be considered anyway if we want to go beyond the Ott-Antonsen ansatz solution, as it was pointed out in Chapter 2.

We then apply the method sketched in Chapter 2 for the (stochastic) Kuramoto model: write down a Fokker-Planck equation, expand it in Fourier series, and then identify the Fourier harmonics with the Kuramoto-Daido order parameters. In this case, $Z_k = \overline{p}_k$, since all the frequencies are set to ω. The result of the computations is given by (Shinomoto and Kuramoto 1986b; Zaks et al. 2003)

$$\dot{Z}_k = Z_k(i\omega k - \frac{k^2\sigma^2}{2}) + \frac{ak}{2}(Z_{k+1} - Z_{k-1}) + \frac{Jk}{2}\left(Z_1 Z_{k-1} - \bar{Z}_1 Z_{k+1}\right) \tag{4.5}$$

where the bar stands for complex conjugate. Now the idea is to use different low-dimensional closures to analyse the infinite set of equations. The Ott-Antonsen ansatz is enough to give a qualitatively correct

view of the phase diagram, sketched in Fig. 4.2, although more refined closures are necessary in order to predict the exact position of the bifurcation lines (Zaks et al. 2003; Tyulkina et al. 2018) (see Appendix C). In order to visualize system behaviour we use the first Kuramoto-Daido parameter, since $Z_1 = R_1 e^{i\psi_1}$ gives information about synchronization (through R_1) and the global phase of the oscillators ψ_1. Although, as we discussed earlier, only one parameter is not enough to render complete knowledge of the system, it suffices to gain intuition on the different phases. The system presents three dynamical regimes: synchronization, seen as a limit cycle in Z_1, which makes $R_1 > 0$, while ψ_1 is a periodic function. Asynchronous states, where R_1 decreases[3]. And collective excitable states, where all oscillators are fixed to the same phase ψ_1, fluctuating around this state. An external input to the system is able to elicit a collective response, making the system spike.

The synchronized state and the collective excitable are separated by a SNIC transition, which is crossed when the excitability a is increased at low noise, and hence it is remnant of the single oscillator SNIC –since all oscillators are synchronized, they behave in a similar way. The boundary between the synchronous and asynchronous states is a Hopf bifurcation, and it can be found by increasing the noise σ at a fixed excitability, analogously to the Kuramoto model. Note that in an excitable medium, these bifurcations would correspond to excitability classes I and II in the Hodgin classification (see Chapter 2). We decided to extend this classification to "synchronization classes", since the way of recruiting oscillators to spike together is very different in both transitions. In *type-I synchronization*, oscillations emerge at the transition point with infinite period but finite amplitude, while in *type-II synchronization* oscillations emerge with fixed, non-vanishing frequency (Buendía et al. 2020b). This means that in type-I synchronization, almost all oscillators become locked when the transition is crossed, while in type-II synchronization there is a growing cluster of synchronized individuals.

Now, there is a small region where both bifurcations come close to each other. At this point, we find a small region of bistability (the green area in Fig. 4.2a) (Sakaguchi et al. 1987; Zaks et al. 2003; Childs and

[3]It never reaches $R_1 = 0$ because, as discussed above, this would require a homogeneous distribution of phases in the case $J = 0$, which is not the case for non-linear oscillators.

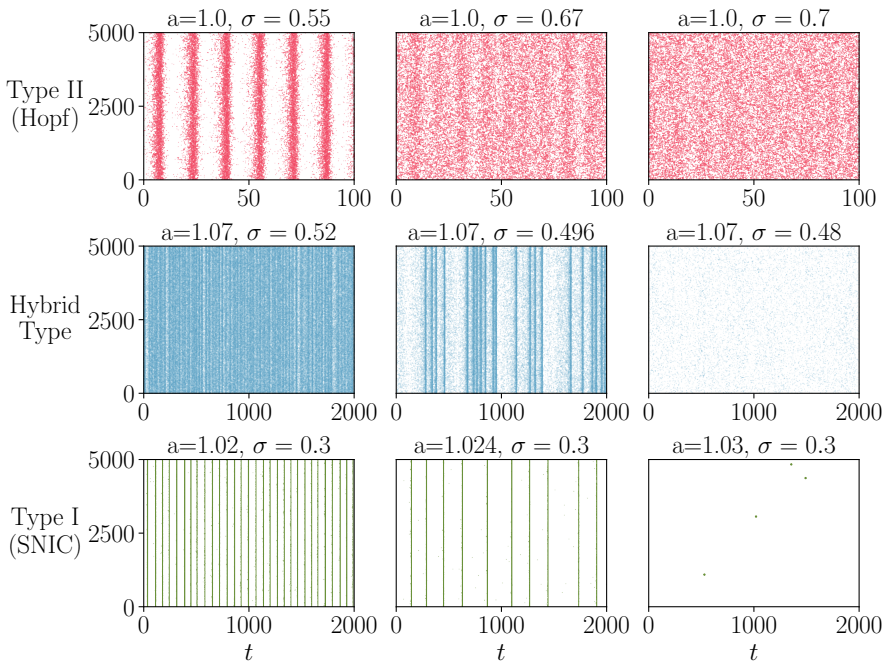

Figure 4.3: **Raster plots at different synchronization classes.** Mean-field raster plots for each one of the three considered cases in the synchronous phase (left), right at the transition point (central column), and in the asynchronous phase (right)

Strogatz 2008). This region has triangular shape, and its vertices are co-dimension 2 bifurcations: a Bogdanov-Takens (BT), a saddle-node-loop (SNL) and a cusp. All of these were already introduced in Chapter 1. At the bottom part of the bistability region, collective excitability coexists with a small limit cycle –partial synchronization–, but as noise increases the limit cycle shrinks through the Hopf bifurcation, leading to coexistence between collective excitability and the asynchronous state (stable equillibrium). Then, in order to understand synchronization transitions, one should not only consider the standard scenarios, as type-I and type-II, but also more diverse, complex scenarios. Near codimension-2 points we can find mixed, or hybrid, synchronization types[4]. Hence, call the transition from synchronous to the bistable

[4]As it happens with excitability at the Bogdanov-Takens bifurcation (Izhikevich 2006)

phase *hybrid type synchronization transition*. Now it remains to study whether the critical behaviour at this transition is different from type-I and type-II.

In order to find the bifurcation diagram with the maximum accuracy possible, we complemented the analytical results with direct numerical analyses, simulating either the full stochastic system (writing an implementation of the Euler-Milstein algorithm for $N = 10^4$ oscillators) or solving (4.5) truncated at sufficiently high orders (up to $k = 50$, so $Z_{k>51} = 0$). Note that the Fokker-Planck method assumes that we are at the thermodynamic limit $N \to +\infty$, so in this case finite size effects are ignored. Results of such analyses are both shown in Figure 4.2c. We see that the shape of the phase diagram is qualitatively identical to the one predicted by the Ott-Antonsen ansatz, but the bistability region has been shrunk into a very small region. Actually, the region is so small, that the exact location of the codimension-2 points, as well as the region boundaries, are both affected by finite size effects in direct simulations.

4.3 Avalanches at hybrid synchronization

4.3.1 Mean-field

We now perform a systematic analysis of avalanche behaviour at the different transitions. First, Fig. 4.3 shows representative raster plots at each one the bifurcations, including the type-I, type-II and HT synchronization transitions. Here the difference between all synchronization types is evident: type-I confers a very coherent, regular structure to the system near the transition, while type-II presents a blurry structure over a background noise. On the other hand, the hybrid-type synchronization transition displays a coherent, synchronous irregular firing over a sparse activity. which is typical of neuronal systems (Brunel 2000; Bellay et al. 2015).

The standard protocol for measuring avalanches is then applied (see Appendix A) at all the phases, as well as at the transitions among them. The results are displayed in Fig. 4.4 for mean-field. Insets show

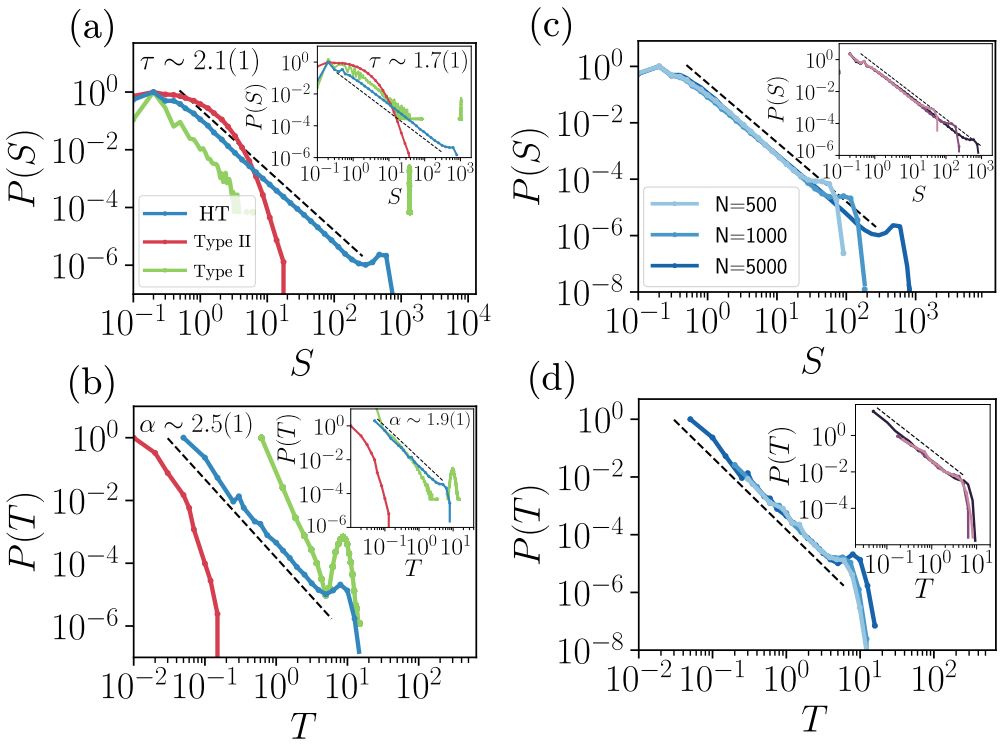

Figure 4.4: **Avalanche distributions at the different bifurcations. (a,b)** Avalanche size and duration distributions for three different types of synchronization transitions (right at the transition points): type-I (SNIC) transition (green lines, $a = 1.024$, $\sigma = 0.3$); type-II (Hopf) transition (red lines, $a = 1.04$, $\sigma = 0.575$), and HT transition (blue lines, $a = 1.07$, $\sigma = 0.499$) in mean-field systems ($N = 5000$). Only the last one exhibits clear cut power-law behavior, both for size and duration distributions. **Insets:** As in the main Figure but for simulations in a 2D lattice (size 64^2): type-I transition ($a = 0.99$, $\sigma = 0.05$), type-II transition ($a = 0.60$, $\sigma = 0.64$), and HT synchronization transition ($a = 0.98$, $\sigma = 0.185$). **(c,d)** Finite-size scaling analysis of $P(S)$ and $P(T)$ in FC networks of different sizes (as specified in the legend) in the HT regime: As in the main Figures but for 2D lattices of sizes ($N = 16^2$, $N = 32^2$, $N = 64^2$).

also the results for two-dimensional systems, that will be discussed in detail later. Scale-free avalanches do not emerge at the type-II (Hopf) transition, nor at the type-I. However, the HT transition displays clean power-law distributed avalanches at criticality. These span over several decades, obey finite-size scaling, and fulfill the hyperscaling relation (1.31). In mean-field, we obtain exponent values $\tau \approx 2.1(1)$, $\alpha \approx 2.5(1)$ and $\gamma^{-1} \approx 0.75(5)$ using a Kolmogorov-Smirnov test (Clauset et al. 2009; Alstott et al. 2014), which are compatible with the values found in mean-field by Liang *et al.* (Liang et al. 2020).

We also have studied the behaviour of the scale-free avalanches when we slightly deviate from the hybrid type transition. A slight reduction in excitability is not enough to completely destroy the power-law distribution of the avalanches, as show in Figure 4.5, as long as we lie near the bistability region. When we took points with larger excitability, avalanches quickly disappear. This suggests that the determination of the bistability phase –which was performed solving (4.5) up to $k = 50$– suffers from finite size effects, due to the small size of such a region. Moreover, remember that almost critical systems also present power-law distributed avalanches spanning some decades, and in practice one of the bests way to determine is looking for the larger span and then performing finite size scaling, since at criticality power-law behaviour holds for any N –subcritical systems at the end fall exponentially, while supercritical ones saturate (Hinrichsen 2000; Binney et al. 2001; Muñoz 2018). Separating both effects is a difficult task numerically, but finding a small parameter range with avalanches distributed as power laws falls under what we could expect from the traditional theory of critical systems.

If we insist in moving away from the HT transition, scale-free avalanches break down, either by changing excitability or noise, as illustrated in Fig. 4.6. This demonstrates that scale-free behaviour can be seen only in a very small region, near the HT transition, at $a_{HT} = 1.07$, $\sigma_{HT} = 0.496$.

Finally, as a complementary measure of complexity, we have computed the distribution of interevent intervals, and the coefficient of variation (see Appendix A). Results are shown in Figure 4.7. We found that only around the HT transition, the coefficients of variation are large CV > 1, and they are accompanied by broad distributions of IEI values. These results indicate that the dynamical richness at the HT bi-

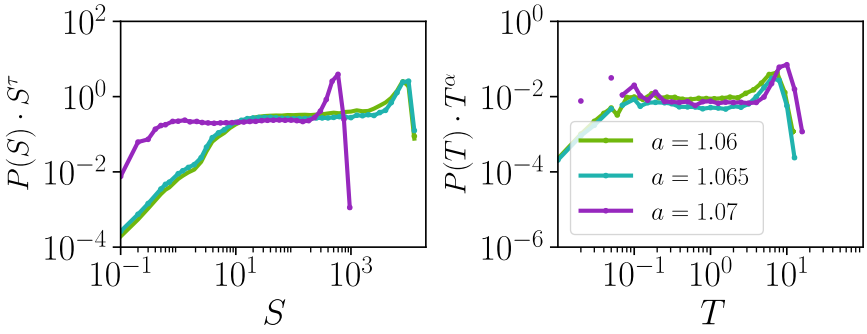

Figure 4.5: **Avalanches close to the hybrid type synchronization transition.** Size and duration distributions for a network of size $N = 5000$ evaluated at the hybrid type synchronization transition ($a_{HT} = 1.07$, $\sigma_{HT} = 0.496$) and two other nearby points, slightly to the left of it. Power law behavior is observed only in the bistable region close to the hybrid-type synchronization.

furcation and the bistability regime is way larger than any other. Then, even when type-I and type-II synchronization transitions are formally critical (Ohta and Sasa 2008; Hong et al. 2015), they are not able to generate the macroscopic level of complexity required for scale-free avalanches.

4.3.2 Two dimensions

In addition to mean-field analyses, we performed a study of the system in two-dimensional systems. This is justified by the organization of the cortical columns in the brain (Breakspear 2017), that has also inspired models such as the Landau-Ginzburg (di Santo et al. 2018a).

We used the same computational tools in order to obtain the phase diagram in two-dimensions, revealing a very similar diagram to the mean-field case, as demonstrated by Fig. 4.8. The same three states (synchronous, asynchronous and collective excitable) can be found in the low-dimensional system. At the asynchronous regime, activity fluctuates randomly, creating smalls clusters that appear and propagate locally. The average synchronization is zero, although there

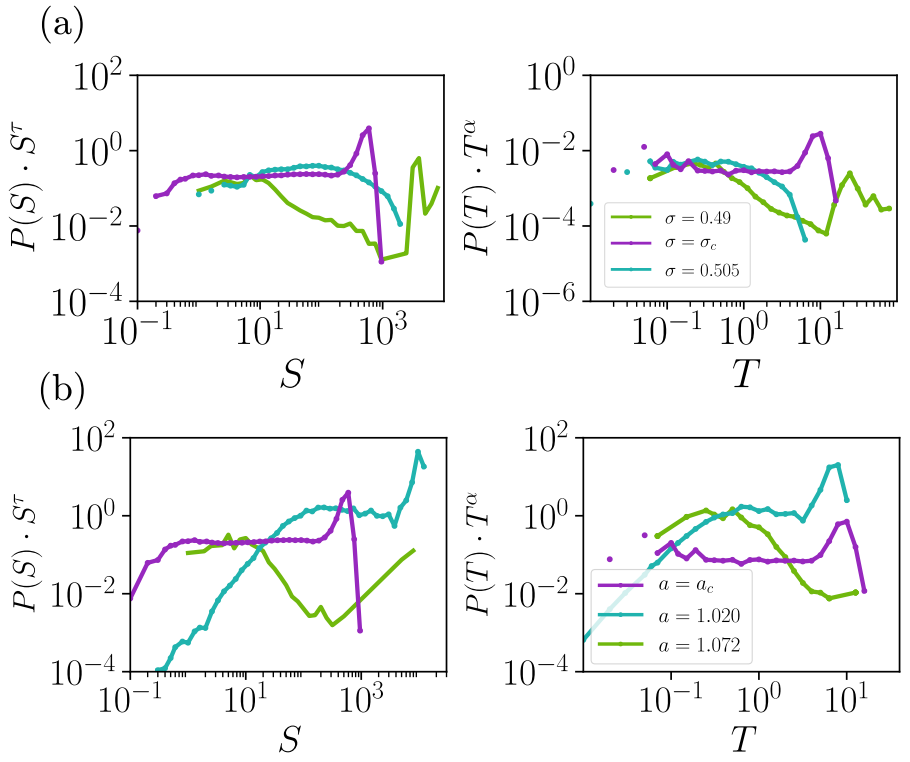

Figure 4.6: **Avalanches away from the hybrid type synchronization transition.** Size and duration distributions for a network of size $N = 5000$ evaluated at the hybrid type synchronization transition ($a_{HT} = 1.07$, $\sigma_{HT} = 0.496$), and two nearby points: **(a)** by varying noise σ at constant excitability and **(b)** by varying excitability a at constant noise. Power law behavior is observed only at the hybrid type transition

is a certain activity. On the other hand, at the synchronous phase the system "breathes", and oscillators behave in way similar to the single unit. Therefore, the system is silent most of times, and all neurons spike together in a small time window. Although visually this activations seems to be wave-like, it is the closest it can get to a perfect synchronization. In two-dimensional systems, topological defects prevent completely coherent oscillations (Mermin and Wagner 1966; Shinomoto and Kuramoto 1986a; Kardar 2007a). Finally, the collective excitable system is always pinned at the "down" state, but it is susceptible to external inputs. Let us discuss in detail what happens

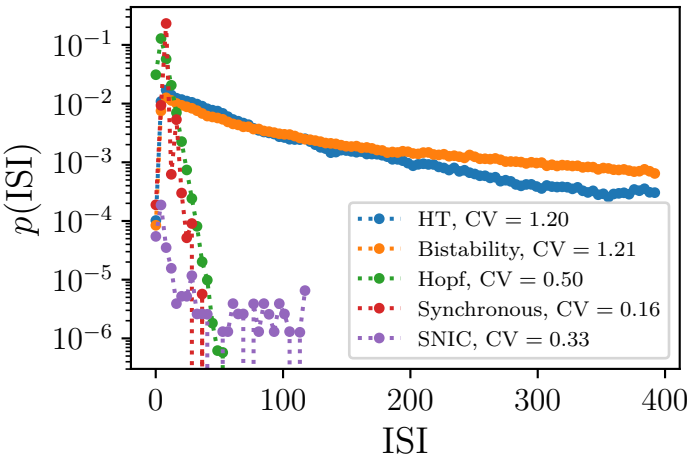

Figure 4.7: **ISI distributions and CVs for mean-field systems.** Each color represents the probability distribution of interspike interval at different phases and their bifurcations, as well as the coefficient of variation, as shown in the legend. Parameter values: Synchronous regime, $\sigma = 0.5$, $a = 0.5$; Hopf bifurcation, $a = 0.5$, $\sigma = 0.92$; collectively excitable phase, $\sigma = 0.5$, $a = 1.12$; hybrid type synchronization transition: $\sigma = 0.5$, $a = 1.07$; bistable regime: $\sigma = 0.5$, $a = 1.072$. Network size $N = 5000$.

at the different bifurcation lines (see also Fig. 4.9).

1. Near the SNIC bifurcation, there is oscillating activity, that moves as spiral travelling waves along the system.

2. Near the Hopf bifurcation, activity slightly oscillates in time, growing and shrinking in spatially distributed, fragmented clusters.

3. At the HT synchronization transition, the dynamical behaviour is richer, being a mixture of the previous two. Travelling waves are alternated with fluctuations that lead the system to the collective excitable state for a while, which is a reflection of the bistability.

Then, richer dynamics are found at the HT synchronization transition, where the key features of both types live together. We then com-

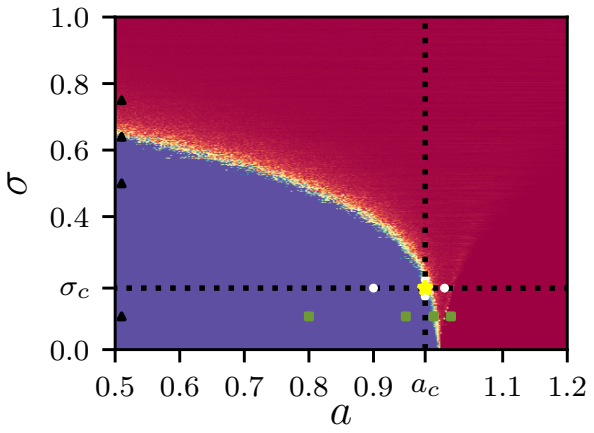

Figure 4.8: **Phase diagram in two dimensions.** The region where avalanches are found is marked at the intersection of the dashed, black lines. Additional points show regions where simulation videos were recorded (available at the published version of the paper, see Fig. 4.9 for some examples).

puted avalanche distributions, finding again that scale-free distributed avalanches emerge only at the hybrid synchronization transition. The results are in the insets in Fig. 4.4, and critical exponents are $\tau \approx 1.7(1)$, $\alpha \approx 1.9(1)$ and $\gamma^{-1} \approx 0.75(5)$, compatible with the values observed in experiments, as well as with the Landau-Ginzburg model (di Santo et al. 2018a). Note that exponents changed with respect to the mean-field ones, except the γ, which is similar to the universal value proposed by Fontenele *et al.* (Fontenele et al. 2019). This result, both for mean-field systems and two-dimensional ones, is illustrated in Fig. 4.10.

4.4 Discussion

We have demonstrated here that the paradigmatic synchronization transition of the Kuramoto model is not enough in order to understand the observed critical behaviour, and more ingredients have to be taken in account. In particular, we have classified synchronization bifurca-

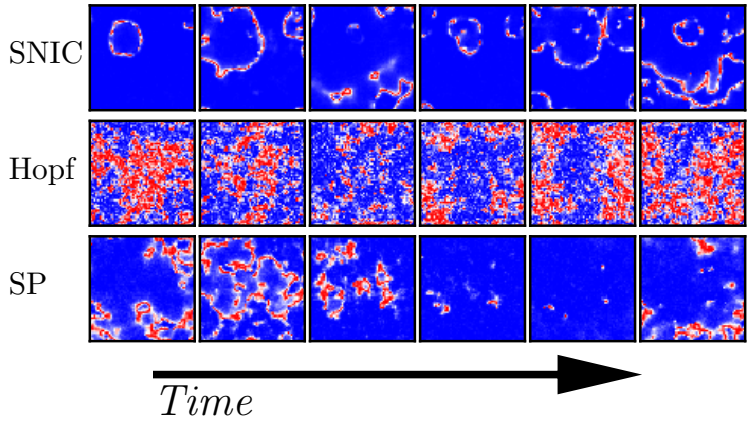

Figure 4.9: **Spatio-temporal dynamics on two-dimensional systems.** The figure shows three rows, each one with six different snapshots of a two-dimensional simulation, for the following cases: Upper row: SNIC bifurcation ($a = 1$, $\sigma = 0.08$); central row: Hopf bifurcation ($a = 0.5$, $\sigma = 0.65$); and lower row: hybrid type synchronization transition ($a = 0.98$, $\sigma = 0.185$). Blue color indicates lack of activity, while red color stands for maximum levels of activity (identified as $1 + \sin\varphi_j$). Simulations performed for $N = 64^2$ with periodic boundary conditions.

tions in a way analogous to that of the Hodgin excitability classes, and have demonstrated that critical scale-free avalanches, with exponents compatible with those found in experiments, emerge only near a *hybrid type* synchronization transition. However, this does not entirely solve all theoretical problems. The next natural question to wonder is which one of the dynamical ingredients confer such a special behaviour to the HT transition. We will present some possible explanatory scenarios for such dynamical complexity. The first scenario could be the proximity to one of the codimension-2 points. Remarkably, the saddle-node-loop (SNL) bifurcation has been previously argued to be necessary for the generation of high variability and dynamical richness in neural networks (Hesse et al. 2017; Schleimer et al. 2019); but it has also been established that the crucial features of critically balanced excitation/inhibition neural networks –a robust observation in experiments– stem from a phase diagram organized around a BT

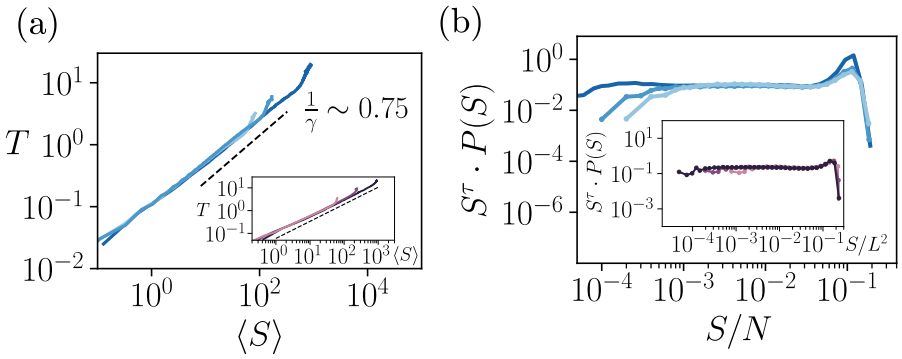

Figure 4.10: **Exponents accuracy analysis (a)** Averaged avalanche size as a function of the duration for different system sizes. **(b)** Same as (a), but we multiply by s^τ to obtain an asymptotically flat curve – allowing easier visual inspected– and re-scaled as a function of the system size to collapse the different curves. As expected from true scale invariance, avalanches become flat and collapse for the different system sizes. Inset: the same information, but for two-dimensional systems. Parameters: (a, σ) for mean-field systems, $N = 500$: $(1.07, 0.520)$, $N = 1000$: $(1.07, 0.505)$; $N = 5000$: $(1.07, 0.496)$ and 2D networks, $L = 16$: $(0.995, 0.192)$; $L = 32$: $(0.982, 0.190)$; $L = 64$: $(0.98, 0.185)$. Theoretical lines are shown as black dashed lines for comparison.

bifurcation (Benayoun et al. 2010; Cowan et al. 2016; Buendía et al. 2020b).

Unfortunately, the bistability region is so small in parameter space that distinguishing all those points numerically is very difficult, specially owing to finite-size effects. The only computational answer we can provide is that scale-free avalanches appear when entering the synchronous phase from the bistability region, in close vicinity with codimension-2 points.

The second scenario comes precisely from the interplay between criticality and bistable regimes. In theory, these two are largely incompatible, since they correspond to either second-order or first-order phase transitions, respectively. However, stochastic jumps between excitable and partially synchronous states are likely to increase the complexity of the system, which could be enhanced at the boundary of the phase, where fluctuations are maximized by criticality. Moreover, note that many experiments and models (Liu et al. 2014; di Santo et

al. 2016; Jercog et al. 2017; Tartaglia and Brunel 2017; di Santo et al. 2018a; Schleimer et al. 2019) remark the importance of bistability in neuronal systems and its role on dynamical richness. As we will see in the next chapter, bistability can lead to oscillations in self-organized scenarios. This could mean that a critical transition that leads to a bistable regime, or a self-organized system to its Maxwell point, might display critical-like dynamics. If this is true, one would argue that bistability should also be present in other models such as (Liang et al. 2020).

We would like to remark that the topology of the phase diagram, specially the bistable region surrounded by the SNL-BT-Cusp triangle can be found in many models of neuronal dynamics, at very different scales, and hence we argue that it could be a key feature of neuronal systems. For example, the Morris-Lecar neuron (Liu et al. 2014) posses this "triangle" at the individual level. Systems composed by theta-neurons also display a very similar phase diagram at the collective level (Luke et al. 2013; Luke et al. 2014). In particular, the popular Wilson-Cowan model for brain dynamics presents the same kind of bifurcations (Borisyuk and Kirillov 1992). Therefore, the phenomenology discussed here is rather universal and not model-specific. It is noteworthy that other scenarios have been described to connect lines of type-I and type-II transitions –e.g., subcritical Hopf bifurcations followed by a fold of limit cycles– which also involve a regime of bistability (Fontenele et al. 2019; Buendía et al. 2020b).

Although the model studied here is not meant to be realistic, it provides us insights on the key dynamical mechanism needed to generate features observed in real systems. We hypothesize that cortical avalanches emerge at the HT transition, and that the key ingredients in this model (excitability, synchronization, bistability) should be present in many others, but have been overlooked up to this point. Of course, even if critical-neuro models present HT transitions –or, at least, some its main ingredients– this will not be enough in order to affirm that the brain works at a critical point. As it was pointed out at the beginning, models are of no use without the backing of data, and hence a "data-driven" approach is needed in order to understand the dynamical regime of the cortex, and discriminate which is the most accurate theoretical model among all th proposals.

Adaptation and Self-Organization

"Any man could, if he were so inclined, be the sculptor of his own brain."

- Santiago Ramón y Cajal.

Thus far, we studied models where (a)synchronous states are delimited by phase transitions, and discussed the possibility of explaining the experimental observations by tuning these models at criticality. In particular, the *hybrid synchronization* hypothesis seems to be a good candidate to explain neuronal avalanches and complex dynamics observed in the real brain.

However, the study of criticality in biology always comes with another implicit question. How did the system *become* critical? In physical systems, phase transitions are rare and usually need the fine tuning of at least one control parameter. As we explained in Chapter 1, the theory of self-organization (Bak et al. 1987; Bak 1996) gives a general answer to this problem: if the control parameters can adapt as a function of the current thermodynamic phase, they might present an equilibrium at critical points, organizing the system to criticality without the need of any external tuning. In practice, the problem relies on identifying the physical mechanisms underlying these adaptation processes.

The brain has several *plasticity mechanisms* that could help to bring the brain to critical points. In this chapter, we briefly review some of these mechanisms, as well as the theory of self-organized criticality, including the recently proposed concept of self-organized bistability (di Santo et al. 2016). Finally, these are applied to the study of the Landau-Ginzburg model of the brain (di Santo et al. 2018a).

5.1 Neuroplasticity

The capacity of the brain to re-wire, change, and adapt itself is known with the name of neuroplasticity, or brain plasticity in general (Kandel et al. 2000). Plasticity takes place at different scales through different mechanisms, ranging from individual neurons to rewiring whole regions (Kandel et al. 2000; Turrigiano and Nelson 2004), although the effects and timescales of each mechanism are wildly different (Froemke 2015). For a long time, it was thought that brain was susceptible to modification only during its early development, i.e., during childhood. However, current evidence suggests that many plasticity mechanisms remain at the mature brain, so it reorganizes during our whole life (Kandel et al. 2000).

We focus on the different mechanisms of functional plasticity –that is, mechanisms that act over already existing neurons and synapses. These include homeostatic mechanisms (Turrigiano and Nelson 2004) and synaptic plasticity[1] (Mateos-Aparicio and Rodríguez-Moreno 2019). Some aspects of the latter were already briefly pointed out in Chapter 2, where we discussed that synaptical function is constrained by the number of neurotransmitters in the synaptic vesicles. Once the vesicles are empty, the synapse cannot transmit the action potential to the postsynaptic neuron, until the neurotransmitters are recovered. This is a basic mechanism for *short-term* plasticity, that leads to *synaptic depression*. On the other hand, presynaptic spikes can lead to an increase of residual Ca^{2+}, which is known to facilitate vesicle release (Kandel et al. 2000). In this case, a second spike arriving to the synapse might have a greater effect due to the accumulation of calcium, known as *synaptic facilitation* (Mateos-Aparicio and Rodríguez-Moreno 2019). Other mechanisms such as augmentation and potentiation, which rely on more complex biochemical pathways, also facilitate spiking, but they operate in longer timescales[2] (Cheng et al. 2018). Both depression and facilitation happen at the same time, so models usually deal with

[1] There is a world of different regulatory mechanisms, and a complete classification lies outside of the scope of this work.

[2] Facilitation acts in the order of 10^{-2} seconds, augmentation on the second, and potentiation in the order of minutes.

an effective net change in the synaptic conductivity (Tsodyks and Markram 1997; Levina et al. 2007; Mattia and Sanchez-Vives 2012; Froemke 2015; Cheng et al. 2018). Non-synaptic plasticity involves, for example, the variation of excitability of the neuronal membrane, facilitating –or hindering– the cell to depolarize and spike (Kandel et al. 2000).

Long-term synaptic plasticity relies on more diverse chemical mechanisms, modulating the density of post-synpatic neuron receptors, or involves synaptogenesis (Kandel et al. 2000; Mateos-Aparicio and Rodríguez-Moreno 2019; Millán et al. 2019). One of the most important forms of long-term adaptation is Hebbian dynamics (Sumner et al. 2020). The Hebb postulate indicates that synapses are strengthened as a result of correlated activity between pre- and post-synaptic neurons (Sumner et al. 2020). For example, long-term plasticity makes us able to learn, memorise, and even modify our conduct, being the physiological core of psychological behaviour theory, according to activity-dependent plasticity (Jokić-Begić 2010; Månsson et al. 2016; Mateos-Aparicio and Rodríguez-Moreno 2019; Sumner et al. 2020). In this section we consider plasticity-inspired mechanisms, from the point of view of the theory of self-organized criticality, and discuss some of the aspects that would allow neuroplasticity to play a role on the critical brain hypothesis.

5.2 Self-Organization Mechanisms

In Chapter 1, we briefly introduced the work of Bak, Tang and Wiesenfield on "self-organized criticality" (SOC) (Bak 1996), an idea that deeply changed our perspective of dynamical complexity in natural systems, and created a renewed interest on critical phenomena and its applications. The idea is that adaptation mechanisms are able to tune system's control parameters to the vicinity of a critical point, thus explaining the ubiquitous observations of scale-free phenomena in natural systems (Bak 1996).

Initially, the theory of SOC was explained using sandpile toy mod-

els[3], and the study of self-organization using such tools remains active until today (Bak et al. 1987; Zhang 1989; Grassberger and Manna 1990; Manna 1991; Maslov and Zhang 1995; Christensen et al. 2004). In discrete sandpile models, grains are slowly added into the network sites. The total number of grains is a measure of the system "energy". When the number of grains in a lattice site exceeds certain threshold, toppling grains are redistributed into neighbouring sites. If the system is open, grains falling outside the boundaries are lost, therefore dissipating the available energy. When the system has low energy, no redistribution can take place, so energy is charged as new grains are added. However, when energy is very high, a new grain can cause a redistribution avalanche, which will dissipate a large amount of energy at the boundaries. At large times, this charge-dissipation procedure will self-tune the sandpile into a critical state, where avalanches follow power-law distributions (Jensen 1998; Christensen et al. 2004; Pruessner 2012).

From the conceptual point of view, the key point is that both processes (driving and dissipation) take place at very different timescales (Bak and Chen 1991; Jensen 1998; Christensen and Moloney 2005). In simulations, it is formally possible to obtain an infinite separation of timescales by means of an *offline driving* procedure: grains are added one by one, until an avalanche is triggered. While the avalanche takes place, grains are no longer added. When finite timescales are present in the macroscopic system, the scale-free behaviour is limited (Grinstein et al. 1990; Socolar et al. 1993).

Many variations can be added to these models. Although the first attempts for the model were deterministic (Bak et al. 1987), it was discovered that deterministic models does not formally present true scaling behaviour, but anomalous scaling (Tebaldi et al. 1999; Ktitarev et al. 2000; De Menech and Stella 2000; Bagnoli et al. 2003). On the other hand, numerical simulations on the stochastic sandpile (Manna 1991) were enough to demonstrate scaling and universality. But since critical points are the hallmark of second-order phase transitions, there were also efforts to map the stochastic sandpiles with other physical models at criticality, such as pinning-depinning transition of interfaces in random media, (Narayan and Middleton 1994; Nunes Amaral

[3]Which do not actually represent very well the physics of real sandpiles. Surprisingly, ricepiles seem to be more adequate (Pruessner 2012).

and Lauritsen 1997; Pruessner 2003) or systems exhibiting absorbing-active phase transitions (Vespignani et al. 1998; Dickman et al. 2000; Vespignani et al. 2000; Pastor-Satorras and Vespignani 2000; Rossi et al. 2000). The mappings were first heuristic, but rigorous analyses finally became available (Le Doussal and Wiese 2015).

Let us focus on the absorbing-active transition, which is of our interest here. In order to understand the relationship between second-order phase transitions and the sandpile models, we could play with fixed-energy sandpiles, where periodical boundary conditions are considered, and no grains are added. This system presents two distinct phases, depending on the energy E as the control parameter (Vespignani et al. 1998; Dickman et al. 2000; Vespignani et al. 2000; Dickman et al. 2001). Here, "activity" ρ, is to be understood as the number of sites with grains over the threshold, which can be redistributed: for $E < E_c$, there is no enough grains to sustain activity indefinitely, so at the end all grains redistribute to a frozen state –the absorbing state[4] $\rho = 0$; on the other hand, for $E > E_c$, there are so many grains that at least one site is always over the threshold, meaning that avalanches run indefinitely with $\rho > 0$. A second-order, continuous transition takes place at the critical energy E_c, a fact that was formally demonstrated recently (Dickman et al. 2010; Sidoravicius, Teixeira, et al. 2017). In this way, the scaling features of SOC can be explained from the formalism of non-equilibrium phase transitions. However, fixed energy sandpiles differ from the directed percolation (DP) universality class since energy is conserved, a symmetry that is not present in DP systems and that is relevant for universality (Rossi et al. 2000; Huynh et al. 2011; Bonachela and Muñoz 2008; Bonachela and Muñoz 2009; da Cunha et al. 2014).

We review the main ingredients of theory of SOC, as well as its "imperfect" counterpart, self-organized *quasi* criticality. We will do the same for the new proposed theory of *self-organized bistability*, which extends the concepts of SOC to first-order phase transitions.

[4] This is actually a set of different absorbing states; any microscopic state compatible with the macroscopic condition $\rho = 0$ is absorbing.

5.2.1 Self-organized Criticality

In order to analyse SOC systems, Langevin equations at the macroscopic level are considered. The order parameter in the sandpile is the activity, while the (self-organized) control parameter is the energy. In order to model it, one can take the Landau prescription, writing the most simple equation for the dynamics of the activity. Since the fixed-energy sandpile displays a continuous absorbing-active transition, the Reggeon field theory obtained in Chapter 1, eq. (1.30) can be used, backed by universality arguments. For fixed-energy sandpiles, one can write

$$\partial_t \rho(\vec{x},t) = (-a+\omega E)\rho - b\rho^2 + D\vec{\nabla}^2\rho(\vec{x},t) + \sigma\sqrt{\rho(\vec{x},t)}\eta(\vec{x},t) \qquad (5.1)$$

where the coefficients of the linear and quadratic terms are $a, b > 0$. The coefficient ω can be set $\omega = 1$ without losing any generality. As in the first chapter, D and σ are diffusion and noise constants, respectively, and $\eta(\vec{x},t)$ is a zero-mean Gaussian noise with $\left\langle \eta(\vec{x},t)\eta(\vec{x'},t)\right\rangle = \delta(\vec{x}-\vec{x'})\delta(t-t')$. For now, let us focus on homogeneous, noiseless, mean-field systems ($D = \sigma = 0$). In this case, the critical energy is located at $E_c = a$. When we move from fixed-energy sandpiles to SOC, the control parameter becomes a dynamical variable itself, increasing by slow accumulation of grains, and dissipating due to avalanche events. A simple way to model this process is using the equation

$$\partial_t E(t) = h - \epsilon\rho(t). \qquad (5.2)$$

where h and ϵ are the rates for driving and dissipation, respectively, and the spatial dependence has been dropped for simplicity. Note that the (mean-field) fixed point of the activity in this case is given by $\rho^* = h/\epsilon$, which inserted in eq. (5.1) returns a fixed point $E_{SOC} = a + bh/\epsilon$ to which the system self-organizes. Now, we consider the limit at which the energy is conserved $h, \epsilon \to 0$. However, as discussed above, a key ingredient of SOC is timescale separation, so the limit will be taken with $h \ll \epsilon$, or equivalently, $\Delta \equiv h/\epsilon \to 0$. When this limit is taken, one has $\rho^* \to 0$ and $E_{SOC} \to E_c$. If the energy is (almost) conserved, at

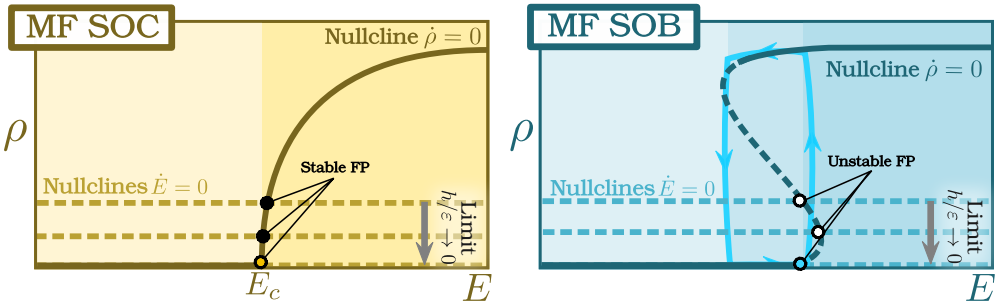

Figure 5.1: **Mean-field analyses of nullclines.** A sketch representing the nullclines $\partial_t \rho = 0$ and $\partial_t E = 0$. The latter is always given by horizontal dashed lines, and represented for three different values of $\Delta = h/\epsilon \to 0$. In the SOC case (left), nullclines collide at a stable fixed point, while in SOB (right) they do in unstable equilibria, creating a stable limit cycle around.

infinite timescale separation, the self-organized energy is the same as the critical control parameter[5](Tang and Bak 1988).

Looking at eq. (5.2), the SOC mechanism relies on the dependence of the energy dynamics on the current phase. If there is no activity, then $\dot{E} = h$, so E grows slowly until reaching the active phase. On the other hand, when $\rho > 0$, then $\dot{E} \simeq -\epsilon\rho$ for a large enough timescale separation, decreasing the energy to the absorbing phase. This mechanism makes the control parameter to fluctuate around E_{SOC}, and drives the energy exactly to E_c in the infinite timescale separation. Then, the existence of a control mechanism that acts differentially on each phase creates a feedback loop that self-organizes the system to the very edge of the transition (Grinstein et al. 1990; Dickman et al. 2000; Moreau and Sontag 2003; Bonachela and Muñoz 2009; Buendía et al. 2020c).

Let us return to the spatially extended, stochastic description. The demographic noise also vanishes in the absorbing state, so once the activity goes to zero the dynamics freezes. Fixed-energy sandpiles can be modelled just by letting $\partial_t E(\vec{x}, t) = \nabla^2 \rho(\vec{x}, t)$ describing the redistribution of energy among neighbouring sites in the lattice. Now, the control parameter is the energy density $\overline{E}$ in the lattice, i.e., the integral over

[5]We insist that the derivation was performed in deterministic mean-field, although numerical evidence will demonstrate that this is also the case in lower dimensions.

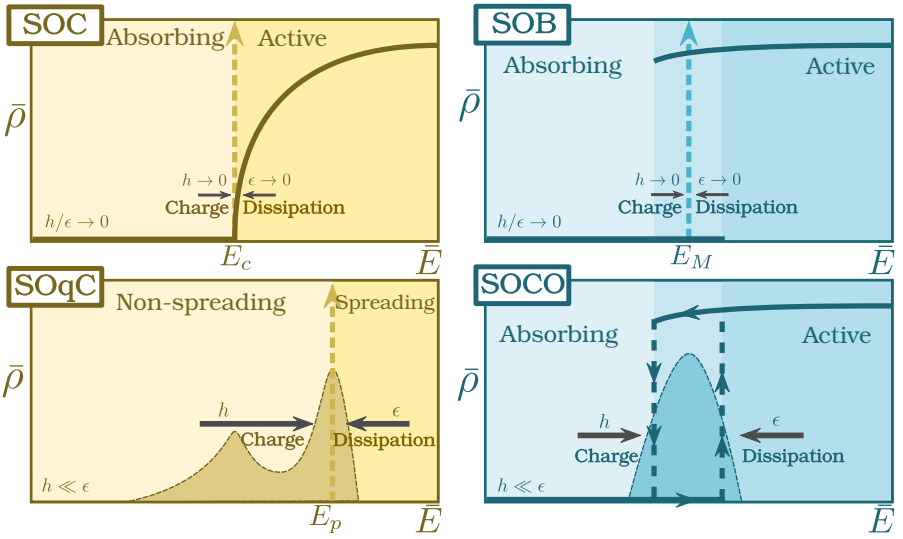

Figure 5.2: **Mechanisms for self-organization.** The left panels show self-organization to a continuous, second-order phase transition, while the right ones display self-organization to a first-order one; top panels are for perfect timescale separation, and the bottom ones are for non-conserved cases. In SOC, the system self-organizes to the critical point E_c, while the probability distribution of the non-conserved version tends to peak around the percolation point E_p between spreading phases. In SOB, they are always self-organized to the Maxwell point E_M, where both phases are equally stable.

$\vec{x}$ of the energy field divided by the volume, which is always globally conserved. As in mean field, if $\bar{E} > E_c$, redistributions take place all the time, making $\rho > 0$, while if $\bar{E} < E_c$ the system falls into the absorbing state (Dornic et al. 2005). Although this dynamics has been justified just by phenomenological arguments, it can be formally derived from microscopic dynamics on (Rossi et al. 2000; Wiese 2016).

In order to perform the simulations, there are two options, offline or online driving, as mentioned earlier. In offline driving, one adds a small amount of activity and energy initially, and let the system evolve until falling into the absorbing state, with open boundary conditions to allow dissipation. Then, the process is repeated. The energy will then converge to the critical point of the (two-dimensional transition). Another possibility is to consider an *online driving*, modifying the equa-

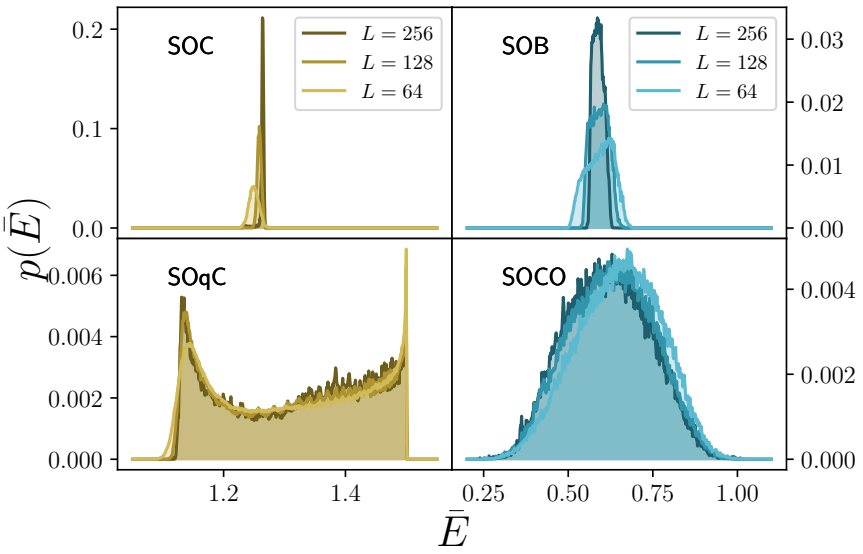

Figure 5.3: **Distribution of average energy density.** The distributions have been computed for both perfect and imperfect timescale separation (top and bottom rows, respectively) and three different system sizes each in order to appreciate scaling. Note that in SOqC and SOCO cases the distribution remains broad even in the thermodynamic limit. Parameters: (SOC) $a = -1$, $b = 1$; (SOB) $a = -1$, $b = -1.5$, $c = 1$. The corresponding non-conserved counterparts additionally use: (SOqC) $\gamma = 0.2$, $h = 1.0$, $\epsilon = 0.1$, $E_{\max} = 1.5$; (SOCO) $\gamma = 0.02$, $h = 1.0$, $\epsilon = 0.1$, $E_{\max} = 1.3$ with offline updating (eqs. (5.6)).

tion as in eq. (5.2) to allow both driving and dissipation, as

$$\partial_t \rho(\vec{x}, t) = (-a + E(\vec{x}, t))\rho - b\rho^2 + D\nabla^2\rho + \sigma\sqrt{\rho(\vec{x}, t)}\eta(\vec{x}, t), \tag{5.3a}$$

$$\partial_t E(\vec{x}, t) = \nabla^2\rho(\vec{x}, t) + h(\vec{x}, t) - \epsilon\rho(\vec{x}, t), \tag{5.3b}$$

where now a slight perturb to the activity can drive the system out of the absorbing state. The difference between these equations and the offline method is that here $\overline{E}$ is no longer constant during avalanches.

The equivalence between the stationary point E_{SOC} of these equations and the actual value E_c of the low-dimensional system is difficult to prove analytically, but computational data consistently report

that $E_{SOC} \simeq E_c$ in the large timescale separation limit (Bonachela and Muñoz 2009).

Figures 5.3 and 5.4 show results from the numerical simulation[6] of these equations, performed using the Dornic *et al.* algorithm that allows exact integration of the system (Dornic et al. 2005). Figure 5.3 shows the probability distribution of finding an energy density $\overline{E}$ in the offline procedure, which becomes more peaked around E_c as the system size increases, leading to $\delta\left(E_c - \overline{E}\right)$ in the thermodynamic limit. Note that increasing the system size has the effect of obtaining a better timescale separation, since boundary dissipation is equivalent to set a dissipation rate $\epsilon \propto L^{-1}$, while energy addition in the bulk rate grows as $h \propto 1/N = L^{-2}$ in the two-dimensional case.

Let us go back to the problem of the universality class of stochastic SOC models. As it was discussed earlier, activity was chosen to follow the DP universality class, and at first sight it could seem that the sandpiles are also compatible with DP. However, there are several evidences that the SOC universality class is different, being so-called conserved directed percolation (C-DP) or Manna class (Dornic et al. 2005). One is the energy conservation law, which introduces relevant perturbations at the renormalization group level. Moreover, the pinning-depinning transition in random media, which has been formally mapped to the sandpile models, is inherently different from DP (Alava and Muñoz 2002; Bonachela et al. 2007; Bonachela et al. 2009; Le Doussal and Wiese 2015; Grassberger et al. 2016).

The C-DP class is explicitly clear in one or two dimensional systems, where it can be seen that critical exponents are different from those of DP (Rossi et al. 2000; Huynh et al. 2011; Bonachela and Muñoz 2008; Bonachela and Muñoz 2009; da Cunha et al. 2014), including recent extensive numerical experiments (Grassberger et al. 2016). On the analytical side, a renormalization group is still missing, despite of all the attempts in the literature (Vespignani et al. 1998; van Wijland 2002; Pruessner 2013; Janssen and Stenull 2016).

[6] Performed using a package originally written by Paula Villa, which I later improved. The code for integration is open-source, and can be found on GitHub at https://github.com/pvillamartin/Dornic_et_al_integration_class.

5.2.2 Self-organized Bistability

SOC describes how a system self-organizes to the critical point of a second-order phase transition. A natural question is to wonder if there exists an analogous mechanism for self-organization to first-order transitions, that usually present a region of bistability between the active and absorbing states.

This is a recent proposal (Gil and Sornette 1996; di Santo et al. 2016) and the basic idea is the same as in SOC, taking a minimum model for the activity, and letting the control parameter to adapt depending on the model's dynamical state. In order to do this, one could get a third-order polynomial, which is the most simple model for bistability, and write

$$\partial_t \rho(\vec{x},t) = (-a + E(\vec{x},t))\rho - b\rho^2 - c\rho^3 + D\nabla^2\rho + \sigma\sqrt{\rho(\vec{x},t)}\eta(\vec{x},t), \quad (5.4a)$$

$$\partial_t E(\vec{x},t) = D_E\nabla^2\rho(\vec{x},t) + h(\vec{x},t) - \epsilon\rho(\vec{x},t), \quad (5.4b)$$

where now $b < 0$ and $a, c > 0$. Homogeneous, noiseless, mean-field solutions ($D = \sigma = 0$) of these equations lead to a limit cycle in the phase space, when the timescale separation is large enough. Let us analyse in detail the mean-field dynamics of this system, in order to understand in detail how the self-organization works here.

For a fixed energy value of energy, the activity equation has the typical S-shape characteristic of first order transitions with hysteresis. The absorbing state $\rho_0 = 0$ is stable as long as $E \leq a \equiv E_2^*$. A solution $\rho_\pm = b/2 \pm \sqrt{b^2/4 + E - a}$ emerges via a saddle-node bifurcation at the point $E_1^* = a - b^2/4$. The equilibrium ρ_+ is stable for $E > E_1^*$, while ρ_- becomes stable –but negative– for $E > a$. Therefore, the solution ρ_- only has physical sense in the interval $E_1^* < E < E_2^*$, where it is unstable. Hence, this provides the region of bistability, where the absorbing and the ρ_+ solutions both are stable, with their stable manifolds separated by ρ_-. This is shown in Fig. 5.2, which is nothing but a cut of Fig. 1.8.

When we include the energy dynamics, the system behaviour becomes richer. As in SOC, the energy tends to charge slowly during the absorbing phase, and discharge fast when $\rho > 0$. However, now the hysteresis cycle allows the system to oscillate: energy charge continues up to the point $E = E_2^*$, where the absorbing state becomes unstable,

and then it is forced to jump to the active phase. At the active phase, energy is dissipated, but up to $E = E_1^* < E_2^*$ following the upper branch of the hysteresis cycle. This leads to the oscillations shown in Fig. 5.2. It is possible to demonstrate that the period of such cycle scales as $T \sim bh/(2\epsilon) = b\Delta/2$, so when the infinite timescale separation is taken, the period of oscillations becomes infinitely slow –conforming an infinite period bifurcation. We will discuss more in detail what happens in the case of "imperfect" timescales later.

Now it is possible to go beyond the mean-field description, as it was done for SOC. Numerical evidence shows that for fixed energy the bistable region survives in low-dimensional, stochastic systems[7]. In the bistable region, instead of the critical point, the system self-organizes to the *Maxwell point* E_M at which both phases are equally stable, as the "edge" of phase coexistence. Simulations show that when we allow the energy to self-organize (either following offline or online procedures), the system converges to $\overline{E} \simeq E_M$, being exact at the thermodynamic limit.

It is possible to do avalanche statistics, as in the case of SOC. Surprisingly, avalanches in SOB also present power-law distributions, even in the absence of a critical point (di Santo et al. 2016). However, the exponents characterising the universality class are different, and coincide instead with those of the mean-field DP: $\tau = 3/2$ and $\alpha = 2$, in contrast with the Manna class. It is striking that these oscillations are even to display "mean-field" exponents even at low dimensionality. The reason behind this is that energy is self-organized to the Maxwell point, where both phases are equally stable, and then the system behaves similarly to a voter model, which presents DP scaling properties (Hinrichsen 2000; Marro and Dickman 2005; Henkel et al. 2008; Ódor 2008), but the critical upper dimension is $d = 2$ (Dornic et al. 2001; Henkel et al. 2008).

It is important to remark that the avalanche distribution presents a typical scale, in the shape of activity bursts that span the whole system almost deterministically, taking all system energy, and usually called *dragon kings*[8] in the literature (Sornette and Ouillon 2012; di Santo et

[7] As long as the parameter b is greater than certain tricritical value. Lower values allow fluctuations to soften the transition, making it continuous (Villa Martín et al. 2015).

[8] The poetic name refers to events that are both rare ("dragon") and large ("kings").

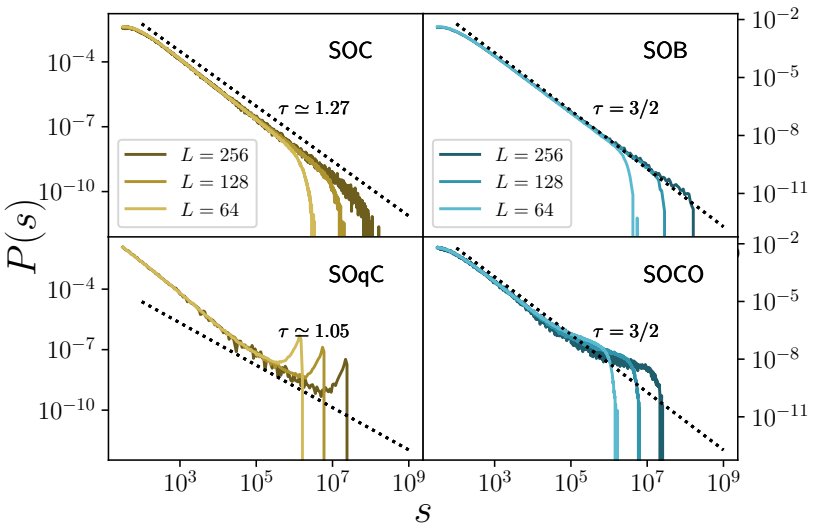

Figure 5.4: **Avalanche size distributions for the diverse self-organization mechanisms.** For SOC and SOB (upper panels) the avalanche distribution is scale-free, only cut due to the finite system size. The avalanche size distribution scales as the system size, as expected by the theory of critical phenomena. For imperfect cases, SOqC and SOCO, the power laws can be fitted only approximately, even in the thermodynamic limit, since the systems do not lie exactly at criticality. Parameters are as in fig 5.3, except $\gamma = 0.1$, $h = 0.1$, $D_E = 0.1$ in the SOqC case.

al. 2016). These dragon kings comes from the slow mean-field oscillatory behaviour. Fluctuations deplete small amounts of energy, but if the system is able to charge enough in order to complete the limit cycle, all the sites become active for some time, leading to this strong temporal scale. However, remember that the period of such collective oscillations increases as we approach the perfect timescale separation (i.e., as system size grows), so as we increase the system we find larger spanning power-law distributions.

The value of $|b|$ has an impact in the scale-free avalanches observed

They were introduced in the context of predictability in economical crises. It is noteworthy to see the coincidence in name with Chinese mythology, where the Dragon King is a deity that controls watery, weather... and of course, dragons!

in SOB, since it controls both the amplitude and frequency of the oscillations. For small jumps from the quiescent to active state, power laws span for many decades, as can be seen in Fig. 5.4. However, larger values of $|b|$ lead to more frequent appearance of dragon kings.

Finally, let us remark that sandpiles can be modified in order to display SOB properties (di Santo et al. 2016), just by changing the redistribution rules of the classical sandpile. A way to do this is including a facilitation mechanism that fosters the creation of activity at the redistribution of grains, a common way of generating discontinuous transitions (Villa Martín et al. 2015). The behaviour of such sandpiles is perfectly explained by SOB dynamics, showing power-law distributed avalanches with the same exponents, as well as the outburst, dragon-king avalanches (di Santo et al. 2016). Actually, this behaviour seems to resemble better the dynamic of real sandpiles than SOC itself, and could be underlying physical process of microfracture experiments (Papanikolaou et al. 2012).

5.3 Imperfect self-organization

We have considered that both SOC and SOB theories have a perfect separation of timescales so far, and hence the energy is only dissipated at boundaries. These are key aspects in order to preserve an exact self-organization to criticality, or, in the case of SOB, to the Maxwell point. However, real natural phenomena do not usually present a perfect timescale separation, and energy is not exactly conserved, but dissipation happens also at the bulk level. Many SOC models are, indeed, non-conserved: earthquake models (Bak and Tang 1989; Olami et al. 1992) and forest-fire models (Bak et al. 1990; Grassberger and Kantz 1991; Drossel and Schwabl 1992) are both classical examples. In the case of the brain, SOC has been proposed as a tentative self-organization mechanism to criticality in several works (Levina et al. 2007; de Arcangelis et al. 2006; Millman et al. 2010; Hesse and Gross 2014), but the system is non-conserved due to the leaky nature of both neurons and synapses (Choi et al. 2012). As we commented above, neuronal plasticity is composed of very different timescales, usually

much larger than the spiking dynamics, but still not the formal infinite separation. Then, it is important to understand how are SOC and SOB results modified under these "imperfect" conditions. Although the non-conserved systems are not truly critical, they display approximate scaling laws (Grassberger and Kantz 1991; Grassberger 1994; Bröker and Grassberger 1997; Grassberger 2002; Wissel and Drossel 2006; Zierenberg et al. 2020) that could be the source of the claimed criticality in the brain.

5.3.1 Self-organized quasi-criticality (SOqC)

Our first step is to speak of imperfect self-organized criticality, usually called *self-organized quasi-criticality* or SOqC. We start by performing a simple modification to include energy dissipation in the SOC equations, as

$$\partial_t \rho(\vec{x},t) = (-a + E(\vec{x},t))\rho - b\rho^2 + D\nabla^2\rho + \sigma\sqrt{\rho(\vec{x},t)}\eta(\vec{x},t), \tag{5.5a}$$

$$\partial_t E(\vec{x},t) = D_E\nabla^2\rho(\vec{x},t) - \epsilon\rho(\vec{x},t), \tag{5.5b}$$

where now set $h = 0$, and ϵ is no longer constrained to vanish in the infinite size limit. The system is integrated as before, either using an online or offline rule. The offline rule has to be slightly changed, in order to account for the loss of energy in the bulk. Every time the system falls at the absorbing state, a small perturbation of activity is performed, generating a spark of activity in a certain location, and the energy is increased at every site as well, to compensate for bulk dissipation. In summary, the offline charge goes as

$$\rho(\vec{x}_0, 0) \to h, \tag{5.6a}$$

$$E(\vec{x}, 0) \to E(\vec{x}, 0) + \gamma(E_{\max} - \overline{E}), \tag{5.6b}$$

where γ is an external driving, $E_{\max}$ the maximum allowed energy in the system, and $\vec{x}_0$ a random position in the lattice. This is the update rule used the Figures 5.3 and 5.4.

How does dissipation change the behaviour of the system? The first important effect is that the self-sustained active phase disappears. If the energy equation is integrated and substituted into the activity one,

we find a non-Markovian term, $-\epsilon\rho(\vec{x},t)\int_0^t dt'\rho(\vec{x},t')$, which is characteristic of *dynamical percolation* (Cardy and Grassberger 1985; Janssen 1985; Grassberger 1983; Muñoz et al. 1996; Buendía et al. 2020a). In this kind of systems, the two phases are a non-spreading and a spreading (excitable) phases. In the latter, a small perturbation can percolate through the whole system, persisting for some time before falling down again into the absorbing phase. Therefore, the universality class of SOqC is that of dynamical percolation, rather than C-DP (Bonachela and Muñoz 2009). As it was commented before, the symmetry corresponding to energy conservation is relevant for universality classes.

In this case, the system charges energy slowly until finally reaching the spreading phase, at which avalanches are able to percolate, dissipating in their way all the system energy, and pushing it deep into the non-spreading again. Then, the average energy density "wanders" around the (percolation) critical point, but never reaching the edge of the phase transition exactly, as shown in Figs. 5.2 and 5.3. The energy does not adapt to the critical value, but jumps alternating between sub- and super-critical states, for any system size. Numerical results reveal that this sweeping through the phase transition point might suffice to induce approximate scaling behavior, but not true scale invariance (Sornette 1994; Bonachela and Muñoz 2009; Palmieri and Jensen 2018; Buendía et al. 2020a).

If instead of the offline perturbation the online driving is considered, a term $+h$ has to be added (or $+h\,(E_{\max} - E\,(\vec{x},t))$, if we want to set a maximum level for the energy) to the energy equation in eqs. (5.5). Now, note that it is possible to tune the (finite) value of h so it compensates the dissipation level, leading to energy conservation, and hence recover the C-DP universality class, although the imperfect separation of timescales does not allow to obtain a truly critical point. This could be expected from the fact that in this case the same equation as in SOC is being used, but the limit of perfect timescale separation is no longer imposed. In this case, the ration between the driving and dissipation constants $\Delta = h/\epsilon$ acts as a control parameter that can be freely tuned –and therefore the system is not completely "self-organized" in this sense. Actually, if dissipation dominates, the system becomes subcritical, while if we make Δ large, then we go to the supercritical phase. However, for a broad range of choices for Δ, the system will hover around the critical state, showing imperfect scaling behaviour.

There is still a comment that will prove very important for the study of self-organization in the brain. We said that the offline version of SOqC belongs to the dynamical percolation universality class, while the online one belongs to C-DP. The only (formal) difference between both algorithms is just the term $+h$, the way of charging the energy. So, what happens in the online algorithm if we take the limit $h \to 0$? As Fig. 5.4 shows for SOqC, for small avalanche sizes and durations, the distribution scales with the exponents of C-DP, while larger ones show the dynamical percolation scaling. The value of h (among other parameters) determine the span of the dynamical percolation region, that grows as $h \to 0$. But as long as $h > 0$, this scaling will end at some point, finally showing the true scaling behaviour of the system. However, very large system sizes might be needed for small values of the driving –otherwise the true C-DP behaviour may be hindered. Additionally, in offline updating, low values of γ do not allow the system to enter into the spreading phase, making the energy to hover around E_c, and retrieving C-DP avalanches (see (Buendía et al. 2020a)).

5.3.2 Self-organized collective oscillations (SOCO)

Finally, in order to discuss all the possible cases, we focus on self-organization of systems at a first order transition in which the timescale separation is not perfect. A simple way to do this is to study arbitrary dissipation and driving, using offline or online rules as the ones discussed in the earlier section. The imperfect version of SOB does not depend on the update procedure used. It suffices to assume that h and ϵ do not vanish in eqs. (5.4) with online updating. We remind that the energy nullcline gives the fixed point of the energy, $\rho^* = h/\epsilon$, which is a simple horizontal nullcline that intersects with the S-shaped cubic nullcline set by $\partial_t \rho = 0$, generating a stable limit cycle. The fact that this nullcline is horizontal becomes very important as we increase the timescale separation, because the tangential cut with the absorbing state is the ultimate reason for the infinite-period bifurcation at $\Delta = 0$, as we will demonstrate later. As long as the timescale separation is large enough, $\Delta < 1$ the system "self-organizes" to collective oscillations, and hence the name *self-organized collective*

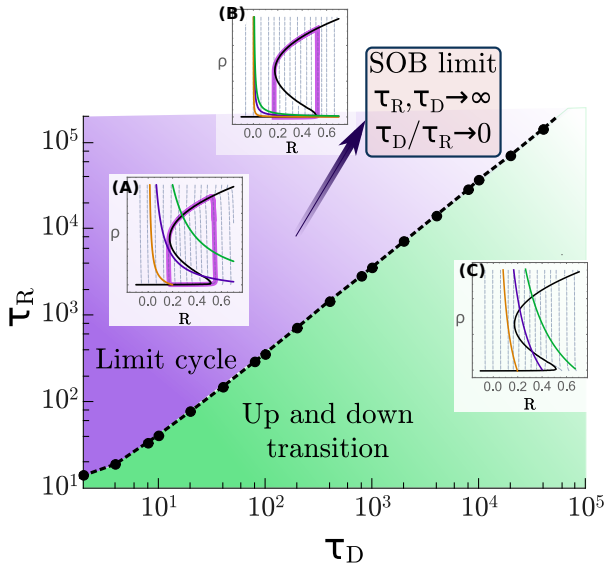

Figure 5.5: **Equivalence between SOB and the Landau-Ginzburg model.** In a single unit, noiseless mean-field system, for $\Delta < 1$ (i.e., $\tau_R/\tau_D > 1$), the Landau-Ginzburg model presents an oscillatory regime. As the timescales become larger, but always with $\tau_R \gg \tau_D$, the null-clines for the different values of ξ (shown in insets as yellow, purple, and green colours) tend to become the same, making the system behave as in SOB. On the other hand, if $\Delta > 1$, we have the bistability between down and up states. Parameters: (A) $\Delta = 0.1$, $\tau_R = 10^3$. Nullclines are $\xi = 0.2, 1.5, 3.5$, respectively (B) $\Delta = 10^{-3}$, $\tau_R = 10^7$. Nullclines are $\xi = 1, 5, 10$, respectively. (C) $\Delta = 10$. Nullclines are $\xi = 0.2, 1.5, 3.5$, All cases use $a = 0.6$, $b = 1.3$.

oscillations for the imperfect SOB model. On the other hand, if $\Delta > 1$, the mean-field system still displays a bistability reminiscent of the individual unit, although this case is not as interesting because it means that driving dynamics is way faster than dissipation.

Therefore, we jump directly into a more applied situation, by analysing the Landau-Ginzburg model by di Santo *et al.* (di Santo et al. 2016). We demonstrate that this system could be also a paradigmatic example of SOCO itself, with little difference with our discussion above. Note that the equations for the single unit of the Landau-Ginzburg model, eqs. (2.26) have already the same shape for the

activity that SOC and SOB, and only the energy variable (that was called "R" in that case) differs. Let us rewrite the timescales $h = \tau_R^{-1}$, $\epsilon = \tau_D^{-1}$, the control parameter[9] $\xi \equiv E_{\max}$, and $R \equiv E$. Then, the equations read[10]

$$\partial_t \rho(\vec{x},t) = (-a + E(\vec{x},t))\rho - b\rho^2 - c\rho^3 + D\nabla^2\rho + \sigma\sqrt{\rho(\vec{x},t)}\eta(\vec{x},t), \quad (5.7a)$$

$$\partial_t E(\vec{x},t) = D_E\nabla^2\rho(\vec{x},t) + h(\xi - E) - \epsilon E\rho. \quad (5.7b)$$

As a small side note, the diffusion term was not present in the original model, so it could be disregarded without changing the universality class (Buendía et al. 2020c). Here dynamics are not conserved, so the system cannot truly self-organize, as it was already discussed for the SOqC case. Actually, control parameters remain, such as ξ and $\Delta = h/\epsilon$. Let us first remind in detail how the deterministic single unit works ($D = D_E = 0$ and $\sigma = 0$). We assume that $\Delta < 1$, since the case $\Delta > 1$, as it happens in the standard SOCO, is uninteresting for us –just the bistability, see Fig. 5.5. The model shows several phases depending on the amount of synaptical resources, ξ:

- If $\xi < a$ obviously $E < a$, and then the linear term in the activity equation becomes negative, leaving the absorbing state as the only possible stable phase. Both nullclines intersect inside the absorbing phase. It is very easy to confirm analytically the existence of this equilibrium, since the exact state is $\rho_0 = 0$, $E_0 = \xi$. It loses stability at $\xi = a$ via a homoclinic bifurcation.

- If we let $\partial_t E = 0$, the fixed points lies at $E^* = h\xi/[(h+\varepsilon)\rho^*]$, which is defined outside of the absorbing phase. If we make a large timescale separation, then we get $E^* \simeq \Delta\xi/\rho^*$. It is possible to show that this point is unstable, and it is surrounded by the limit cycle created through the homoclinic bifurcation. Actually, a simple reasoning is able to show the existence of the limit cycle. If we are in the absorbing state, energy has to slowly grows

[9] We remind that it originally represents availability of Ca^{2+}, essential to facilitate spiking activity.

[10] In (Buendía et al. 2020a), we performed the analysis using $h(\xi - \overline{E})$ instead of $h(\xi - E(\vec{x},t))$, an irrelevant change in mean-field, and qualitatively non important in smaller dimensions.

since at $\rho = 0$ we have $\partial_t E = h(\xi - E)$. If $\xi > a$, at some point we get $E = a$, making the absorbing state unstable, hence jumping to the active phase, making $\rho > 0$ and rendering E^* the only possible stable equilibrium. Now the energy has to change in order to accommodate to E^*. When Δ is very small, we have $E^* \simeq 0$, which is again *inside* the absorbing state, so the system as to dissipate the energy again. But, as soon as we fall into the absorbing –and before reaching E^*–, the solution E^* no longer exists, and energy is forced to start charging again, in a never-ending loop (see also (Mikkelsen et al. 2013)).

- When we let the control parameter ξ to be larger, then the nullclines can intersect in the stable up state, preventing the oscillations. From the point of view of the system dynamics, what happens is that after leaving the absorbing state, the stable energy $E^* \simeq \Delta\xi/\rho^*$ is reached before falling again to the absorbing. Therefore, we are basically compensating the small value of Δ with larger values of ξ. As the infinite timescale separation is approached, larger values of ξ are needed in order to compensate Δ, and in the limit $\Delta \to 0$, a value $\xi \to +\infty$ is required to destabilize the limit cycle, which disappears following a Hopf bifurcation.

This intermediate phase can be maximized by approaching the perfect timescale separation limit so the Landau-Ginzburg model converges to SOB in this limit –displaying also scale-free avalanches, in the sense that SOqC converges to SOC. This procedure is illustrated in Fig. 5.6. A large timescale separation allows the system to self-organize at the edge of a synchronous state, very similar to SOB dynamics. Then, let us recap from Chapter 2 the phase diagram collective state of the Landau-Ginzburg system:

- If ξ is small enough, then the system has not enough synaptical resources and falls into the absorbing state, without any activity. If it is very large, then the system poses at an active phase, where each individual site becomes active and inactive alternatively, depending on its locally available resources. This is done in an asynchronous way, leading to a constant average activity.

- Between both regimes, there is two additional phases characterized by oscillations of the individual units, that can be either

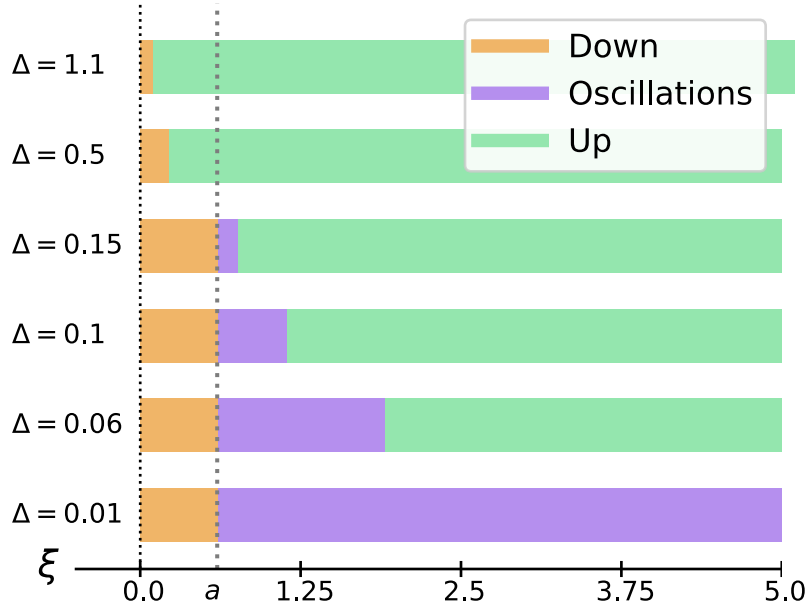

Figure 5.6: **Maximization of the mean-field oscillatory phase.** This diagram shows the length spanned by each phase as a function of the control parameter ξ, depending on the timescale separation Δ. As we make $\Delta \to 0$, the oscillatory phase tends to span larger portions of the parameter space, until completely taking it, hence making the system almost independent on ξ.

synchronized or asynchronous (see Chapter 2). The synchronous phase resembles very well the activity observed in SOB systems. Actually, di Santo *et al.* (di Santo et al. 2018a) demonstrated scale-free avalanches emerge at the edge between the synchronous and asynchronous states.

Notice that in the single unit, when we take $\Delta \to 0$, the oscillatory phase is stable for a wide range of ξ values. Therefore, at the collective level we could then wonder what happens with the synchronization phase transition in this limit. Taking $\Delta \to 0$ makes the system identical to SOB, so we know that adopting the perfect timescale separation, the system is fully independent of ξ and scale-free avalanches can be found at almost any value of the control parameter.

We have also studied the full two-dimensional system numerically. In particular, simulations of eqs. (5.7) were performed for several lat-

tice sizes, running up to 10^8 simulations for different values of the control parameter. Online updating is used in the simulations, and therefore avalanches are measured by analysing the continuous time series, and defining a small threshold (we set it to $\rho_T = 10^{-6}$) that is used to define avalanche start and end. Later, the distribution of avalanche area over the threshold, and its duration, its studied (see also Appendix A) (di Santo et al. 2016).

As it can be seen in Figure 5.8, simulations reveal power-law distributed avalanches for several values of the control parameter ξ, with exponents compatible with those of predicted by SOB theory, as well as large "dragon king" outbursts that scale with system size. Then, the Landau-Ginzburg model with perfect timescale separation is able to self-organize at the edge of the discontinuous phase transition, as it happens in SOB.

One could wonder then what happens with hybrid-type synchronization. If a large timescale separation is able to approximately bring the Landau-Ginzburg model to a Maxwell point, explaining the emergence of critical-like avalanches, isn't it the end of the story? We could then argue that the Landau-Ginzburg model works as a kind of approximate self-organization, and its universality class is the same as in SOB. We examine this possibility in the next section with detail.

5.4 SOB in the Landau-Ginzburg model

When SOB was proposed in the first place, it was already hypothesized that it could be relevant to explain the emergence of scale-free avalanches in neuronal activity (di Santo et al. 2018a): SOB avalanches present the same critical exponents as the unbiased branching process, as it was initially argued for the brain (Beggs and Plenz 2003; Beggs and Plenz 2004). Moreover, SOB relies on self-organizing over a bistable transition, which have been argued to play an important role during the last chapter. Bistability between up and down states has been observed in the brain in conditions as deep sleep or anesthesia (Tsodyks and Markram 1997; Mongillo et al. 2012; Stepp et al. 2015). Under this light, it was proposed that SOB could be fit the experimen-

tal observations better than the usual SOC (de Arcangelis et al. 2006; Levina et al. 2007; Millman et al. 2010; Bonachela et al. 2010).

In parallel with SOB, the Landau-Ginzburg theory also presents a first-order phase transition, and the only difference is the dynamics of the self-adapting variable. In SOB, this is the "energy" field, that in the Landau-Ginzburg description takes the role of synaptical resources. As it was argued in the last section, the Landau-Ginzburg model can be seen as an imperfect SOB, or SOCO, so there is still parameters that can be tuned. These are the timescales of charge and depletion of calcium ions (τ_R and τ_D, respectively) in the extracellular medium, and their the maximum concentration, ξ. As we pointed out before, the timescales can be readily identified with the driving and dissipation rates in non-conserved SOB, while the calcium concentration is analogous to $E_{\max}$. In order to determine the actual role of self-organizing dynamics, we work with biologically motivated values for the ratio between the timescales, that will be kept small but finite –so, no perfect separation of timescales is possible.

Given a fixed separation of timescales, the Landau-Ginzburg model still retains ξ as a control parameter. The collective behaviour of the system depends on ξ, ranging from the absorbing ("down") state, to an asynchronous ("up") state, crossing another phase of "synchronous regular" bursts. Between the synchronous regular and the asynchronous phases, at ξ_c, the system displays a synchronization transition, where scale-free avalanches are found, as long as diverging susceptibility and rich wave propagation in two-dimensions (di Santo et al. 2018a). The main question at this point is: could such a synchronization transition be obtained in a self-organized, parameter-free model?

The question can be answered by revisiting the detailed mean-field analysis of the individual unit of eqs. (5.7) (so we make assume $D = D_E = 0$, $\sigma = 0$). The first step is to see that the separation of timescales, which can be resumed in the parameter $\Delta = h/\epsilon = \tau_D/\tau_R$, is increased in the limit $\Delta \to 0$. The SOB limit will also require each one of the rates to vanish in order to achieve energy conservation, i.e., $h, \epsilon \to 0$, so both processes become infinitely slow. This limit is illustrated in Figure 5.7. Formally, the nullcline $\dot{E} = 0$ leads to $E^* \simeq \Delta\xi/\rho$, so as the separation of timescales increases, the nullcline arrives sooner at a horizontal asymptote. Remember that the SOCO system (eqs. (5.4) with

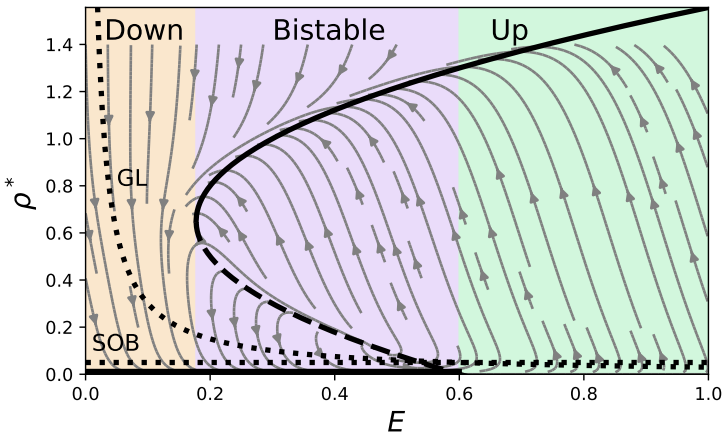

Figure 5.7: **Nullclines of SOCO vs the Landau-Ginzburg model.** Both models share the S-shaped nullcline for the activity $\partial_t \rho = 0$, represented as a thick, black line. Dotted lines represent the energy nullclines $\partial_t E = 0$ for the SOB model and the Landau-Ginzburg (LG), respectively. Note how similar they are when they collide with the unstable equilibrium of the activity nullcline. Both tend to become parallel as the timescale separation increase. Parameters: $a = 0.6, b = 1.3, h = 0.005, \epsilon = 0.1, \xi = 1.0$.

$\Delta > 0$) displayed a horizontal nullcline, so this means that when the limit $\Delta \to 0$ is taken changing ξ does not affect the nullcline shape, making the parameter irrelevant in the perfect timescale separation limit. Therefore, as one could expect, the "perfect timescale" separation eliminates also any dependence on the control parameter. For criticality, this means that reducing Δ leads to a larger range of possible values of ξ where scale-free avalanches can be found, as seen in Figure 5.8. Please note that this is related, but not direct consequence, of the maximization of the oscillatory phase displayed in Figure 5.6. While the maximization of the oscillatory phase affects the individual unit, avalanches are collective phenomena. Such maximization could have ended either in synchronous or asynchronous behaviours, but SOB-like dynamics ensures the system self-organizes to the transition.

Therefore, in order to consider that a model is "self-organized", it is essential to study the relationship between the timescales needed to recover the SOB limit. Experimental observations for the case

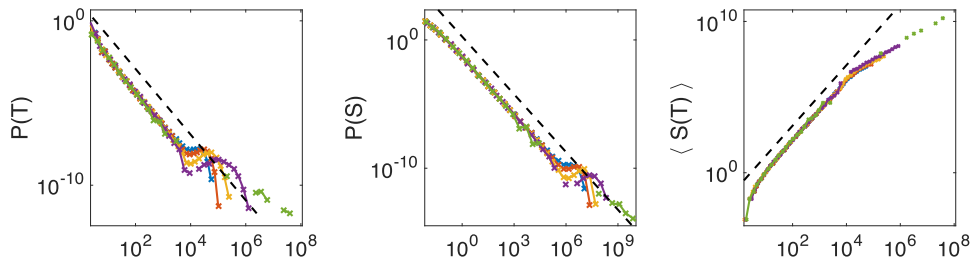

Figure 5.8: **Independence on the control parameter.** Avalanche distributions obtained for two-dimensional, noisy systems with a large separation of timescales, for different values of the control parameter ξ, namely $\xi = 1, 3, 5, 7, 10$. Dashed lines indicate theoretical distributions of the unbiased branching process avalanches. Parameters: $b = 0.5$, $a = 1$, $\tau_D = 10^4$, $\tau_R = 10^6$, $D = D_E = 1$.

of short-synaptic plasticity, which is the main mechanism behind the Landau-Ginzburg model, yield differences in the range from milliseconds to few seconds (Tsodyks and Markram 1997; Buzsáki 2006; Mattia and Sanchez-Vives 2012) that fall outside of the proposed SOB limit, which requires a larger separation. In the case of the Landau-Ginzburg model, if the depletion timescale is of the order of milliseconds, that would need a driving of the order of minutes –ten times larger than the observed ones.

In addition to that, the scale-free power laws have been observed in many different contexts, as resting state, cultured networks, or even during tasks (see Chapter 1). Therefore, there should be a way of distinguishing these scenarios, beyond the parameter-free proposal of self-organization. This hints that self-organization in the way of SOB is not a plausible mechanism to explain all the observed features of cortical activity, at least not by considering only the short-term plasticity adaptation in the way the Landau-Ginzburg model does. For example, the original proposal by Tsodyks-Markram (Tsodyks and Markram 1997) also implements a facilitation with a longer timescale, which allow the self-organization to happen. As we discussed at the beginning of the chapter, there is a plethora of different neuroplasticity mechanisms, with many different timescales and effects, such as the intrinsic

change of excitability in the neurons, long term Hebbian plasticity, or synaptic augmentation. The effects of the different regulatory mechanisms is left as a future, promising work.

In order to sum up, the SOB model can be seen as the limit of the Landau-Ginzburg for a perfect timescale separation. Both cases are able to display scale-free avalanches with exponents compatible with the ones empirically observed in neuroscience. However, the observed separation of timescales is not enough in order to explain the criticality observed in the Landau-Ginzburg model as self-organized, neither to determine its universality class –which, in the proper limit, is to be shared with SOB.

Chapter 6

Perspectives and future work

"Most important part of doing physics is the knowledge of approximation."

- Lev Landau.

After having presented the main results from the thesis, we discuss some of the ideas that emerged from such results, and how could they impact the research in theoretical neuroscience and the criticality hypothesis. In particular, I think that the most stimulating aspects to discuss are the open questions: those issues which we could not answer just by looking at the models, those we do not understand, and what are our hopes for near-future experimental data that could confirm or discard some of the hypotheses presented in this text. As it was indicated in Chapter 1, experimental evidence has the last word on the model reality, and although sometimes theoretical advances indicate what to look for, models should not be driven by models exclusively.

However, in order to compare with experiments, toy models are often not sufficient. All the previously analysed models from chapters 3 to 5 are abstract representations of possible neuronal systems, or their effective dynamics, and directly linking them to experiments is –to say the least– adventurous. We argue that finding the universality class(es) relevant to neuronal dynamics is enough in order to understand their underlying processes (Binney et al. 2001; Ódor 2008). But using that argument implies that we are assuming *already* that the brain is critical, and hence finding its "normal form" near the transition will explain it. But, what happens if the brain is not critical? Then the universality argument is (possibly) not valid –and then toy models may represent different faces or ingredients of the system, but a whole synthesis, with a more detailed description[1], would be needed in order to recover brain

[1] I am not against the main idea of statistical physics, that putting the right microscopical ingredients will yield correct results at the collective level, but just stating that identifying those ingredients in very complex, non-critical phenomena could be

dynamics as a whole (Bunge 2003). This calls for the necessity to check criticality in the brain not only by simple arguments and toy models, but also taking more realistic scenarios, doing a complete bottom-up approach –or synthesis– to connect all levels of explanation with experimental evidence. I would also like to remark that more complex models might not be necessarily more realistic dynamical systems for the individuals, but the use of a more realistic topology, or the addition of new key ingredients in a simple form.

I devote this section to demonstrate how our toy arguments apply in more realistic scenarios, showing some of the preliminary research result performed during the last months prior to the thesis writing.

6.1 Networks of theta-neurons

In chapter 4, we studied the synchronization transition using a system of active oscillators. The key ingredient of such oscillators was excitability, a fundamental aspect of neuronal dynamics that is missing in the stochastic Kuramoto model.

It was possible to obtain precise results on the topology of the phase diagram and their critical bifurcations due to the possibility of working with a simple phase model. This lead to periodicity in the angle distribution $P(\varphi, t)$, so it could be expanded in Fourier series, allowing us to decompose the Fokker-Planck equation into an infinite set of differential equations. One possible criticism is that neurons (or even neuronal regions) are not oscillators, but excitable units. However, near a limit-cycle bifurcation they can be always regarded as non-linear oscillators, as demonstrated by Ermentrout and Kopell (Ermentrout and Kopell 1986) or as argued by Izhikevich (Hoppensteadt and Izhikevich 1997). Actually, note that the form of the active rotator presented in Chapter 4, eq. (4.2), is very similar to eq. (2.29) (which models a quadratic integrate and fire neuron with a leaky membrane), for a fixed intensity $I \simeq 1$, as we demonstrated in Chapter 2. Therefore, our simple, the model still captures the essential properties of excitable type-I units.

But our proposed model still presents important differences with

a very difficult task.

real integrate-and-fire models, thus we decided to test whether the hybrid excitability transition could be found on systems of theta-neurons, which are still regarded as a simple model written in terms of phases (so the analytical machinery can be applied), but it is more realistic than the active rotator model.

Actually, the key difference between both equations is coupling. The toy model uses a Kuramoto-like coupling while the theta-neuron uses current (or synaptical) coupling. This detail is an important difference, since the Kuramoto coupling includes both excitatory and inhibitory couplings in an effective way. The term $\sin\left(\varphi_i - \varphi_j\right)$, for $\varphi_i > \varphi_j$ is positive (excitatory) for the i-th neuron, but negative (inhibitory) for the j-th. We later show explicitly that adding inhibition enriches the dynamics of the theta-neuron networks, which becomes similar to the macroscopic phase diagram obtained for the active oscillators described in Chapter 4.

Our objective in this section is to show that the formalism developed during the thesis to study systems of coupled oscillators is of use in more realistic systems, as well as comparing the phase diagram of the theta-neurons to the active-rotator model.

6.1.1 Mean-field theory

Let us study the behaviour of theta-neurons in mean-field first. We start by recovering the equation for the theta-neuron, eq. (2.28), for a system of N neurons,

$$\dot{\varphi}_j = \left(I_j(t) + 1\right) + \left(I_j(t) - 1\right)\cos\varphi_j, \tag{6.1}$$

where φ_j is the angle that codes the neuron membrane potential and I_j is the input current to neuron j. Remember that the theta-neuron is derived from a quadratic integrate-at-fire exactly near a type-I excitability bifurcation, so it can be seen that neurons are at rest when $\varphi_j = -\pi$, and spiking at $\varphi_j = \pi$ (see Chapter 2).

Let us first say a few words about the input current. In the absence of current, the neuron is posed exactly at a SNIC bifurcation, hence reacting to any external perturbation, no matter how small it is. A way to solve this problem, and confer a "threshold" to the neuron, is

to assume that a constant (negative) current is applied at all times to the system. Then, assuming that all couplings are homogeneous, but subject to stochastic noise, we have

$$I_j(t) = I_j^d(t) + I_j^s(t) = -q_j + Jr(t) + \sigma\eta_j(t), \tag{6.2}$$

where q_j is the external current applied to neuron j, σ is the noise intensity, $\eta_j(t)$ is a Gaussian white noise, J is the coupling intensity, and $r(t)$ is the instantaneous firing rate, that can be understood as the number of spikes arriving to the neuron in a very small time window for fast synapses (see also the section on synaptic inputs in Chapter 2). Note that, since the system is a mean-field one, all neurons receive the same input, which is the global system activity multiplied by a factor: $Jr(t)$. The external currents to each neuron play a similar role to angular speed in individual oscillators, and we could set any distribution $g(q)$ for them. Finally, we have defined $I_j^d = -q_j + Js$ and $I_j^s = \sigma\eta_j(t)$, in order to separate the deterministic and stochastic parts of the current.

Let us study the simplest case, the deterministic ($\sigma = 0$, so $I_j^s = 0$) system with $g(q)$ a Lorentzian of mean q_0 and spread Δ. It is then possible to follow the procedure in Chapter 2 in order to obtain

$$\dot{Z}_1 = \frac{iI^d}{2}(1+Z_1)^2 - \frac{iI^d}{2}(1-Z_1)^2 \tag{6.3}$$

for the Kuramoto order parameter under the Ott-Antonsen ansatz, with $I^d = q_0 + i\Delta + Jr(t)$. Then, the only thing that remains is to identify the mean-field input $r(t)$ to the neuron with the Kuramoto-Daido order parameters. The conformal map

$$W = \frac{1-\overline{Z}_1}{1+\overline{Z}_1} \tag{6.4}$$

allow us to write eq. (6.3) as

$$\dot{W} = -iW^2 + i(q_0 + Jr(t)), \tag{6.5}$$

and it can be furthermore demonstrated that $W = \pi r + iV$, where V is the mean membrane potential of the associated quadratic integrate-and-fire neuron (Montbrió et al. 2015). In this way, it is possible to obtain equations for the average firing rate and membrane potential,

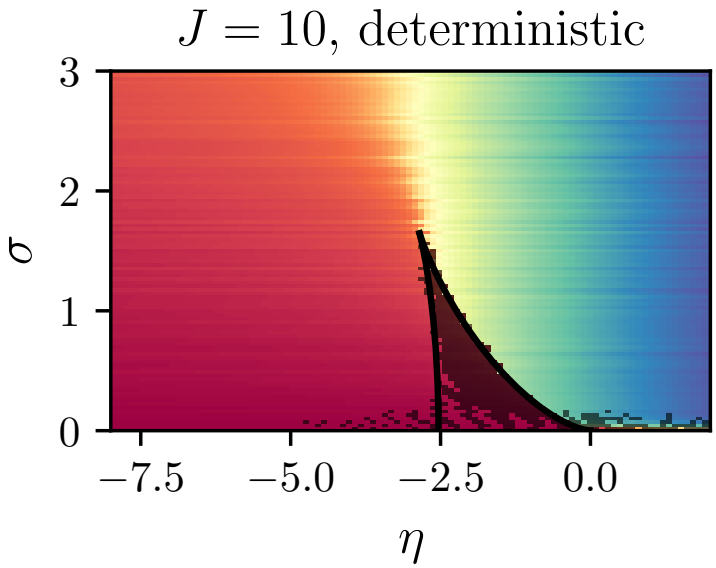

Figure 6.1: **Phase diagram of deterministic excitatory QIF neurons.** Simulations are performed for a mean-field system of excitatory quadratic integrate and fire neurons, using q_0 and Δ as parameters. Red zone is a "down" phase, with low firing rates and membrane potential below the threshold. Blue colors indicate a constant firing of the neurons. Shaded region indicates a bistable region, as detected numerically. This region is surrounded by a saddle-node bifurcation, obtained by performing bifurcation analyses on eqs. (6.6)

$$\dot{r} = \frac{\Delta}{\pi} + 2rV, \tag{6.6a}$$

$$\dot{V} = V^2 - q_0 + Jr - \pi^2 r^2. \tag{6.6b}$$

Figure 6.1 shows a comparison of the predicted phase diagram obtained from theory and numerical simulations, respectively, when only excitatory neurons with spike-like currents are considered. In numerics, the input current is computed just by counting the number of neurons that spiked in time interval $[t-\tau, t]$, with $\tau \ll 1$. The system displays two different phases: a "down" state, with almost zero firing rate, and an "up" state with constant firing. For certain values of q_0 and Δ,

it is also possible to find a bistability region, where the system goes to up or down states depending on initial conditions.

For analytics, it is possible to demonstrate that the instantaneous firing rate $r(t)$ in the Ott-Antonsen ansatz is given by

$$r(t) = \frac{1}{2\pi}\frac{1-|Z_1|^2}{|1+Z_1|^2}. \tag{6.7}$$

as done by (Laing 2014; Montbrió et al. 2015). Actually, this can be easily done by computing the density of neurons at π, $P(\varphi = \pi, t)$, a computation that is immediate taking the Fourier expansion of the probability density, as shown in detail in Section 6.2 and (Montbrió et al. 2015).

Finally, let us consider what happens when we introduce stochastic noise. For clarity, set $g(q) = \delta(q - q_0)$ this time. Then, we can write the Fokker-Planck equation,

$$\partial_t P(\varphi, t) = -\partial_\varphi \{A(\varphi) P(\varphi, t)\} + \frac{1}{2}\partial_\varphi \left\{B(\varphi)\,\partial_\varphi [B(\varphi) P(\varphi, t)]\right\} \tag{6.8a}$$

$$A(\varphi, t) = \left(I^d(t) + 1\right) + \left(I^d(t) - 1\right)\cos\varphi \tag{6.8b}$$

$$B(\varphi) = \sigma(1 + \cos\varphi) \tag{6.8c}$$

which indicates us the probability of finding a particle at phase φ in a time t. Note that $A(\varphi, t)$ and $B(\varphi)$ are respectively the deterministic part and the multiplicative noise, respectively. We remark since we set all the external inputs to q_0, then the probability density does not depend on q. If the assumption is relaxed, we would have $P(\varphi, q, t)$. Following again the steps explained in Chapter 2, it is again possible to obtain an infinite set of equations for the Kuramoto-Daido order parameters. The computations are more involved than the previous ones due to the appearance of multiplicative noise, but there is no additional conceptual difficulties. The result is

$$\dot{Z}_k = i\left(1 + I^d\right)kZ_k - \frac{i\left[1 - I^d\right]k}{2}(Z_{k+1} + Z_{k-1}) + \\ + \frac{\sigma^2}{8}\left[k(2Z_{k-1} - 2Z_{k+1} + Z_{k-2} - Z_{k+2}) - k^2(6Z_k + 4Z_{k-1} + 4Z_{k+1} + Z_{k-2} + Z_{k+2})\right], \tag{6.9}$$

where the deterministic and stochastic contributions have been separated for clarity. Note that the multiplicative noise comes from the fact that we added the noise in the input current of the quadratic integrate-and-fire neuron. After the change of variables to phases, it becomes multiplicative, coupling larger orders into the equation.

The phase diagram, however, is qualitatively identical to the one for the deterministic neuron: down and up states, and bistability between them. Therefore, a mean-field, excitatory theta-neurons system displays a first-order phase transition from down to up states for low values of noise, while the change of phase is continuous over the cusp (see Figure 6.1). The dynamics is more complex than the simple stochastic model by Larremore *et al.* analysed in Chapter 3 –where a network composed only by excitatory units leads to all active or inactive–, but still not as much as the active rotators model.

6.1.2 Inhibitory neurons

Besides the more complicated shape of eq. (6.9), it is clear that theta-neurons are lacking something that was present in the active rotators models: by comparing both, the answer turns out to be inhibition.

As we discussed earlier, the sinusoidal coupling typical of Kuramoto systems is able to mimic inhibition in a very coarse way. We already remarked several times during the thesis the importance of inhibition in the brain, and in the present context it is also fundamental in order to increase complexity and generate richer dynamical regimes. Thus, we introduce an extension of the theory presented so far in order to work with E-I networks.

Analytically, we have two different populations, the excitatory one and the inhibitory one. Each one will have its own instantaneous firing rate, denoted respectively $r_e(t)$ and $r_i(t)$. The excitatory population receives a deterministic current $I_e^d(t) = -q_e + \omega_{ee} r_e(t) - \omega_{ei} r_i(t)$, while the inhibitory one receives $I_i^d(t) = -q_i + \omega_{ie} r_e(t) - \omega_{ii} r_i(t)$. For simplicity, let us add an additive noise to the equations, that is formally equivalent to assume a Lorentzian distribution for the external currents. Noise is different for each population, with intensities σ_e and σ_i, respectively. Additionally, each population is described by its own set of Kuramoto-

Daido parameters, and hence we have Z_k^e and Z_k^i. However, in this case the Fokker-Planck equation is two-dimensional, as $P(\varphi_e, \varphi_i, t)$, so the Fourier coefficients form a matrix. Therefore, if we want to reconstruct the probability distribution, in principle, we need the Kuramoto-Daido order parameters

$$Z_{kl} = \left\langle e^{ik\varphi_e} e^{il\varphi_i} \right\rangle = \int d\varphi_e d\varphi_i e^{ik\varphi_e} e^{il\varphi_i} P(\varphi_e, \varphi_i, t). \tag{6.10}$$

This definition leaves the Kuramoto-Daido parameters for each population as $Z_k^e = Z_{k0}$ and $Z_k^i = Z_{0k}$. Looking at the Langevin equations, one realises that generalising eq. (6.3) is straightforward,

$$\begin{aligned} \dot{Z}_{kl} = i\left(1 + I_e^d\right) k Z_{kl} - \frac{i\left[1 - I_e^d\right] k}{2} (Z_{k+1,l} + Z_{k-1,l}) + \\ + i\left(1 + I_i^d\right) l Z_{kl} - \frac{i\left[1 - I_i^d\right] l}{2} (Z_{k,l+1} + Z_{k,l-1}) - \\ - \frac{\sigma^2\left(k^2 + l^2\right)}{2} Z_k. \end{aligned} \tag{6.11}$$

If we were to generalise eq (6.9), a similar procedure would suffice. Although equations (6.11) are very complicated to solve, one could immediately notice that setting $k = 0$ and $l = 0$ alternatively almost decouples the equations,

$$\dot{Z}_k^e = i\left(1 + I_e^d\right) k Z_k^e - \frac{i\left[1 - I_e^d\right] k}{2} (Z_{k+1}^e + Z_{k-1}^e) - \frac{\sigma^2 k^2}{2} Z_k^e \tag{6.12a}$$

$$\dot{Z}_k^i = i\left(1 + I_i^d\right) k Z_k^i - \frac{i\left[1 - I_i^d\right] k}{2} (Z_{k+1}^i + Z_{k-1}^i) - \frac{\sigma^2 k^2}{2} Z_k^i \tag{6.12b}$$

where the coupling between Z_k^e and Z_k^i is inside the input currents. Although we do not have general information about Z_{kl}, Z_k^e and Z_k^i modes are enough to recover the dynamics of the single populations, allowing us to reconstruct the partial probability distributions $P(\varphi_e, t)$ and $P(\varphi_i, t)$. Indeed, it is reasonable to assume that $P(\varphi_e, \varphi_i, t) = P(\varphi_e, t) P(\varphi_i, t)$ from the beginning. However, within

this approximation it is possible to generalize the method for more complex problems. For example, in a case where the noise matrix in the Fokker-Planck is not diagonal, we could have expected couplings from arbitrary Z_{kl} to Z_k^e and Z_k^i.

Finally, note that the order parameters we have used are *for each population*. Therefore, we could have the Kuramoto order parameters $\left|Z_1^e\right| = \left|Z_1^i\right| = 1$, meaning that both the excitatory and inhibitory populations are synchronized, but this does not imply that both populations are synchronized together. In order to do so, one would need to compute the order parameters for all the angles, without looking if the particular neurons are excitatory or inhibitory,

$$Z_k = \left\langle e^{ik\varphi} \right\rangle = \int d\varphi \frac{P_1(\varphi,t) + P_2(\varphi,t)}{2} e^{ik\varphi} = \frac{1}{2}\left(Z_k^e + Z_k^i\right) \tag{6.13}$$

with $P_1(\varphi,t) = \int d\varphi_2 P(\varphi,\varphi_2,t)$ and $P_2(\varphi) = \int d\varphi_1 P(\varphi_2,\varphi,t)$. The Fourier series was used in order to evaluate all the integrals, yielding the Kuramoto order parameters of the population. Then, notice that obtaining the Kuramoto-Daido order parameters Z_k^e and Z_k^i allowed us to obtain all the information about the system. Montbriò *et al.* (Montbrió et al. 2015) derived mean-field equations for this problem within the Ott-Antonsen ansatz, but they did not present any results regarding the two-dimensional system. Apart from the extending their analytical results, we gave some insights about the model in the simplest approximation. Assuming the ansatz $Z_k^{e,i} = \left(Z_1^{e,i}\right)^k$ and applying the conformal mapping (Montbrió et al. 2015; Laing 2018) one gets

$$Z_1^{e,i} = \frac{1 - \overline{W}_{e,i}}{1 + \overline{W}_{e,i}} \tag{6.14}$$

with $W_{e,i} = \pi r_{e,i} + i V_{e,i}$ it is possible to write equations for the average membrane potential and instantaneous firing rate of the populations,

$$\dot{r}_e = \frac{\sigma_e}{\pi} + 2 r_e V_e \tag{6.15a}$$

$$\dot{V}_e = V_e^2 + I_e^d - (\pi r_e)^2 \tag{6.15b}$$

$$\dot{r}_i = \frac{\sigma_i}{\pi} + 2 r_i V_i \tag{6.15c}$$

$$\dot{V}_i = V_i^2 + I_i^d - (\pi r_i)^2 \tag{6.15d}$$

A further change of variables is needed in order to make explicit the fraction α of individuals in the system, since the averages are defined as $V_{e,i} = N_{e,i}^{-1} \sum_{j=1}^{N_{e,i}} V_j$, instead of dividing by the total number of neurons N. The first thing we can observe is that, if we make all the couplings equal ($\omega_{ee} = \omega_{ei} = \omega_{ie} = \omega_{ii} = J$), then the average membrane potential $V = (V_e + V_i)/2$ and firing rate $r = (r_e + r_i)/2$ have exactly the same shape as the excitatory-only system, but with an effective, reduced coupling $J(1 - 2\alpha)$, in an analogous way of what happens to the Larremore *et al.* model (Larremore et al. 2014). However, it was not possible to find any hint of the LAI phase in this system, when a sparse Erdös-Rényi network is employed.

Allowing for more freedom on the couplings should lead to a richer phase diagram, as it happens in the Wilson-Cowan model (Wilson and Cowan 1972; Borisyuk and Kirillov 1992) but a more careful bifurcation analysis should be performed. We are currently analysing such phase diagrams, in order to compare with other models and look for richer behaviours, such as limit cycles (synchronization) or asynchronous regimes, in an ongoing research project. In addition to that, the behaviour of the model in more complex topologies remains to be studied. As it was mentioned before, for preliminary analyses, we have studied the behaviour of theta neurons in Erdös-Rényi networks, with the hope to find an asynchronous irregular regime, or deviations from mean-field theory. No hints of different qualitative dynamics has been found so far, meaning that Erdös-Rényi networks behave very similarly to mean-field predictions. This could be, as we discuss later in this Chapter, due to the presence of threshold in neurons (in this case, the negative external current applied to neuron populations) but more research is needed in order to elucidate these issues. We have also implemented these models in real topologies, such as the connectome or synthetic hierarchical-modular networks (see for example (Zamora-López et al. 2016)), but results have yet to be analysed.

6.2 A continuous measure for firing rates

A possible drawback for the analysis of the theta-neurons is that the spike train coupling usually employed is difficult to write as angular variables. Instead, many studies (Luke et al. 2013; Laing 2014; Luke et al. 2014; Laing 2018) use a function that mimics the spike behaviour. Since the spike is produced at $\varphi = \pi$, the function $(1+\cos\varphi)^n$ tends to be larger around $\varphi = \pi$ as n increases, hence it is possible to use it as current input function instead of the usual Kuramoto coupling.

We demonstrate here that is possible to make the process for infinite n, mapping exactly QIF and theta neurons. First, recalling expression (2.8) for the general current input, and assuming that the system is fully connected, one can write

$$I(t) = \frac{1}{N}\sum_{j=1}^{N}\sum_{\left\{t_m^j\right\}}\int_{-\infty}^{t} dt' G_\tau\left(t_m^j - t'\right)\delta\left(t_m^j - t'\right), \tag{6.16}$$

where N is the total number of neurons, $\left\{t_m^j\right\}$ are the set of times at which the j-th neuron spiked, and $G_\tau(t)$ is a kernel that returns the strength of the interaction, which presents a typical time τ. Note that at all the spike times, the phase of the j-th neuron must be π. Then, $\delta\left(t_m^j - t'\right) = \delta\left(\pi - \varphi_j(t')\right)$. Using the following equivalence,

$$\delta(\pi-\varphi) = \lim_{n\to+\infty}\sqrt{\frac{n}{4\pi}}\left(\frac{1-\cos\varphi}{2}\right)^n, \tag{6.17}$$

which is very easy to demonstrate, it is possible to insert this expression into the synaptical current equation eq. (6.16), to get

$$I(t) = \lim_{n\to\infty}\sqrt{\frac{n}{4\pi}}\frac{1}{N}\sum_{j=1}^{N}\sum_{\left\{t_m^j\right\}}\int_{-\infty}^{t} dt' G_\tau\left(t_m^j - t'\right)\left(\frac{1-\cos\varphi_j(t')}{2}\right)^n. \tag{6.18}$$

The "spike times" delta has been effectively encoded into the function $\varphi_j(t')$. Taking the limit at which the typical time of the kernel $\tau \to 0$,

it is possible to eliminate the integral, since in that case $G_\tau(0 \leq t \leq \tau) \simeq 1/\tau$ and then

$$\sum_{\left\{t_m^j\right\}} \int_{-\infty}^{t} dt' G_\tau\left(t_m^j - t'\right) f(t') \simeq \tau^{-1} \int_{t-\tau}^{t} dt' f(t') \simeq f(t) + \mathcal{O}(\tau). \quad (6.19)$$

Notice that when take this limit, we are assuming that the only spikes affecting the neuron are the ones that are present exactly at this time t, thus the input current would be the instantaneous firing rate $r(t)$ of the network.

Now, let us rewrite the term with trigonometrical functions in order to change all the powers into cosines of multiples of φ, which can be readily substituted by Kuramoto-Daido order parameters. In order to do this, the following identity turns out to be useful,

$$(1-\cos\phi)^n = \frac{1}{2^{n-1}}\left[\binom{2n-1}{n} + \sum_{k=1}^{n}\binom{2n}{n-k}(-1)^k \cos(k\phi_j)\right], \quad (6.20)$$

which can be proved by induction with some effort. This identity allow us to rewrite all the cosines as $\mathfrak{Re} Z_k$, absorbing the summation over all neurons. Applying all these changes, we finally arrive at

$$I(t) = r(t) = \lim_{n\to\infty} \sqrt{\frac{n}{4\pi}}\frac{2}{4^n}\left[\binom{2n-1}{n} + \sum_{k=1}^{n}\binom{2n}{n-k}(-1)^k \mathfrak{Re} Z_k\right], \quad (6.21)$$

where now only the last sum and the limit remain to be evaluated. Unfortunately, it is not possible to compute the sum analytically at this point unless we take the Ott-Antonsen ansatz, setting $Z_k = Z_1^k$. Writing the real part as $\mathfrak{Re} Z = (Z + \bar{Z})/2$ and using that

$$\sum_{k=1}^{n}\binom{2n}{n-k}(-Z_1)^k = -Z_1\binom{2n}{n-1}{}_2F_1(1, 1-n; 2+n; Z_1), \quad (6.22)$$

where ${}_2F_1(a,b;c;z)$ represents the hypergeometric function, it is possible to finally evaluate the limit $n \to \infty$. In order to do this, we employ the asymptotic expansion of the binomial coefficients. For the hypergeometric function, recalling its definition

$$ {}_2F_1(1, 1-n; 2+n; Z_1) = \sum_{k=0}^{\infty} \frac{(2-n-k)_k}{(2+n+1)_k} (-Z_1)^k \to \frac{1}{1+Z_1}, \tag{6.23} $$

where to evaluate the limit for large n we used that both Pochammer symbols scale as n^k, leaving a geometric series. We can finally substitute everything, leading to

$$ r(t) = \frac{1}{2\pi} \left[1 - \frac{Z_1}{1+Z_1} - \frac{\bar{Z}_1}{1+\bar{Z}_1} \right] = \frac{1}{2\pi} \frac{1-|Z_1|^2}{|1+Z_1|^2}. \tag{6.24} $$

Notice that eq. (6.24) coincides with the result derived by Montbrió *et al.* (Montbrió et al. 2015) when one solves for the firing rate[2]. However, here we obtained this equation from first principles, working only from the phase description of the oscillators. There are two important consequences from this result: first, interaction (6.18) can be formally used to count spikes, as usually done in leaky integrate-and-fire neurons, and making the theta-neuron *exactly identical* to QIF neurons. Second, in (Montbrió et al. 2015) , the Ott-Antonsen ansatz is used from the very beginning, while the derivation here uses it at the end, generalizing their results. If eq. (6.21) is used instead of applying the Ott-Antonsen ansatz, all harmonics can be taken in account, leading to more accurate results when the system is noisy. Equation (6.21) can complement the system of equations obtained above for theta-neurons, giving a fully macroscopic description of a noisy set of QIF neurons at any order k in an exact way.

Finally, note that if we work with phase oscillators from the very beginning, we can just count the number of individuals that spiking,

[2]Except for a factor of 2 (i.e., the expression given by Montbrió *et al.* is divided by π^{-1} instead of $(2\pi)^{-1}$). This factors just shifts the coupling to $J \to J/2$. However, in the original derivation by Montbrió and collaborators there is no need to re-shift anything in order to fit the numerical simulations, as we showed before. On the other hand, both Luke and Barreto (Luke et al. 2013) and Laing (Laing 2014) normalize the Dirac delta to 2π instead of unity ($J \to \pi J$). Laing gives explicitly the result for (6.24), which coincides exactly with the one we present here, multiplied by 2π as we could expect. The direct computation of the number of spiking neurons via $P(\varphi = \pi, t)$ also yields the factor $(2\pi)^{-1}$. It seems that for simulations where we are counting spikes with small time windows (instead of making neurons interact through finite n) there is a "correct" normalization factor, which I do not understand, nor I could find any detail in the literature.

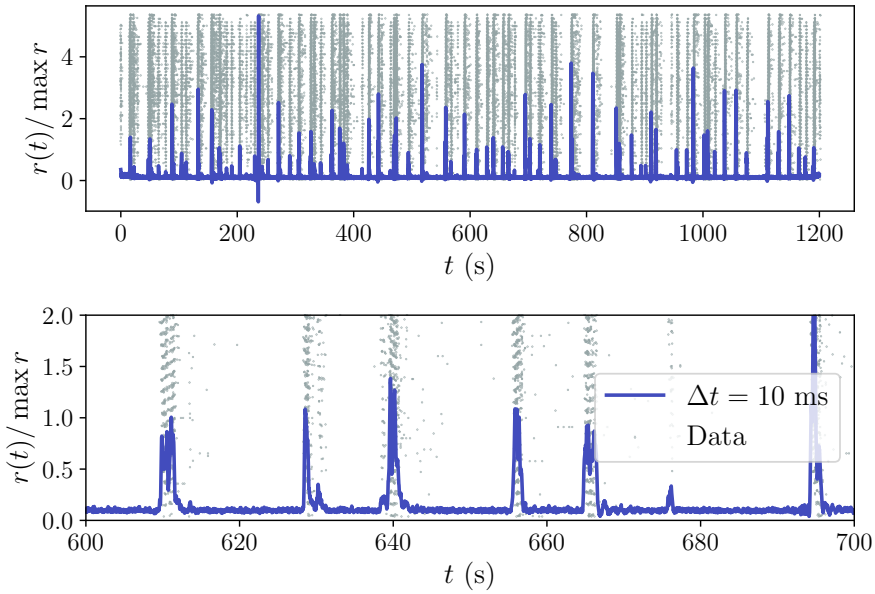

Figure 6.2: **Measuring firing rates through synchronization.** Experimental data used with permission of Jordi Soriano. In-vitro culture of $N =$ neurons. Phases were identified by setting $\varphi = \pi$ at each spike, and $\varphi = -\pi$ just before the event, then performing linear interpolation with $\Delta t = 10$ ms. Decreasing the value does not affect the result. Then the Kuramoto-Daido order parameters computed, and the firing rate obtained using (6.21). Notice that each spike is convoluted with the function $(1-\cos\varphi)^n$, and hence the method lose fine synchronization details inside fast bursting events.

i.e., those that are at $\varphi = \pi$. Then, the instantaneous firing rate will be the density of oscillators at such a phase, that can be readily computed, even for heterogeneous oscillators

$$P(\varphi = \pi, t) = \int dq P(\pi, q, t) = \frac{1}{2\pi}\left[1 + 2\sum_{k=1}^{+\infty}(-1)^k \,\mathfrak{Re}\,(Z_k)\right] \tag{6.25}$$

where we used that $Z_k(t) = \int dq g(q)\overline{p}_k(q,t)$. It is clear that this constitutes a simpler version of eq. (6.21). Moreover, using the Ott-Antonsen ansatz yields again (6.24). One could wonder why it would be necessary to perform all the complicated computations presented above,

instead of this simple evaluation. The reason is that it serves to link exactly theta-neurons with QIF, as it was already commented, and that it allows to see what is the effect of convoluting the spike with a kernel, which can be useful in several applications.

Another remarkable detail is that the derivation of the equivalence between the spike counting and interaction (6.18) is model-agnostic. This means that it is possible to compute the firing rate of any set of neurons via phase interpolation. The usual procedure to compute the firing rate of a set of N neurons is to bin the time with a small timebin τ and count all spikes inside the bins. However, the choice of the time bin is arbitrary is related with the system size N, as explained in Appendix A. If, instead, one discretizes the time, interpolates the phases, and computes the firing rate via the Kuramoto-Daido parameters (either in its complete, or Ott-Antonsen formulations), it is possible to get a real, continuous, firing rate function that does not depend on time binning -which could be of great value to experimentalists. I checked this fact against experimental data provided by Prof. Jordi Soriano in Barcelona[3], of neuronal networks growing *in vitro*. Figures 6.2 and 6.3 show the results, which are very consistent against data.

I also tested the firing rate with fake, simulated data, in order to see if has all the properties one could expect from the instantaneous firing rate. It turns out that it behaves quite well, taking eq. (6.21) with up to $n = 50$ or $n = 100$. Some facts about this measure are as follows:

- A completely asynchronous system has $r(t) \simeq 1/(2\pi)$, as one can readily check from (6.24), no matter how fast is the individual neuron firing rate. This is in contrast with the time-binned measure usually employed, where the time-bin is sensible to the firing rate of individual neurons[4].

- Time bins are still needed to interpolate the phases. However, the interpolation converges as the bin size goes to zero, so the measure $r(t)$ converges accordingly. In contrast, time-windows always end up having no spikes when they are made sufficiently small, due to the finite size of the network.

[3] Data from M. Montalà *et al.*, eNEURO, submitted.

[4] Larger rates allow more spikes inside the same time-window. Although usually one divides through $N\tau$, finite-size effects have a marked effect here.

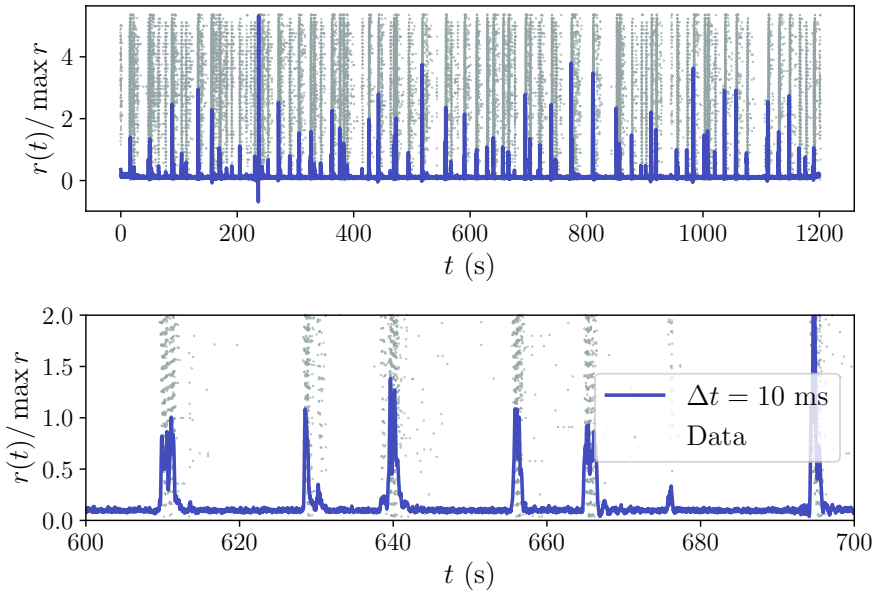

Figure 6.3: **Using the distribution increases sensitivity.** Same dataset, but analysed using eq. (6.25) instead of (6.21). Since here the distribution is working directly with the Dirac delta instead of the "kernel" for large n, the method is more sensitive to structure inside bursting events, as it can be appreciated in zoom. Notice how instantaneous peaks are also larger. The price to pay is that finer discretizations are needed to converge, as the negative event makes clear.

- Time binning also leads to problem in finite sizes: suppose that all the neurons in the system spike at the same individual firing rate. If we duplicate the number of neurons, each bin will have more spikes, so firing rates must be computed *per neuron* (or reduce the time windows as $N^{-1/2}$). However, this measure is robust against any change of system size, just converging for $N \to +\infty$.

I am now trying to contrast this measure with more data, possible using it to study the effect on avalanche measures. I think that, if used correctly, this measure could be of great impact in the neuroscientific community, even for experimentalists.

6.3 On Jensen's force and synchronization

In the Larremore *et al.* model we found that Jensen's force was directly related with the appearance of the asynchronous irregular state. Although we were able to demonstrate the causal relationship between the two phenomena, performing all the analytical computations, there is still some unanswered questions about the mechanism which allows the asynchronous irregular state to emerge.

6.3.1 Benayoun: the importance of "just one term"

For example, I was not able to locate the LAI phase in the model by Benayoun *et al.* (Benayoun et al. 2010) in numerical experiments, although its equations are very similar to the ones corresponding the Larremore *et al.* model (see Chapter 2). The only difference between both equations was actually the term corresponding to the input, which is just $\langle f(\Lambda)\rangle$ for the Larremore model, but $\langle(1-s)f(\Lambda)\rangle$ for Benayoun *et al.* Therefore, I suspect that the difference lies in the following: while in the Larremore model it suffices to obtain input fluctuations in order to perform averages as $\langle f(\Lambda)\rangle$, the Benayoun *et al.* model requires the full probability distribution for the activity in order to being able to evaluate such quantities. Making $\langle(1-s)f(\Lambda)\rangle \simeq (1-\langle s\rangle)\langle f(\Lambda)\rangle$ and applying the analytical techniques we developed for the Larremore *et al.* model would be incorrect, since such an approximation is already assuming the mean-field hypothesis.

It is worth to note that the term $(1-s)$ means that if all the neurons are simultaneously active, then nobody else can become active, which is what actually happens in real systems. On the other hand, in the Larremore *et al.* model once all the neurons are simultaneously active, it feedbacks itself to remain in that (absorbing) state. Actually, at γ_c the model is very similar to a voter model, displaying just two symmetrical absorbing states, $s^* = 0$ and $s^* = 1$. It is just matter of time and fluctuations to fall in one of both. In the Benayoun *et al.* model, fluctuations can drive the network to high activity, but after a high fluctuation, the

system must always fall again. In this case, the only absorbing state is $s^* = 0$.

Another detail that surprises me from the Benayoun *et al.* model is that the mean-field macroscopic limit of this system are the Wilson-Cowan equations, even when it apparently lacks a refractory period. If we review the derivation of Wilson-Cowan equations (presented in Chapter 2), the first assumption is the existence of a refractory period r, that leads at the end to the saturation term $(1 - rs)$. In the Benayoun *et al.* model neurons are assumed to be active for a typical time $1/\beta$, which is the typical timescale for a spike. In the Wilson-Cowan model, spikes are Dirac delta functions, but neurons must remain refractory for a time r. Hence, maybe the correct interpretation of the Benayoun *et al.* model would be to take $r = 1/\beta$, and reinterpret the "active" state of the neurons as "refractory" instead, with a discrete spike at the time t at which the transition happened[5]. Then, the difference with the Larremore *et al.* model –at which a neuron is continuously active while it receives enough input– becomes evident: in Larremore *et al.* excitability is missing, but this ingredient is present in the Benayoun *et al.* model, which again lead to possibilities of bifurcations compatible with those of the hybrid synchronization.

Finally, given the complexity of the phase diagram of the (mean-field) Wilson-Cowan equations, probably an asynchronous irregular regime is hidden in a small parameter range (see Chapter 2). The diagram with multiplicative noise (the Benayoun *et al.* model) should be then analysed with care, in order to find such states. From the point of view of synchronization transitions, they probably exist –because in the Wilson-Cowan equations there are limit cycles–, and studying such regimes would give more information about the behaviour of the Jensen's force for more realistic systems.

[5]Using a three-state model, quiescent, spiking, and refractory for the neurons, would also probably allow us to recover part of the fast oscillating variables integrated out in the Wilson-Cowan equations.

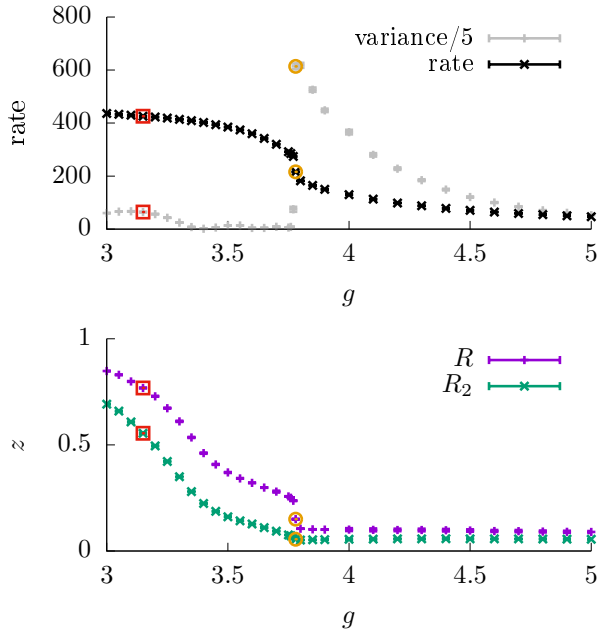

Figure 6.4: **LIFLS model phase diagram.** As with the Brunel model, the LIFLS present a synchronous-asynchronous transition near $g = 4$ (marked with yellow circles). The leftmost transition, marked in red, is a change from monostable to bistable collective firing rates, as hinted by the increase of the second Kuramoto-Daido parameter. Parameters: coupling $J = J_{ext} = 2$ mV, $N = 2000$, $\tau_m = 20$ ms, $\tau_s = 5$ ms, $\tau_r = 2$ ms, $V_r = -10$ mV, $V_h = 10$ mV, $V_l = 0$ mV, $\theta_T = 20$ mV.

6.3.2 Jensen force in I&F neurons

We discussed the possibility to find the asynchronous irregular state in more realistic models in Chapter 3. One of the most concerning issues when the research on Jensen's force was published (Buendía et al. 2019) was the lack of truly *self-sustained* irregular phases in leaky integrate-and-fire neurons, which suffer from strong dissipation. However, in the literature there are some recent candidates to display such self-sustained, low activity regimes, that could be explained using the Jensen's force approach (Kriener et al. 2014; Borges et al. 2020).

A later revisit of the Larremore *et al.* model shows that, when the transfer function presents a threshold, the LAI phase might disappear.

In the Larremore *et al.* model, a node can be activated by a single active neighbour –even when it is very improbable– in contrast to real neurons that need many active neighbours to overcome the membrane potential threshold and start spiking. Hence, LAI phase might be hindered when a threshold is considered, which might explain why it is so difficult to find irregular phases in the absence of external input for more realistic models. On the other hand, when the external input is added, it compensates the threshold, allowing the neuron to spike more easily. This is the case, for example, of the Brunel model (Brunel 2000), now regarded as a paradigmatic model of simple integrate and fire neurons which are able to display very different behaviours. This model presents several bifurcations and phases, including an asynchronous irregular phase for inhibition dominated regimes with certain external input. When the system is excitation dominated, it experiences a synchronization phase transition to a synchronous regular regime. The transition happens just at the point of balance between excitation and inhibition.

We analysed in detail the dynamic of this transition, in collaboration with Prof. Johannes Zierenberg, who was studying the dynamics of neurons at the transition. This turned out to be bistable, producing small "synchronization clusters" that change dynamically. We discovered that such a bistability in the individual neurons comes from input fluctuations. This mechanism is not particular of the Brunel model, and it is displayed also for leaky integrate and fire neurons with leaky synapses (LIFLS model). This model is defined by simple leaky integrate-and-fire neurons

$$\tau_m \dot{V}_j = -\left(V_j - V_l\right) + I_j^e + I_j^i + I_j^{ext}, \tag{6.26}$$

where each intensity is convoluted by an exponential kernel $\tau_s \dot{I}_j = -I_j$. The model is complemented by a reset rule: each time surpasses a threshold, $V \geq \theta_T$, the membrane potential is hold to $V = V_h$, and the current for neighbouring neighbours is increased by J (or gJ in the case of inhibitory neurons). Then the neuron is refractory for τ_r milliseconds, after which the membrane potential returns to $V = V_r$. The external current is set as a random Poisson process of spikes. As the Brunel model, this presents a synchronization phase transition at the balanced state (see Figure 6.4) around $g_c \simeq 4$, where bistability in individual's firing rate is found. Moreover, such fluctuations are not

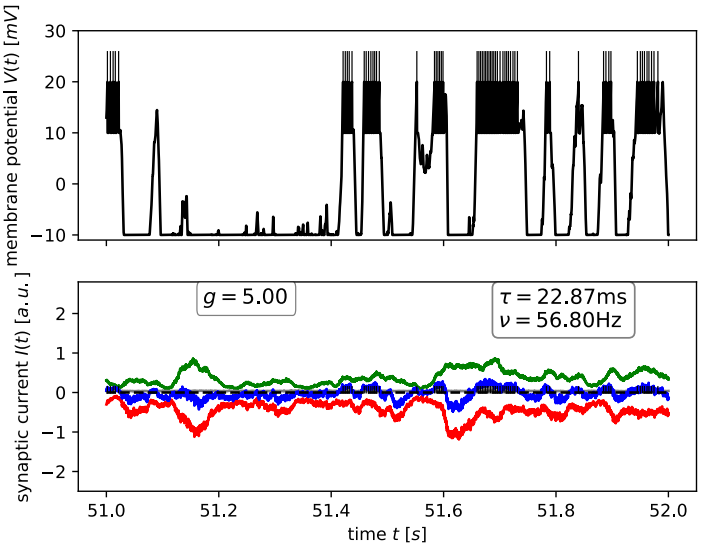

Figure 6.5: **Jensen's force in the LIFLS neuron.** Time series for an individual neuron in the model (top), and the corresponding input current (bottom). The input current is divided in excitatory (green) inhibitory (red) and total (blue). Spikes are marked with vertical lines. The average spiking frequency an autocorrelation times are indicated. Parameters are as in Fig. 6.4, with $g = 5$.

white-noise, but present a certain correlation time –due to τ_s–, so they are able to sustain the neuron firing for some time. This is an important difference with the Larremore *et al.* model, in which fluctuations are completely random. In the inhibition dominated regime ($g > g_c$), inhibition is able to decorrelate the time series, leading to the asynchronous irregular states, where the neurons spike only due to almost random fluctuations. In the excitatory regime, the input current is always large enough in order to make neurons spike tonically, leading to a synchronization in the long-term. Moreover, large excitation leads to bistability in the collective firing rate.

Near the balanced transition, large autocorrelation times are able to present "up and down" states in the individual neurons and synchronization clusters that change dynamically, as displayed in Figure 6.5. Therefore, here Jensen's force is acting in a more complicated (but realistic) way, facilitating bistability for the individual firing rates. Avalanche behaviour remains to be studied, but this

synchronization transition could be of interest to compare with the active oscillators model. However, a recent model by Girardi-Schappo *et al.* (Girardi-Schappo et al. 2020), similar in spirit to the Larremore *et al.* model, reproduces the phase diagram of Brunel, claiming that scale-free avalanches are present only at the edge with the absorbing state, and that they belong to the usual universality class of directed percolation. The model is actually able to self-organize (through a mechanism similar to SOqC) to the balanced, critical point. The avalanches were measured the same way as in formal non-equilibrium systems, in contrast with the usual method employed in neuroscience (see Appendix A).

Chapter 7

Overview and conclusions

"Now tell me what happened –in words. I want your translation of the mathematics"

- Isaac Asimov, in *Second Foundation*, 1953

After sketching the current lines of research derived from the thesis results, I would like to discuss some of them, sharing some of my concerns and thoughts, from a broader perspective.

7.1 Overview

The first issue I want to discuss is the data-driven approach to model whole-brain dynamics by authors such as Deco, Cabral, Daffertshofer, or Tagliazzuchi (Deco et al. 2009; Cabral et al. 2011; Cabral et al. 2014; Jobst et al. 2017; Daffertshofer et al. 2018b; Daffertshofer et al. 2018a). The idea is the following: using neuroimaging techniques, one can infer the topology of the structural connectome, and then assign a dynamical system to each one of the network nodes –that represent mesoscopic regions. Finally, one can compare the simulated temporal series of activity with those obtained experimentally, fitting models to observations. Data of the structural connectome are already widely accessible, allowing to perform many analyses (Haimovici et al. 2013; Villegas et al. 2014; Cabral et al. 2017; Ódor and Kelling 2019; Atasoy et al. 2019) which correlate the known structure with the observed function. In the whole-brain models I am discussing, the objective is usually to check whether the observed global data can be explained by the criticality hypothesis. I believe that this idea is actually very powerful, and has the potential to settle the criticality debate if carefully analysed, so let me discuss this issue in-depth.

Despite of being an overall good strategy, I believe it has both technical and philosophical pitfalls. One of the most concerning technical problems with such a method is that, if the experimental signal is very complex, a simple dynamical system with two different phases needs to be at criticality in order to fit the data (Mora and Bialek 2011). In this situation, where we have a *network* of nodes, not all the nodes have to be posed at criticality, but it is important to keep in mind "overfitting" due to large amount of degrees of freedom available.

Then, it is important to distinguish bifurcations at the individual level with those at the collective one. Cabral and collaborators consider a network of Stuart-Landau oscillators (Cabral et al. 2014). These are nothing but the normal form of a Hopf bifurcation. When compared with the data, it turns out that a system composed by (mostly) critical Hopf oscillators is the one that fit best. How could we put this together with our first result in Chapter 4, which discards the Hopf bifurcation as a source of complexity and critical avalanches? The answer lies at the scale at which we look at the outcomes. The Stuart-Landau *units* are able to reproduce the experimental results near their Hopf bifurcation, but at the macroscopic level, we do not know which is the resultant dynamical regime; on the other hand, in the Kuramoto model, the Hopf bifurcation is collective, for the *whole system*, while each oscillator is just rotating with speed ω_0. Notice that at the HT transition, the individual oscillators are very near their individual SNIC bifurcation[1] ($a = 1.07$, with the individual SNIC happening at $a_c = 1$). Therefore, the key question is: if one computes the collective phase diagram of the coupled system of homogeneous Stuart-Landau oscillators, what macroscopic regime corresponds to all individuals tuned at the Hopf bifurcation?

This problem was already addressed by Hoppensteadt and Izhikevich (Hoppensteadt and Izhikevich 1997), who tried to analyse the problem of collective neuronal behaviour from the point of view of universality. Neurons are excitable systems, and they can spike through type-I or type-II excitability classes. Therefore, building a canonical model for each excitability class, and studying its collective,

[1] It's actually so close, that if the brain was working near the HT transition, and I decided to fit the model to the data, I would probably claim that the oscillators need to be near a SNIC transition... but we saw they SNIC bifurcations do not generate any avalanches at the collective level!

macroscopic behaviour, would suffice to uncover much of the possible system dynamics. Hence, Hoppensteadt and Izhikevich already studied systems of coupled Stuart-Landau oscillators (type-II) as well as our active rotators (type-I) (Hoppensteadt and Izhikevich 1997) but 23 years ago the powerful reductions by Ott and Antonsen (Ott and Antonsen 2008) were not yet available, and the analyses are obscure and based on the "weakly correlated" approximation. Given the results obtained in this thesis, I believe that performing a rigorous analysis of the normal forms of type-I and type-II mean-field oscillators is of central importance right now, a challenge actually able to shed light on the dynamical state of the brain, which could constitute a notorious advance both from theoretical and experimental sides. There is already numerical machinery to perform accurate fits from networks to experimental data recordings, which are obtained via modern neuroimaging techniques. The remaining (difficult) task is to understand the collective behaviour emerging from such a fit, linking it to possibly realistic neuronal models. For example, recently Deco, Daffertshofer and their collaborators (Deco et al. 2009; Daffertshofer et al. 2018b) have also analysed the Wilson-Cowan model, fitting it to experimental data, but it is always looked near the Hopf bifurcation –so it should keep similarities with the canonical type-II model, the Stuart-Landau oscillators.

I mentioned before that the problems are not only technical, but also philosophical. This is in the sense that setting a simple model and performing a fit is a purely *instrumentalist* point of view, and it should be taken with care. A realist would be concerned about choosing an adequate model to represent the dynamics of the region. Such a model should be justified by theory or experimental observations. If not, one could just set up any model able to display a large repertoire of dynamical complexity (e.g., a chaotic system), or even a simple model which is able to display such emerging complexity at the macroscopic level, and fit the data accurately, just because the model has enough degrees of freedom to do it. Let me give a practical example. Suppose that the mean-field, the collective phase diagram of excitable type-I and type-II oscillators turned out to be similar, with the same bifurcation lines and phases (at least, locally). Then, since the fit is done at the macroscopic level, both models should be able to fit the data equally well. However, it is clear that a type-II model is not adequate for a type-I region, and

viceversa. Just putting a model on a node because it is "simple" could give misleading answers to our conceptual questions, specially if one talks about the properties of individual regions.

Hence, it is very important to pay attention also to lower scales, going for a bottom-to-top synthesis. Given the evidence in the literature, it is worth to wonder: if a critical type-II oscillator is model adequate for mesoscopic regions, how do the neurons self-organize to such a point at this scale? Why should be then possible to find avalanches by looking at only that region, when we know that Hopf bifurcations do not yield scale free avalanches[2]? These questions make it clear that only working from philosophical realism, using a bottom-up approach, we will be able to settle the debate on brain criticality.

Another relevant issue worth to be discussed is the relationship between the balanced brain and criticality. Balance between excitation and inhibition is one of the most robust observations at this point, both in experiments and theoretically (Brunel 2000; Shew et al. 2011; Poil et al. 2012; Bellay et al. 2015; Denève and Machens 2016; Politi et al. 2018; Sadeh and Clopath 2020). However, balanced states are usually linked to asynchronous irregular activity (Vreeswijk and Sompolinsky 1996; Denève and Machens 2016; Politi et al. 2018; Buendía et al. 2019), which are characterized by extremely de-correlated systems, in contrast with the large correlations associated with criticality. On one hand, such large correlations are usually invoked as an advantage for information transmission in biological systems (Beggs 2008; Shew and Plenz 2013; Muñoz 2018), but it has been demonstrated that the irregular activity is also a good candidate for computation and information processing (Denève and Machens 2016; Rubin et al. 2017; Sadeh and Clopath 2020). Balanced states have been found in concomitance with neuronal avalanches experimentally (Shew et al. 2011; Poil et al. 2012), and criticality has been related with such balance in many models (Brunel 2000; Vogels et al. 2011; Poil et al. 2012; Denève and Machens 2016; Politi et al. 2018; Ullner et al. 2018). However, both exhibit some aspects that seem to be in contradiction with each other. In our analyses of the dynamical balance states, we saw that at criticality, correlations exhibit a peak (Buendía et al. 2019) but still seems to decrease as the system size is increased. Neuronal balance in some models is

[2] I have the feeling that the answer to this question is closely related with the previous footnote.

intrinsically linked with synchronization transitions, as it happens in the Brunel model (Brunel 2000), where the balance between excitatory and inhibitory interactions leads to a transition between asynchronous irregular and synchronous regular collective spikes. It is possible that, if the brain lives near the edge of a synchronization transition, it could jump between the irregular de-correlated and synchronous correlated states in a flexible way. The remaining question is what happens with the correlations at criticality –which are expected to diverge, at least for the macroscopic field, or displaying large spatially correlated domains (as spin clusters in the Ising model). In our low-dimensional systems, synchronization manifest itself as travelling and spiral waves, which are a distinctive feature of excitable, noisy spatiotemporal systems. Although both the Landau-Ginzburg and the active oscillators present larger spatial correlations at criticality, it is actually difficult to discern whether if the synchronization clusters sizes are power-law distributed or not, i.e., if the correlation distance diverges at criticality. Temporal correlations of the models are more suggestive, with a Hurst exponent near 1 for the Landau-Ginzburg model (di Santo et al. 2018a) which is indicative of long-time autocorrelations. We also performed classical measures of autocorrelation times in the active oscillators system, finding larger correlations near the hybrid type bifurcation –but discriminating if they were scale-free or not was actually very difficult.

However, models such as the active rotators and the Landau-Ginzburg itself consider inhibition only in an effective way[3], so they say nothing about the role of synchronization in balanced networks. On the other hand, they serve as a test field to measure correlations near synchronization transitions. A more systematic study of how angular variables (and their related activity) are correlated in excitable models, would be needed in order to understand what is the difference with models that belong to the mean-field DP universality class. Correlation functions are a classical measure in the study of critical phenomena and there is already studies for several variants of the Kuramoto model (Hong et al. 2005; Hong et al. 2015; Wüster and Bhavna 2020), and I would expect similar results (power-law distributed events) in the non-linear oscillator system –which does not seem to be the case. The relationship between the nature of the transition

[3]For the Landau-Ginzburg, only net activity is considered, while in the active rotators it is introduced in the Kuramoto coupling.

corresponding to E-I balance, synchronization transitions, and how correlations work in the synchronous-asynchronous spectrum is also left as an important future work.

Finally, I would like to state my doubts on the method used to measure critical avalanches in neuroscience experiments, pioneered by Beggs and Plenz (Beggs and Plenz 2003), and explained in detail in Appendix A. The idea of the method, at the end of the day, is to construct a continuous temporal series of neural activity based on the coarse-grained events measured by the electrodes. In order to do this, it is mandatory to choose a bin width to cluster some of the spike events, and this choice is arbitrary. As Beggs and Plenz admit in their seminal paper, the simplest rational choice would be to use the average inter-spike interval of the neurons –compute mean time between two consecutive spikes, and average along neurons– but the events are so sparsely distributed that doing so misses the internal structure of the bursts. Then, the solution is to use the average inter-event interval, which is the mean time between two consecutive events, no matter what neuron spiked. The critical exponents depend on the time bin width choice (Beggs and Plenz 2003; Beggs and Plenz 2004), and up to my knowledge there is no formal mathematical reason to think that the mean inter-spike interval is superior to any other choice –apart from obtaining consistently the unbiased branching process exponents. Moreover, the method does not seem to be fully consistent. Di Santo demonstrated that it is possible to obtain power-law like avalanches in randomly shuffled synchronous signals, as well as in the synchronous irregular phase of the Brunel model (a find also noticed by Touboul and Destexhe (Touboul and Destexhe 2017)). This is indeed a problem, since the synchronous irregular phase is not critical at all –but the method returns avalanches, so, if avalanches were the only information we had about the system, we could end up thinking it is indeed critical. The method does, however, detect correctly the critical dynamics of the contact process (di Santo 2018). In the Landau-Ginzburg model, avalanches in the activity cannot be found through usual non-equilibrium time series analyses[4] but avalanches are recovered when using the "neuroscience standard" method, with the correct critical exponents. These inconsistencies make me think

[4]Using a small threshold and integrating the signal above. This was confirmed by personal communication with the authors.

that we do not fully understand what this measurement is actually doing, and if we want to discern criticality in the brain, it is key to really know what is formally going under the hood. This is an open project for which we have already several ideas, and it is soon to start after finishing this work.

7.2 Conclusions

In this thesis, we have studied different models with the aim to shed light on the problem of the criticality hypothesis in the brain, and its relation with synchronization dynamics. In Chapter 1, we reviewed the state of the art, and after the thesis, it is time to assess the impact of our results for the theoretical neuroscience community, and the issue of brain criticality in particular.

In the literature, the hypothetical critical transition at which the brain is supposed to operate was claimed to belong to the mean-field directed percolation universality class, a result backed by many theoretical and experimental studies (Beggs and Plenz 2003; Levina et al. 2007; Levina et al. 2009; Hahn et al. 2010; Millman et al. 2010; Poil et al. 2012; Bellay et al. 2015; Girardi-Schappo et al. 2020). However, recent experiments and models suggest that the associated critical exponents can differ from those of the critical branching process (Pasquale et al. 2008; Friedman et al. 2012; di Santo et al. 2018a; Fontenele et al. 2019), and hence one has to look for other mechanisms, such as a different universality class, Griffith phases, or even non-critical phenomena. Our results are consistent with a new universality (Buendía et al. 2020c), which would be the corresponding to the *hybrid type synchronization transition* (HT). This transition emerges due to the excitable behaviour of the system, and, although we could not elucidate its origin exactly, it seems to suggest that bistability and oscillations play a prominent role. I confirmed that the conditions present in our active rotator model can be found in many well-known scenarios, as theta-neuron networks (Luke et al. 2013; Luke et al. 2014), Morris-Lecar neurons (Liu et al. 2014), or the Wilson-Cowan model (Borisyuk and Kirillov 1992). Additionally, I found several models in the litera-

ture which I think that would be worth revisiting conceptually using the concept of HT transitions (Schleimer et al. 2019; Porta and Copelli 2019; Liang et al. 2020).

The dynamical richness and complexity the active rotators phase diagram was early noticed by Borisyuk and Killinov (Borisyuk and Kirillov 1992) in the Wilson-Cowan model. But note that although our active rotator model is oriented to capture mesoscopic properties, its similarities with neuronal models such as the theta-neuron make it an adequate one to study collective properties from individuals, with minor modifications.

In principle one can insist on using a canonical excitable type-I model such as the active rotators to represent whole regions. The phase diagram derived from active rotators in actually used as a paradigmatic example of complexity by Cofré *et al.* (Cofré et al. 2020). In this paper, the authors discuss the state of the art of whole-brain models, highlighting the role of dynamical systems. In spite of the difficulties that modelling with simple models present (which are extensively discussed above from both the methodological and philosophical perspectives), gaining understanding from simple models is always the first step to illuminate the behaviour of the complete system. The results obtained by Deco, Tagliazzuchi, and other researchers (Cabral et al. 2011; Deco et al. 2009; Cabral et al. 2014; Jobst et al. 2017; Daffertshofer et al. 2018b; Daffertshofer et al. 2018a) are very promising and follow a similar philosophy to the active rotator model, which is to couple simple models that are representative of an excitability class for mesoscopic regions in order to capture the macroscopic rhythms of the brain. Therefore, I believe that one of the main objectives would be to compare these results with those obtained by type-I excitable systems in more heterogeneous setups, adding more realistic topologies, and heterogeneity in individual units. The outcome of such studies would shed light on the (collective) dynamical regime of the cortex, advancing our knowledge towards the solution of the criticality hypothesis. This would allow us to construct more realistic models, obtaining more accurate pictures of the behaviour of each neuronal region, thus effectively connecting the scales from the neuronal level to the whole-brain.

Finally, self-organization is a powerful tool in order to understand emergent phenomena in the brain. The concept of SOB (di Santo et al. 2016; Buendía et al. 2020a) brings together bistability with oscillations,

and it could provide us with answers to the mechanisms underlying scaling in the brain. Plasticity does not only impact on brain dynamics, but the structural connectivity itself: it is known that plasticity plays a key role in the development of the brain, a process in which dynamics and topology are highly interconnected (Kandel et al. 2000; Millán et al. 2018). The analysis of self-organization performed in this thesis focuses mostly on the dynamical part, considering either simple mean-field or two-dimensional systems. In spite of this limitation, relevant models (such as the Landau-Ginzburg) can be explained in terms of self-organized collective oscillations (Buendía et al. 2020c). Therefore, I think that studying plasticity and network topology under the lens of self-organization could lead to a deeper understanding of collective complexity in the brain. For example, preliminary studies over the model of Larremore *et al.* showed that plasticity rules can induce synchronized states, and allowed e.g. Girardi-Schappo to construct a simple model with synchronization transitions (Girardi-Schappo et al. 2020), as discussed earlier. Under my point of view, plasticity is key in neuronal dynamics, and at least short-term plasticity should be considered more often when constructing physical models of neuronal networks.

In order to summarize, I think that the present work will serve to shed light on synchronization dynamics in the brain, as well as its relationship with the criticality hypothesis. In this thesis, I have introduced some new concepts, as the Jensen's force for excitatory-inhibitory populations, and hybrid synchronization transitions, that I believe that will be of use in the next years. Although their final impact will be assessed by time, experiments, and long discussions, I have the feeling that they have the potential to lead to new discoveries and partially clarify issues about criticality and synchronization.

Additionally, I tried my best to be formal, both in analytics and numerics, putting all my efforts to get to the root of the details, with the idea of illuminating all the conceptual elements that might be hidden at first sight. I am sure that some of these details entail relevant answers, as I am fairly convinced that the debate on the brain's criticality hypothesis will not last very long, due to the current interest in the issue and the quality of new experimental data. Unfortunately, although providing valuable insights, solving the issue of criticality still does not solve the neuroscience "soft problem", for which it is necessary

to invest more efforts, both in the experimental and theoretical sides. However, the global picture is exciting: many scientists from very diverse backgrounds are now synchronized to understand *how the brain works*, at all scales, from the neuron to the emotions. I find the implications of such a knowledge fascinating, from theoretical arguments and clinical applications to the consequences on psychology, sociology, and philosophy. I hope that, after obtaining answers to the soft problem, we will have a chance to understand the "hard" one –which could yield many answers about ourselves and our position in the world.

Appendix A

On avalanche measurements

In Chapter 1, we have introduced the concept of avalanche in non-equilibrium physical systems (in particular, in the contact process) as outbursts of activity when the system is perturbed from the absorbing state. In simple systems, it is possible to obtain analytically approximations for the critical exponent values, which can be computed numerically. As it was sketched in Chapter 1, there two usual ways of measuring these events formally:

- The avalanches are rare outbursts that happen at the time series, so a way of measuring them is to set a small threshold above the time series average, and look for events that cross this threshold for a certain time. The duration of the avalanche is the time between two threshold crossings, and the duration is the area between the curve and threshold. For a sufficiently large time series, it is possible to obtain statistics on these events, and compute the distribution.

- In the case of the absorbing-active transitions, it is possible to set the system initially at the absorbing state and perturb it slightly, computing the time it needs to go back to the absorbing phase. The size of the avalanche is integrated activity over all time. Then it is possible to repeat the process as necessary to obtain good statistics.

The second method can be mapped into the first just by adding a small rate of spontaneous activation at the microscopic system. Then, it should be clear that both ways of measuring the avalanches are formally almost identical.

However, both methods make two important assumptions: that we have complete information about the activity in the system, and infinite precision measuring temporal events. Neither of those are true in the case of neuroscience experimental setups. In the simplest, in-vitro case considered by Beggs and Plenz (Beggs and Plenz 2003), there is a set of electrodes, separated by a certain distance, which measure the

potential of a neuronal slice. Each electrode is not measuring the activity of individual neurons, but the integrated activity of collective groups. Therefore, an event in an electrode means that many neurons fired in a collective way. There is no way –in contrast with our simple non-equilibrium models– to know how many neurons spiked or what is the total "activity" of the system using this measure.

So what Beggs and Plenz proposed was the following experimental procedure:

1. Select a small activity threshold for each electrode. If the signal exceeds the threshold, we then assume that an "event" happened at the peak of the activity, and assign it a weight proportional to the area between the signal and the threshold. This is very similar to our first procedure for non-equilibrium systems, but it is done for each individual.

2. Put all the weighted events in a *raster plot*, i.e. a graph that represents the events that happened at every time. Then, one computes the *mean interevent interval*, called $\langle \text{IEI} \rangle$, which is the average time between two events produced by any electrode.

3. Finally, the time is divided in bins with width $\Delta t = \langle \text{IEI} \rangle$, and avalanches are defined as events that take place between two empty bins. The duration is the time elapsed between the two empty timebins, while the size is computed summing all the (weighted) events inside. For sufficiently large time series, we can evaluate the statistics of the avalanches.

In models, it is possible to mimic this procedure, either but computing the average activity of a small group of simulated neurons, or using mesoscopic models. It is possible to generalize this method to individual neurons, setting the individual spikes as (unweighted) events, if necessary. An important remark is avoid confusing the average interevent interval of the system $\langle \text{IEI} \rangle$, with the average interspike interval, $\overline{\text{ISI}}$, which gives the average of times between spikes of a single neuron. The mean and variance over different neurons of the interspike interval are used to define the coefficient of variation, a common measure to quantify the irregularity in spiking behaviour that is em-

ployed in Chapters 3 and 4. This is defined as

$$CV = \frac{\sigma^2\left(\overline{\mathrm{ISI}}\right)}{\left\langle\overline{\mathrm{ISI}}\right\rangle}. \tag{A.1}$$

Note that this measure does not depend on any time-binning procedure. However, discretizing the time in bins is typical in neuroscience experiments. For example, it is also employed for computing firing rates in systems of individual neurons. In this case, the system is also binned (usually with $\Delta t = 100$ ms or $\Delta t = 500$ ms (Gerstner 2014)), and the firing rate is computed by counting spikes and normalizing dividing by the number of individuals and bin size, as $r = N_{\mathrm{spikes}}/(N\Delta t)$. When $\Delta t \to 0$, this is known as the instantaneous firing rates.

Therefore, what the experimental avalanche measure actually does is to compute the "firing rates" for a certain time bin, and set the avalanches to those events between two "absorbing" bins, in analogy with the measure in non-equilibrium systems. As we discuss in Chapter 7, the problem here is that Δt is chosen arbitrarily. If we think about a finite, asynchronous system, it is always possible to set a time bin such that there is empty bins, leading to avalanche distributions. However, in the thermodynamic limit, there is no time without an event, and everything is homogeneous. This problem is discussed more in depth in Chapter 7.

Appendix B

Weakly coupled oscillators

Here we present the procedure to perform a phase reduction to a general system of coupled oscillators. We start considering the dynamical system

$$\frac{d\vec{x}_j}{dt} = \vec{F}\left(\vec{x}_j\right) + \sum_{i=1}^{N} g_{ij}\left(\vec{x}_i, \vec{x}_j\right), \tag{B.1}$$

where $\vec{x}_j \in \mathbb{R}^n$ are the variables that identify the state of the oscillator j, $\vec{F}\left(\vec{x}_j\right)$ represents the dynamics of the single oscillator, and $g_{ij}\left(\vec{x}_i, \vec{x}_j\right)$ gives the interaction between different oscillators. Each individual oscillator is characterised by a single stable limit cycle, so after sufficient time the variables $\vec{x}_j(t)$ will fall inside this limit cycle. Since the function $\vec{F}$ is the same for each individual, all individual oscillators are identical, and share the same period T.

Once the system is posed at limit cycle, the angular variables can be chosen via a homeomorphism between the limit cycle with a unit circle, so the phase corresponding to $t = 0$ is $\varphi = 0$ and the phase corresponding to $t = T$ is $\varphi = 2\pi$, linearly interpolating between both values. What happens with points outside the limit cycle? In practice, such points can be disregarded by "thermalization", i.e., waiting a time enough for the system to reach the limit cycle. However, formally speaking the cycle is just asymptotically approached, thus a phase must be defined for any point of the phase space. For a single oscillator, each point $\vec{x}^{\mathrm{L}}(t)$ in the cycle has well-defined phase, so the idea for arbitrary points $\vec{x}(t)$ in the phase space is to assign a phase $\varphi(\vec{x}) = \varphi\left(\vec{x}^{\mathrm{L}}\right)$ such that $\varphi(\vec{x}(t \to +\infty)) = \varphi\left(\vec{x}^{\mathrm{L}}(t)\right)$. Therefore, all the points outside the cycle in the trajectory that link $\vec{x}(t)$ with $\vec{x}^{\mathrm{L}}(t)$ share the same phase, and they form a *isochron* (Izhikevich 2006; Nakao 2016). In this way the points inside the stable manifolds have a phase assigned.

This definition allow us to define perturbations along the limit cycle. If we have a point at the cycle $\vec{x}_1^{\mathrm{L}}$, and push it with a short-time

pulse $\vec{x}^{\mathcal{L}} + \vec{h}$, then the phase jumps from $\varphi_1 = \varphi\left(\vec{x}^{\mathcal{L}}\right)$ to $\varphi_2 = \varphi\left(\vec{x}^{\mathcal{L}} + \vec{h}\right)$. The system will return to the stable limit cycle at a new point through the isochron, hence maintaining φ_2. Then, we can define the *phase response curve* as

$$PRC\left(\varphi_1, \vec{h}\right) = \varphi_2 - \varphi_1, \tag{B.2}$$

where the dependency on the magnitude of the perturbation $\vec{h}$ is encoded in φ_2. This definition works fairly well to be applied directly in numerical and experimental situations, since it is easy to perturb oscillatory behaviour with short pulses. In neuronal systems, it suffices to do patch clamp on individual neurons, but the technique can be used even at larger and more complex scales, obtaining PRCs even for circadian rhythms (VanderLeest et al. 2007; Ukai and Ueda 2010; Monti et al. 2017). The PRC is useful to determine if an oscillator can be entrained to an external signal: a positive PRC means that the oscillator is able to adapt its period to match faster signals (at a certain phases), while a negative PRC allows the oscillator to slightly decrease its period. The PRC method allows one to include slight perturbations easily. By Taylor expanding φ_2 around $\vec{h} = 0$ the PRC near small perturbations, we find

$$PRC\left(\varphi, \vec{h}\right) = \vec{\nabla}\varphi\left(\vec{x} = \vec{x}^{\mathcal{L}}\right) \cdot \vec{h} \equiv \vec{\chi}(\varphi) \cdot \vec{h} \tag{B.3}$$

where $\vec{\chi}(\varphi)$ is the linear response function, which can be also evaluated by taking the derivative of the PRC at zero perturbation (Nakao 2016). Experimentally, it can be obtained by applying very small perturbations to the signal and computing the changes in periods. It is possible to intuitively understand that an oscillator rotating with a fixed frequency ω, behaves as the input multiplied by the linear response when it is perturbed by an external input,

$$\dot{\varphi} = \omega + \chi(\varphi) I(t). \tag{B.4}$$

This can be formally demonstrated in detail (which can be found e.g. in (Nakao 2016; Izhikevich 2006)), but it will be of little use here. Now, we write (B.1) using (B.4), identifying the coupling as the input $I(t)$, effectively reducing the nN-dimensional system to just a N-dimensional one. It is possible to perform this change as long as the strength of the interaction is low, and therefore this formalism is only adequate

for weakly interacting oscillators. Then, changing variables to a co-rotating frame with speed ω, all the free oscillators would seem to be stuck. If we assume that the changes in phase due to the coupling are of a slower timescale than those happening due to the "natural" frequency ω, it is possible to apply temporal coarse graining (as in (2.23)), by defining

$$H_{ij}(\varphi) = \frac{1}{T}\int_0^T dt' \chi_j(t') g_{ij}(\vec{x}_i(\omega t'), \vec{x}(\omega t' + \varphi)) \tag{B.5}$$

being $\vec{x}(\varphi)$ the inverse transformation to $\varphi(\vec{x})$. With this change of variables, the final system reads

$$\frac{d\varphi_j}{dt} = \omega_j + \sum_{j\neq i} H_{ij}\left(\varphi_i - \varphi_j\right), \tag{B.6}$$

where $\omega_j = H_{jj}(0)$ is the deviation of angular velocity of the j-th oscillator with respect to ω. This expression is usually difficult to tackle analytically, so usually only the first term of the Fourier series of H_{ij} is considered in the computations,

$$\frac{d\varphi_j}{dt} = \omega_j + \sum_i c_{ij} \sin\left(\varphi_i - \varphi_j + \psi_{ij}\right) \tag{B.7}$$

which is nothing but the celebrated Kuramoto-Shinomoto model of synchronization (Izhikevich 2006). Therefore, we see that this simple popular model arises from any general set of coupling limit cycles, when the systems are assumed to interact weakly, and taking just the first interaction harmonic.

Bifurcation analysis of active rotators

C.1 Equations for different ansatzs

In Chapter 4, we derived an infinite set of ODEs for the dynamics of the Kuramoto-Daido order parameters. In this Appendix, we give indications about bifurcation analyses for different closures, and compare their results. Let us start by recalling eq. (4.5)

$$\dot{Z}_k = Z_k(i\omega k - \frac{k^2\sigma^2}{2}) + \frac{ak}{2}(Z_{k+1} - Z_{k-1}) + \frac{Jk}{2}\left(Z_1 Z_{k-1} - \bar{Z}_1 Z_{k+1}\right) \quad \text{(C.1)}$$

where $Z_k = \left\langle e^{ik\varphi} \right\rangle$ are the Kuramoto-Daido order parameters, ω is the angular frequency, a is the excitability, J the coupling between oscillators, and σ^2 the noise intensity.

When the system is deterministic, the Ott-Antonsen ansatz (Ott and Antonsen 2008), which is given by $Z_k(t) = [Z_1(t)]^k$, is able to provide an exact solution for the Kuramoto-Daido parameters. However, the active rotator system is stochastic, meaning that such an ansatz only provides correct solutions up to order $\mathcal{O}\left(\sigma^2\right)$ (Goldobin et al. 2018; Tyulkina et al. 2018), and higher-order corrections or a more adequate ansatz are needed.

As it was already pointed out in Chapter 2, the Ott-Antonsen ansatz is equivalent to assume that the distribution of angles $P(\varphi, t)$ is Lorentzian. Given the high synchronization of the oscillators conferred by the excitable behaviour, one could think that the Gaussian distribution would be more adequate for this case. Then, writing the wrapped Gaussian distribution (2.47) with mean $\psi(t)$ and variance $\Delta(t)$,

$$P(\varphi, t) = \frac{1}{\sqrt{2\pi\Delta}} \sum_{k=-\infty}^{+\infty} \exp\left[-\frac{(\psi - \varphi + 2\pi k)^2}{2\Delta}\right], \quad \text{(C.2)}$$

it is possible to obtain explicitly an expression of the Kuramoto-Daido order parameters just by integration,

$$Z_k(t) = \int d\varphi P(\varphi, t) e^{ik\varphi} = e^{-\frac{1}{2}k^2\Delta(t)} e^{ik\psi(t)}. \tag{C.3}$$

From eq. (C.3) one can demonstrate (2.48), which is similar to the usual form of the Ott-Antonsen ansatz. However, it is easier to just plug eq. (C.3) into (C.1), to obtain

$$\dot{\psi} = \omega + a e^{-\Delta/2} \cosh\Delta \sin\psi, \tag{C.4a}$$
$$\dot{\Delta} = \sigma^2 + 2\sinh\Delta \left(a e^{-\Delta/2} \cos\psi - J e^{-\Delta} \right). \tag{C.4b}$$

as derived by Zaks *et al.* (Zaks et al. 2003). Finally, one can perform a bifurcation analysis on this reduced two-dimensional system, which yields the phase diagram sketched in Figure 4.2, although some of the bifurcation lines do not coincide very well with those obtained numerically. This was already appreciated by Zaks *et al.* (Zaks et al. 2003), and we will compare how well it performs against the other two options, the Ott-Antonsen and the second-order cumulant expansion proposed by Tyulkina, Goldobin *et al.* (Goldobin et al. 2018; Tyulkina et al. 2018).

Then, let us work on the Ott-Antonsen ansatz and its expansion. As we already sketched in Chapter 2, it is possible to change from variable Z_k to the *circular cumulants* ϑ_k. The advantage of the cumulants is that at the Ott-Antonsen solution, $\vartheta_1 = Z_1$, while all other $\vartheta_{k>1} = 0$. Therefore, it is possible to expand order by order from the Ott-Antonsen manifold (see Chapter 2 for more details). Let us take the second order, setting $\vartheta_{k>3} = 0$, so $Z_3 = Z_1^3 + 3Z_1\vartheta_2$, with $\vartheta_2 = Z_2 - Z_1^2$. Then, the system reads

$$\dot{Z}_1 = \frac{1}{2}\left(J - \sigma^2 + 2i\omega\right) Z_1 + a\left(Z_1^2 - 1 + \vartheta_2\right) - J\left(Z_1|Z_1|^2 + \vartheta_2 \bar{Z}_1\right), \tag{C.5a}$$
$$\dot{\vartheta}_2 = 2\vartheta_2(i\omega + aZ_1) - \sigma^2(2\vartheta_2 + Z_1^2) - 2J\vartheta_2|Z_1|^2. \tag{C.5b}$$

Note that imposing $\vartheta_2 = 0$ gives the same result as the Ott-Antonsen ansatz, as expected. This closure provides us with a noticeable quantitative improvement on the location of the Hopf and SNIC bifurcations, which coincide very well with the results of numerical integrations (Buendía et al. 2020b). We checked the accuracy in the predic-

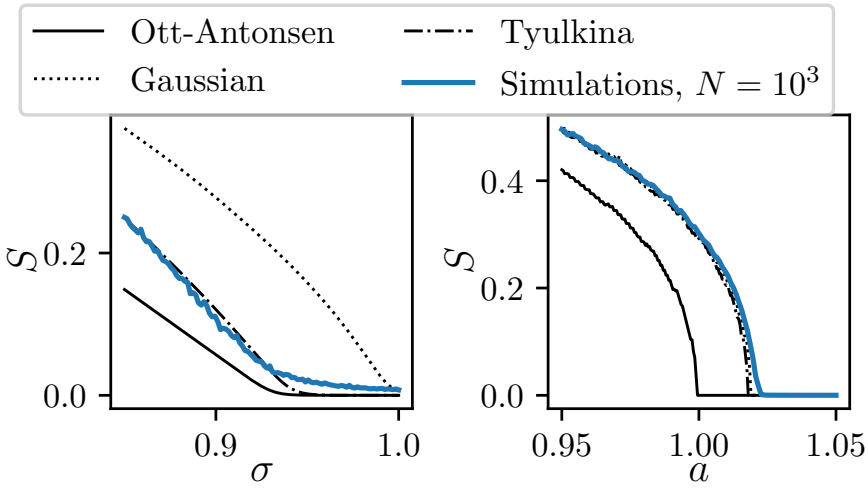

Figure C.1: **Comparison between analytical closures and numerical simulations.** The value of the Shinomoto-Kuramoto order parameter S along the Hopf and SNIC bifurcations, both for analytical results (black lines, see legend) and numerical simulations (blue line). Parameters: $\omega = 1$, $J = 1$; Hopf, $a = 0.5$. SNIC, $\sigma = 0.275$. In numerical simulations, $N = 1000$.

tion of the bifurcation lines by contrasting the results from the considered closures with direct numerical simulations of $N = 1000$ active rotators. In order to avoid pitfalls from the non-linearities in the angular phase with the Kuramoto order parameter, we used instead the Shinomoto-Kuramoto order parameter (Shinomoto and Kuramoto 1986b; Shinomoto and Kuramoto 1986a; Lima Dias Pinto and Copelli 2019) which detects the presence or lacks of oscillations in a reliable way, and it is defined as

$$S = \sqrt{\langle |Z_1|^2 \rangle_t - |\langle Z_1 \rangle_t|^2}. \tag{C.6}$$

where $\langle \cdot \rangle$ indicates a temporal average. This parameter is also used for the visualization of the phase diagram in Fig. 4.2.

The main conclusion from this analysis is that the best results in both bifurcations are obtained from the ansatz proposed by Tyulkina *et al.* (Tyulkina et al. 2018). As we discussed above, the Gaussian ansatz captures very well the dynamics sear the SNIC bifurcation, since at

this bifurcation oscillators are highly synchronized. Finally, the Ott-Antonsen ansatz fails to predict the coordinates of any of the bifurcations, since they are studied for values of σ away from its applicability region.

C.2 Bifurcation analysis of the Ott-Antonsen equations

Following Childs and Strogatz (Childs and Strogatz 2008), we present here the bifurcation analysis of the most simple case, the one corresponding to the Ott-Antonsen ansatz. Making $\vartheta_2 = 0$, and writing $Z_1 = R\sin\psi$, the closure equations read

$$\dot{R} = \frac{1}{2}R\left[J\left(1-R^2\right)-\sigma^2\right] - \frac{1}{2}a\left(1-R^2\right)\cos\psi, \tag{C.7a}$$

$$\dot{\psi} = \omega + \frac{a\left(1+R^2\right)\sin\psi}{2R}. \tag{C.7b}$$

Several observations are important. First, making $a = 0$ recovers the case for the stochastic Kuramoto model, eq. (2.44) (notice that the definition of noise in Chapter 2 is slightly different). Second, if the Kuramoto order parameter is constant, then the collective phase evolves through the normal form of the SNIC bifurcation (see Chapter 1). This means that a partially synchronous phase of a system of type-I oscillators behaves exactly as a type-I oscillator, with redefined excitability $a' = a\left(1+R^2\right)/(2R) > a$. In general, having less synchronization accounts for more excitability at the macroscopic level, as one could have expected intuitively.

In order to perform a bifurcation analyses, we follow the prescription by Strogatz and Childs (Childs and Strogatz 2008). We know that in the limit $a = 0$ the system behaves as the stochastic Kuramoto, so it must undergo a Hopf bifurcation at $J = \sigma^2$; on the other hand, individual oscillators with $J = 0$ present a SNIC bifurcation.

The normal procedure would be to obtain the equilibria by imposing $\dot{R} = 0$ and $\dot{\psi} = 0$, then insert these solutions (R^*, ψ^*) into the Jacobian

$Q(R,\psi)$, diagonalize it, and checking the bifurcation conditions on the eigenvalues. However, not even the first step –obtaining analytic expressions for R^* and ψ^* is possible. Despite of that, it is possible to obtain the bifurcation curves as it was pointed out at the end of Chapter 1. Hopf bifurcation fulfills $\mathrm{Tr}\, Q(R^*,\psi^*) = 0$, while the condition for the saddle node is $\det Q(R^*,\psi^*) = 0$ in two dimensional systems Notice that the equilibria values are bounded, since $0 \leq R \leq 1$ and $0 \leq \psi < 2\pi$. Hence, one can use the bifurcation condition in conjunction with the condition for the fixed points to obtain the bifurcation curves as parametric equations that depend on the values of (R^*,ψ^*), without having to compute explicitly the equilibria location. There are six unknowns: R^*, ψ^*, ω, a, J, and σ. One of the parameters can be set to one with a change of variable, without loss of generality. We choose $\omega = 1$. For the moment, let us fix J, and use the remaining four as variables. For the system of equations, we choose to solve for R^*, $\cos\psi^*$ and $\sin\psi^*$. The last two are not independent conditions, but $\cos^2\psi + \sin^2\psi = 1$ allow one to extract the excitability in an easy way,

$$a_H = \sqrt{\frac{J-\sigma^2}{J+\sigma^2}}\,\frac{\sqrt{4\omega^2(J+\sigma^2)^2 + J^2(J-\sigma^2)^2}}{2J}. \tag{C.8}$$

We could have solved the system directly for R, ψ^* and a, but the algebra is simpler in this way (Childs and Strogatz 2008). This is a parametric curve for the Hopf bifurcation, $a_H = a_H(\omega, J, \sigma)$, that was obtained without knowing R^* and ψ^* explicitly. Actually, since we set $\omega = 1$ and fixed J then $a_H = a_H(\sigma)$.

For the saddle-node bifurcation line, the computation is more difficult. In this case we want to avoid the variable R^* at all, since solving for it implies solving high-order polynomials. Then, we choose to solve for ω, $\cos\psi^*$ and $\sin\psi^*$, to eliminate the dependence on ψ^*. The result is

$$\omega_S = \frac{(1+R^2)^{3/2}}{2(1-R^2)^2}\sqrt{J(1-R^2)(2\sigma^2 - J(1-R^2)^2) - \sigma^4(1+R^2)}, \tag{C.9a}$$

$$a_S = \frac{\sqrt{2}R^2}{(1-R^2)^2}\sqrt{(J(1-R^2)-\sigma^2)(2\sigma^2 - J(1-R^2)^2)}. \tag{C.9b}$$

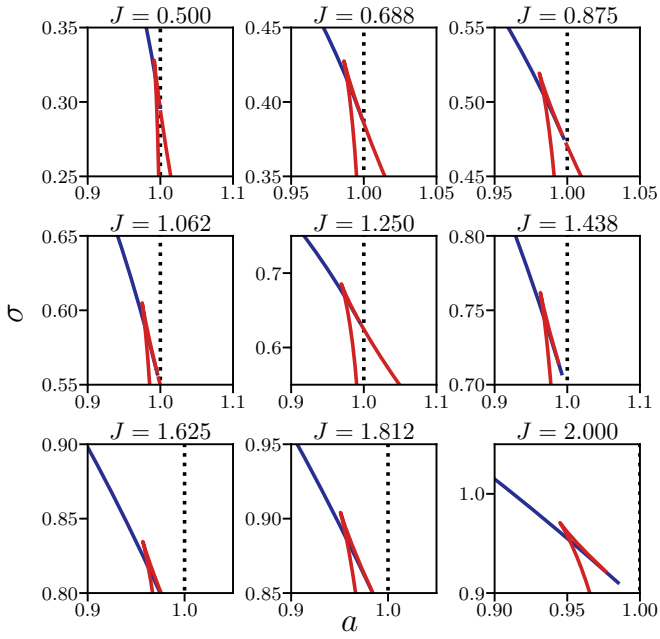

Figure C.2: **Bifurcation lines predicted by the Ott-Antonsen ansatz.** The bifurcation lines in the (a, σ) plane for the Ott-Antonsen ansatz. Hopf bifurcations (eq. (C.8)) are represented by blue lines, while red ones correspond to saddle-nodes (eqs. (C.9)). All plots are zooms to remark the bistable region, which exists for all the values of coupling displayed here.

Since R is bounded, the bifurcation line in the (a, σ) plane can be obtained by making $\omega_S = 1$ and solving for σ in the first equation to obtain $\sigma_S = \sigma_S(R)$, $a_S = a_S(R)$ (remember that J is fixed) and then moving the parameter R from 0 to 1.

In Figure C.2, we show different cut of the Hopf and saddle node bifurcations obtained for several values of the coupling J. The bistability region delimited by the small triangle is present for many values of J, but decreases until vanishing for low enough values of the coupling.

References

Abeles, M. (1991). *Corticonics: Neural Circuits of the Cerebral Cortex*. Cambridge University Press.

Acebrón, J. A., L. L. Bonilla, C. J. Pérez Vicente, F. Ritort, and R. Spigler (2005). "The Kuramoto Model: A Simple Paradigm for Synchronization Phenomena". *Reviews of Modern Physics* 77.1, pp. 137–185.

Aguilar-Velázquez, D. and L. Guzmán-Vargas (2019). "Critical Synchronization and 1/ f Noise in Inhibitory/Excitatory Rich-Club Neural Networks". *Scientific Reports* 9.1, p. 1258.

Alava, M. and M. A. Muñoz (2002). "Interface Depinning versus Absorbing-State Phase Transitions". *Physical Review E* 65.2, p. 026145.

Albrecht, U. (2012). "Timing to Perfection: The Biology of Central and Peripheral Circadian Clocks". *Neuron* 74.2, pp. 246–260.

Alstott, J., E. Bullmore, and D. Plenz (2014). "Powerlaw: A Python Package for Analysis of Heavy-Tailed Distributions". *PloS one* 9.1.

Anderson, P. W. (1972). "More Is Different". *Science* 177.4047, pp. 393–396.

Arieli, A., A. Sterkin, A. Grinvald, and A. Aertsen (1996). "Dynamics of Ongoing Activity: Explanation of the Large Variability in Evoked Cortical Responses". *Science* 273.5283, pp. 1868–1871.

Atasoy, S., G. Deco, and M. L. Kringelbach (2019). "Playing at the Edge of Criticality: Expanded Whole-Brain Repertoire of Connectome-Harmonics". *The Functional Role of Critical Dynamics in Neural Systems*. Ed. by N. Tomen, J. M. Herrmann, and U. Ernst. Springer Series on Bio- and Neurosystems. Cham: Springer International Publishing, pp. 27–45.

Bagnoli, F., F. Cecconi, A. Flammini, and A. Vespignani (2003). "Short-Period Attractors and Non-Ergodic Behavior in the Deterministic Fixed-Energy Sandpile Model". *EPL (Europhys. Lett.)* 63.4, p. 512.

Bak, P. (1996). *How Nature Works: The Science of Self-Organized Criticality*. Copernicus New York.

Bak, P. and K. Chen (1991). "Self-Organized Criticality". *Scientific American* 264.1, pp. 46–53.

Bak, P. and C. Tang (1989). "Earthquakes as a Self-Organized Critical Phenomenon". *Journal of Geophysical Research* 94.B11, p. 15635.

Bak, P., C. Tang, and K. Wiesenfeld (1987). "Self-Organized Criticality: An Explanation of the 1/f Noise". *Physical review letters* 59.4, p. 381.

REFERENCES

Bak, P., K. Chen, and C. Tang (1990). "A Forest-Fire Model and Some Thoughts on Turbulence". *Physics letters A* 147.5-6, pp. 297–300.

Barral, J. and A. D. Reyes (2016). "Synaptic Scaling Rule Preserves Excitatory–Inhibitory Balance and Salient Neuronal Network Dynamics". *Nature Neuroscience* 19.12, p. 1690.

Beggs, J. M. (2008). "The Criticality Hypothesis: How Local Cortical Networks Might Optimize Information Processing". *Phil Trans R Soc A* 366.1864, pp. 329–343.

Beggs, J. M. and D. Plenz (2003). "Neuronal Avalanches in Neocortical Circuits". *Journal of neuroscience* 23.35, pp. 11167–11177.

Beggs, J. M. and D. Plenz (2004). "Neuronal Avalanches Are Diverse and Precise Activity Patterns That Are Stable for Many Hours in Cortical Slice Cultures". *Journal of Neuroscience* 24.22, pp. 5216–5229.

Beggs, J. M. and N. Timme (2012). "Being Critical of Criticality in the Brain". *Frontiers in Physiology* 3.

Bellay, T., A. Klaus, S. Seshadri, and D. Plenz (2015). "Irregular Spiking of Pyramidal Neurons Organizes as Scale-Invariant Neuronal Avalanches in the Awake State". *eLife* 4. Ed. by F. K. Skinner, e07224.

Benayoun, M., J. D. Cowan, W. van Drongelen, and E. Wallace (2010). "Avalanches in a Stochastic Model of Spiking Neurons". *PLoS Comput. Biol.* 6.7, e1000846.

Binney, J. J., N. J. Dowrick, A. J. Fisher, and M. E. J. Newman (2001). *The Theory of Critical Phenomena: An Introduction to the Renormalization Group*. Oxford Univ. Press.

Boldog, E. et al. (2018). "Transcriptomic and Morphophysiological Evidence for a Specialized Human Cortical GABAergic Cell Type". *Nature Neuroscience* 21.9, pp. 1185–1195.

Bonachela, J. A. and M. A. Muñoz (2009). "Self-Organization without Conservation: True or Just Apparent Scale-Invariance?" *J. Stat. Mech.* P09009.

Bonachela, J., S. de Franciscis, J. Torres, and M. A. Muñoz (2010). "Self-Organization without Conservation: Are Neuronal Avalanches Generically Critical?" *J. Stat. Mech.* 2010.02, P02015.

Bonachela, J. A. and M. A. Muñoz (2008). "Confirming and Extending the Hypothesis of Universality in Sandpiles". *Physical Review E* 78.4, p. 041102.

Bonachela, J. A., H. Chaté, I. Dornic, and M. A. Muñoz (2007). "Absorbing States and Elastic Interfaces in Random Media: Two Equivalent Descriptions of Self-Organized Criticality". *Physical review letters* 98.15, p. 155702.

Bonachela, J. A., M. Alava, and M. A. Muñoz (2009). "Cusps, Self-Organization, and Absorbing States". *Physical Review E* 79.5, p. 050106.

Börgers, C. and N. Kopell (2005). "Effects of Noisy Drive on Rhythms in Networks of Excitatory and Inhibitory Neurons". *Neural Computation* 17.3, pp. 557–608.

Börgers, C., M. Krupa, and S. Gielen (2010). "The Response of a Classical Hodgkin–Huxley Neuron to an Inhibitory Input Pulse". *Journal of Computational Neuroscience* 28.3, pp. 509–526.

Borges, F. S. et al. (2020). "Self-Sustained Activity of Low Firing Rate in Balanced Networks". *Physica A: Statistical Mechanics and its Applications* 537, p. 122671.

Borisyuk, R. M. and A. B. Kirillov (1992). "Bifurcation Analysis of a Neural Network Model". *Biological Cybernetics* 66.4, pp. 319–325.

Breakspear, M. (2017). "Dynamic Models of Large-Scale Brain Activity". *Nature neuroscience* 20.3, pp. 340–352.

Breakspear, M., S. Heitmann, and A. Daffertshofer (2010). "Generative Models of Cortical Oscillations: Neurobiological Implications of the Kuramoto Model". *Front. Human Neurosci.* 4, p. 190.

Brochini, L. et al. (2016). "Phase Transitions and Self-Organized Criticality in Networks of Stochastic Spiking Neurons". *Scientific Reports* 6.1, p. 35831.

Bröker, H.-M. and P. Grassberger (1997). "Random Neighbor Theory of the Olami-Feder-Christensen Earthquake Model". *Physical Review E* 56.4, p. 3944.

Brunel, N. (2000). "Dynamics of Sparsely Connected Networks of Excitatory and Inhibitory Spiking Neurons". *Journal of Computational Neuroscience* 8.3, pp. 183–208.

Brunel, N. and M. C. W. van Rossum (2007). "Lapicque's 1907 Paper: From Frogs to Integrate-and-Fire". *Biological Cybernetics* 97.5, pp. 337–339.

Brunel, N. and X.-J. Wang (2003). "What Determines the Frequency of Fast Network Oscillations with Irregular Neural Discharges? I.

Synaptic Dynamics and Excitation-Inhibition Balance". *Journal of Neurophysiology* 90.1, pp. 415–430.

Buehlmann, A. and G. Deco (2010). "Optimal Information Transfer in the Cortex through Synchronization". *PLoS Computational Biology* 6.9.

Buendía, V. et al. (2019). "Jensen's Force and the Statistical Mechanics of Cortical Asynchronous States". *Scientific Reports* 9.1, p. 15183.

Buendía, V., S. di Santo, J. A. Bonachela, and M. A. Muñoz (2020a). "Feedback Mechanisms for Self-Organization to the Edge of a Phase Transition". *Frontiers in Physics* 8, p. 333.

Buendía, V., P. Villegas, R. Burioni, and M. A. Muñoz (2020b). "Hybrid-Type Synchronization Transitions: Where Marginal Coherence, Scale-Free Avalanches, and Bistability Live Together". *arXiv:2011.03263 [cond-mat, physics:nlin, q-bio]*.

Buendía, V., S. di Santo, P. Villegas, R. Burioni, and M. A. Muñoz (2020c). "Self-Organized Bistability and Its Possible Relevance for Brain Dynamics". *Physical Review Research* 2.1, p. 013318.

Buice, M. A. and J. D. Cowan (2007). "Field-Theoretic Approach to Fluctuation Effects in Neural Networks". *Phys. Rev. E* 75.5, p. 051919.

Bunge, M. (2003). *Emergence and Convergence: Qualitative Novelty and the Unity of Knowledge*. University of Toronto Press.

Buzsáki, G. (2006). *Rhythms of the Brain*. Oxford ; New York: Oxford University Press.

Cabral, J., E. Hugues, O. Sporns, and G. Deco (2011). "Role of Local Network Oscillations in Resting-State Functional Connectivity". *Neuroimage* 57.1, pp. 130–139.

Cabral, J., M. L. Kringelbach, and G. Deco (2014). "Exploring the Network Dynamics Underlying Brain Activity during Rest". *Progress in Neurobiology* 114, pp. 102–131.

— (2017). "Functional Connectivity Dynamically Evolves on Multiple Time-Scales over a Static Structural Connectome: Models and Mechanisms". *NeuroImage*. Functional Architecture of the Brain 160, pp. 84–96.

Cabrera, J. L., J. Hoenicka, and D. Macedo (2013). "A Small Morris-Lecar Neuron Network Gets Close to Critical Only in the Small-World Regimen". *Journal of Complex Systems* 2013, pp. 1–7.

Cardy, J. L. and P. Grassberger (1985). "Epidemic Models and Percolation". *Journal of Physics A: Mathematical and General* 18.6, p. L267.

Chalmers, D. J. (1995). "Facing Up to the Problem of Consciousness". *Journal of Consciousness Studies* 2.3, pp. 200–19.

Chen, X. and R. Dzakpasu (2010). "Observed Network Dynamics from Altering the Balance between Excitatory and Inhibitory Neurons in Cultured Networks". *Physical Review E* 82.3, p. 031907.

Cheng, Q., S.-H. Song, and G. J. Augustine (2018). "Molecular Mechanisms of Short-Term Plasticity: Role of Synapsin Phosphorylation in Augmentation and Potentiation of Spontaneous Glutamate Release". *Frontiers in Synaptic Neuroscience* 10.

Childs, L. M. and S. H. Strogatz (2008). "Stability Diagram for the Forced Kuramoto Model". *Chaos: An Interdisciplinary Journal of Nonlinear Science* 18.4, p. 043128.

Choi, H. W., S. E. Maeng, and J. W. Lee (2012). "Self-Organized Criticality of a Simple Integrate-and-Fire Neural Model". *Journal of the Korean Physical Society* 60.4, pp. 657–659.

Christensen, K and N. Moloney (2005). *Complexity and Criticality*. London: Imperial College Press.

Christensen, K., N. R. Moloney, O. Peters, and G. Pruessner (2004). "Avalanche Behavior in an Absorbing State Oslo Model". *Physical Review E* 70.6.

Clauset, A., C. R. Shalizi, and M. E. J. Newman (2009). "Power-Law Distributions in Empirical Data". *SIAM Review* 51.4, pp. 661–703.

Cofré, R. et al. (2020). "Whole-Brain Models to Explore Altered States of Consciousness from the Bottom Up". *Brain Sciences* 10.9, p. 626.

Corral, Á., C. J. Pérez, A. Díaz-Guilera, and A. Arenas (1995). "Self-Organized Criticality and Synchronization in a Lattice Model of Integrate-and-Fire Oscillators". *Phys. Rev. Lett.* 74.1, pp. 118–121.

Cowan, J. D., J. Neuman, and W. van Drongelen (2016). "Wilson–Cowan Equations for Neocortical Dynamics". *The Journal of Mathematical Neuroscience* 6.1, p. 1.

Cunden, F. D., P. Facchi, M. Ligabò, and P. Vivo (2017). "Universality of the Third-Order Phase Transition in the Constrained Coulomb Gas". *Journal of Statistical Mechanics: Theory and Experiment* 2017.5, p. 053303.

da Cunha, S. D., L. R. da Silva, G. M. Viswanathan, and R. Dickman (2014). "Activity, Diffusion, and Correlations in a Two-Dimensional

Conserved Stochastic Sandpile". *Journal of Statistical Mechanics: Theory and Experiment* 2014.8, P08003.

Daffertshofer, A., R. Ton, M. L. Kringelbach, M. Woolrich, and G. Deco (2018a). "Distinct Criticality of Phase and Amplitude Dynamics in the Resting Brain". *NeuroImage*. Brain Connectivity Dynamics 180, pp. 442–447.

Daffertshofer, A., R. Ton, B. Pietras, M. L. Kringelbach, and G. Deco (2018b). "Scale-Freeness or Partial Synchronization in Neural Mass Phase Oscillator Networks: Pick One of Two?" *NeuroImage*. Brain Connectivity Dynamics 180, pp. 428–441.

Davidson, E. and M. Levin (2005). "Gene Regulatory Networks". *Proc. Natl. Acad. of Sci. (USA)* 102.14, pp. 4935–4935.

de Arcangelis, L., C. Perrone-Capano, and H. J. Herrmann (2006). "Self-Organized Criticality Model for Brain Plasticity". *Physical Review Letters* 96.2, p. 028107.

De Menech, M. and A. L. Stella (2000). "From Waves to Avalanches: Two Different Mechanisms of Sandpile Dynamics". *Physical Review E* 62.4, R4528.

Deco, G. and V. K. Jirsa (2012). "Ongoing Cortical Activity at Rest: Criticality, Multistability, and Ghost Attractors". *Journal of Neuroscience* 32.10, pp. 3366–3375.

Deco, G., V. K. Jirsa, P. A. Robinson, M. Breakspear, and K. Friston (2008). "The Dynamic Brain: From Spiking Neurons to Neural Masses and Cortical Fields". *PLoS Comput. Biol.y* 4.8.

Deco, G., V. Jirsa, A. R. McIntosh, O. Sporns, and R. Kötter (2009). "Key Role of Coupling, Delay, and Noise in Resting Brain Fluctuations". *Proceedings of the National Academy of Sciences* 106.25, pp. 10302–10307.

Deco, G. et al. (2014). "How Local Excitation–Inhibition Ratio Impacts the Whole Brain Dynamics". *Journal of Neuroscience* 34.23, pp. 7886–7898.

Dehghani, N. et al. (2012). "Avalanche Analysis from Multielectrode Ensemble Recordings in Cat, Monkey, and Human Cerebral Cortex during Wakefulness and Sleep". *Frontiers in Physiology* 3.

Dehghani, N. et al. (2016). "Dynamic Balance of Excitation and Inhibition in Human and Monkey Neocortex". *Scientific Reports* 6, p. 23176.

Denève, S. and C. K. Machens (2016). "Efficient Codes and Balanced Networks". *Nature Neuroscience* 19.3, pp. 375–382.

Destexhe, A. (2009). "Self-Sustained Asynchronous Irregular States and up–down States in Thalamic, Cortical and Thalamocortical Networks of Nonlinear Integrate-and-Fire Neurons". *Journal of Computational Neuroscience* 27.3, p. 493.

di Santo, S, P Villegas, R Burioni, and M. Muñoz (2017). "A Simple Unified View of Branching Process Statistics: Random Walks in Balanced Logarithmic Potentials". *Physical Review E*.

di Santo, S. (2018). "Criticality in the Brain: From Neutral Theory to Self-Organization and Synchronization". PhD Thesis. Parma.

di Santo, S., R. Burioni, A. Vezzani, and M. A. Muñoz (2016). "Self-Organized Bistability Associated with First-Order Phase Transitions". *Phys. Rev. Lett.* 116.24, p. 240601.

di Santo, S., P. Villegas, R. Burioni, and M. A. Muñoz (2018a). "Landau–Ginzburg Theory of Cortex Dynamics: Scale-Free Avalanches Emerge at the Edge of Synchronization". *Proc. Natl. Acad. of Sci. (USA)* 115.7, E1356–E1365.

— (2018b). "Non-Normality, Reactivity, and Intrinsic Stochasticity in Neural Dynamics: A Non-Equilibrium Potential Approach". *Journal of Statistical Mechanics: Theory and Experiment* 2018.7, p. 073402.

Dickman, R., M. A. Muñoz, A. Vespignani, and S. Zapperi (2000). "Paths to Self-Organized Criticality". *Brazilian Journal of Physics* 30.1, pp. 27–41.

Dickman, R. et al. (2001). "Critical Behavior of a One-Dimensional Fixed-Energy Stochastic Sandpile". *Physical Review E* 64.5, p. 056104.

Dickman, R., L. T. Rolla, and V. Sidoravicius (2010). "Activated Random Walkers: Facts, Conjectures and Challenges". *Journal of Statistical Physics* 138.1-3, pp. 126–142.

Ditlevsen, S. and P. Greenwood (2013). "The Morris–Lecar Neuron Model Embeds a Leaky Integrate-and-Fire Model". *Journal of Mathematical Biology* 67.2, pp. 239–259.

Dornic, I., H. Chaté, J. Chave, and H. Hinrichsen (2001). "Critical Coarsening without Surface Tension: The Universality Class of the Voter Model". *Physical Review Letters* 87.4, p. 045701.

Dornic, I., H. Chaté, and M. A. Muñoz (2005). "Integration of Langevin Equations with Multiplicative Noise and the Viability of Field The-

ories for Absorbing Phase Transitions". *Physical Review Letters* 94.10, p. 100601.
Drossel, B. and F. Schwabl (1992). "Self-Organized Critical Forest-Fire Model". *Physical Review Letters* 69.11, p. 1629.
El Boustani, S. and A. Destexhe (2009). "A Master Equation Formalism for Macroscopic Modeling of Asynchronous Irregular Activity States". *Neural Computation* 21.1, pp. 46–100.
Ermentrout, G. B. and N. Kopell (1986). "Parabolic Bursting in an Excitable System Coupled with a Slow Oscillation". *SIAM Journal on Applied Mathematics* 46.2, pp. 233–253.
Ferrari, F. A., R. L. Viana, S. R. Lopes, and R. Stoop (2015). "Phase Synchronization of Coupled Bursting Neurons and the Generalized Kuramoto Model". *Neural Networks* 66, pp. 107–118.
Feuillet, L., H. Dufour, and J. Pelletier (2007). "Brain of a White-Collar Worker". *The Lancet* 370.9583, p. 262.
Fontenele, A. J. et al. (2019). "Criticality between Cortical States". *Physical review letters* 122.20, p. 208101.
Friedman, N. et al. (2012). "Universal Critical Dynamics in High Resolution Neuronal Avalanche Data". *Physical review letters* 108.20, p. 208102.
Froemke, R. C. (2015). "Plasticity of Cortical Excitatory-Inhibitory Balance". *Annual Review of Neuroscience* 38.1, pp. 195–219.
Gardiner, C. (2009). *Stochastic Methods: A Handbook for the Natural and Social Sciences*. Springer Series in Synergetics. Springer.
Gerstner, W. (2014). *Neuronal Dynamics: From Single Neurons To Networks And Models Of Cognition*. UK ed. edition. Cambridge, United Kingdom: Cambridge University Press.
Gil, L and D Sornette (1996). "Landau-Ginzburg Theory of Self-Organized Criticality". *Physical Review Letters* 76.21, p. 3991.
Ginzburg, I. and H. Sompolinsky (1994). "Theory of Correlations in Stochastic Neural Networks". *Physical Review E* 50.4, pp. 3171–3191.
Girardi-Schappo, M., L. Brochini, A. A. Costa, T. T. A. Carvalho, and O. Kinouchi (2020). "Synaptic Balance Due to Homeostatically Self-Organized Quasicritical Dynamics". *Phys. Rev. Res.* 2.1, p. 012042.
Gireesh, E. D. and D. Plenz (2008). "Neuronal Avalanches Organize as Nested Theta- and Beta/Gamma-Oscillations during Development

of Cortical Layer 2/3". *Proceedings of the National Academy of Sciences* 105.21, pp. 7576–7581.
Goldobin, D. S., I. V. Tyulkina, L. S. Klimenko, and A. Pikovsky (2018). "Collective Mode Reductions for Populations of Coupled Noisy Oscillators". *Chaos: An Interdisciplinary Journal of Nonlinear Science* 28.10, p. 101101.
Golombek, D. A. and R. E. Rosenstein (2010). "Physiology of Circadian Entrainment". *Physiological Reviews* 90.3, pp. 1063–1102.
Grassberger, P and S. Manna (1990). "Some More Sandpiles". *Journal de Physique* 51.11, pp. 1077–1098.
Grassberger, P. (1983). "On the Critical Behavior of the General Epidemic Process and Dynamical Percolation". *Mathematical Biosciences* 63.2, pp. 157–172.
— (1994). "Efficient Large-Scale Simulations of a Uniformly Driven System". *Physical Review E* 49.3, p. 2436.
— (2002). "Critical Behaviour of the Drossel-Schwabl Forest Fire Model". *New Journal of Physics* 4.1, p. 17.
Grassberger, P. and H. Kantz (1991). "On a Forest Fire Model with Supposed Self-Organized Criticality". *Journal of Statistical Physics* 63.3-4, pp. 685–700.
Grassberger, P., D. Dhar, and P. Mohanty (2016). "Oslo Model, Hyperuniformity, and the Quenched Edwards-Wilkinson Model". *Physical Review E* 94.4, p. 042314.
Gray, C. M., P. König, A. K. Engel, and W. Singer (1989). "Oscillatory Responses in Cat Visual Cortex Exhibit Inter-Columnar Synchronization Which Reflects Global Stimulus Properties". *Nature* 338.6213, pp. 334–337.
Grinstein, G, D.-H. Lee, and S. Sachdev (1990). "Conservation Laws, Anisotropy, and "Self-Organized Criticality"in Noisy Nonequilibrium Systems". *Physical review letters* 64.16, p. 1927.
Hahn, G. et al. (2010). "Neuronal Avalanches in Spontaneous Activity in Vivo". *Journal of neurophysiology* 104.6, pp. 3312–3322.
Haider, B., A. Duque, A. R. Hasenstaub, and D. A. McCormick (2006). "Neocortical Network Activity in Vivo Is Generated through a Dynamic Balance of Excitation and Inhibition". *Journal of Neuroscience* 26.17, pp. 4535–4545.
Haimovici, A., E. Tagliazucchi, P. Balenzuela, and D. R. Chialvo (2013). "Brain Organization into Resting State Networks Emerges at Criti-

cality on a Model of the Human Connectome". *Physical Review Letters* 110.17.

Harris, K. D. and A. Thiele (2011). "Cortical State and Attention". *Nature Reviews Neuroscience* 12.9, p. 509.

Henkel, M., H. Hinrichsen, and S. Lübeck (2008). *Non-Equilibrium Phase Transitions: Absorbing Phase Transitions*. Theor. and Math. Phys. Berlin: Springer London.

Hesse, J. and T. Gross (2014). "Self-Organized Criticality as a Fundamental Property of Neural Systems". *Frontiers in Computational Neuroscience* 8.

Hesse, J., J.-H. Schleimer, and S. Schreiber (2017). "Qualitative Changes in Phase-Response Curve and Synchronization at the Saddle-Node-Loop Bifurcation". *Physical Review E* 95.5.

Hidalgo, J., L. F. Seoane, J. M. Cortés, and M. A. Muñoz (2012). "Stochastic Amplification of Fluctuations in Cortical Up-States". *PloS one* 7.8, e40710.

Hinrichsen, H. (2000). "Non-Equilibrium Critical Phenomena and Phase Transitions into Absorbing States". *Advances in Physics* 49.7, pp. 815–958.

Hodgkin, A. L. (1948). "The Local Electric Changes Associated with Repetitive Action in a Non-Medullated Axon". *The Journal of Physiology* 107.2, pp. 165–181.

Hohenberg, P. C. and B. I. Halperin (1977). "Theory of Dynamic Critical Phenomena". *Reviews of Modern Physics* 49.3, pp. 435–479.

Hong, H., H. Park, and M. Y. Choi (2005). "Collective Synchronization in Spatially Extended Systems of Coupled Oscillators with Random Frequencies". *Physical Review E* 72.3.

Hong, H., H. Chaté, L.-H. Tang, and H. Park (2015). "Finite-Size Scaling, Dynamic Fluctuations, and Hyperscaling Relation in the Kuramoto Model". *Physical Review E* 92.2.

Hoppensteadt, F. C. and E. M. Izhikevich (1997). *Weakly Correlated Neural Networks*. Applied Mathematical Sciences 126. Springer.

Huynh, H. N., G. Pruessner, and L. Y. Chew (2011). "The Abelian Manna Model on Various Lattices in One and Two Dimensions". *Journal of Statistical Mechanics: Theory and Experiment* 2011.09, P09024.

Isaacson, J. S. and M. Scanziani (2011). "How Inhibition Shapes Cortical Activity". *Neuron* 72.2, pp. 231–243.

Izhikevich, E. M. (2003). "Simple Model of Spiking Neurons". *IEEE Transactions on Neural Networks* 14.6, pp. 1569–1572.

Izhikevich, E. M. (2006). *Dynamical Systems in Neuroscience: The Geometry of Excitability and Bursting*. The MIT Press.

Janssen, H. K. (1985). "Renormalized Field Theory of Dynamical Percolation". *Zeitschrift für Physik B Condensed Matter* 58.4, pp. 311–317.

Janssen, H.-K. and O. Stenull (2016). "Directed Percolation with a Conserved Field and the Depinning Transition". *Physical Review E* 94.4, p. 042138.

Jensen, H. J. (1998). *Self-Organized Criticality: Emergent Complex Behavior in Physical and Biological Systems*. Cambridge: Cambridge university press.

Jercog, D. et al. (2017). "UP-DOWN Cortical Dynamics Reflect State Transitions in a Bistable Network". *eLife* 6. Ed. by M. C. van Rossum, e22425.

Jobst, B. M. et al. (2017). "Increased Stability and Breakdown of Brain Effective Connectivity During Slow-Wave Sleep: Mechanistic Insights from Whole-Brain Computational Modelling". *Scientific Reports* 7.1, p. 4634.

Jokić-Begić, N. (2010). "Cognitive-Behavioral Therapy and Neuroscience: Towards Closer Integration". *Psychological Topics* 19.2, pp. 235–254.

Kandel, E. R., J. H. Schwartz, T. M. Jessell, S. A. Siegelbaum, and A. J. Hudspeth (2000). *Principles of Neural Science*. Vol. 4. McGraw-hill New York.

Kardar, M. (2007a). *Statistical Physics of Fields*. Cambridge ; New York: Cambridge University Press.

— (2007b). *Statistical Physics of Particles*. Cambridge : New York: Cambridge University Press.

Karimipanah, Y., Z. Ma, J.-e. K. Miller, R. Yuste, and R. Wessel (2017). "Neocortical Activity Is Stimulus- and Scale-Invariant". *PLOS ONE* 12.5, e0177396.

Kinouchi, O. and M. Copelli (2006). "Optimal Dynamical Range of Excitable Networks at Criticality". *Nature Physics* 2.5, pp. 348–351.

Klaus, A., S. Yu, and D. Plenz (2011). "Statistical Analyses Support Power Law Distributions Found in Neuronal Avalanches". *PLoS ONE* 6.5. Ed. by M. Zochowski, e19779.

Kriener, B. et al. (2014). "Dynamics of Self-Sustained Asynchronous-Irregular Activity in Random Networks of Spiking Neurons with Strong Synapses". *Frontiers in Computational Neuroscience* 8, p. 136.

Ktitarev, D., S Lübeck, P Grassberger, and V. Priezzhev (2000). "Scaling of Waves in the Bak-Tang-Wiesenfeld Sandpile Model". *Physical Review E* 61.1, p. 81.

Kuznetsov, Y. A. (2004). *Elements of Applied Bifurcation Theory*. Ed. by S. S. Antman, J. E. Marsden, and L. Sirovich. Vol. 112. Applied Mathematical Sciences. New York, NY: Springer New York.

La Camera, G. et al. (2006). "Multiple Time Scales of Temporal Response in Pyramidal and Fast Spiking Cortical Neurons". *Journal of Neurophysiology* 96.6, pp. 3448–3464.

Laing, C. R. (2014). "Derivation of a Neural Field Model from a Network of Theta Neurons". *Physical Review E* 90.1.

— (2018). "The Dynamics of Networks of Identical Theta Neurons". *The Journal of Mathematical Neuroscience* 8.1.

Landau, L. D. and E. M. Lifshitz (1964). *Statistical Physics*. Second. Vol. 5. Revert\'e.

Larremore, D. B., W. L. Shew, E. Ott, F. Sorrentino, and J. G. Restrepo (2014). "Inhibition Causes Ceaseless Dynamics in Networks of Excitable Nodes". *Physical Review Letters* 112.13, p. 138103.

Latham, P. E., B. J. Richmond, P. Nelson, and S. Nirenberg (2000). "Intrinsic Dynamics in Neuronal Networks. I. Theory". *Journal of Neurophysiology* 83.2, pp. 808–827.

Le Bellac, M. (1991). *Quantum and Statistical Field Theory*. Clarendon Press Oxford.

Le Doussal, P. and K. J. Wiese (2015). "Exact Mapping of the Stochastic Field Theory for Manna Sandpiles to Interfaces in Random Media". *Physical review letters* 114.11, p. 110601.

Levina, A. and V. Priesemann (2017). "Subsampling Scaling". *Nature Communications* 8.1, p. 15140.

Levina, A., J. M. Herrmann, and T. Geisel (2007). "Dynamical Synapses Causing Self-Organized Criticality in Neural Networks". *Nature Physics* 3.12, pp. 857–860.

— (2009). "Phase Transitions towards Criticality in a Neural System with Adaptive Interactions". *Physical Review Letters* 102.11, p. 118110.

Lewin, R. (1980). "Is Your Brain Really Necessary?" *Science* 210.4475, pp. 1232–1234.

Liang, J., T. Zhou, and C. Zhou (2020). "Hopf Bifurcation in Mean Field Explains Critical Avalanches in Excitation-Inhibition Balanced Neuronal Networks: A Mechanism for Multiscale Variability". *arXiv preprint arXiv:2001.05626*.

Lima Dias Pinto, I. and M. Copelli (2019). "Oscillations and Collective Excitability in a Model of Stochastic Neurons under Excitatory and Inhibitory Coupling". *Physical Review E* 100.6, p. 062416.

Lindner, B (2004). "Effects of Noise in Excitable Systems". *Physics Reports* 392.6, pp. 321–424.

Litwin-Kumar, A. and B. Doiron (2012). "Slow Dynamics and High Variability in Balanced Cortical Networks with Clustered Connections". *Nature Neuroscience* 15.11, p. 1498.

Liu, B.-h. et al. (2011). "Broad Inhibition Sharpens Orientation Selectivity by Expanding Input Dynamic Range in Mouse Simple Cells". *Neuron* 71.3, pp. 542–554.

Liu, C., X. Liu, and S. Liu (2014). "Bifurcation Analysis of a Morris–Lecar Neuron Model". *Biological Cybernetics* 108.1, pp. 75–84.

Luke, T. B., E. Barreto, and P. So (2013). "Complete Classification of the Macroscopic Behavior of a Heterogeneous Network of Theta Neurons". *Neural Computation* 25.12, pp. 3207–3234.

— (2014). "Macroscopic Complexity from an Autonomous Network of Networks of Theta Neurons". *Frontiers in Computational Neuroscience* 8.

Ma, T. and S. Wang (2011). "Third-Order Gas-Liquid Phase Transition and the Nature of Andrews Critical Point". *AIP Advances* 1.4, p. 042101.

Mandelbrot, B. B. (1983). *The Fractal Geometry of Nature*. W.H Freeman and Co.

Manna, S. S. (1991). "Two-State Model of Self-Organized Criticality". *Journal of Physics A: Mathematical and General* 24.7, pp. L363–L369.

Månsson, K. N. T. et al. (2016). "Neuroplasticity in Response to Cognitive Behavior Therapy for Social Anxiety Disorder". *Translational Psychiatry* 6.2, e727–e727.

Markram, H. (2006). "The Blue Brain Project". *Nature Reviews Neuroscience* 7.2, pp. 153–160.

Markram, H. et al. (2015). "Reconstruction and Simulation of Neocortical Microcircuitry". *Cell* 163.2, pp. 456–492.

Marro, J. and R. Dickman (2005). *Nonequilibrium Phase Transitions in Lattice Models*. Collection Aléa-Saclay. Cambridge University Press.

Maslov, S. and Y.-C. Zhang (1995). "Exactly Solved Model of Self-Organized Criticality". *Physical review letters* 75.8, p. 1550.

Mateos-Aparicio, P. and A. Rodríguez-Moreno (2019). "The Impact of Studying Brain Plasticity". *Frontiers in Cellular Neuroscience* 13.

Mattia, M. and M. V. Sanchez-Vives (2012). "Exploring the Spectrum of Dynamical Regimes and Timescales in Spontaneous Cortical Activity". *Cogn. Neurodyn.* 6.3, pp. 239–250.

Mermin, N. D. (2004). "Could Feynman Have Said This?" *Physics Today* 57.5, pp. 10–11.

Mermin, N. D. and H. Wagner (1966). "Absence of Ferromagnetism or Antiferromagnetism in One-or Two-Dimensional Isotropic Heisenberg Models". *Physical Review Letters* 17.22, p. 1133.

Michiels van Kessenich, L., D. Berger, L. de Arcangelis, and H. J. Herrmann (2019). "Pattern Recognition with Neuronal Avalanche Dynamics". *Physical Review E* 99.1, p. 010302.

Mikkelsen, K., A. Imparato, and A. Torcini (2013). "Emergence of Slow Collective Oscillations in Neural Networks with Spike-Timing Dependent Plasticity". *Physical Review Letters* 110.20, p. 208101.

Millán, A. P., J. J. Torres, S. Johnson, and J. Marro (2018). "Concurrence of Form and Function in Developing Networks and Its Role in Synaptic Pruning". *Nature Communications* 9.1, p. 2236.

Millán, A. P., J. J. Torres, and J. Marro (2019). "How Memory Conforms to Brain Development". *Frontiers in Computational Neuroscience* 13.

Miller, A. (2019). "Realism". *The Stanford Encyclopedia of Philosophy*. Ed. by E. N. Zalta. Winter 2019. Metaphysics Research Lab, Stanford University.

Miller, K. J., L. B. Sorensen, J. G. Ojemann, and M. den Nijs (2009). "Power-Law Scaling in the Brain Surface Electric Potential". *PLOS Computational Biology* 5.12, e1000609.

Miller, S. R., S. Yu, and D. Plenz (2019). "The Scale-Invariant, Temporal Profile of Neuronal Avalanches in Relation to Cortical γ–Oscillations". *Scientific Reports* 9.1, pp. 1–14.

Millman, D., S. Mihalas, A. Kirkwood, and E. Niebur (2010). "Self-organized criticality occurs in non-conservative neuronal networks during 'up' states". *Nature Physics* 6.10, pp. 801–805.

Mongillo, G., D. Hansel, and C. van Vreeswijk (2012). "Bistability and Spatiotemporal Irregularity in Neuronal Networks with Nonlinear Synaptic Transmission". *Physical Review Letters* 108.15, p. 158101.

Montbrió, E., D. Pazó, and A. Roxin (2015). "Macroscopic Description for Networks of Spiking Neurons". *Physical Review X* 5.2.

Montejo, N., M. N. Lorenzo, V. Pérez-Villar, and V. Pérez-Muñuzuri (2005). "Noise Correlation Length Effects on a Morris-Lecar Neural Network". *Physical Review E* 72.1.

Monti, M., D. K. Lubensky, and P. R. ten Wolde (2017). "Optimal Entrainment of Circadian Clocks in the Presence of Noise". *arXiv preprint arXiv:1706.02226*.

Mora, T. and W. Bialek (2011). "Are Biological Systems Poised at Criticality?" *J. Stat. Phys.* 144.2, pp. 268–302.

Moreau, L. and E. Sontag (2003). "Balancing at the Border of Instability". *Physical Review E* 68.2, p. 020901.

Moretti, P. and M. A. Muñoz (2013). "Griffiths Phases and the Stretching of Criticality in Brain Networks". *Nature Communications* 4.1, p. 2521.

Muller, L., F. Chavane, J. Reynolds, and T. J. Sejnowski (2018). "Cortical Travelling Waves: Mechanisms and Computational Principles". *Nature Reviews Neuroscience* 19.5, p. 255.

Muñoz, M., G Grinstein, R Dickman, and R Livi (1996). "Critical Behavior of Systems with Many Absorbing States". *Physical review letters* 76.3, p. 451.

Muñoz, M., R Dickman, A Vespignani, and S Zapperi (1999). "Avalanche and Spreading Exponents in Systems with Absorbing States". *Phys. Rev. E* 59.5, pp. 6175–6179.

Muñoz, M. A. (2018). "Colloquium: Criticality and Dynamical Scaling in Living Systems". *Rev. Mod. Phys.* 90.3, p. 031001.

Murphy, B. K. and K. D. Miller (2009). "Balanced Amplification: A New Mechanism of Selective Amplification of Neural Activity Patterns". *Neuron* 61.4, pp. 635–648.

Nakao, H. (2016). "Phase Reduction Approach to Synchronisation of Nonlinear Oscillators". *Contemporary Physics* 57.2, pp. 188–214.

Narayan, O. and A. A. Middleton (1994). "Avalanches and the Renormalization Group for Pinned Charge-Density Waves". *Physical Review B* 49.1, p. 244.

Nunes Amaral, L. A. and K. B. Lauritsen (1997). "Universality Classes for Rice-Pile Models". *Physical Review E* 56.1, pp. 231–234.

Ódor, G. (2008). *Universality in Nonequilibrium Lattice Systems: Theoretical Foundations*. Singapore: World Scientific.

Ódor, G. and J. Kelling (2019). "Critical Synchronization Dynamics of the Kuramoto Model on Connectome and Small World Graphs". *Scientific Reports* 9.1, p. 19621.

Ohta, H. and S. I. Sasa (2008). "Critical Phenomena in Globally Coupled Excitable Elements". *Physical Review E* 78.6, p. 065101.

Okun, M. and I. Lampl (2008). "Instantaneous Correlation of Excitation and Inhibition during Ongoing and Sensory-Evoked Activities". *Nature Neuroscience* 11, 535 EP.

Olami, Z., H. J. S. Feder, and K. Christensen (1992). "Self-Organized Criticality in a Continuous, Nonconservative Cellular Automaton Modeling Earthquakes". *Physical review letters* 68.8, p. 1244.

Ott, E. and T. M. Antonsen (2008). "Low Dimensional Behavior of Large Systems of Globally Coupled Oscillators". *Chaos: An Interdisciplinary Journal of Nonlinear Science* 18.3, p. 037113.

Ozbudak, E. M., M. Thattai, H. N. Lim, B. I. Shraiman, and A. Van Oudenaarden (2004). "Multistability in the Lactose Utilization Network of Escherichia Coli". *Nature* 427.6976, p. 737.

Palmieri, L. and H. J. Jensen (2018). "The Emergence of Weak Criticality in SOC Systems". *EPL (Europhysics Letters)* 123.2, p. 20002.

Palmigiano, A., T. Geisel, F. Wolf, and D. Battaglia (2017). "Flexible Information Routing by Transient Synchrony". *Nature Neuroscience* 20.7, pp. 1014–1022.

Palva, J. M. et al. (2013). "Neuronal Long-Range Temporal Correlations and Avalanche Dynamics Are Correlated with Behavioral Scaling Laws". *Proceedings of the National Academy of Sciences of the United States of America* 110.9, pp. 3585–3590.

Papanikolaou, S. et al. (2012). "Quasi-Periodic Events in Crystal Plasticity and the Self-Organized Avalanche Oscillator". *Nature* 490.7421, pp. 517–521.

Pasquale, V, P Massobrio, L. Bologna, M Chiappalone, and S Martinoia (2008). "Self-Organization and Neuronal Avalanches in Networks

of Dissociated Cortical Neurons". *Neuroscience* 153.4, pp. 1354–1369.

Pastor-Satorras, R. and A. Vespignani (2000). "Field Theory of Absorbing Phase Transitions with a Nondiffusive Conserved Field". *Physical Review E* 62.5, R5875–R5878.

Pastor-Satorras, R., C. Castellano, P. Van Mieghem, and A. Vespignani (2015). "Epidemic Processes in Complex Networks". *Reviews of Modern Physics* 87.3, p. 925.

Pathria, R. K. and P. D. Beale (2011). *Statistical Mechanics*. Third. Elsevier.

Petermann, T. et al. (2009). "Spontaneous Cortical Activity in Awake Monkeys Composed of Neuronal Avalanches". *Proceedings of the National Academy of Sciences* 106.37, pp. 15921–15926.

Pikovsky, A., M. Rosenblum, and J. Kurths (2003). *Synchronization: A Universal Concept in Nonlinear Sciences*. Vol. 12. Cambridge: Cambridge university press.

Pittorino, F., M. Ibáñez–Berganza, M. di Volo, A. Vezzani, and R. Burioni (2017). "Chaos and Correlated Avalanches in Excitatory Neural Networks with Synaptic Plasticity". *Physical Review Letters* 118.9, p. 098102.

Plenz, D. and E. Niebur (2014). *Criticality in Neural Systems*. John Wiley & Sons.

Poil, S.-S., R. Hardstone, H. D. Mansvelder, and K. Linkenkaer-Hansen (2012). "Critical-State Dynamics of Avalanches and Oscillations Jointly Emerge from Balanced Excitation/Inhibition in Neuronal Networks". *Journal of Neuroscience* 32.29, pp. 9817–9823.

Politi, A., E. Ullner, and A. Torcini (2018). "Collective Irregular Dynamics in Balanced Networks of Leaky Integrate-and-Fire Neurons". *The European Physical Journal Special Topics* 227.10-11, pp. 1185–1204.

Ponce-Alvarez, A., A. Jouary, M. Privat, G. Deco, and G. Sumbre (2018). "Whole-Brain Neuronal Activity Displays Crackling Noise Dynamics". *Neuron* 100.6, 1446–1459.e6.

Porta, L. D. and M. Copelli (2019). "Modeling Neuronal Avalanches and Long-Range Temporal Correlations at the Emergence of Collective Oscillations: Continuously Varying Exponents Mimic M/EEG Results". *PLOS Computational Biology* 15.4, e1006924.

Pouille, F., A. Marin-Burgin, H. Adesnik, B. V. Atallah, and M. Scanziani (2009). "Input Normalization by Global Feedforward Inhibition Expands Cortical Dynamic Range". *Nature Neuroscience* 12.12, p. 1577.

Prescott, S. A. (2014). "Excitability: Types I, II, and III". *Encyclopedia of Computational Neuroscience*. Ed. by D. Jaeger and R. Jung. New York, NY: Springer New York, pp. 1–7.

Priesemann, V. and O. Shriki (2018). "Can a Time Varying External Drive Give Rise to Apparent Criticality in Neural Systems?" *PLOS Computational Biology* 14.5, e1006081.

Priesemann, V., M. H. Munk, and M. Wibral (2009). "Subsampling Effects in Neuronal Avalanche Distributions Recorded in Vivo". *BMC Neuroscience* 10.1, p. 40.

Priesemann, V. et al. (2014). "Spike Avalanches in Vivo Suggest a Driven, Slightly Subcritical Brain State". *Frontiers in Systems Neuroscience* 8.

Pruessner, G. (2003). "Oslo Rice Pile Model Is a Quenched Edwards-Wilkinson Equation". *Physical Review E* 67.3, p. 030301.

— (2012). *Self-Organised Criticality: Theory, Models and Characterisation*. Cambridge University Press.

— (2013). "A Field Theory for Self-Organised Criticality". *Proceedings of the European Conference on Complex Systems 2012*. Springer, pp. 79–86.

Recio, I. and J. J. Torres (2016). "Emergence of Low Noise Frustrated States in E/I Balanced Neural Networks". *Neural Networks* 84, pp. 91–101.

Renart, A. et al. (2010). "The Asynchronous State in Cortical Circuits". *Science* 327.5965, pp. 587–590.

Ribeiro, T. L. et al. (2010). "Spike Avalanches Exhibit Universal Dynamics across the Sleep-Wake Cycle". *PLOS ONE* 5.11, e14129.

Rossi, M., R. Pastor-Satorras, and A. Vespignani (2000). "Universality Class of Absorbing Phase Transitions with a Conserved Field". *Physical Review Letters* 85.9, pp. 1803–1806.

Rothman, J. S. (2013). "Modeling Synapses". *Encyclopedia of Computational Neuroscience*. Ed. by D. Jaeger and R. Jung. New York, NY: Springer, pp. 1–15.

Rubin, R., L. F. Abbott, and H. Sompolinsky (2017). "Balanced Excitation and Inhibition Are Required for High-Capacity, Noise-Robust Neuronal Selectivity". *Proc. Natl. Acad. of Sci. (USA)*, p. 201705841.

Sadeh, S. and C. Clopath (2020). "Inhibitory Stabilization and Cortical Computation". *Nature Reviews Neuroscience*, pp. 1–17.

Sakaguchi, H., S. Shinomoto, and Y. Kuramoto (1987). "Local and Grobal Self-Entrainments in Oscillator Lattices". *Progress of Theoretical Physics* 77.5, pp. 1005–1010.

Scarpetta, S., I. Apicella, L. Minati, and A. de Candia (2018). "Hysteresis, Neural Avalanches, and Critical Behavior near a First-Order Transition of a Spiking Neural Network". *Physical Review E* 97.6, p. 062305.

Schleimer, J.-H., J. Hesse, and S. Schreiber (2019). "Spike Statistics of Stochastic Homoclinic Neuron Models in the Bistable Region". *arXiv:1902.00951 [q-bio]*.

Segev, R., Y. Shapira, M. Benveniste, and E. Ben-Jacob (2001). "Observations and Modeling of Synchronized Bursting in Two-Dimensional Neural Networks". *Physical Review E* 64.1, p. 011920.

Serazzi, G. and S. Zanero (2004). "Computer Virus Propagation Models". *Performance Tools and Applications to Networked Systems*. Springer, pp. 26–50.

Shew, W. L. and D. Plenz (2013). "The Functional Benefits of Criticality in the Cortex". *The Neuroscientist* 19.1, pp. 88–100.

Shew, W. L., H. Yang, T. Petermann, R. Roy, and D. Plenz (2009). "Neuronal Avalanches Imply Maximum Dynamic Range in Cortical Networks at Criticality". *Journal of Neuroscience* 29.49, pp. 15595–15600.

Shew, W. L., H. Yang, S. Yu, R. Roy, and D. Plenz (2011). "Information Capacity and Transmission Are Maximized in Balanced Cortical Networks with Neuronal Avalanches". *Journal of Neuroscience* 31.1, pp. 55–63.

Shinomoto, S. and Y. Kuramoto (1986a). "Cooperative Phenomena in Two-Dimensional Active Rotator Systems". *Progress of Theoretical Physics* 75.6, pp. 1319–1327.

— (1986b). "Phase Transitions in Active Rotator Systems". *Progress of Theoretical Physics* 75.5, pp. 1105–1110.

Shu, Y., A. Hasenstaub, and D. A. McCormick (2003). "Turning on and off Recurrent Balanced Cortical Activity". *Nature* 423.6937, p. 288.

Sidoravicius, V., A. Teixeira, et al. (2017). "Absorbing-State Transition for Stochastic Sandpiles and Activated Random Walks". *Electronic Journal of Probability* 22.

Sippy, T. and R. Yuste (2013). "Decorrelating Action of Inhibition in Neocortical Networks". *Journal of Neuroscience* 33.23, pp. 9813–9830.

Socolar, J., G Grinstein, and C Jayaprakash (1993). "On Self-Organized Criticality in Nonconserving Systems". *Physical Review E* 47.4, p. 2366.

Softky, W. R. and C. Koch (1993). "The Highly Irregular Firing of Cortical Cells Is Inconsistent with Temporal Integration of Random EPSPs". *Journal of Neuroscience* 13.1, pp. 334–350.

Soriano, J., M. R. Martínez, T. Tlusty, and E. Moses (2008). "Development of Input Connections in Neural Cultures". *Proc. Natl. Acad. of Sci. (USA)*.

Sornette, D. (1994). "Sweeping of an Instability: An Alternative to Self-Organized Criticality to Get Powerlaws without Parameter Tuning". *J. de Physique I* 4.2, pp. 209–221.

Sornette, D. and G. Ouillon (2012). "Dragon-Kings: Mechanisms, Statistical Methods and Empirical Evidence". *Eur. Phys. J. Spec.Top.* 205.1, pp. 1–26.

Stepp, N., D. Plenz, and N. Srinivasa (2015). "Synaptic Plasticity Enables Adaptive Self-Tuning Critical Networks". *PLoS Computational Biology* 11.1.

Strogatz, S. H. (1994). *Nonlinear Dynamics and Chaos: With Applications to Physics, Biology, Chemistry, and Engineering*. Studies in Nonlinearity. Reading, Mass: Addison-Wesley Pub.

— (2000). "From Kuramoto to Crawford: Exploring the Onset of Synchronization in Populations of Coupled Oscillators". *Physica D: Nonlinear Phenomena* 143.1-4, pp. 1–20.

Sumner, R. L., M. J. Spriggs, S. D. Muthukumaraswamy, and I. J. Kirk (2020). "The Role of Hebbian Learning in Human Perception: A Methodological and Theoretical Review of the Human Visual Long-Term Potentiation Paradigm". *Neuroscience & Biobehavioral Reviews* 115, pp. 220–237.

Tang, C. and P. Bak (1988). "Mean Field Theory of Self-Organized Critical Phenomena". *Journal of Statistical Physics* 51.5-6, pp. 797–802.

Tartaglia, E. M. and N. Brunel (2017). "Bistability and up/down State Alternations in Inhibition-Dominated Randomly Connected Networks of LIF Neurons". *Scientific Reports* 7.1, p. 11916.

Tebaldi, C., M. De Menech, and A. L. Stella (1999). "Multifractal Scaling in the Bak-Tang-Wiesenfeld Sandpile and Edge Events". *Physical Review Letters* 83.19, p. 3952.

Touboul, J. and A. Destexhe (2010). "Can Power-Law Scaling and Neuronal Avalanches Arise from Stochastic Dynamics?" *PLOS ONE* 5.2, e8982.

— (2017). "Power-Law Statistics and Universal Scaling in the Absence of Criticality". *Physical Review E* 95.1.

Treviño, M. (2016). "Inhibition Controls Asynchronous States of Neuronal Networks". *Frontiers in Synaptic Neuroscience* 8, p. 11.

Tsodyks, M. V. and H. Markram (1997). "The Neural Code between Neocortical Pyramidal Neurons Depends on Neurotransmitter Release Probability". *Proceedings of the National Academy of Sciences* 94.2, pp. 719–723.

Tsumoto, K., H. Kitajima, T. Yoshinaga, K. Aihara, and H. Kawakami (2006). "Bifurcations in Morris–Lecar Neuron Model". *Neurocomputing* 69.4, pp. 293–316.

Turrigiano, G. G. and S. B. Nelson (2004). "Homeostatic Plasticity in the Developing Nervous System". *Nature Reviews Neuroscience* 5.2, pp. 97–107.

Tyulkina, I. V., D. S. Goldobin, L. S. Klimenko, and A. Pikovsky (2018). "Dynamics of Noisy Oscillator Populations beyond the Ott-Antonsen Ansatz". *Physical Review Letters* 120.26.

Ukai, H. and H. R. Ueda (2010). "Systems Biology of Mammalian Circadian Clocks". *Annual Review of Physiology* 72.1, pp. 579–603.

Ullner, E., A. Politi, and A. Torcini (2018). "Ubiquity of Collective Irregular Dynamics in Balanced Networks of Spiking Neurons". *Chaos: An Interdisciplinary Journal of Nonlinear Science* 28.8, p. 081106.

van Wijland, F. (2002). "Universality Class of Nonequilibrium Phase Transitions with Infinitely Many Absorbing States". *Physical review letters* 89.19, p. 190602.

VanderLeest, H. T. et al. (2007). "Seasonal Encoding by the Circadian Pacemaker of the SCN". *Current Biology* 17.5, pp. 468–473.

Vespignani, A, R Dickman, M. Muñoz, and S Zapperi (1998). "Driving, Conservation, and Absorbing States in Sandpiles". *Physical Review Letters* 81.25, p. 5676.

Vespignani, A., R. Dickman, M. A. Muñoz, and S. Zapperi (2000). "Absorbing-State Phase Transitions in Fixed-Energy Sandpiles". *Physical Review E* 62.4, p. 4564.

Villa Martín, P., J. A. Bonachela, S. A. Levin, and M. A. Muñoz (2015). "Eluding Catastrophic Shifts". *Proc. Nat. Acad. of Sci.* 112.15, E1828–E1836.

Villegas, P., P. Moretti, and M. A. Muñoz (2014). "Frustrated Hierarchical Synchronization and Emergent Complexity in the Human Connectome Network". *Scientific Reports* 4, p. 5990.

Vogels, T. P. and L. F. Abbott (2009). "Gating Multiple Signals through Detailed Balance of Excitation and Inhibition in Spiking Networks". *Nat. Neurosci.* 12.4, p. 483.

Vogels, T. P., H. Sprekeler, F. Zenke, C. Clopath, and W. Gerstner (2011). "Inhibitory Plasticity Balances Excitation and Inhibition in Sensory Pathways and Memory Networks". *Science* 334.6062, pp. 1569–1573.

Vreeswijk, C. van and H. Sompolinsky (1996). "Chaos in Neuronal Networks with Balanced Excitatory and Inhibitory Activity". *Science* 274.5293, pp. 1724–1726.

Vreeswijk, C. van and H. Sompolinsky (1998). "Chaotic Balanced State in a Model of Cortical Circuits". *Neural Computation* 10.6, pp. 1321–1371.

Wang, G., W. Jin, and C. Hu (2013). "The Complete Synchronization of Morris–Lecar Neurons Influenced by Noise". *Nonlinear Dynamics* 73.3, pp. 1715–1719.

Wiese, K. J. (2016). "Coherent-State Path Integral versus Coarse-Grained Effective Stochastic Equation of Motion: From Reaction Diffusion to Stochastic Sandpiles". *Physical Review E* 93.4, p. 042117.

Wilson, H. R. and J. D. Cowan (1972). "Excitatory and Inhibitory Interactions in Localized Populations of Model Neurons". *Biophysical Journal* 12.1, pp. 1–24.

Wilting, J. and V. Priesemann (2019). "Between Perfectly Critical and Fully Irregular: A Reverberating Model Captures and Predicts Cortical Spike Propagation". *Cerebral Cortex* 29.6, pp. 2759–2770.

Winfree, A. T. (2001). *The Geometry of Biological Time*. Vol. 12. Springer Science & Business Media.

Wissel, F. and B. Drossel (2006). "Transient and Stationary Behavior of the Olami-Feder-Christensen Model". *Physical Review E* 74.6, p. 066109.

Wolfart, J., D. Debay, G. Le Masson, A. Destexhe, and T. Bal (2005). "Synaptic Background Activity Controls Spike Transfer from Thalamus to Cortex". *Nature Neuroscience* 8.12, p. 1760.

Wüster, S. and R. Bhavna (2020). "Spatial Correlations in a Finite-Range Kuramoto Model". *Physical Review E* 101.5, p. 052210.

Yaghoubi, M. et al. (2018). "Neuronal Avalanche Dynamics Indicates Different Universality Classes in Neuronal Cultures". *Scientific reports* 8.1, p. 3417.

Yang, D.-P., H.-J. Zhou, and C. Zhou (2017). "Co-Emergence of Multi-Scale Cortical Activities of Irregular Firing, Oscillations and Avalanches Achieves Cost-Efficient Information Capacity". *PLoS Computational Biology* 13.2, e1005384.

Yang, H., W. L. Shew, R. Roy, and D. Plenz (2012). "Maximal Variability of Phase Synchrony in Cortical Networks with Neuronal Avalanches". *Journal of Neuroscience* 32.3, pp. 1061–1072.

Yu, S., A. Klaus, H. Yang, and D. Plenz (2014). "Scale-Invariant Neuronal Avalanche Dynamics and the Cut-off in Size Distributions". *PloS one* 9.6, e99761.

Yu, S. et al. (2017). "Maintained Avalanche Dynamics during Task-Induced Changes of Neuronal Activity in Nonhuman Primates". *eLife* 6. Ed. by C. Chestek, e27119.

Zaks, M. A., A. B. Neiman, S. Feistel, and L. Schimansky-Geier (2003). "Noise-Controlled Oscillations and Their Bifurcations in Coupled Phase Oscillators". *Physical Review E* 68.6.

Zamora-López, G., Y. Chen, G. Deco, M. L. Kringelbach, and C. Zhou (2016). "Functional Complexity Emerging from Anatomical Constraints in the Brain: The Significance of Network Modularity and Rich-Clubs". *Scientific Reports* 6.1, p. 38424.

Zhang, Y.-C. (1989). "Scaling Theory of Self-Organized Criticality". *Physical Review Letters* 63.5, p. 470.

Zierenberg, J., J. Wilting, V. Priesemann, and A. Levina (2020). "Description of Spreading Dynamics by Microscopic Network Models

and Macroscopic Branching Processes Can Differ Due to Coalescence". *Physical Review E* 101.2, p. 022301.